Time-Resolved Proteomic Analysis in Zebrafish and Cultured Neurons Using Bioorthogonal Noncanonical Amino Acid Tagging

Thesis by

Sophie Miller

In Partial Fulfillment of the Requirements for the

Degree of

Doctor of Philosophy in Chemical Engineering

CALIFORNIA INSTITUTE OF TECHNOLOGY

Pasadena, California

2025

Defended May 19, 2025

Sophie Eve Miller
ORCID: 0000-0001-6805-7036

ACKNOWLEDGEMENTS

As I begin to write these acknowledgements, I am sitting on the balcony of the chemical engineering building at Stanford—the place that inspired me to pursue this PhD and where, almost exactly 10 years ago, I made the decision to continue my studies at Caltech. The years that have passed between then and now have been a great privilege and immensely rewarding, but they have not been without their challenges, both academic and personal. Nevertheless, my heart is filled with an overwhelming sense of gratitude: gratitude for the opportunity to have gotten to contribute my small drop in the bucket of scientific knowledge, gratitude for the opportunity to learn and expand my mind and push my intellectual limits surrounded by some of the most brilliant people on the planet, and—most of all—gratitude for the people who supported me every step of the way and without whom I could not have made it across the finish line. This section is for all of you.

I must begin by thanking my advisor, **Prof. David Tirrell**. It's incredible to think that the same 16-year-old Sophie that came to visit Caltech and met with you to inquire about chemical engineering is now wrapping up her PhD as your last ever graduate student. Thank you for giving me the freedom and support to research the scientific questions that I was compelled to answer, even if they were outside the lab's typical areas of expertise. It is rare for a PhD student to be trusted to work with the level of independence that you encouraged me to embrace. I am honored to have received your mentorship, and your integrity, intellectual rigor, patience, and optimism will always be an inspiration to me.

I would also like to acknowledge the other members of my thesis committee: **Prof. David Prober**, **Prof. Tsui-Fen Chou**, and **Prof. Mikhail Shapiro**. **David**: Thank you for taking me in as an honorary member of your lab. Your lab was a second home to me on campus, and I will forever be grateful for all that you provided me: the opportunity to work with zebrafish, the chance to learn about the biology of sleep, an environment where I could surround myself with neuroscientists, another group of labmates to work alongside as my primary lab slowly shrank in size, and a mountain-facing desk in the shiny new Chen building

to escape the temperature-dysregulated on-the-brink-of-collapse Spalding. **Tsui-Fen**: I am overwhelmed with gratitude for your extreme generosity with me. You have given so much of your time, at times in 2 or 3 hour-long stretches, to talk to me about my work and provide invaluable scientific guidance. Your proteomics expertise, as well as the facility on campus you help run, has been indispensable, but I am above all grateful for the genuine caring and support I have received from you over the years. **Mikhail**: Thank you for taking the time out of your incredibly busy schedule to serve as my committee chair. Even though we only ever met a few times about my research, you were always engaged, asked thoughtful questions, and provided me with useful directions for my projects, including the suggestion to use heat shock as a proof-of-concept for my BONCAT work in zebrafish, which ended up being the key to completing that story. I will also always be grateful for your letting me TA your undergraduate chemical engineering fluid mechanics class, as it had been a dream of mine to teach that material ever since I took Prof. Gerry Fuller's version of the course my junior year at Stanford. You are a huge role model for me, and I have always admired your academic vigor, your passion for both academic and entrepreneurial endeavors, and your non-linear career path to becoming a professor.

There have been various other faculty at Caltech (or previously affiliated with Caltech in some capacity) whose guidance and support have meant a great deal to me over the course of my PhD. To **Prof. Henry Lester**: Thank you for allowing me to take over your tissue culture room and to absorb your and your lab members' wisdom as I embarked upon research involving drugs and cultured primary neurons. I am especially appreciative of the kindness and warmth you have always shown me, and for always believing in me and in my potential as a scientist, especially during moments I may have felt discouraged. To **Prof. Erin Schuman**: I cannot imagine what my PhD would have been like were it not for your influence and support. From opening the doors to your lab in Frankfurt for a summer to take advantage of your lab's incredible facilities and expertise, to encouraging me to take the neurobiology course at the Marine Biological Laboratory in Woods Hole, to providing me with the idea to work on BONCAT proteomics in zebrafish, to looking over PowerPoint slides with me before my talk at a conference in India, to taking the time out of your

Thanksgiving holiday in New York City to meet with me for a coffee, you have been unbelievably generous toward me with your time and energy. You are an inspiration to me, and I am so grateful to be able to look up to you.

The support from Caltech or Caltech-affiliated faculty does not end there. To **Prof. Shelly Tzlil**: While I wish the circumstances that brought you and Noa to Caltech had been different, I am grateful that I got to meet and get to know you both. Thank you for always being willing to chat, for bringing a wonderful, inquisitive burst of energy and healthy dose of Israeli candidness to the lab, and for the caring you have shown me. To **Prof. Mike Vicic**: Thank you for your wisdom and advice, for your willingness to lend a compassionate ear, and for all you do to help Caltech chemical engineers. You make this department an immeasurably better place. To **Prof. Julia Greer**: I am humbled and honored to have you as a mentor. I do not know how you have the time to go on coffee walks with me and remember anything about my life between running a lab doing incredible research, being a mother to three amazing kids, going to the gym and being in insane shape, and shredding the slopes at Mammoth, where you have even opened the doors of your awesome condo to me. Thank you for the guidance you have given me and the inspiring example you set for me. To **Prof. Julie Kornfield**: I owe a great deal of my being where I am today to you, and every time I bump into you on campus puts a smile on my face. Working in your lab as a SURF student during the summer of 2013, between my sophomore and junior years at Stanford, showed me what a phenomenal place Caltech is to do research and was the inspiration for the Honors thesis project I went on to do in Zhenan's lab, which turned into my first independent research experience, several conference awards, my first scientific paper, and opened so many academic doors to me. The email you sent me after I was turned down for the Rhodes and Marshall Scholarships but before I heard back from the Churchill Scholarship was one of the most meaningful emails I have received, and it remains starred in my email inbox to this day. To **Prof. Rustem Ismagilov**: Thank you for giving me the opportunity to TA for your undergraduate chemical engineering thermodynamics class two times. Helping teach your course was one of the most rewarding experiences of my PhD, and it gave me a sense of fulfillment and lifted me up during the hardest months of my life. Finally, to **Prof. Sarah**

Heilshorn: You probably do not remember who I am, but our conversations when I was deciding between undergraduate and graduate programs were pivotal in my deciding to go to Stanford and Caltech, respectively, and you have been an academic role model to me for many years. Your thesis has sat on the shelves above my desk and has inspired me throughout my PhD.

There is one more Caltech faculty member who requires particularly special recognition. **Prof. Justin Bois**: It almost feels strange to put you alongside other professors when you feel as much like a friend as you do a mentor. Thank you for redefining the bar for what it means to be a good teacher and for trusting me to TA for you two times, granting me a behind the scenes look into the heroic level of time and thought you put into your courses. Thank you for teaching me how to properly analyze and visualize data—you change the way hundreds of Caltech students do their research for the better. Thank you for being there for me during some of my lowest points and supporting me when I needed it the most, striking the perfect balance between empathetic understanding and practical advice. Thank you for sharing your love of the Magic Castle and of LAFC with me, and for being an appreciator of Uruguayan soccer, even if it is only because some players from La Celeste have also donned your beloved black and gold. Thank you for being the husband to the coolest, kindest, and most brilliant woman, **Ramit Mizrahi**. You two remind me what to never settle for less than in a future partner. I am extraordinarily grateful to you both for being the biggest and most generous supporters of the Caltech Jewish community. Thank you both, as well, for inviting me stay with you and Ben at your house when my apartment was uninhabitable.

There are professors and teachers from my college and high school years who left an indelible mark on me both intellectually and personally, and I would like to acknowledge a handful without whom I would not be where I am today. **Prof. Zhenan Bao**: My heart is filled with gratitude every time I think about the fact that, despite leading a lab of 50 or more people doing groundbreaking research, you have taken time over the years to write me countless letters of recommendation, go on Dish hikes together, and give me advice over long phone calls. I am awestruck by your ability to balance everything you do and somehow make it

look easy. I feel blessed to have you as both a scientific role model and as a mentor. By giving me the opportunity to work in your lab as an undergraduate, and by letting me work on a completely independent project that you helped me turn into my first first-author peer-reviewed paper, you set me on the course that led me to this PhD, and your support since has been instrumental in helping me accomplish this goal. **Prof. Channing Robertson**: Watching your lectures on YouTube when I was in high school sparked my interest in studying chemical engineering. Little did I know then, or when I met you as a starry-eyed 11th grader with the gumption to reach out to you when visiting Stanford, that you would become like an academic grandfather to me (not because of your age, I must emphasize, but because of the nature of the caring and love you have shown me). I will forever be grateful to you and to Donna for always believing in me and for supporting me over the years. I treasure our chats for the perspective they give me, as they allow me to zoom out from whatever struggles I may be experiencing and remind me that the ups and downs are all part of the greater scientific trajectory I am on. To **Dr. Palfrey** and **Mr. Worrall**: Attending Horace Mann was an immense privilege, and the most incredible part of that experience was the quality of teachers like you. Thank you for nurturing the budding young scientist, mathematician, and engineer in me. You gave me the confidence to believe I could tackle challenging problems, but even more importantly, you showed me how exhilarating and beautiful science and math can be.

My time in the Tirrell Lab would not have been the same without the wonderful scientists with whom I shared bench and office space: **Elliot, Grace, Stephanie, Hanwei, Xinyan, Yue, Bradley, Maiko, Xinran, Sam, Mark, Shannon, Peter, Seth, Kelly, Josh,** and **Seu**. I am so fortunate to have been surrounded by so many intelligent, hard-working, kind, and collaborative scientists and engineers. You all pushed me to be a better researcher and made coming into lab infinitely more fun than it otherwise would have been. Thank you for your tough questions at group meetings, your technical expertise around the lab, and your camaraderie. I would like to give extra thanks out to those of you who became not just coworkers but also friends. **Dr. Elliot MacKrell**: You are a shining example of a thoughtful and thorough researcher, amaze me with all you were able to do with the computational skills

you picked up during your co-op, and always brightened my day with our conversations. **Dr. Grace Wang**: Your friendship and support, as well as all the amazing food we got to eat together around the San Gabriel Valley, made a huge difference in my being able to push through the hardest times of this PhD. You are one of the most determined and tough scientists I know. **Dr. Stephanie Breunig**: Your kindness, helpfulness, and positive attitude made every day in lab better, and I will always admire how hard-working, patient, and dedicated you are as a scientist. **Dr. Sam Ho**: Thank you for setting such an amazing example for what it looks like to do beautiful science, overcome challenges in the lab, and be an amazing mentor and friend to those below you. **Dr. Josh Baccile**: I am so grateful to have you as a friend. You made me laugh more than any other person in the lab, without question, and the prospect of debriefing each other on our dreams and laughing at your unfiltered commentary gave me something to look forward to every day in lab. Thank you for providing real-talk when I needed real-talk, and for being a pseudo-big-brother in the lab for so many of us when we needed support. **Dr. Seunghyun Sim**: I am lucky to have a scientist like you to look up to. You balance work and life with grace and I am so grateful we have kept in touch and for your continued caring and support. **Dr. Kelly Burke**: Thank you for taking me under your wing during my first quarter at Caltech. You showed me what it means to work smart, to have a balanced approach to this experience, and to take control of your PhD and know when it is time to switch paths. It is also because of you that I was first exposed to neuroscience, which changed the course of my research and opened my mind to an entire world of scientific questions I did not know about before but have since captivated me. I would also like to acknowledge to **Dr. Alborz Mahdavi**: I am inspired by what you have built with Protomer, and I appreciate your genuine friendliness to me over the years.

I had the fortune to also be embraced as an honorary member of a second lab on campus: the Prober Lab: **Amina, Grigorios, Andrey, Uli, Chanpreet, Dan, Steve, Jin, Rongwei, Andrew, Altyn, Desi, Jasmine, Marina, Yun, Olivia, Alexis, Tasha, Brianna, Hannah, Cristina, Alex, Axel, Ryan, Barbara,** and **Caressa**. You have all been so kindhearted toward me and have made me feel like a true part of the group. You have also all provided encouragement and support over the last five years of my PhD, and I am so grateful to have

been embraced by a whole new set of labmates as the Tirrell lab gradually dwindled in size. Thank you for teaching me the patience required to do biological research and for sharing with me your collective expertise about zebrafish, the brain, sleep, and more. I would like to give special thanks to those of you that have spent time helping me with my projects and gone above and beyond the normal duties of labmates. **Dr. Grigorios Oikonomou**: It is because of our chat after deciding to change PhD projects that I decided to work with the Prober lab. From Matlab code, plasmids, and VT plate loading tricks to always asking engaged and thoughtful questions at every lab meeting, the knowledge and wisdom you have shared with me and everyone else in the lab has been invaluable. **Altyn Rymbek**: Thank you for taking the time out of your own research to help me with injections and for always being willing to go out of your way to help me and others. You are one of the kindest souls I have met at Caltech, and I will never forget our chats around the lab or late at night in the injection room. Your curiosity and genuine caring touched my heart and brightened my days. **Tasha Cammidge**: The Prober lab has been so incredibly lucky to have had you as a lab manager. You are unbelievably kind, patient, and knowledgeable, and your hard work every day has kept the lab running smoothly and been an indispensable part of every project in the lab. You always ask what you can do to help, and you make everything feel like no problem, even when it involves setting up dozens of fish matings or counting and sorting thousands of embryos. I'm so excited to see the impact you make in your next role with Green Labs. Thank you for everything.

I am grateful to have had the opportunity to collaborate with phenomenal scientists in other labs who have taught me so much and helped me with various projects over the years. None of the chapters in my thesis would have been possible without my coworkers at the Proteome Exploration Laboratory (PEL) at Caltech. It is an incredible privilege to have access to the technological resources of the PEL and, even more importantly, the expertise of the scientists that work there. **Dr. Ting-Yu Wang** and **Dr. Baiyi Quan**: You have both spent so many hours helping me run more BONCAT samples than I can count on the mass spectrometers, as well as going back and forth with me over e-mail about the best ways to analyze my datasets, even late at night or on holidays. You treated my samples with the same care and

dedication I would have, which is rare and something I do not take for granted. You are also both extremely kind and caring. Working with you two has been an absolute pleasure. **Dr. Jeff Jones**: Thank you for your expertise in analyzing proteomics data. The pipeline you developed for the PEL has facilitated my research and that of everyone else who has had their data processed with your tidyproteomics package.

I would also like to acknowledge members of other labs with whom I got to work closely over the years. **Dr. Aaron Nichols**: From gabbing about true crime podcasts to scraping ketamine-treated neurons off dishes together, the prospect of getting to chat with you was probably the thing I most looked forward to every time I had to do something in the lab on the third floor of Kerckhoff. You are one of the friendliest people I have had the pleasure to meet at Caltech, and I am so grateful for your willingness to help me in the lab. You are a phenomenal teacher and mentor, and anyone that gets to work with or for you in the future will be so lucky. **Dr. Zack Blumenfeld**: I am so grateful we both ended up collaborating with the Prober lab. Your suggestion to me after one of my lab meetings that I use BONCAT to study antidepressants *in vitro* planted the seed that became the second chapter of this thesis. I had so much fun devising and working on our Chen Innovator Grant project together, and having the chance to work on a project related to antidepressants gave my PhD work a lot of meaning. I enjoyed chatting with you about everything from medicine to our athletic hobbies to philosophy, and I have no doubt you'll make a fantastic doctor and scientist. **Dr. Sabine Brinkmann-Chen**: If there were a queen of lab managers, I am pretty sure it would be you. Even while you are busy running a tight ship in the Arnold lab and saving the third floor of Spalding (and perhaps the whole building) from chaos, infestation, anarchy, or collapse, you always take the time to chat with me and help me with whatever it is I might need. Whether helping me send an international package on dry ice, managing purchase orders for centrifuge maintenance, or giving me tips on gym training through injury rehab, you have generously given to me of your time and energy. Thank you for always cheering for me from down the hall. **Dr. Susanne tom Dieck**: Your knowledge about primary neuron cultures and BONCAT were tremendously helpful to me and most of my PhD work would have been impossible without the knowledge and technical know-how you shared with me. Working in

the Schuman Lab in 2018 was an incredible experience, and you were instrumental in making that as enriching as it was. I will also never forget how you picked me up at the airport in Frankfurt less than two weeks after my father passed away. Thank you for your kindness, generosity, and help over the years. **Dr. Sonia Gasmi**: I am so grateful for our chats about research and the struggles of BONCAT over the last couple of years. You are a wonderful human and a fearless researcher—not many would be as brave as you have been getting BONCAT to work in squid. Thank you for your warmth and friendliness.

There are many others who work tirelessly behind the scenes to make everything we do in the Tirrell Lab and in the chemical engineering department possible. **Irina Meininger**: Thank you for your help with everything from overseeing and managing lab funding to helping me get on Dave's busy calendar. Your work has kept the lab afloat, and the warmth and caring you have shown me over the years have made a lasting positive impact on my time here. **Allison Kinard**: The Caltech chemical engineering graduate program is unbelievably lucky to have you running the show. You are amazing at your job, and I cannot think of a single time where you did not have the answer to a question I had. Thank you for the kindness and positivity you bring to every one of our interactions, be it an informal visit to the second floor of Spalding or some urgent problem for which you always have a solution.

There are others on campus whose work often goes unrecognized, but whose seemingly small contributions to our day-to-day lives at Caltech add over the weeks and years to make a huge impact. From the baristas at the Red Door Café that kept me caffeinated, to the custodians in the lab buildings where I worked who would arrive before dawn to keep our workspaces clean and tidy, these people brightened even the darkest days. **Martha Oropesa** y **Guillermina De La Torre**: Gracias por todos los cappuccinos que me han hechos con tanto cariño durante estos años en Caltech. Simepre me saludan con una sonrisa y con amor y preguntan por mi salud y mi familia. **Jaime** y **Sergio**: Gracias por trabajar tan duro para que los laboratorios donde trabajamos esten impecables. Siempre han sido tan amables conmigo. Siempre me alegran el día cuando los veo en Spalding o en Chen. Los extrañaré todos mucho.

I have had many—perhaps too many, some might say—creative, athletic, and social outlets during my time at Caltech and living in Los Angeles. These activities allowed me to get my mind off my experiments and brought me joy that was better than medicine to me. Rowing has been more than a hobby to me. It has been meditation, medicine, therapy, and transcendence disguised in a beautiful, albeit at times painful, sport. Every Saturday and Sunday, I had the opportunity to watch the sun rise over glassy water, and pushing off the dock allowed me to leave my worries on the shore and enter my tranquil, lung-burning bubble for as long as my quads could handle. Thank you to the **Churchill College Boat Club** for introducing me to this beautiful sport and to the **Cambridge University Boat Club** for exposing me to what it looks like at the highest level. Thank you to **Anna Liberovsky** for spending dozens of hours following me in a launch over the years and for being such an incredible coach and coxswain. All you taught me about rowing, from sculling to sweep, will be with me for the rest of my life. I would like to thank the many friends I made at the **Long Beach Rowing Association** over countless early mornings at the boathouse—you have all been such a wonderful community and have always been so kind to me. I cannot imagine a better way to have spent my weekend mornings than with you all. I would be remiss not to thank **Brie Larson** for producing the AppleTV+ series adaptation of one of my favorite books, *Lessons in Chemistry*, as it gave me the coolest day of my life rowing on set for a big-time Hollywood production and getting to experience "The Industry" during my time living in the city of Stars. I would also like to thank **American Family Insurance** for the extra cushion in my checking account from residuals for their ad that I rowed in, providing a welcome supplement to my humble graduate student salary. I now understand why so many people move to LA to catch their big break.

Playing with the Caltech Jazz Band has been a great honor and privilege, and getting to be a part of more concerts with this incredibly talented group was one of the best silver linings of having my PhD take as long as it did. Thank you **Barb Catlin** for making it such an enriching experience, for bringing in so many legendary guest artists for us to play with, and such a reliable source of happiness every Wednesday evening. Thank you, as well, for going above and beyond with the thoughtfulness and caring you have shown me over the years. I would

also like to acknowledge **Dr. Steve Snyder**: Thank you for going out of your way to show me kindness, to open up your home to the saxophone section for rehearsals and brats and whiskey, for helping me fix my saxophone, and for showing me that it is possible to continue play music at a high level even with a career outside of academia.

Only at Caltech can someone who has never played water polo in her life end up being listed on the athletic roster for a Division III NCAA women's water polo team as a Volunteer Assistant Coach. **Coach Jon Bonafede**: Thank you for letting me be a small part of the growth of the incredible program you have built here. Playing with the squad gave me an incredible opportunity to be a part of a team, learn a new sport, push myself physically, and meet an incredible group of women during grad school, and I am extremely grateful for this part of my Caltech experience. I would also like to thank the various undergrads I got to practice alongside a couple times a week: seeing you juggle athletics with your insane courseloads reminded me I can always make time for the things I love.

I am profoundly grateful to have been able to find a welcoming and tight-knit Jewish community at Caltech, and I am honored to have been able to serve the community for several years as the leader of two Jewish student groups on campus. **Rabbi Hershy and Sheva Stolik**: You both work tirelessly to create a home-away-from-home for so many Jewish students, faculty, and staff, dedicating your lives to enriching our souls with the learnings of the Torah and the blessings of its mitzvot. Thank you for the homemade soups when I am sick, for the gefilte fish deliveries for post-surgery Passover seders, for always remembering my dad's yahrzeit and hosting study sessions in his memory, and for always inviting me to Shabbat dinners. You have strengthened my Jewish identity and, as a result, added so much meaning to my life during my PhD. **Prof. Diana Kormos-Buchwald**: Thank you for opening the doors of the Einstein Papers Project house to the Caltech Hillel club and for your support of the Caltech Jewish community over the years. The lunches we had there, particularly our gatherings after October 7, were so meaningful and important, and I am grateful for your making them possible.

I am blessed with many amazing friendships, each of which I treasure deeply. These friends make me laugh till I cry and sit with me while I cry until I laugh. They are my chosen family, and I thank each and every one of them for allowing me to be theirs.

Dr. Annie Marsden: I cannot imagine what my PhD would have been like without you to lean on, even from afar. You have been my rock throughout this entire journey. From Utah to Uruguay, from Sun Valley to Sierra Camp, from the Bay to LA, from the Grand Canyon to Cambridge, from Greenwich to Greece, our adventures together have been the source of so many happy memories during my PhD. Yet it is in the smaller moments—the countless phone calls and texts answered—that friendships are truly made. Few people, if any, understand me and the experience I have had in my PhD better than you. I can always depend on you to pick me up when I am at my lowest, and you somehow always know exactly what I need to hear in any given moment. I am also so grateful for your family and all the warmth, love, compassion, beautiful places, and brain power the Marsden family has shown me. Thank you for being there for me every step of the way.

Julia Enthoven: Thank you for your friendship and support throughout this entire PhD. The joy and memories from times we have spent together and trips I have taken with you and your family have brought so much happiness into these years. Your thoughtful questions always push me to think deeply and be more intentional about the decisions I make. You inspire me with your ability to balance crushing it as a CEO with being an extraordinary friend to me and so many others. I will never forget the way that you showed up for me after my dad passed away, touching down in SF after returning from Australia only to head straight to Greenwich to be by my side during the hardest days of my life. I am so lucky to have you as a friend.

Katie Cacouris: I can always rely on your spontaneous phone calls, cheery hellos, and huge hugs to brighten my day. You always make me feel so loved, and your steadfast support has meant a great deal to me and made a huge difference throughout my life and this PhD experience. I cherish that, even when we pick up the phone and think we have nothing to talk

about, it turns out we have an infinite amount to discuss, and an hour or two end up flying chatting about books, current events, conspiracy theories, work, dating, family, travels, and more. Thank you for being such an amazing friend.

Dr. Greg Heon: I am very grateful that you managed to survive my dragging you up two mountains you probably had no business being on (first a hike up Mount Baldy after you pulled an all-nighter, and later sliding head-first down a double black chute off Lincoln Mountain at Mammoth). Your willingness to lend an ear, big heart, and ability to relate to the challenges of the PhD are all reasons why you were at times the first person I would call when I needed a friend. I hope I can continue to be the best Sophie I can, if for no other reason than to be a good role model for your little Sophie to look up to.

Annalisa Boslough: Thank you for your thoughtfulness, encouragement, and support over these years. You are one of my most loyal cheerleaders and have always celebrated my wins as much as (and often even more than) I do, which is more than any friend could ask for. You always know what to say to cheer me up and I can always count on you to be on my team no matter what. Our trip this year to San Luis Obispo will always be a particularly special memory, as it was exactly what I needed to lift my spirits and recharge my heart and mind before heading into this final push.

Nicole Himmel: I feel like my time in LA could be separated into before-Nicole and after-Nicole, with the latter being filled with so much more love, brightness, perfectly planned SoCal day trips, and delicious Italian food than the former. You are one of the sweetest and most caring people I know, and I am so grateful to have a friend that always knows, sees, and reminds me of the core of who I am, even when I might be feeling down. Thank you for being such a special part of this experience.

Alissa Bernstein: I was not sure whether to put you in the family or friends section, but I did not want to offend any family members that would have gotten fewer words than you. You have had such a positive impact on my life during my time in LA, and I have been so blessed

to get to have you nearby both while at Stanford and now at Caltech. Thank you for all the hugs, sleepovers, silly singing sessions, Shabbat dinners, farmers' market sample raids, and road trips. You are fiercely loving and empathetic, and I know I can always show up exactly as I am and be embraced by you and have a great time. You are someone I have always counted on to help me get through some of my hardest days.

Dr. Connor McMahan: I am so grateful to have met you during my first week at Caltech. You have been a rock for me throughout this experience. Many of my fondest memories from my time at Caltech are with you, including early drives to Long Beach to row, playing and listening to music together, and watching movies that you loved but I often found to be weird. Thank you for your gentle, patient kindness and for always lending an ear or a shoulder when I have needed them most. I have made so many other wonderful friends, each of whom I could write several sentences about how much their friendship has

Kelsey Dietz: It is an incredible blessing to have a friendship that spans schools, coasts, and continents not just survive but thrive for 25 years. You are one of my most thoughtful friends and know me so well, always sending the most perfect gifts and kind messages that brighten my day and make me smile. Thank you for always there to celebrate my happiest moments and support me in my hardest. Your loyalty, love, and kindness have meant the world to me.

Prof. Michelle Teplensky: You are the friend I always go to and trust the most for advice about anything related to graduate school, research, or academia. Thank you for always picking up the phone when I am having an academic existential crisis—I can always count on you to reassure me and guide me in the right direction. I am also so grateful to have someone like you to look up to as a friend crushing it on the professorial path, working so hard with such determination and passion toward your goals. You remain to this day my absolute favorite co-author.

To my incredible Taco Tuesday friends: **Dr. Alex Welch, Jamie Goldfield, Dr. Megan Phelan, Kendall Fagan, Amy Han, Alex Cureton, Taylor Szala, Alexander Dewing, Claire Mallon, Spencer Jackson, Ipek Demirdag, Jason West, Lauren Friedman, Éowyn Lucas, John Welch, John Stayner, Nathan Roberson, Cori Brendel, Ivo Andov, Alex Samuels, Jackie Dowling, and Sydney Corona.** It is rare for a group of friends to stick to a biweekly standing commitment for over six years, even through a global pandemic. You are such a fun, kind, and brilliant group of humans, and I could always count on our every-other-week Taco Tuesday dinners and various other gatherings and trips together to brighten my day. So many of you were also my core group of ski friends during my time in graduate school, and our many winter trips to Mammoth over the years were the perfect weekend getaways and one of my favorite parts of my years living in Los Angeles.

I would like to acknowledge two particularly special members of this group with whom I had the privilege of living during my time at Caltech. **Dr. Alex Welch**: My entire Caltech experience would not have been the same were it not for your reaching out to me months before the start of our first year to ask about being roommates. You were an amazing roommate and have been a great friend to me, including during the year of my life after losing my dad. I am so grateful for the warmth and kindness I have received from you and from your whole wonderful family. It is also through you that I got to meet my core friend group in LA, which has been such a blessing during my time here. **Dr. Megan Phelan**: You are one of the most loyal, dependable, thoughtful, strong, and resilient people I know. I am so grateful to have gotten to live with you and to have you as a close friend, and to share with you a love of water sports, reggaeton, and spicy food. I am constantly inspired by your faith, mental and physical toughness, and positive attitude. You, your mom, your dad, and Gabriel have been such a source of love, comfort, and support to me.

I am fortunate to have made many meaningful friendships during my time at Caltech that have been such a source of joy and comfort to me over the years. I could write multiple sentences about each of these people, the happy memories I have with them, and times when each of them lifted me up with love and support in ways that made a difference along my

PhD journey. **Dr. Lee Rosenthal, Dr. Ethan Pickering, Dr. Sophia Charan**, **Jacob Wasserman, Dr. Oren Mizrahi, Danielle Resheff, Will Rosencrans, Roey Lazarovitz, Michael Wolman, Helen Wexler, Dr. Zachary Sercel, Dr. Ruben Mirzoyan, Dr. Karen Mirzoyan, and Meital Carmi**. And to my Pasadena friends **Eric Hallett** and **Erin Goodwin**: thank you for bringing so much laughter, music, and thoughtful conversation into my life these last few years of my PhD.

I also have so many friends that, even from afar, have shown me they care and have each been there for me along the way in ways that have meant a great deal to me: **Sarah Sicular, Maya Chung, Pooja Pradhan, Arynne Wexler, Kaitlyn Baab, Lindsey Schmid, Dr. Nalini Tata, Dr. Noam Rosenthal, Gabriella Chan, Dr. Charlotte Poplawski, Dr. Evaline Tsai, Dr. Devon McMahon, Andrew Demas, Victoria Nguyen, Prof. Hannah Wayment-Steele, Dr. Jesse Freeman, Lucy Thomson,** and **Arthur Kuenzi:** through our friendships over the years, each of you have made my heart feel so full and have made me feel like I can fly and soar to heights even higher than I believed possible for myself.

I would also like to acknowledge **Dr. Emily McGrath**: You helped me get me through the toughest period of my life and overcome many challenging moments that tested me along this journey. Thank you for the compassion you have shown me, the perspective and wisdom you have shared with me, and your patience. Even though I am not perfect and sometimes need reminders of the things you have taught me, I know I can rely on you for help when I need it the most.

Thank you to my friends that are really more like family: **Dr. Diana Kaplan, Sabina Young, Lara Young, Ronit Felzer, Carlos Naibryf, Mica Naibryf, Tali Naibryf, Patti Weeks,** and **Louis Gramling**. When I think about the love you all show me, my heart feels like it could explode. Knowing how deeply each of you cares for me fills me with immense gratitude, and your belief in me fuels my fire to achieve even my most ambitious goals.

By far and away the greatest blessing of my life is my family. I could write an entire thesis about my love and gratitude for my family, and words fail when it comes to capturing the appreciation and love I have for the people in this final portion of these acknowledgements. But if my PhD taught me anything, it is to not fear failure. So here I go.

Laura, Richard, Jack, and Daniela Murawczyk: You have all shown me such an incredible level of love, caring, and support throughout my life, but especially during these years I have been in graduate school. You have helped me celebrate birthdays, successes, and milestones along this journey, even when I have been reluctant to do so myself. Thank you for all the happy memories together, from Shabbat dinners in Menlo Park to Thanksgivings in Greenwich to barbecues at SSC. Thank you for opening your home to me during my many visits up to the Bay. Thank you, Laura, for being on the other end of so many long phone calls and texts, providing a listening ear, an empathetic heart, and much-needed fashion advice. Thank you, Richard, for your wise advice, your belief in me over the years, and your amazing food. Thank you, Jack and Daniela, for keeping me company in the lab one summer and being such fun and wonderful research assistants, for being so brilliant and curious but also hilarious, and for setting such a shining example of the kind of people I hope my future children grow up to be.

Mariel and Andy Katz: You two have been my main source of family support in LA and have been so generous with me over these years. Thank you for letting me tag along for Jewish holiday celebrations and services, for the Sunday morning trips to my favorite farmer's market, for always thinking of me and checking in, for coming to support me at my jazz concerts, and for your constant encouragement over the years. I am so lucky to have had you two nearby during my PhD and will miss you so much when I leave after graduating. **Cami and Alec Katz:** I am so fortunate to have cousins with whom I am so close and who always show me so much love. I cherish all the times I have gotten to spend with you during this PhD and the conversations we have had over the years that make me feel so cared for. Thank you for being such amazing cousins. **Bobby and Jackie Katz:** Thank you for inviting me to be a part of Rosh Hashanah and Passover dinners whenever I have been in LA for the

holidays, for always welcoming me with warmth and kindness, for being both my literal and metaphorical ticket into Sinai Temple, my favorite place to go for High Holiday services, for expert medical advice when I am in a pinch, and for the best LA doctor recommendations.

Dr. Sammy Miller, Russ Valdez, and Vivian Valdez: Thank you for always rooting for me, giving amazing advice, and for all the fun times together from LA to Austin. Sammy, you have given me so much to look up to, and I am honored to be the third Dr. S. Miller in the family. I am so grateful for our chats, whether on the couch in your home or on the phone, which have provided so much wisdom, perspective, patience, and support.

Justin Miller: You are my fiercest protector and one of my most loyal and steadfast supporters, and I am so grateful I could be closer to you during these years in LA. I will cherish my memories with you from my time in graduate school, including dinners together, hanging out together in Brentwood, playing with Bodhi and Sebastian, and spending time with Sascha. Thank you for your unconditional love every day of my life.

Jason, Katie, Emmi, Octavia, Zephyr, Rhett, and Rhodes Aryeh: Thank you all for being such amazing cheerleaders for me throughout this process. I always look forward to spending time with your incredible family, both when you were in Malibu as well as now in Greenwich any time I visit home. You all make my heart feel so full and make me believe that I can tackle any challenge I encounter, which has made a huge difference along this journey.

Auntie Vera: Thank you for the love and caring you have shown me throughout my entire life. I am deeply grateful for your thoughtfulness and generosity, and I am so blessed to always feel your support, even from afar. I cherish the moments we have together, from holidays and birthdays to shows and exhibits, which uplift me and bring me so much joy.

Gloria y **Luis:** Gracias por todo lo que han hecho por mi durante mi vida y especialmente durante estos años de mi PhD para apoyarme. Sus llamadas y mensajes siempre me hacen sonreír. Gracias por siempre estar ahí esperándome con comida rica

cuando llego del aeropuerto y por ayudarme con cualquier cosa que necesito cuando estoy en casa. Gracias por cuidar a mi mamá y a nuestra casa en forma tan especial. A Gloria—te estaré agradecida por venir a ayudarme después de mi cirugía y hasta acompañarme al laboratorio cuando todavía no podia caminar sin muletas. Me quieren como una hija y su cariño me llena el corazón con agradecimiento.

Abu: Tu amor y confianza en mí han sido algunas de mis mayores motivaciones durante mi PhD. Cada vez que hablo contigo, me haces acordar que "¡arriba que podemos!" Aunque nunca podré comprender la profundidad de tu amor hasta que tenga mis propios nietos, lo siento en mi corazón y me sostiene. Estoy segura que todos los besos que me diste en la kepele cuando era chica resultaron en la inteligencia que me permitió llegar a donde estoy hoy. Poder celebrar este logro contigo es el regalo más grande que podría pedir. Gracias por inyectarme amor y vida y por creer en mi siempre.

Audrey: You are my biggest cheerleader and number one hype-woman, and your unwavering encouragement and support have meant more than the world to me. Thank you for always believing in me in every aspect of my life; your bullishness on Sophie even during my most difficult days, along with your thoughtfully curated Spotify playlists and the silly gifts you sent me every day the week after my knee surgery, picked me up countless times and gave me the push I needed to keep going. You know me better than anyone, and even though you may not always answer the phone or respond to my texts, you are without fail there when I need you. We have both been through so much these last several years, together and in parallel, and having a built-in best friend to move through life alongside (and dance up a storm around the globe, from Nocturnal Wonderland to Scorpios) made all the difference. You make my life brighter and the world a more interesting and colorful place to inhabit. I could not ask for a more amazing sister.

Mommy: There is not a single person to whom the phrase "I would not be here if it were not for you" applies more deeply and truthfully than it does to you. You are the literal reason I am here. You gave me life. You gave me love and cared for me since the moment I was born.

You made accessible to me every opportunity to learn and expand my mind and cultivate my curiosity. You instilled in me and nurtured my love for math and science. You taught me the importance of hard work, of asking questions, and of seeking a deep and rigorous understanding of the world around me. You are the most brilliant chemical engineer I know (and yes, I say that knowing all of the incredible and accomplished scientists I mentioned toward the beginning of this Acknowledgements section). You paved the path for me to come to Caltech, another place we now share that has shaped both of us. This experience was not easy for me and, as the person who was at the other end of the phone during almost every single one of my lowest moments and who feels my hardships as if they were your own, I know it was not easy for you, either. I do not know what I would have done without your unconditional and tireless support of me. Having you as my mother and Daddy as my father is the greatest blessing of my life, and there is nothing for which I am more grateful. Although thank you is not nearly enough and no word or words could ever suffice: thank you.

Finally, it feels wrong that the two people whose pride individually would have surpassed the sum of the pride of every single other person mentioned in these acknowledgements are not here in the physical sense to celebrate this achievement with me. I choose to believe that this is because, wherever they are—in my heart, all around me, wherever I go—they are somehow able to celebrate it in an even bigger way than those of us here on Earth can possibly comprehend. **Daddy**: your infinite love for me and your limitless belief in what I am capable of achieving propel me forward every day. Even though I miss you every day, I also know you are always with me: in my creativity, my curiosity, my sensitivity, my determination verging on stubbornness in achieving my goals, and my desperation to find a decent bagel in Los Angeles. **Achis**: Sé que hubieras estado sentado en la primer fila de la audiencia de mi defensa y de mi graduación con tu traje blanco con una gran sonrisa, tan orgulloso de tener una nieta con un Doctorado de Caltech en Ingeniería Química. Es un honor poder lograr sueños que comenzaron contigo. Te dedico esta tesis a ti.

ABSTRACT

Temporally and spatially controlled protein synthesis plays a critical role in orchestrating the molecular events underlying behaviors, stress adaptations, and therapeutic responses to drugs. However, traditional proteomic techniques often fail to capture the dynamic changes in protein expression essential for understanding transient biological phenomena. To overcome this limitation, the work presented in this thesis leverages bioorthogonal noncanonical amino acid tagging (BONCAT) coupled with mass spectrometry to perform time-resolved proteomic analyses in zebrafish larvae and cultured neurons.

Chapter II details the development and validation of BONCAT proteomics in zebrafish, demonstrating that newly synthesized proteins from zebrafish larvae could be reliably labeled, enriched, and identified even over short labeling periods. Proof-of-concept experiments using heat shock revealed that BONCAT proteomics was able to detect changes in expression of proteins known to be induced by heat shock with greater sensitivity than conventional approaches using global proteomics. These results establish BONCAT as a powerful tool for investigating dynamic changes in protein synthesis in zebrafish. In Chapter III, we applied BONCAT to neuronal cultures to profile the proteomic changes induced by sub-anesthetic, antidepressant-relevant doses of ketamine. These studies uncovered rapid alterations in protein synthesis, identifying significantly differentially regulated proteins and pathways involved in synaptic plasticity, cytoskeletal remodeling, cellular signaling, metabolism, and RNA processing. This work provides novel molecular insights into ketamine's rapid-acting antidepressant effects and further illustrates the utility of BONCAT for capturing early, transient proteomic responses to drug treatment. Finally, in Chapter IV, we explore changes in protein expression in zebrafish larvae underlying circadian rhythms and in response to low-dose ketamine treatment. We observed interesting protein synthesis patterns in both biological contexts, but our findings lacked the statistical significance and reproducibility across experiments required to draw strong biological conclusions from our data. Although methodological refinements are required, our work underscores BONCAT's potential to elucidate transient proteomic shifts underlying behavioral phenomena and pharmacological interventions in zebrafish.

TABLE OF CONTENTS

LIST OF FIGURES

LIST OF TABLES

NOMENCLATURE

ACN. Acetonitrile

AGC. Automatic gain control

AHA. Azidohomoalanine

ANL. Azidonorleucine

ANOVA. Analysis of variance.

BONCAT. Bioorthogonal noncanonical amino acid tagging

CSF. Cerebrospinal fluid

CuAAC. Cu(I)-catalyzed [3 + 2] azide-alkyne cycloaddition

DBCO. Dibenzocyclooctyne

dpf. Days post fertilization

ECDF. Empirical cumulative distribution function

EDTA. Ethylenediaminetetraacetic acid

FA. Formic acid

FBS. Fetal bovine serum

FC. Fold change

FDR. False discovery rate

FUNCAT. Fluorescent noncanonical amino acid tagging

GO. Gene ontology

GSEA. Gene set enrichment analysis

HCD. Higher-energy collisional dissociation

iTRAQ. Isobaric tags for relative and absolute quantification

LC-MS/MS. Liquid chromatography tandem mass spectrometry

LFQ. Label-free quantitation

MetRS. Methionyl-tRNA synthetase

mRNA. Messenger RNA

MS. Mass spectrometry

m/z. Mass to charge ratio

PBS. Phosphate buffered saline.

PCA. Principal component analysis

PFA. Paraformaldehyde

RNA. Ribonucleic acid

SDS. Sodium dodecyl sulfate

SILAC. Stable isotope labeling by amino acids in cell culture

SPAAC. Strain-promoted [3 + 2] azide-alkyne cycloaddition

STRING. Search tool for the retrieval of interacting genes/proteins

TBTA. Tris(benzyltriazolylmethyl)amine

TCEP. Tris(2-carboxyethyl)phosphine hydrochloride

Tg. Transgenic

TMT. Tandem mass tags

UHPLC. Ultra-high-performance liquid chromatography

WT. Wild type

Chapter I

INTRODUCTION

Proteins synthesized at precise times and locations drive critical cellular responses underlying behavior[1–4], stress adaptation[5–7], and pharmacological interventions[8–12]. Traditional proteomic methods provide snapshots of protein abundances but often fail to detect dynamic changes that are critical for understanding transient biological phenomena. Bioorthogonal noncanonical amino acid tagging (BONCAT) offers a targeted strategy to address this limitation by allowing selective labeling, enrichment, and identification of newly synthesized proteins within defined time windows[13,14]. Leveraging click chemistry to affinity purify newly synthesized proteins labeled with chemically modified amino acids[15–17], BONCAT enables time-resolved proteomic analyses that can elucidate rapid shifts in protein expression otherwise masked by highly abundant pre-existing proteins.

For my doctoral research, I developed and applied BONCAT proteomics techniques, both *in vivo* in zebrafish larvae and *in vitro* in primary embryonic rat cortical neurons, to investigate temporally regulated protein synthesis in various biological and behavioral contexts. Specifically, I explored BONCAT's utility in dissecting molecular responses to environmental stressors, fast-acting pharmacological treatments, and circadian rhythms. These studies demonstrate the effectiveness and versatility of BONCAT for uncovering biologically relevant changes in protein expression, providing a basis for future mechanistic work aimed at dissecting the roles that specific proteins might play in regulating processes.

In Chapter II, we describe the development and validation of BONCAT proteomics in larval zebrafish, a model organism that has seen widespread use in developmental biology and neuroscience due to its genetic tractability, optical transparency, and quantifiable, evolutionarily conserved behaviors. Our experiments confirmed the successful enrichment and mass spectrometry-based identification of newly synthesized proteins from zebrafish larvae after labeling periods as short as 12 h. As a proof-of-concept, we investigated changes

in protein synthesis in fish subjected to heat shock, detecting differential expression of proteins known to be induced by heat shock with enhanced sensitivity compared to conventional global proteomics. These findings demonstrated BONCAT's ability to reveal transient changes in protein synthesis in zebrafish larvae, paving the way for future time-resolved proteomic analyses addressing other biological questions of interest to the zebrafish research community.

Chapter III focuses on understanding the rapid antidepressant effects of ketamine using BONCAT in primary neuron cultures. Unlike traditional antidepressants characterized by delayed therapeutic effects, ketamine alleviates depressive symptoms within hours to days. Despite extensive research, the molecular mechanisms responsible for ketamine's rapid-acting antidepressant effects remain unclear. Our analysis uncovered rapid and significant proteomic shifts during the first 24 hours of treatment with sub-dissociative, antidepressant-relevant doses of ketamine, observing an overall increase in protein synthesis in ketamine-treated neurons compared to controls. We identified various significantly up- or down-regulated proteins and pathways involved in synaptic plasticity, cytoskeletal dynamics, cellular signaling pathways, metabolism, and RNA processing. Thus, our work provides novel insights into the changes in protein expression underlying ketamine's rapid-acting antidepressant effects and further illustrates the power of BONCAT for capturing early, transient proteomic responses to drug treatment.

In Chapter IV, we used BONCAT proteomics to explore circadian rhythms and low-dose ketamine treatment in zebrafish larvae. Our results showed evidence suggesting increased protein synthesis during the night compared to during the day; however, this pattern was inconsistent across developmental stages, indicating possible context dependency in circadian regulation of protein expression. Additionally, we investigated proteomic responses to treatment with sub-dissociative, antidepressant-level doses in zebrafish larvae, aiming to extend our *in vitro* findings to an *in vivo* context. While we observed several potentially interesting changes in protein synthesis in our proteomic analysis of BONCAT-enriched samples, our findings lacked the statistical significance and reproducibility across

experiments required to draw strong biological conclusions from our data. Nevertheless, these studies emphasize BONCAT's potential for investigating transient changes in protein expression underlying behavioral phenomena in zebrafish while also highlighting methodological challenges that require further optimization.

1.1 References

(1) Davis, H. P.; Squire, L. R. Protein Synthesis and Memory: A Review. *Psychol. Bull.* **1984**, *96* (3), 518–559.

(2) Martin, K. C.; Barad, M.; Kandel, E. R. Local Protein Synthesis and Its Role in Synapse-Specific Plasticity. *Curr. Opin. Neurobiol.* **2000**, *10* (5), 587–592. https://doi.org/10.1016/S0959-4388(00)00128-8.

(3) Agranoff, B. W.; Klinger, P. D. Puromycin Effect on Memory Fixation in the Goldfish. *Science* **1964**, *146* (3646), 952–953. https://doi.org/10.1126/science.146.3646.952.

(4) Laguesse, S.; Ron, D. Protein Translation and Psychiatric Disorders. *Neurosci. Rev. J. Bringing Neurobiol. Neurol. Psychiatry* **2020**, *26* (1), 21–42. https://doi.org/10.1177/1073858419853236.

(5) Feder, M. E.; Hofmann, G. E. HEAT-SHOCK PROTEINS, MOLECULAR CHAPERONES, AND THE STRESS RESPONSE: Evolutionary and Ecological Physiology. *Annu. Rev. Physiol.* **1999**, *61* (Volume 61, 1999), 243–282. https://doi.org/10.1146/annurev.physiol.61.1.243.

(6) Basile, F.; Capaccia, C.; Zampini, D.; Biagetti, T.; Diverio, S.; Guelfi, G. Omics Insights into Animal Resilience and Stress Factors. *Animals* **2021**, *11* (1), 47. https://doi.org/10.3390/ani11010047.

(7) Costa-Mattioli, M.; Walter, P. The Integrated Stress Response: From Mechanism to Disease. *Science* **2020**, *368* (6489), eaat5314. https://doi.org/10.1126/science.aat5314.

(8) Hodas, J. J. L.; Nehring, A.; Höche, N.; Sweredoski, M. J.; Pielot, R.; Hess, S.; Tirrell, D. A.; Dieterich, D. C.; Schuman, E. M. Dopaminergic Modulation of the Hippocampal Neuropil Proteome Identified by Bioorthogonal Noncanonical Amino Acid Tagging (BONCAT). *PROTEOMICS* **2012**, *12* (15–16), 2464–2476. https://doi.org/10.1002/pmic.201200112.

(9) Zhang, G.; Bowling, H.; Hom, N.; Kirshenbaum, K.; Klann, E.; Chao, M. V.; Neubert, T. A. In-Depth Quantitative Proteomic Analysis of de Novo Protein Synthesis Induced by Brain-Derived Neurotrophic Factor. *J. Proteome Res.* **2014**, *13* (12), 5707–5714. https://doi.org/10.1021/pr5006982.

(10) Bowling, H.; Bhattacharya, A.; Zhang, G.; Lebowitz, J. Z.; Alam, D.; Smith, P. T.; Kirshenbaum, K.; Neubert, T. A.; Vogel, C.; Chao, M. V.; Klann, E. BONLAC: A Combinatorial Proteomic Technique to Measure Stimulus-Induced Translational Profiles in Brain Slices. *Neuropharmacology* **2016**, *100*, 76–89. https://doi.org/10.1016/j.neuropharm.2015.07.017.

(11) Schanzenbächer, C. T.; Sambandan, S.; Langer, J. D.; Schuman, E. M. Nascent Proteome Remodeling Following Homeostatic Scaling at Hippocampal Synapses. *Neuron* **2016**, *92* (2), 358–371. https://doi.org/10.1016/j.neuron.2016.09.058.

(12) Schanzenbächer, C. T.; Langer, J. D.; Schuman, E. M. Time- and Polarity-Dependent Proteomic Changes Associated with Homeostatic Scaling at Central Synapses. *eLife* **2018**, *7*, e33322. https://doi.org/10.7554/eLife.33322.

(13) Dieterich, D. C.; Link, A. J.; Graumann, J.; Tirrell, D. A.; Schuman, E. M. Selective Identification of Newly Synthesized Proteins in Mammalian Cells Using Bioorthogonal Noncanonical Amino Acid Tagging (BONCAT). *Proc. Natl. Acad. Sci.* **2006**, *103* (25), 9482–9487.

(14) Dieterich, D. C.; Lee, J. J.; Link, A. J.; Graumann, J.; Tirrell, D. A.; Schuman, E. M. Labeling, Detection and Identification of Newly Synthesized Proteomes with Bioorthogonal Non-Canonical Amino-Acid Tagging. *Nat. Protoc.* **2007**, *2* (3), 532–540. https://doi.org/10.1038/nprot.2007.52.

(15) Rostovtsev, V. V.; Green, L. G.; Fokin, V. V.; Sharpless, K. B. A Stepwise Huisgen Cycloaddition Process: Copper(I)-Catalyzed Regioselective "Ligation" of Azides and Terminal Alkynes. *Angew. Chem. Int. Ed.* **2002**, *41* (14), 2596–2599. https://doi.org/10.1002/1521-3773(20020715)41:14<2596::AID-ANIE2596>3.0.CO;2-4.

(16) Tornøe, C. W.; Christensen, C.; Meldal, M. Peptidotriazoles on Solid Phase: [1,2,3]-Triazoles by Regiospecific Copper(I)-Catalyzed 1,3-Dipolar Cycloadditions of Terminal Alkynes to Azides. *J. Org. Chem.* **2002**, *67* (9), 3057–3064. https://doi.org/10.1021/jo011148j.

(17) Agard, N. J.; Prescher, J. A.; Bertozzi, C. R. A Strain-Promoted [3 + 2] Azide−Alkyne Cycloaddition for Covalent Modification of Biomolecules in Living Systems. *J. Am. Chem. Soc.* **2004**, *126* (46), 15046–15047. https://doi.org/10.1021/ja044996f.

Chapter II

TIME-RESOLVED PROTEOMIC ANALYSIS IN ZEBRAFISH USING BIOORTHOGONAL NONCANONICAL AMINO ACID TAGGING (BONCAT)

2.1 Abstract

Protein synthesis underpins many biological processes, yet tracking time-dependent proteomic changes remains challenging. Bioorthogonal noncanonical amino acid tagging (BONCAT) offers a targeted approach for labeling and identifying newly synthesized proteins within defined time windows of interest. Here, we present the first such application of BONCAT in larval zebrafish, a model organism that has seen widespread use because of its genetic tractability and utility in developmental biology and neuroscience. We successfully enriched, using click chemistry, and identified, via mass spectrometry, azidohomoalanine (AHA)-labeled proteins after labeling durations as short as 12 hours. Proteomic analysis of BONCAT-enriched proteins demonstrated significant signal above background compared to unlabeled controls after both 48 h and 12 h of labeling. As a proof of concept, we investigated proteomic changes in response to heat shock in zebrafish larvae. BONCAT analysis revealed the upregulation of heat shock-induced proteins with greater sensitivity than global proteomics. Gene set enrichment analysis confirmed that known heat shock response proteins were significantly enriched in the BONCAT dataset but not in the global proteomics dataset, highlighting the ability of BONCAT to detect transient molecular responses otherwise masked in conventional global proteomics. Beyond the expected changes in synthesis of heat shock proteins, BONCAT identified differentially expressed proteins implicated in stress responses, lipid metabolism, and neural regulation, offering insights into the zebrafish heat shock response. These findings establish BONCAT as a powerful tool for time-resolved proteomic analysis in zebrafish. Its ability to enhance signal specificity and resolve protein dynamics opens new avenues for studying molecular underpinnings of behavior, stress, and development in this versatile model organism.

2.2 Introduction

Changes in protein expression underlie many behavioral phenomena, driving processes such as learning and stress responses. During learning, the synthesis of particular proteins at specific times leads to synaptic plasticity involved in long-term memory formation[1–3]. Similarly, changes in protein synthesis that occur in response to environmental or chemical stressors play important roles in adaptive processes required for survival[4–6]. Understanding these molecular-level changes can aid in the discovery of novel targets for treating neurological or psychiatric disorders, as well as the identification of pathways that support resilience to stress.

While RNA sequencing methods have been used in many organisms and have generated critical insights into the control of gene expression under a wide variety of conditions, the relationship between mRNA and protein abundances is not simple[7–10]. Factors including post-transcriptional regulation of mRNAs, alternative splicing, polyribosomes, and differences in stability between mRNA and the protein it encodes all contribute to mismatches in the relative amounts of a protein and its corresponding mRNA transcript. Furthermore, analysis at the protein level enables the detection of post-translational modifications, which also have a marked effect on protein function[11–14]. Therefore, innovations in proteomic techniques are necessary for obtaining a more accurate understanding of the functional states of cells or organisms, which depend on the proteins being expressed rather than the mRNAs that are present.

Several computational and methodological advances have enabled the quantification of protein abundances from mass spectrometry-based proteomic analysis. Label-free quantification (LFQ) allows for relative measurements of protein abundances based on measured peptide ion intensities[15,16]. The accuracy of peptide and protein quantitation can be improved using methods such as stable isotope labeling by amino acids in cell culture (SILAC)[17], which introduces heavy isotopes into proteins during synthesis, or the addition of isobaric tags, such as tandem mass tags (TMT)[18] or isobaric tags for relative and absolute quantification (iTRAQ)[19]. Despite these advances, it remains challenging to identify proteins

synthesized during a particular time window of interest, such as in response to environmental perturbation. Even when newly synthesized proteins are tagged using methods like SILAC, their signals are often obscured by highly abundant pre-existing proteins.

Bioorthogonal noncanonical amino acid tagging (BONCAT)[20,21] mitigates the shortcomings of conventional proteomic workflows by enabling the affinity purification of newly synthesized proteins via metabolic labeling with a chemically modified amino acid analog. In the most common BONCAT experiment, the azide-bearing methionine surrogate azidohomoalanine (AHA) is incorporated into newly synthesized proteins in competition with methionine after activation and charging by the endogenous methionyl-tRNA synthetase (MetRS) of the host. AHA-labeled proteins can be covalently attached to affinity tags or to alkyne-functionalized beads for enrichment and subsequent identification via mass spectrometry[20,21], or labeled with fluorescent alkynes for *in situ* visualization (fluorescent noncanonical amino acid tagging, or FUNCAT)[22]. Enrichment or labeling of AHA-tagged proteins is accomplished either by a Cu(I)-catalyzed [3 + 2] azide-alkyne cycloaddition (CuAAC)[23,24], or by a strain-promoted [3 + 2] azide-alkyne cycloaddition (SPAAC)[25]. Because azides and alkynes are rare in living organisms[26–28], the azide-alkyne "click" reaction is highly selective toward AHA-labeled proteins. Although depletion of methionine to enable high levels of replacement by AHA can perturb protein abundances, competitive labeling at modest levels can be accomplished without significant perturbation[29].

BONCAT has been used to perform time-resolved proteomic analyses in a diverse array of biological systems, including bacteria[30,31], immortalized cell lines[20,32–34], primary cultures[20,35–39], tissue sections[40,41], stem cell-derived cultures[42–44], plants[45], *Caenorhabditis elegans*[46–48], *Xenopus laevis*[49,50], and rodents[33,51–54], but not yet in zebrafish. Zebrafish larvae are a powerful and widely used model organism: their rapid developmental timeline has made them a workhorse of developmental biology, while their optical transparency, relatively simple brain anatomy, and expression of evolutionarily conserved genes have made them increasingly popular in neuroscience. As early as 5 days post fertilization (dpf), larval zebrafish exhibit well-characterized, robust, and conserved behaviors, which have

been studied in the context of sleep[55,56], fear[57–59], social interactions[60–63], learning[64–66], and more[67–69]. Moreover, their small size makes them amenable to high-throughput behavioral tracking[70–72], while their optical transparency facilitates whole-brain imaging and non-invasive monitoring of neuronal activity[73,74]. Finally, zebrafish larvae are able to absorb compounds from the medium they swim in, simplifying the delivery of small molecule drugs or metabolic labels, including noncanonical amino acids.

Over a decade ago, Hinz and coworkers reported that AHA could be used to label newly synthesized proteins in zebrafish larvae[75]. More recently, Shahar et al. accomplished cell-type specific labeling of newly synthesized proteins by incorporating the bulkier noncanonical amino acid azidonorleucine (ANL) into the nascent proteome of neurons by expressing a mutant MetRS under the control of a neuron-specific promoter[76]. Both papers showed that azide-labeled proteins could be visualized using FUNCAT and, using western blots, the authors demonstrated that AHA- and ANL-labeled proteins could be affinity purified. However, we are unaware of reports of identification of BONCAT-labeled proteins in zebrafish via LC-MS/MS-based proteomic methods.

Here, we show for the first time that BONCAT can be utilized to perform time-resolved proteomic analysis in zebrafish. We demonstrate that enriched AHA-labeled proteins can be detected via LC-MS/MS at levels above background with labeling times as short as 12 hours. As a proof of concept, we demonstrate that BONCAT captures changes in protein expression in response to heat-induced stress, revealing changes in the expression of heat shock proteins that are not apparent in global proteomic analysis. Thus, this work provides a foundation for future time-resolved studies of protein expression in zebrafish to uncover the molecular bases of behavioral phenomena.

2.3 Results

We set out to evaluate the utility of the BONCAT method for time-resolved proteomic analysis in larval zebrafish. Zebrafish larvae (5-6 dpf) were treated with the methionine analog AHA (Fig. 2.1A) in E3 embryo medium during the time window of interest, resulting in labeling of newly synthesized proteins with azide side chains. AHA-labeled proteins could

be visualized *in situ* or enriched for subsequent identification via LC-MS/MS (Fig. 2.1B). Previously, Hinz et al. demonstrated that AHA-tagged proteins could be fluorescently labeled *in situ* in larval zebrafish (Fig. 2.2A, Fig. S2.1), and that transient labeling with AHA revealed evidence of increased protein synthesis following treatment with the GABA receptor antagonist pentylenetetrazole (PTZ)[75]. We aimed to expand the capabilities of BONCAT in zebrafish larvae to include the identification and quantitative analysis of enriched AHA-labeled proteins.

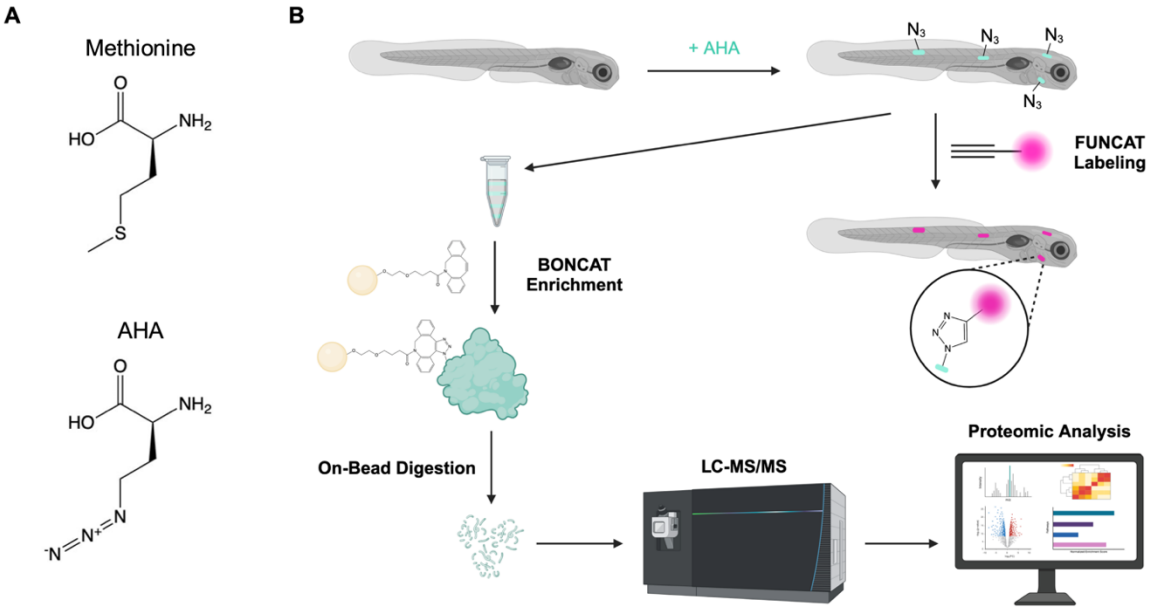

Figure 2.1. Newly synthesized proteins labeled with noncanonical amino acid AHA can be identified (BONCAT) and visualized (FUNCAT) using click chemistry. (A) Chemical structures of methionine and azidohomoalanine (AHA). (B) Schematic showing AHA incorporation into newly synthesized proteins in zebrafish larvae (5-7 dpf). AHA-labeled proteins can be enriched via covalent attachment to DBCO-agarose beads using copper-free strain-promoted [3 + 2] azide–alkyne cycloaddition. Peptides released via on-bead enzymatic digestion can be identified via LC-MS/MS for downstream proteomic analysis. Alternatively, AHA-labeled proteins can be visualized *in situ* via reaction with an alkyne-fluorophore using Cu(I)-catalyzed [3 + 2] azide–alkyne cycloaddition. Created in BioRender. Miller, S. (2025) https://BioRender.com/0kr2egz.

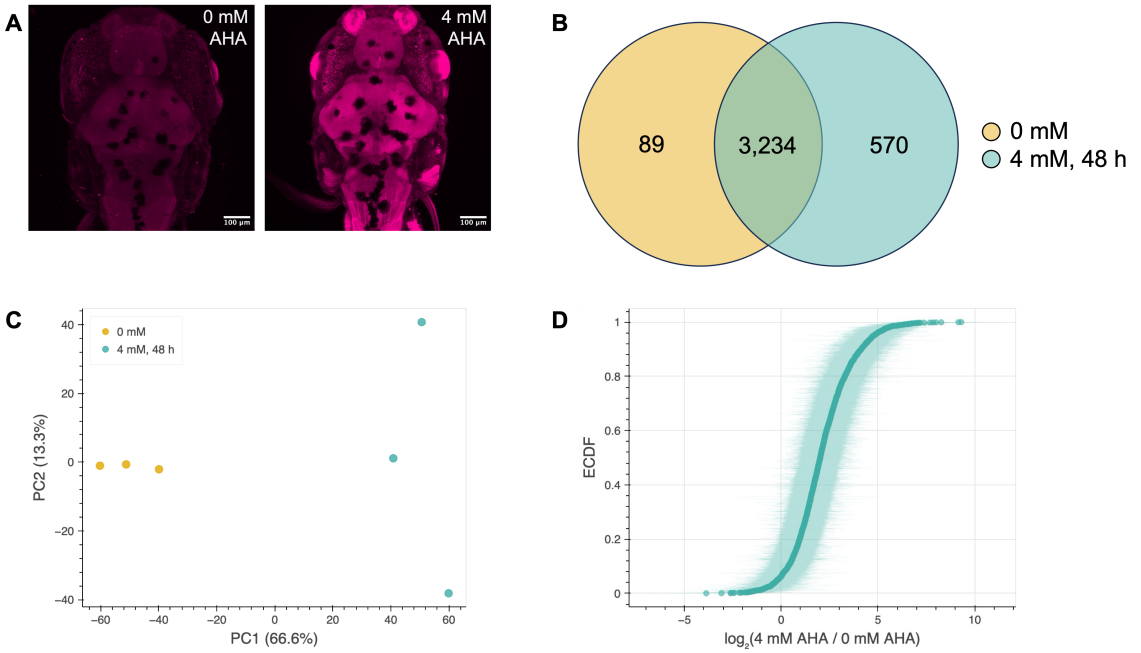

Figure 2.2. BONCAT enables visualization, enrichment, and proteomic analysis of newly synthesized proteins from larval zebrafish treated with AHA for 48 h. (A) *In situ* visualization of AHA-labeled proteins was consistent with FUNCAT results reported by Hinz et al.[75] Zebrafish larvae (7 dpf) were fixed after 48 h metabolic labeling with 4 mM AHA, permeabilized, and treated with 5 µM Cy3 alkyne. Representative images of dorsal views of the head and start of the tail are shown for an unlabeled control zebrafish larva (left, n=3) and a zebrafish larva labeled with 4 mM AHA for 48 h (right, n=3). Scale bar is 100 µm. (B) Venn diagram indicating the numbers of proteins identified via proteomic analysis in control samples of untreated fish and/or in samples of fish treated with 4 mM AHA for 48 h. (C) PCA plot showing separation of control and labeled samples after dimensionality reduction. PCA was performed using raw abundance data. (D) Empirical cumulative distribution function (ECDF) plot showing, for each protein identified in both labeled and unlabeled samples, the log of the ratio of the average raw abundance of that protein in labeled samples to its average raw abundance in unlabeled samples. Shading represents 95% confidence intervals. n = 3 biological replicates for each condition.

Using strain-promoted azide-alkyne click chemistry (SPAAC), we conjugated labeled proteins in zebrafish lysates (150 zebrafish larvae per sample) onto dibenzocyclooctyne (DBCO)-agarose beads. After extensive bead washing, on-bead digestion of the enriched proteins with trypsin and Lys-C, and peptide purification, samples were subjected to LC-MS/MS analysis. Our initial experiments compared fish treated with 4 mM AHA for 48 h to untreated control fish collected at the same time, since Hinz et al. were able to detect robust labeling under these conditions[75]. We identified 4,245 zebrafish proteins, 3,893 of which had at least one quantified raw abundance value (Fig. 2.2B). Principal component analysis (PCA)

revealed distinct separation of labeled samples from unlabeled control samples, particularly along the PC1 axis, which accounts for 66.6% of the variance in the dataset (Fig. 2.2C). The quality of sample clustering in PCA can be quantified using a Silhouette score[77], which is determined by measuring for each sample i the mean distance to other points in the same cluster (a_i) and the mean distance to all points in the nearest cluster (b_i), and then calculating $\frac{1}{n}\sum_{i=1}^{n}\frac{b_i-a_i}{\max(a_i,b_i)}$, where n is the number of samples in the dataset. The final value ranges from -1 to 1, where a negative score indicates that points are assigned to incorrect clusters, a score of zero suggests that clusters are overlapping or points are equally close to points in other clusters as they are to points in their own, and a positive value means clusters are clearly distinguished and well separated from one another. The mean Silhouette score calculated for samples in this PCA was 0.68, providing quantitative confirmation of the clear separation observed between labeled and unlabeled samples.

Most quantified proteins (3,234/3,893) were identified in both control and labeled samples (Fig. 2.2B), indicating the presence of background signal from unlabeled proteins that make it through the enrichment process, likely due to non-specific adsorption onto the agarose beads. However, almost all (94%) of the proteins identified across both AHA-treated and control samples had greater average abundance values in the labeled samples (Fig. 2.2D). There were also more total proteins identified in the AHA-treated samples, with 570 proteins found uniquely in labeled samples compared to 89 uniquely found in control samples (Fig. 2.2B). More proteins were identified across all three replicates in the labeled condition (3,273 proteins) compared to unlabeled controls (2,431 proteins), whereas fewer proteins were identified in only one replicate (199, compared to 413 in unlabeled samples) or only two replicates (372, compared to 479 in unlabeled samples). These results indicate successful enrichment of AHA-labeled proteins.

AHA-labeled proteins from zebrafish larvae exposed to 12 h labeling can be enriched and identified

We then tested whether we could identify AHA-labeled proteins via LC-MS/MS after shorter labeling times, since the value of the information captured by the BONCAT method

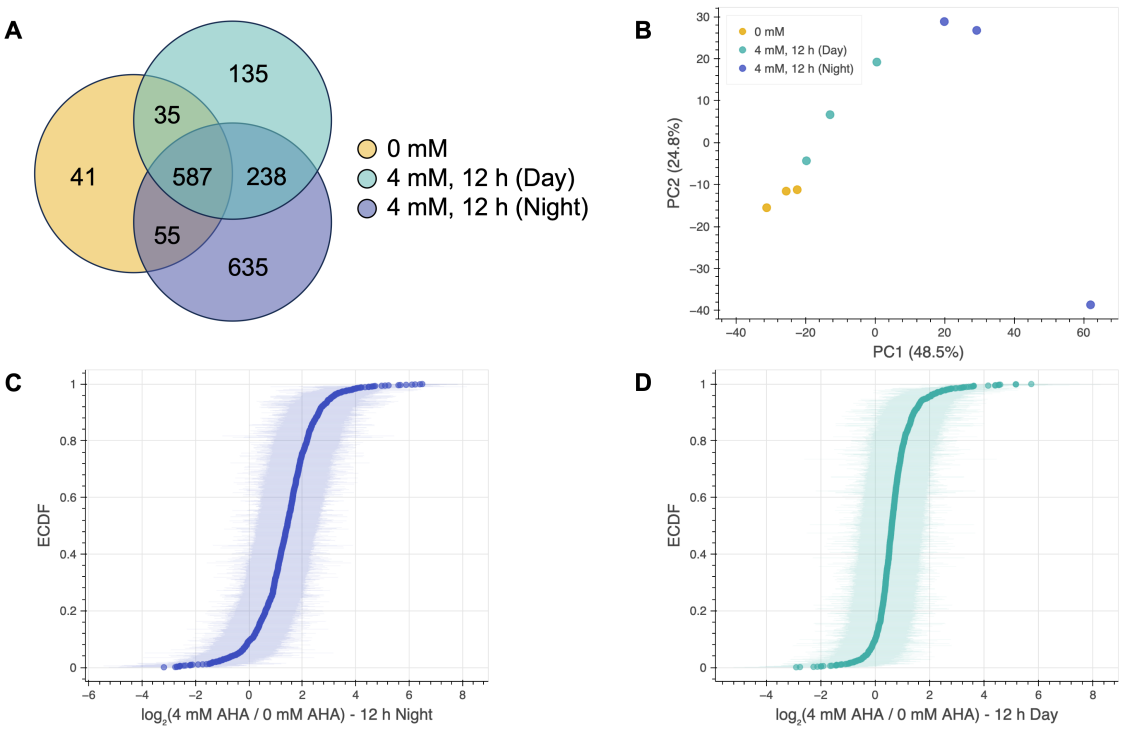

Figure 2.3. Newly synthesized proteins labeled with AHA for 12 h can be enriched via BONCAT for proteomic analysis. (A) Venn diagram indicating the number proteins identified via proteomic analysis in control samples of untreated fish, samples of fish treated with 4 mM AHA for 12 h during the night (9 pm – 9 am), and samples of fish treated with 4 mM AHA for 12 h during the day (9 am – 9 pm). (B) PCA plot showing clustering and linear separability of unlabeled control, daytime AHA-labeled, and nighttime AHA-labeled samples after dimensionality reduction. PCA was performed using raw abundance data. (C) ECDF depicting the log ratios of the average raw abundances of proteins identified in samples labeled with AHA for 12 h during the night to their average raw abundance in control samples. (D) ECDF depicting the log ratios of the average raw abundances of proteins identified in samples labeled with AHA for 12 h during the day to their average raw abundance in control samples. Shading on ECDF curves represents 95% confidence intervals. n = 3 biological replicates for each condition.

increases with improved temporal resolution. We performed BONCAT analysis on samples labeled for 12 h (during the day or during night) and compared them to unlabeled controls. In total, 1,726 proteins were identified across all samples. The samples labeled during the night yielded the largest number of protein identifications, while, as expected, the unlabeled samples yielded the fewest, with only 41 proteins unique to the unlabeled condition (Fig. 2.3A). PCA again revealed clear separation of samples from the three different conditions, particularly along the PC1 axis, which accounts for 48.5% of the variance in the dataset (Fig. 2.3B). The greatest separation was observed between the

unlabeled samples and samples labeled for 12 h at night (Silhouette score = 0.60), although separation between daytime- and nighttime-labeled samples (Silhouette score = 0.32) is indicative of differences in protein expression between day and night. Of the proteins identified in samples labeled with AHA for 12 h during the night as well as in unlabeled controls, 94% had a higher average raw abundance in the labeled samples (Fig. 2.3C). Similarly, 92% of proteins identified in samples labeled for 12 h during the day and in unlabeled samples had higher average raw abundances in the daytime-labeled samples (Fig. 2.3D).

Effect of AHA on larval zebrafish locomotor activity and sleep behavior

Having verified that we can identify BONCAT-enriched proteins via LC-MS/MS at levels above background after 12 hours of labeling in zebrafish larvae, we sought to test the ability of BONCAT to reveal changes in protein synthesis associated with transient biological responses. Intrigued by the possibility that differences in protein expression during day versus night could be captured via BONCAT analysis, we focused initially on trying to distinguish "sleep" vs "wake" proteomes. As a first step, we examined the effect of AHA treatment on sleep behavior, using a video tracking system to assess the locomotor activity and sleep of the fish over a 48-hour period during exposure to 4 mM AHA. We did not expect to see an effect on zebrafish behavior, since Hinz et al. previously showed that treatment with 4 mM AHA for up to 72 hours did not affect spontaneous swimming behavior, visual tracking, or reflexive behaviors in zebrafish larvae[75]. However, although normal circadian changes in activity were maintained, contrary to our hypothesis, we observed a decrease in locomotor activity and an increase in sleep in zebrafish exposed to AHA (Fig. S2.2). In light of the effects of AHA on larval zebrafish sleep behavior, we did not pursue further use of the BONCAT method to probe changes in protein expression underlying natural sleep-wake cycles.

BONCAT reveals changes in protein expression in zebrafish larvae exposed to heat shock

To evaluate the BONCAT method's ability to detect newly synthesized proteins expressed in zebrafish during discrete, biologically relevant time windows, we instead examined the

proteomic response of zebrafish to heat shock. Zebrafish larvae (6 dpf) were treated with AHA and immediately subjected to elevated temperature (32°C) for 12 h, whereas control fish were treated with AHA and kept at 28.5°C for the same amount of time. The experiment was carried out during the night, since we observed that 12 h labeling at night resulted in more proteins identified, better PCA separation from controls, and improved signal above background compared to samples labeled during the day (Figs. 2.3B-D). BONCAT-enriched samples were subjected to LC-MS/MS analysis, resulting in the identification of 2,198 proteins (Fig. 2.4A). Samples clustered well by condition via PCA (Fig. 2.4B), and linear separability of the samples in principal component space (Silhouette score = 0.41) suggests that the experimental conditions drive distinct patterns in the data that are well captured by the first two principal components, even though together they account for less than a third of the total variance.

Differential expression analysis identified 23 proteins that were significantly up- or down-regulated in response to heat shock (FDR-adj. p-value < 0.05 and $|\log_2(\text{Fold Change})| > 1$) (Table S1), with an additional 76 proteins with $|\log_2(FC)| < 1$ that pass the threshold of statistical significance after accounting for multiple hypothesis testing (Fig. 2.4C). We searched all the proteins identified in our experiment for those previously reported to be up-regulated in response to heat shock to check whether their expression was also elevated in our BONCAT proteomics data. To identify proteins in our dataset previously shown to be induced by heat shock, we began by listing all of the proteins in our dataset that overlapped with proteins returned in Zebrafish Information Network (ZFIN) database searches for “heat shock” or “hsp.” We then examined the information and references listed in these proteins’ ZFIN entries, performing a thorough literature search to identify any with published data demonstrating that their expression increases in response to heat shock. This resulted in the identification of 19 proteins in our BONCAT proteomics dataset that have previously been shown to be up-regulated in response to heat shock (Table 1). The raw abundance values for these proteins were distributed across the range of values detected via LC-MS/MS (Fig. S2.3). Some of these proteins (designated “confirmed”) have been reported as showing increased expression, either at the protein or mRNA level, in response to heat shock in

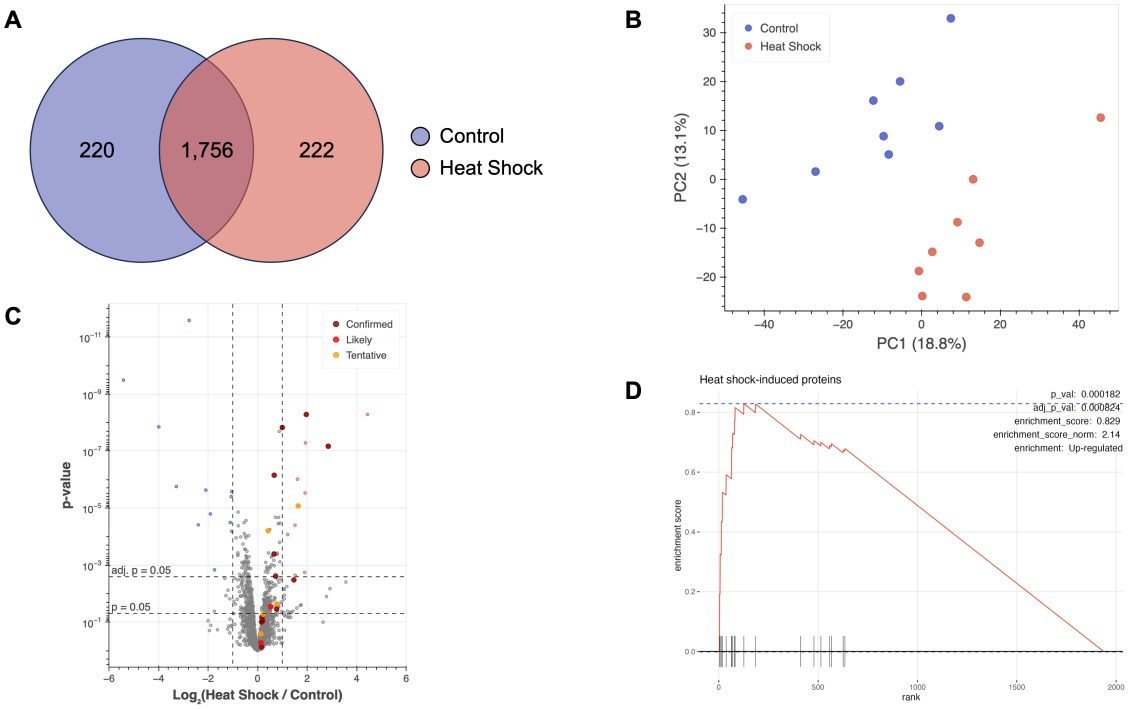

Figure 2.4. Proteomic analysis of BONCAT-labeled proteins from zebrafish larvae exposed to elevated temperatures for 12 h reveals expected up-regulation of heat shock-induced proteins. (A) Venn diagram indicating the number BONCAT-enriched proteins identified via proteomic analysis in samples of control fish treated with 4 mM AHA and kept at 28.5°C and/or in samples of fish treated with 4 mM AHA during incubation at 32°C. (B) PCA plot showing clustering and separation of control fish and fish exposed to heat shock. PCA was performed using median normalized abundance values. (C) Volcano plot comparing expression of BONCAT-enriched proteins identified in zebrafish larvae exposed to heat shock to their expression in controls. Fold change values were calculated via label-free quantification. Proteins significantly up-regulated in fish exposed to heat shock are depicted in light red, whereas proteins significantly down-regulated in fish exposed to heat shock are depicted in blue. Significance threshold was set to $|\log_2(FC)| > 1$ and FDR-adj. $p < 0.05$. Horizontal dashed lines depict $p = 0.05$ and Benjamini-Hochberg false-discovery rate (FDR)-adjusted $p = 0.05$. Enlarged, highlighted points indicate proteins for which data exists demonstrating their up-regulation during heat shock. Dark red ("confirmed") signifies that the protein has been shown to be up-regulated during heat shock in zebrafish. Bright red ("likely") signifies that the protein has been shown to be up-regulated during heat shock in other organisms. Orange ("tentative") indicates that existing data suggests a weak increase or that there are conflicting data in different papers. (D) Gene set enrichment analysis (GSEA) curve for proteins known to be induced by heat shock, which were manually annotated as "Heat shock response" for pathway analysis and are denoted with tick marks along the x-axis. Analysis revealed that this group of proteins is significantly enriched in the dataset based on FDR-adjusted p-values. The number of permutations was set to 10,000 for calculation of p-values. n = 8 biological replicates for each condition.

zebrafish. Others have been shown to increase in expression in response to heat shock in other systems, including other species of fish, insects, or mammalian cell culture ("likely"), or have exhibited weak or conflicting effects in previous reports ("tentative"). Our data showed that all 19 of these proteins had increased abundance ($log_2FC > 0$) in zebrafish exposed to heat shock, although only 8 of these log_2FC values were statistically significant (FDR-adj. p-values < 0.05).

We performed gene set enrichment analysis (GSEA) to identify signaling pathways that are significantly up- or down-regulated in zebrafish in response to heat shock. None of the protein annotations obtained from the Gene Ontology (GO) knowledgebase (Molecular Function, Cellular Component, and Biological Process), the WikiPathways database, or the Reactome pathway database were found to be significantly differentially regulated between treatment conditions. The only annotation in our dataset related to heat shock that was pulled from these databases for zebrafish was "regulation of HSF-1 mediated heat shock response" from the Reactome database. However, the complete entry for this pathway on the Reactome website specifies that this pathway was not assembled from zebrafish data but was instead inferred from human data. To address the lack of heat shock-related annotations for zebrafish proteins, we manually annotated the 19 proteins identified above as "heat shock-induced proteins" (Table 1). Performing GSEA again with this new annotation identified "heat shock-induced proteins" as significantly enriched, with a normalized enrichment score of 2.14 and an associated FDR-adjusted p-value of $8.24x10^{-4}$ (Fig. 2.4D).

Table 2.1. Proteins induced by heat shock in zebrafish identified via proteomic analysis of BONCAT-enriched samples

Protein	Gene Name	Log_2FC	P-Value	FDR-Adj. P-Value	Previously Shown Up-Regulated in Heat Shock
Heat shock protein family A (Hsp70) member 1B	hspa1b	2.860	6.77E-08	1.46E-05	Confirmed[78,79]
Heat shock cognate 70-kd protein, like	hsp70l	1.970	5.20E-09	2.52E-06	Confirmed[80]
DnaJ heat shock protein family (Hsp40) member B1b	dnajb1b	1.640	8.00E-06	9.55E-04	Tentative[81]
Heat shock cognate 70	hsc70	1.470	3.31E-03	5.73E-02	Confirmed[82–84]
Heat shock protein 90, alpha (cytosolic), class A member 1, tandem duplicate 1	hsp90aa1.1	1.000	1.49E-08	4.81E-06	Confirmed[85]

Serpin peptidase inhibitor, clade H (heat shock protein 47), member 1b	serpinh1b	0.770	3.51E-02	2.07E-01	Confirmed[86]
ST13 Hsp70 interacting protein	st13	0.768	2.31E-02	1.69E-01	Tentative[87]
Heat shock protein, alpha-crystallin-related, b11	hspb11	0.730	2.43E-03	4.85E-02	Confirmed[88,89]
Heat shock protein 90, beta (grp94), member 1	hsp90b1	0.674	7.04E-07	1.36E-04	Confirmed[90,91]
Unc-45 myosin chaperone B	unc45b	0.666	4.08E-04	1.64E-02	Confirmed[92–94]
Heat shock protein 4a	hspa4a	0.524	2.87E-01	1.87E-01	Likely[83,95]
Heat shock protein 8	hspa8	0.426	6.30E-05	3.93E-03	Tentative[83,96,97]
Heat shock protein 9	hspa9	0.234	5.29E-02	2.54E-01	Tentative[83,89,95,98]
Heat shock protein 5	hspa5	0.199	9.07E-02	3.29E-01	Confirmed[83,95,99]
Heat shock 10 protein 1	hspe1	0.179	6.71E-02	2.83E-01	Confirmed[82,100]
Heat shock 60 protein 1	hspd1	0.163	9.88E-02	3.44E-01	Confirmed[101]
Hypoxia up-regulated 1	hyou1	0.158	7.47E-01	8.83E-01	Confirmed[83,99]
Heat shock protein family A (Hsp70) member 8B	hspa8b	0.136	5.31E-01	7.56E-01	Likely[83]
Heat shock protein 90, alpha (cytosolic), class B member 1	hsp90ab1	0.130	2.58E-01	5.62E-01	Tentative[85,86]

Fold change values were calculated via label-free quantification. Both non-adjusted p-values as well as p-values adjusted for FDR using the Benjamini-Hochberg procedure are provided. The last column indicates the level of confidence ascribed to the manual annotation for that protein being induced by heat shock. “Confirmed” signifies that the protein has been shown to be up-regulated by heat shock in zebrafish. “Likely” signifies that the protein has been shown to be up-regulated by heat shock in other organisms. “Tentative” indicates that existing data suggests a weak increase or that there are conflicting data in different papers.

In addition to the heat shock-induced proteins identified, we uncovered other proteins significantly up- or down-regulated with potentially interesting biological functions in the context of heat shock (Table S1). For example, nitric oxide synthase-interacting protein (nosip, $\log_2$FC = 1.9363, FDR-adj. p = $1.259\text{x}10^{-5}$) modulates nitric oxide signaling, which can be affected by heat stress[102,103] and is involved in various cellular stress responses[104–106]. Sphingosine-1-phosphate lyase 1 (sgpl1, $\log_2$FC = 1.9363, FDR-adj. p = $1.259\text{x}10^{-5}$), which is involved in lipid metabolism, plays a role in cell survival and apoptosis[107–109], processes that could be influenced by heat stress[110–112]. Periaxin, on the other hand, which plays a crucial role in myelination[113–115], is down-regulated (prx, $\log_2$FC= -1.0413, FDR-adj. p = $3.647\text{x}10^{-4}$), suggesting that heat shock might affect neural development or maintenance.

Similarly, the down-regulation of perilipin (plin2, $log_2FC = -3.2774$, FDR-adj. $p = 2.839x10^{-4}$), a protein associated with lipid droplets, could reflect shifts in energy metabolism in response to heat stress. Finally, heterogenous nuclear ribonucleoprotein K (hnrpkl, $log_2FC= -1.0581$, FDR-adj. $p = 4.794x10^{-4}$) and heterogenous nuclear ribonucleoprotein D (hnrnpd, $log_2FC= -1.2785$, non-adj. $p = 1.176x10^{-2}$), which are involved in mRNA processing and regulation[116,117], both have reduced expression, potentially implicating them upstream of the broader gene expression changes observed with heat shock. Further work is required to dissect the roles (if any) that these proteins play in the heat shock response and how they affect zebrafish physiology under heat-induced stress.

Proteomic analysis of whole lysates does not reveal up-regulation of the heat-shock pathway

To assess the extent to which the time-resolved nature of the BONCAT method reveals new information, we carried out a global proteomic analysis on whole lysates prior to BONCAT enrichment. In order to compare the same samples before and after BONCAT enrichment, we set aside a portion of each sample (heat-shocked and control) before the click reaction and subjected the lysates to LC-MS/MS analysis. As expected, many more proteins were identified in the unenriched samples (12,206 proteins, Fig. 2.5A), since whole lysates reflect the entire proteome, whereas BONCAT enrichment selectively isolates newly synthesized proteins. Using the process described above, we manually annotated proteins in the global proteomics dataset for which data exists demonstrating their up-regulation in response to heat shock as "heat shock-induced proteins." Of the 35 such proteins identified, 8 have unexpected negative log_2FC values in this dataset (Table S2). PCA resulted in poorer clustering with less pronounced separation between heat-shocked and controls samples compared to BONCAT-enriched samples (Silhouette score = 0.18 vs 0.41), and the first two principal components only explain 11.3% and 8.8% of total variance (Fig. 2.5B). Comparison of these PCA results with those of BONCAT-enriched samples indicates that BONCAT enables improved differentiation between heat shock and control samples. This is likely because the presence of pre-existing proteins synthesized before treatment in unenriched whole lysate samples masks heat shock-induced changes in protein expression.

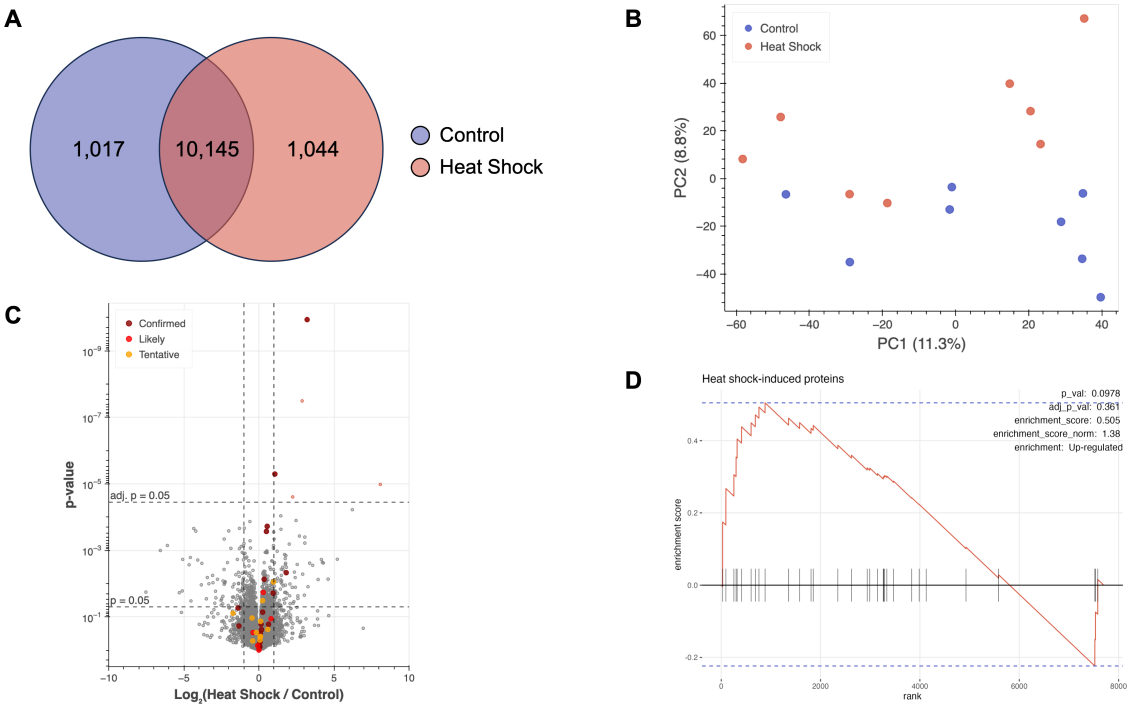

Figure 2.5. Global proteomics performed on zebrafish exposed to heat shock identifies 12,206 proteins, but heat shock-induced proteins are not significantly enriched. (A) Venn diagram indicating the number proteins identified via global proteomics on aliquots of zebrafish lysates set aside prior to BONCAT enrichment. Control fish were treated with 4 mM AHA for 12 h and kept at 28.5°C, while fish exposed to heat shock were treated with 4 mM AHA for 12 h during incubation at 32°C. (B) PCA plot shows less defined clustering and poor separation between control and heat shock samples. PCA was performed using median normalized abundance values. (C) Volcano plot comparing expression of proteins identified in whole lysates of zebrafish larvae exposed to heat shock to their expression in control fish. Fold change values were calculated via label-free quantification. Proteins significantly up-regulated in fish exposed to heat shock are depicted in light red, whereas proteins significantly down-regulated in fish exposed to heat shock are depicted in blue. Significance threshold was set to $|\log_2 FC| > 1$ and FDR-adj. $p < 0.05$. Horizontal dashed lines depict $p = 0.05$ and Benjamini-Hochberg FDR-adjusted $p = 0.05$. Enlarged, highlighted points indicate proteins for which data exists demonstrating their up-regulation during heat shock. Dark red signifies that the protein has been shown to be up-regulated during heat shock in zebrafish. Bright red signifies that the protein has been shown to be up-regulated during heat shock in other organisms. Orange indicates that existing data suggests a weak increase or are conflicting across different reports. (D) Gene set enrichment analysis (GSEA) curve for proteins known to be induced by heat shock, which were manually annotated as "Heat shock response" for pathway analysis and are denoted with tick marks along the x-axis. Analysis revealed that this group of proteins is not significantly enriched. The number of permutations was set to 10,000 for calculation of p-values. n = 8 biological replicates for each condition.

Differential expression analysis of these whole lysate samples revealed only two proteins known to be induced by heat shock that were significantly up-regulated in heat shock samples

($log_2FC > 1$ and FDR-adj. p-value < 0.05), with only five significantly up-regulated proteins and no significantly down-regulated proteins in the dataset (Fig 2.5C). Moreover, GSEA on global proteomics data did not return "heat shock-induced proteins" as a significantly up-regulated gene set (normalized enrichment score = 1.38, FDR-adj. p-value = 0.361) (Fig. 2.5D). In fact, no pathways in the annotation databases considered were found to be significantly enriched.

Examining the log_2FC values of the known heat shock-induced proteins identified in the BONCAT and global proteomics datasets revealed that the heat shock-induced proteins rank more highly relative to other proteins in the BONCAT data (Fig. 2.6A), whereas in the global

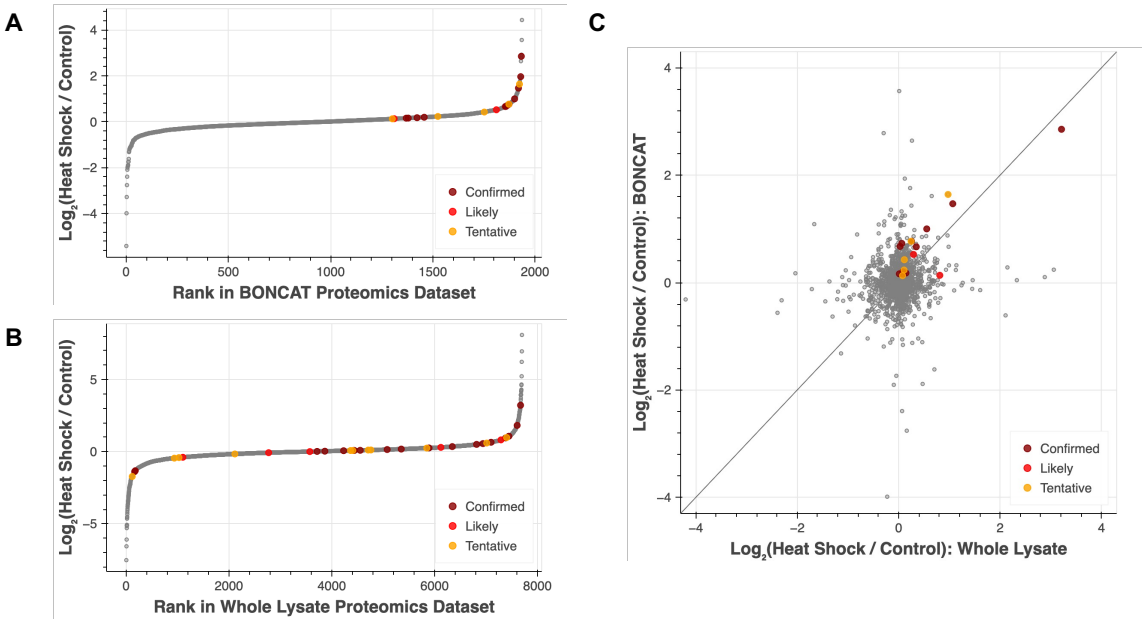

Figure 2.6. Proteins induced by heat shock are more enriched in BONCAT proteomics data compared to global proteomics data. (A, B) Ranked log2FC values for proteins identified in both heat shock and control samples in BONCAT-enriched samples (A) and in whole lysate samples (B). log2FC > 1 corresponds to greater expression in heat shock samples, whereas log2FC < 1 corresponds to greater expression in control samples. (C) Scatter plot showing log2FC values for all proteins identified both via BONCAT proteomics and via traditional global proteomics. While the overall distribution of protein log2FC values is similar in both datasets, heat shock-induced proteins had significantly higher log2FC values in the BONCAT proteomics dataset than their corresponding log2FC value in the global proteomics data (Wilcoxon signed-rank test, p = 0.010). In all plots, colored dots highlight proteins for which data exists demonstrating their up-regulation during heat shock. Dark red ("confirmed") signifies that the protein has been shown to be up-regulated during heat shock in zebrafish. Bright red ("likely") signifies that the protein has been shown to be up-regulated during heat shock in other organisms. Orange ("tentative") indicates that existing data suggests a weak increase or that there are conflicting data in different papers.

proteomics data they are more broadly distributed across the range of values detected (Fig. 2.6B). While a Kolmogorov-Smirnov test confirms that the distribution of heat shock-induced protein log_2FC values is not drawn from the same underlying distribution as the rest of the proteome in either experiment, the p-value associated with this difference is much lower in the BONCAT data (KS test $p = 6.69x10^{-9}$) compared to the global proteomics data (KS test $p = 0.0341$). Furthermore, direct comparison of the log_2FC values of the 18 heat shock-induced proteins identified in both datasets reveals that all but two have higher log_2FC values in the data from BONCAT-enriched samples than in the unenriched sample data (Fig. 2.6C) and that this overall increase is statistically significant (Wilcoxon signed-rank test, $p = 0.0104$). The stronger up-regulation of heat shock-induced proteins in the BONCAT proteomics dataset compared to the global proteomics dataset provides further evidence that BONCAT enables improved detection of biologically relevant, stimulus-evoked changes in protein expression.

2.4 Discussion

Here, we report for the first time the use of BONCAT in zebrafish to perform time-resolved proteomic analysis. While the labeling of newly synthesized proteins in whole zebrafish larvae using AHA[75] and in specific cell-types using ANL[76] has been reported previously, enrichment and analysis of BONCAT-labeled proteins via mass spectrometry-based proteomics have not. We found that AHA-labeled proteins could be enriched and identified after labeling periods as short as 12 hours, although more proteins were identified after more extended labeling. After 12 hours, the number of proteins we identified (~2000) is typical of other published zebrafish proteomics experiments[118–126] and a substantial improvement over older methods that used 2D gels[120,127,128].

Using heat shock as a proof of concept, we then demonstrated the ability of the BONCAT method to detect changes in protein synthesis associated with a transient response that were not identified via conventional global proteomics. Notably, we were able to do this at 32°C, which is at the low end of temperatures known to induce a heat shock response in zebrafish (32-39°C)[129–133]. Although global proteomics enables researchers to identify a greater

number of proteins overall, BONCAT was more successful at uncovering biologically meaningful changes in protein expression. Our global proteomics experiment identified more proteins than any previously published proteomics data in zebrafish (12,206 proteins, whereas the largest dataset to date had consisted of 8,363 proteins[126]), yet our BONCAT proteomics data revealed a greater number of heat shock proteins to be significantly up-regulated via differential expression analysis. BONCAT proteomics also revealed heat shock response to be the most significantly altered pathway via GSEA, whereas it did not pass the threshold of statistical significance in traditional global proteomics using whole lysates.

The majority of proteomics studies in zebrafish to date have been global analyses of whole lysates, in which the background proteome can obscure changes in protein synthesis that occur in response to transient signals or environmental stresses, as we observed in our heat shock experiments. Ribosome profiling and SILAC have been applied in zebrafish to obtain more time-resolved information about protein expression[134–139]. Ribosome profiling provides snapshots of protein synthesis at specified time points by pulling down and sequencing ribosome-bound mRNAs, whereas SILAC enables the quantitative investigation of protein expression and turnover dynamics using heavy isotope-labeled amino acids. BONCAT combines advantages of both of these techniques: enrichment of newly synthesized proteins prevents high-abundance, unlabeled proteins from overwhelming the signal of lower abundance proteins of interest, while the use of tagged amino acids enables examination of protein expression during a user-defined time window of interest.

Future work will lead to further advancements in the sensitivity of BONCAT proteomics in zebrafish. Time resolution could be improved by reducing labeling times to less than 12 hours. Pushing the limits further, BONCAT could be used for cell-type specific time-resolved proteomics in zebrafish, taking advantage of more recent work demonstrating the ability to label newly synthesized proteins in neurons[97,98]. Specifically, fish engineered to express a mutant methionyl-tRNA synthetase under the control of a neuron-specific promoter are able to incorporate the bulkier amino acid ANL into newly synthesized proteins in neurons. Cell-type specific BONCAT proteomics has the potential to reveal changes in

protein expression underlying behavioral phenomena studied in zebrafish, including sleep, social behavior, learning and memory, stress, and locomotion. However, enriching ANL-labeled proteins from neurons poses challenges, as the ratio of unlabeled to labeled protein will be higher than that encountered in AHA-labeling, highlighting the need for improvement in the BONCAT workflow. While we were able to reduce the number of non-specifically adsorbed proteins that make it through the enrichment process by using a smaller quantity of beads in our experiments involving 12 h AHA labeling (30 μL per sample) than in our experiment with 48 h AHA labeling (40 μL per sample), further optimization of the BONCAT enrichment protocol described here will be crucial for performing proteomic analyses of ANL-labeled proteins in zebrafish. Finally, these techniques could be extended beyond larval zebrafish to juvenile or adult fish, which may be more useful for answering certain research questions, could reduce the number of fish needed per experiment as each provides more tissue, and would facilitate the physical dissection of specific organs of interest.

2.5 Materials and Methods

Zebrafish Husbandry

Animal husbandry and all experimental procedures involving zebrafish were performed in accordance with the California Institute of Technology Institutional Animal Care and Use Committee (IACUC) guidelines and by the Office of Laboratory Animal Resources at the California Institute of Technology (animal protocol 1836). All experiments used wildtype (hybrid TLAB) zebrafish 4-7 days post fertilization (dpf). Sex is not yet defined at this stage of development. Fish were raised in an incubator at 28.5°C in petri dishes containing E3 embryo medium (5 mM NaCl, 0.17 mM KCl, 0.33 mM $CaCl_2$, 0.33 mM $MgSO_4$) at a density of 50 zebrafish larvae per dish.

Video tracking of larval zebrafish behavior

In the evening (~8 p.m.), individual 4 dpf zebrafish larvae were placed into wells of 96-well plates (Whatman, 7701–1651) containing approximately 700 μL of E3 medium. Recording and analysis of larval zebrafish behavior were performed as previously described[72,140]. In

brief, each 96-well plate was loaded into a custom-modified Zebrabox (Viewpoint Life Sciences) equipped with a Dinion one-third inch monochrome camera (Point Grey, Dragonfly 2) fitted with a fixed-angle megapixel lens (Computar, M5018-MP) and infrared filter. Boxes were continuously illuminated with infrared LEDs and illuminated with white LEDs from 9 a.m. to 11 p.m. to simulate daylight. The chamber containing the 96-well plate was filled with continuously circulating water from a tank to maintain a constant temperature of 28.5°C. Fish movements were captured at 15 Hz and recorded in quantization mode with 1-min time bins. The parameters used for detection were: sensitivity, 30; bursting, 900; freezing, 10, which were determined empirically. A movement was defined as a pixel displacement between adjacent video frames preceded and followed by a period of inactivity of at least 67 ms (the limit of temporal resolution). A minute of sleep was defined as any continuous one-minute period with no movement based on arousal threshold changes established by past work[70]. Average activity was defined as the average amount of activity in seconds/hour, including sleep bouts.

At 9 a.m. on 5 dpf, warm E3 was added to each well to bring the volume of all wells back to 700 µL to account for evaporation overnight. Using a multi-channel pipette, a 280 µL volume was subsequently removed from each well. For wells designated as controls, this was replaced with 280 µL of E3. For treated wells, 280 µL of a filtered and pre-warmed solution of 10 mM AHA (Iris Biotech, HAA9280) in E3 was added to achieve a final concentration of 4 mM AHA. Every 12 hours for the duration of the treatment (48 h), wells were replenished with E3 to return their volume to 700 µL.

Analysis of zebrafish behavioral data from video trackers

Data collected by the Viewpoint video tracker systems were processed in Matlab (R2023b, The Mathworks, Inc.) using custom scripts (modified from Prober et al., 2006). VTs_to_DATA_new_machines_middur.m is a Matlab script that that converts data acquired by the video trackers to a format that is useful for analysis using Matlab. VT_analysis_2019b.m is a Matlab script that analyzes data collected by the Viewpoint video tracker system to quantify several metrics, including locomotor activity, wake activity, sleep,

sleep architecture and sleep latency. These scripts and detailed instructions on their use will be provided upon request.

AHA labeling for BONCAT and FUNCAT in zebrafish larvae

To initiate labeling of newly synthesized proteins in zebrafish larvae, E3 was removed from petri dishes and replaced with 20 mL 4 mM AHA (Iris Biotech, HAA9280) dissolved in E3, filtered with a 0.2 μM filter, and brought to 28.5°C prior to treatment. Fish exposed to 48 h labeling were treated at 5 dpf beginning at 9 am, whereas fish treated with AHA for 12 h were administered AHA either at 6 dpf at 9 am (day) or at 6 dpf at 9 pm (night). Untreated control fish had E3 removed from their dishes and replaced with 20 mL fresh E3. Petri dishes with zebrafish larvae in the 4 mM AHA solution were left in the 28.5°C incubator for the duration of treatment. After the desired labeling time, the 4 mM AHA solution was removed from the dishes, and fish were rinsed three times with E3 prior to collection. Zebrafish larvae to be used for FUNCAT imaging experiments were collected in 1.5-mL Eppendorf tubes (6 fish per tube) and placed on ice for euthanasia via rapid cooling. Zebrafish larvae to be used for BONCAT proteomics experiments were collected in 5-mL Eppendorf tubes (150 fish collected from three dishes per 5-mL tube) and placed on ice for euthanasia. After 1 hour, fish were transferred from the 5-mL tubes to 1.5-mL Eppendorf tubes provided by the BeatBox Tissue Kit 24x (PreOmics, P.O.00128) with the magnetic bead removed and set aside. All E3 was removed from the tube, and the remaining pellet of zebrafish was stored at -80°C until subsequent lysis and chemical enrichment.

FUNCAT imaging of newly synthesized proteins in zebrafish larvae

The FUNCAT protocol was performed as previously described[75,76] with some minor modifications. Zebrafish euthanized on ice were fixed in a solution of 4% paraformaldehyde (PFA), 4% sucrose, and 0.25% Triton X-100 (Thermo Scientific, 85111) in 1X PBS (Gibco, 10010-023) on a rocker at 4°C overnight. Fixed zebrafish larvae were washed twice with 50% methanol in 1X PBS and twice with 100% methanol before storing in methanol at −20ºC for at least two nights. Fish were then rehydrated through successive 5 min washes with 75% methanol in PBST (1X PBS with 0.1% Tween-20, Thermo Scientific, 85113), 50%

methanol in PBST, 25% methanol in PBST, and PBST. Samples were then washed three times with PBDTT (PBST with 1% DMSO and 0.5% Triton X-100), followed by digestion with 1 mg/mL collagenase (Sigma-Aldrich, C0130) in PBST for 45 min at room temperature. After two quick washes with PBST, fish were post-fixed for 20 min in 4% PFA, 4% sucrose, and 0.25% Triton X-100 in 1X PBS. Fish were once again washed twice briefly with PBST, followed by three 5-min washes with PBDTT. Permeabilized zebrafish larvae were then incubated in blocking solution composed of 5% bovine serum albumin (Sigma-Aldrich) and 10% normal goat serum (Sigma-Aldrich, G9023) in PBDTT for 3 h at 4°C on a rocker. Samples were then washed three times for 10-15 min in PBST adjusted to pH 7.8.

Click reaction solution (0.2 mM TBTA, 0.5 mM TCEP, 5 μM Cy3 alkyne, 0.2 mM $CuSO_4$) was prepared in a 15-mL Eppendorf tube as follows: the amount of PBST needed to provide 1 mL solution per sample was added, followed by tris(benzyltriazolylmethyl)amine (TBTA, Sigma-Aldrich, 678937), vortexing for 10 seconds, adding tris(2-carboxyethyl)phosphine hydrochloride (TCEP, Sigma-Aldrich, C4706) vortexing for 10 seconds, adding Cy3 alkyne (Vector Laboratories, CCT-TA117), vortexing for 10 seconds, adding $CuSO_4$ (Merck Millipore, 1.02790), and vortexing for 30 seconds. The solution was filtered through a 0.22 μm filter and then added to samples, which were incubated overnight at room temperature on a rotary tube mixer set to a low speed. The next day, samples were washed four times for 30 min in PBDTT with 0.5 mM EDTA (Invitrogen, AM9260G) then washed twice for 1 h in PBDTT. Samples were rinsed briefly twice and then washed three times for 5 min with PBTx (1X PBS with 0.25% Triton X-100). Samples were then washed once for 5 min in 1X PBS before being transferred to Vectashield (Vector Laboratories, H-1000-10) gradually, first to a 10% solution, then 25%, 50%, 75%, and finally 100%, waiting until fish sink to the bottom of the tube before transferring to the next solution. Fish mounted in Vectashield were imaged using a Zeiss LSM 780 confocal microscope with a Plan-Apochromat 10x/0.45 air objective. Sulfo-Cy3 was excited with a 561 nm laser, and emitted light was detected between 538-680 nm. All image processing was carried out using ImageJ (NIH).

BONCAT labeling during heat shock treatment of zebrafish larvae

For heat shock experiments, E3 was replaced with 20 mL 4 mM AHA in E3 at 9 pm at 6 dpf. Fish and solution were transferred from petri dishes to 50 mL Falcon tubes. Control fish were placed in a tube rack in the 28.5°C incubator while fish exposed to heat shock were placed in a water bath set to 32°C. Animals were exposed to light for the first two hours (9 pm to 11 pm) and then incubated in the dark from 11 pm until 9 am. The lights in the incubator automatically turn off during this time window to simulate nighttime, and the water bath was covered to mimic these dark conditions. At 9 am, the fish were rinsed, collected, euthanized, and stored as described above.

Preparation of zebrafish lysates

After thawing, 500 µL lysis buffer containing 0.2% (w/v) n-dodecyl-β-maltoside (Thermo Fisher Scientific, 329370010), 2.5% (w/v) sodium dodecyl sulfate (Sigma-Aldrich, L5750), and 1:1000 EDTA-free protease inhibitors (Millipore, 539134) in 1X PBS was added to each tube containing zebrafish larvae. The magnetic bead set aside earlier from the PreOmics BeatBox Tissue Kit was added back to the tube. Prior to homogenization, 1 µL benzonase (Sigma-Aldrich, E8263-25KU) was added to each tube and allowed to sit for 5-10 min. Tubes were then placed in the PreOmics BeatBox tissue homogenizer for 10 min on the standard setting. Samples were then heated at 95°C for 10 min, and then subjected to one more cycle of homogenization and heating. Lysates were cleared by centrifugation (20 min, 20,600 g, 4°C) and the supernatants were transferred to Protein LoBind tubes (Eppendorf, 02243108). Protein concentrations in each lysate were measured using the Pierce™ BCA Protein Assay Kit (performed on aliquots of lysates diluted 10-fold to ensure the concentrations measured were within the assay's dynamic range) and normalized across all samples using 2.5% SDS in PBS, resulting in each sample containing the same mass of protein (typically 1-3 mg) in a total volume of 500 µL. Lysates were stored at −80°C for further processing.

Sample preparation for mass spectrometry

For BONCAT analysis, lysates were first alkylated by treatment with 100 µL of 600 mM chloroacetamide (Sigma-Aldrich, C0267) in 0.8% SDS/PBS and incubation on a tube shaker at 65°C for 30 min in the dark at 1200 RPM. Following alkylation, 600 µL of 8 M urea / 0.85 M NaCl in PBS were added to the lysate (final concentration of urea: 4 M) along with 30 or 40 µL aza-dibenzocyclooctyne (DBCO) agarose beads (Vector Laboratories, CCT-1034). Lower bead volumes were used for samples with shorter AHA labeling times to reduce the amount of non-specifically adsorbed proteins that make it through the enrichment process as background. The copper-free click reaction was incubated on a rotary wheel at a low speed in the dark at room temperature for 24 h. Samples were centrifuged at 1.5k RCF for 1 min, the supernatant was removed, and samples were reduced by adding 500 µL of 5 mM dithiothreitol (Sigma-Aldrich, 43815) in 0.8% SDS/PBS to each sample and incubating on a tube shaker for 15 min at 70°C and 1200 RPM in the dark. After centrifugation and removal of supernatant, samples were subjected to another alkylation step using 500 µL of 40 mM chloroacetamide and placement on a rotary wheel in the dark at room temperature for 30 min. Beads were then subjected to a series of thorough wash steps to remove nonspecifically bound proteins, first with 50 mL 0.8% (w/v) SDS in PBS, then with 50 mL urea in 100 mM tris hydrochloride (pH = 8.0), and finally with 50 mL 20% (v/v) acetonitrile (ACN) in doubly distilled water. Washed beads were transferred to 1.5-mL Protein LoBind tubes using 10% ACN in 50 mM ammonium bicarbonate, using 500 µL, then 300 µL, then 300 µL solution to ensure maximal resuspension and collection of beads from the columns. Samples were centrifuged at 1.5k RCF for 1 min and all but 100 µL of the supernatant was removed.

On-bead digestion was carried out by adding 0.1 µg trypsin and 0.05 µg endoproteinase LysC to each sample and incubating overnight on a tube shaker at 37°C and 1200 RPM. The following morning, samples were spun down at 1.5k RCF for 1 min and the peptide-containing supernatants were transferred to Pierce™ Centrifuge Columns (Thermo Scientific, 89868). The process of collecting peptides was repeated with two additional bead washes, each using 50 µL of the STOP solution from the PreOmics Phoenix Kit (P.O.00023, Lot Number 0000444362) which were combined with the supernatants in the columns.

Samples were then centrifuged at 1.5k RCF for 1 min to remove any DBCO-agarose resin carried over in the supernatants. Samples were desalted and purified using the PreOmics Phoenix Kit following instructions provided by the manufacturer. After the final elution step, samples were vacuum concentrated to dryness and resuspended in 10 µL 0.2% formic acid for subsequent LC-MS/MS analysis.

For global proteomic analysis, a small volume of the concentration-normalized lysates from AHA-treated fish was set aside prior to BONCAT enrichment. For each sample, the volume of lysate corresponding to 50 µg protein was digested in an S-Trap micro spin column (Protifi, USA, C02-micro) according to the manufacturer's instructions. After elution and drying, samples were desalted using Pierce™ C18 spin columns (Thermo Scientific, 89870) lyophilized, and then resuspended in 2% acetonitrile, 0.2% formic acid for subsequent LC-MS/MS analysis.

LC-MS/MS analysis

All samples were analyzed on an Eclipse mass spectrometer (Thermo Fisher Scientific, USA) coupled to a Vanquish Neo UHPLC system (Thermo Fisher Scientific, USA). Peptides from BONCAT-enriched samples were separated on an Aurora UHPLC Column (25 cm x 75 µm, 1.7 µm C18, AUR3-25075C18-TS, Ion Opticks) with a flow rate of 0.35 µL/min for a total duration of 1 h and ionized at 1.6 kV in the positive ion mode. The gradient was composed of 6% solvent B (3.5 min), 6-25% B (41.5 min), 25-40% B (15 min), 40–98% B (2 min), and 98% B (5min), with the remaining volume composed of solvent A, where solvent A is 2% acetonitrile (ACN, Fisher Scientific, A9554) and 0.2% formic acid (FA, Fisher Scientific, A11750) in water, and solvent B is 80% ACN and 0.2% formic acid in water. For samples from whole lysates, 2 µg of peptides were separated on an Aurora Frontier™ column (60 cm × 75 µm, 1.7 µm C18, AUR3-60075C18, Ion Opticks) at 0.30 µL/min for a total duration of 2 h and ionized at 1.8 kV. The gradient was composed of 6% solvent B (7.5 min), 6-25% B (82.5 min), 25-40% B (30 min), 40–98% B (1 min), and 98% B (9 min). MS1 scans were acquired in the Orbitrap at the resolution of 120,000 from 375 to 1,600 m/z. Automatic gain control (AGC) was set to a target of 106 and a maximum injection time of 50 ms. MS2 scans

were acquired in the ion trap using fast scan rate on precursors with 2-7 charge states and quadrupole isolation mode (isolation window: 1.2 m/z) with higher-energy collisional dissociation (HCD, 30%) activation type. Dynamic exclusion was set to 30 s. Ion transfer tube temperature was 300°C and the S-lens RF level was set to 30.

Proteomic data processing and analysis

MS raw files were searched against the Uniprot *Danio rerio* proteome (UP000000437) using the Proteome Discoverer 3.0 software based on the SequestHT algorithm. Oxidation / +15.995 Da (M), deamidated / +0.984 Da (N) were set as dynamic modifications; carbamidomethylation / +57.021 Da (C) was set as a fixed modification. The precursor mass tolerance was set to 10 ppm; fragment mass tolerance was set to 0.6 Da. The maximum false peptide discovery rate was specified as 0.01 using the Percolator Node validated by q-value. The relative abundance of parental peptides was calculated by integration of the area under the curve of the MS1 peaks using the Minora LFQ node. The mass spectrometry data have been deposited to the ProteomeXchange Consortium via the PRIDE[141] partner repository with the dataset identifier PXD063084.

Raw protein quantification data exported from Proteome Discoverer 3.0 was imported into R and analyzed using the Tidyproteomics package (version 1.7.3) (https://jeffsocal.github.io/tidyproteomics/index.html)[142]. Once imported, the data were filtered for common protein contaminants and normalized between runs via median normalization. Differential expression analysis was performed in the Tidyproteomics package using the limma algorithms (https://bioinf.wehi.edu.au/limma/). All plots, with the exception of gene set enrichment plots, were generated using a separate analysis pipeline in Python. Jupyter notebooks with Python code can be provided upon request. Gene set enrichment analysis to identify significantly up- or down-regulated pathways was performed in R using the Bioconductor fgsea package (https://bioconductor.org/packages/release/bioc/html/fgsea.html)[143]. Pathway annotations were drawn from the Gene Ontology (GO) database for biological process, molecular function, and cellular component, as well as from the WikiPathways and Reactome Pathways

databases. Annotations for heat shock-induced proteins were added manually based on a search of the literature for data showing increase in expression in response to heat shock. All code can be provided upon request.

2.6 Supplementary Information

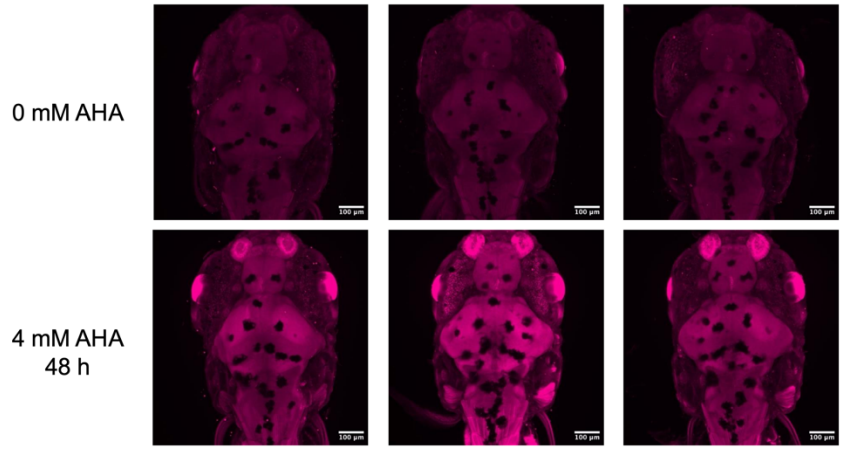

Figure S2.1. Images of FUNCAT-labeled proteins after 48 h labeling with 4 mM AHA. 7 dpf zebrafish larvae were fixed after 48 h metabolic labeling with 4 mM AHA, permeabilized, and reacted with with 5 μM Cy3 alkyne. Maximum Z-projections of dorsal views of the head and start of the tail are shown for three unlabeled control larvae (top row) and three larvae labeled with 4 mM AHA for 48 h (bottom row). Dark spots are pigment spots on the skin of the larvae characteristic of this stage of development. Scale bar is 100 μm.

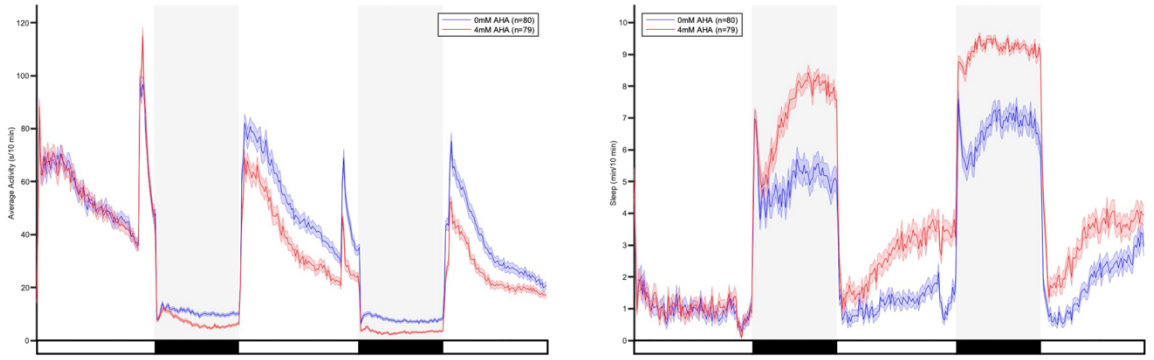

Figure S2.2. Wildtype zebrafish larvae treated with 4 mM AHA are less active and sleep more than untreated larvae. Locomotor activity (left) and sleep (right) traces for untreated control larvae (n=80, blue) and larvae treated with AHA (n=79, red). Zebrafish were loaded onto video trackers at 7 pm at 4 dpf, and data acquisition began at 9 am at 5 dpf. Treated fish were given AHA beginning at 9 pm at 5 dpf, and E3 medium was added to every 12 hours, including at the beginning of data acquisition, to replenish well volumes that decrease over time due to evaporation. Line and shading represent mean ± SEM. White and black bars on the x-axis indicate day (14 hours, 9 am to 11 pm) and night (10 hours, 11 pm to 9 am), respectively.

Table S2.1. Significantly up- and down-regulated proteins in BONCAT-enriched samples from zebrafish larvae exposed to heat shock.

Description	Gene Name	Log_2(FC)	P-Value	FDR Adj. P-Value
Protein-tyrosine-phosphatase	ptprr	4.437	5.21E-09	2.52E-06
Heat shock protein family A (Hsp70) member 1B	hspa1b	2.855	6.77E-08	1.46E-05
Heat shock cognate 70-kd protein,-like	hsp70l	1.967	5.20E-09	2.52E-06
Sphingosine-1-phosphate lyase 1	sgpl1	1.936	5.20E-08	1.26E-05
Si:dkeyp-67a8.4	si:dkeyp-67a8.4	1.919	2.96E-06	3.82E-04
Zinc finger and BTB domain-containing 11	zbtb11	1.905	1.79E-03	3.88E-02
DnaJ heat shock protein family (Hsp40) member B1b	dnajb1b	1.642	8.39E-06	9.55E-04
Nitric oxide synthase-interacting protein	nosip	1.612	9.70E-07	1.71E-04
Zinc finger protein X-linked	zfx	1.525	2.31E-03	4.65E-02
Zinc finger protein 1027	znf1027	1.514	4.01E-05	2.77E-03
Proteasome 26S subunit ubiquitin receptor, non-ATPase 2	psmd2	1.216	8.46E-05	4.82E-03
Periaxin	prx	-1.041	2.64E-06	3.65E-04
Zinc finger protein 1011 (Fragment)	znf1011	-1.045	6.51E-05	3.94E-03
Heterogeneous nuclear ribonucleoprotein K	hnrnpk	-1.058	3.96E-06	4.79E-04
Ras-related protein Rab	rab38c	-1.102	3.22E-05	2.62E-03
Nucleoside diphosphate kinase	nme2b.2	-1.737	1.47E-03	3.35E-02
Biogenesis of lysosome-related organelles complex 1 subunit 3	bloc1s3	-1.905	1.61E-05	1.64E-03
Si:ch211-1i11.3	si:ch211-1i11.3	-2.088	2.35E-06	3.50E-04
Titin, tandem duplicate 2 (Fragment)	ttn.2	-2.393	3.87E-05	2.77E-03
Periostin, osteoblast-specific factor a	postna	-2.759	2.60E-12	5.04E-09
Perilipin	plin2	-3.277	1.76E-06	2.84E-04
Cystathionine gamma-lyase	cth	-3.988	1.42E-08	4.81E-06
Coiled-coil domain containing 88C	ccdc88c	-5.413	3.26E-10	3.16E-07

Proteins listed have $|\log_2(FC)| > 1$ and Benjamini-Hochberg false discovery rate adjusted $p < 0.05$. Red rows are significantly up-regulated proteins whereas blue rows are significantly down-regulated proteins.

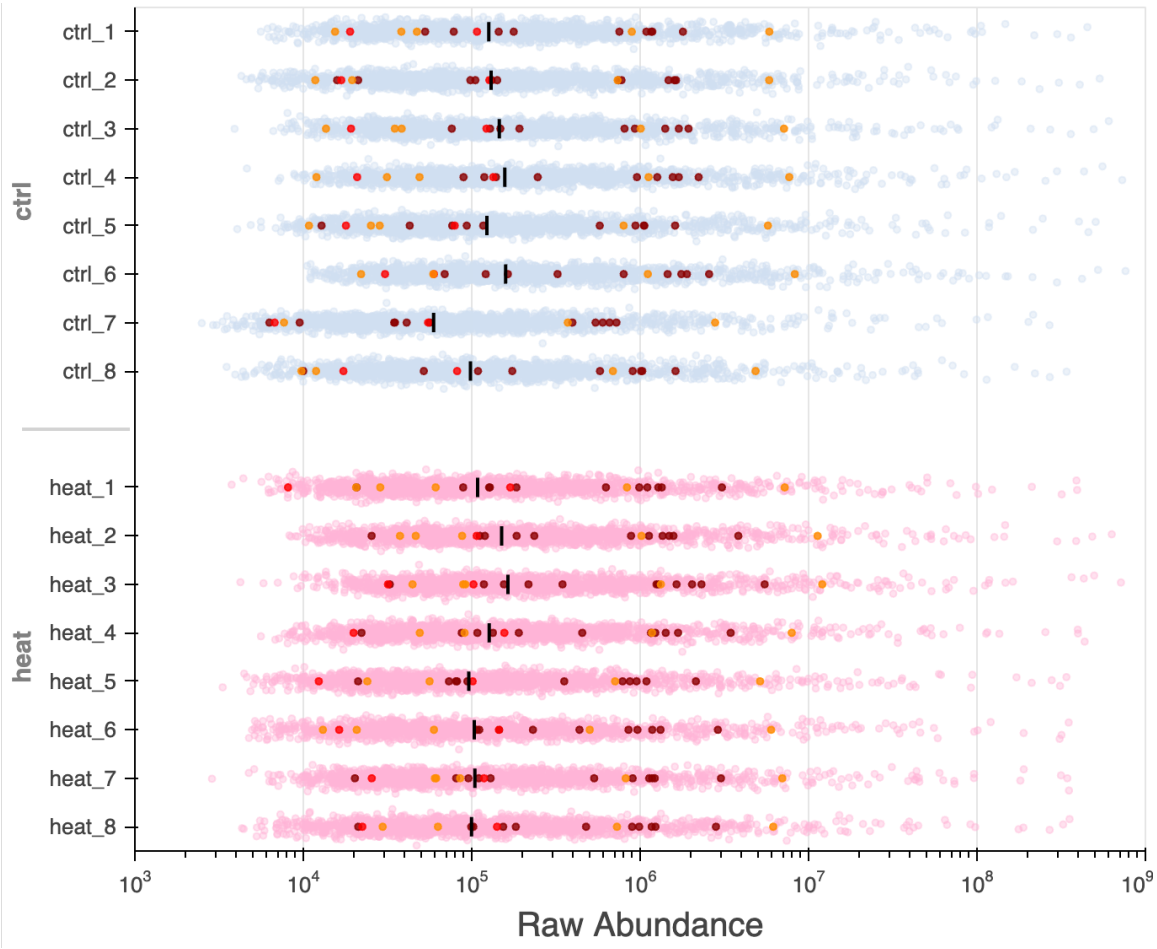

Figure S2.3. Raw abundances of proteins known to be induced by heat shock identified via BONCAT proteomics are spread across the range of abundances detected. Raw abundance values for all proteins identified in each biological replicate were calculated using the Proteome Discoverer software based on peptide abundances measured via LC-MS/MS. Highlighted in yellow are proteins previously shown to be up-regulated by heat shock, either in zebrafish or in other organisms. Black dash represents the median raw protein abundance in each sample.

Table S2.2. Heat shock proteins identified via proteomic analysis of whole lysates.

Protein	Gene Name	Log_2(FC)	P-Value	FDR-Adj. P-Value	Previously Shown Up-Regulated in Heat Shock
Heat shock protein family A (Hsp70) member 1B	hspa1b	3.210	1.16E-10	8.90E-07	Confirmed[78,79]
Heat shock cognate 70-kd protein, tandem duplicate 2	hsp70.2	1.820	4.68E-03	3.87E-01	Confirmed[80]
Heat shock cognate 70	hsc70	1.070	5.00E-06	1.30E-02	Confirmed[82–84]
DnaJ heat shock protein family (Hsp40) member B1b	dnajb1b	0.974	8.91E-03	4.48E-01	Tentative[81]
Heat shock protein, alpha-crystallin-related, 1	hspb1	0.946	1.94E-02	5.47E-01	Confirmed[82,88,89,144,145]
Heat shock protein family A (Hsp70) member 8B	hspa8b	0.812	1.14E-01	7.16E-01	Likely[83]
HSPA (heat shock 70kDa) binding protein, cytoplasmic cochaperone 1	hspbp1	0.647	1.68E-01	7.52E-01	Confirmed[80,82]
DnaJ (Hsp40) homolog, subfamily C, member 3a	dnajc3a	0.594	2.38E-01	7.94E-01	Tentative[146]
Heat shock protein 90, alpha (cytosolic), class A member 1, tandem duplicate 1	hsp90aa1.1	0.554	1.90E-04	1.21E-01	Confirmed[85]
Heat shock protein 90, alpha (cytosolic), class A member 1, tandem duplicate 2	hsp90aa1.2	0.500	2.70E-04	1.21E-01	Confirmed[80,82]
Unc-45 myosin chaperone B	unc45b	0.357	7.40E-03	4.47E-01	Confirmed[92–94]
Heat shock protein 4a	hspa4a	0.293	1.84E-02	5.44E-01	Likely[83,95]
Serpin peptidase inhibitor, clade H (heat shock protein 47), member 1b	serpinh1b	0.253	7.23E-02	6.83E+01	Confirmed[86]
ST13 Hsp70 interacting protein	st13	0.246	3.25E-02	6.05E-01	Tentative[87]
AHA1, activator of heat shock protein ATPase homolog 1b	ahsa1b	0.175	2.44E-01	7.95E-01	Confirmed[147]
Heat shock 10 protein 1	hspe1	0.143	1.66E-01	7.52E-01	Confirmed[82,100]
Heat shock protein 8	hspa8	0.112	1.36E-01	7.31E-01	Tentative[83,96,97]
Heat shock protein 9	hspa9	0.107	3.88E-01	8.50E-01	Tentative[83,89,95,98]
Hypoxia up-regulated 1	hyou1	0.090	3.16E-01	8.22E-01	Confirmed[83,99]
Heat shock protein 5	hspa5	0.080	3.76E-01	8.41E-01	Confirmed[83,95,99]
Crystallin, alpha A	Cryaa	0.079	5.70E-01	9.05E-01	Confirmed[88,89]
Heat shock protein 90, alpha (cytosolic), class B member 1	hsp90ab1	0.076	3.93E-01	8.50E-01	Tentative[85,86]
Heat shock protein 4b	hspa4b	0.073	4.97E-01	8.84E-01	Confirmed[83,95]
Heat shock protein, alpha-crystallin-related, b11	hspb11	0.06	7.95E-01	9.55E-01	Confirmed[88,89]
Heat shock protein 90, beta (grp94), member 1	hsp90b1	0.029	7.31E-01	9.43E-01	Confirmed[90,91]
Heat shock 60 protein 1	hspd1	0.013	8.78E-01	9.74E-01	Confirmed[101]
Huntingtin interacting protein K	Hypk	0.001	9.97E-01	9.99E-01	Likely[148]
DnaJ (Hsp40) homolog, subfamily C, member 8	dnajc8	-0.076	7.26E-01	9.43E-01	Likely[149]
Prostaglandin E synthase 3b (cytosolic)	ptges3b	-0.164	2.94E-01	8.13E-01	Tentative[150]
DnaJ (Hsp40) homolog, subfamily C, member 9	dnajc9	-0.393	2.95E-01	8.13E-01	Likely[151]
DnaJ (Hsp40) homolog, subfamily C, member 3b	dnajc3b	-0.415	5.29E-01	8.93E-01	Tentative[146]

Prostaglandin E synthase 3a (cytosolic)	ptges3a	-0.454	1.08E-01	7.13E-01	Tentative[150,152]
AHA1, activator of heat shock protein ATPase homolog 1a	ahsa1a	-1.330	1.88E-01	7.59E-01	Confirmed[147]
Heat shock protein b8	hspb8	-1.380	5.39E-02	6.64E-01	Confirmed[82,88]
Heat shock transcription factor 1	hsf1	-1.720	7.80E-02	6.90E-01	Tentative[82,153–156]

Fold change values were calculated via label-free quantification. Both non-adjusted p-values as well as Benjamini-Hochberg-adjusted p-values are provided. The last column indicates the level of confidence ascribed to the manual annotation for that protein being induced by heat shock. “Confirmed” signifies that the protein has been shown to be up-regulated during heat shock in zebrafish. “Likely” signifies that the protein has been shown to be up-regulated during heat shock in other organisms. “Tentative” indicates that existing data suggests a weak increase or that there are conflicting data in different papers.

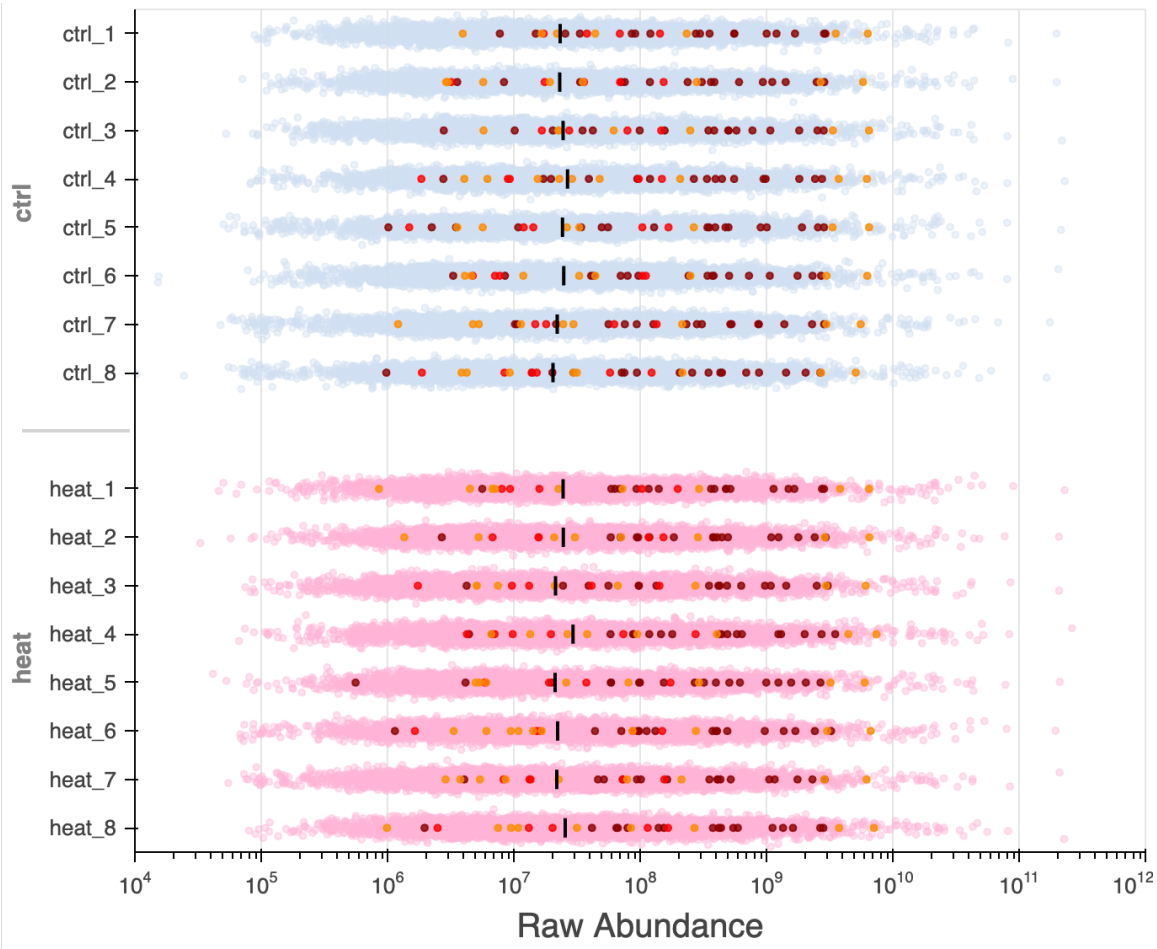

Figure S2.4. Raw abundances of proteins identified in whole lysates. Raw abundance values for all proteins identified in each biological replicate were calculated using the Proteome Discoverer software based on peptide abundances measured via LC-MS/MS. Highlighted in bright green are proteins previously shown to be up-regulated by heat shock, either in zebrafish or in other organisms. Black dash represents the median raw protein abundance in each sample.

2.7 References

(1) Davis, H. P.; Squire, L. R. Protein Synthesis and Memory: A Review. *Psychol. Bull.* **1984**, *96* (3), 518–559.

(2) Martin, K. C.; Barad, M.; Kandel, E. R. Local Protein Synthesis and Its Role in Synapse-Specific Plasticity. *Curr. Opin. Neurobiol.* **2000**, *10* (5), 587–592. https://doi.org/10.1016/S0959-4388(00)00128-8.

(3) Agranoff, B. W.; Klinger, P. D. Puromycin Effect on Memory Fixation in the Goldfish. *Science* **1964**, *146* (3646), 952–953. https://doi.org/10.1126/science.146.3646.952.

(4) Feder, M. E.; Hofmann, G. E. HEAT-SHOCK PROTEINS, MOLECULAR CHAPERONES, AND THE STRESS RESPONSE: Evolutionary and Ecological Physiology. *Annu. Rev. Physiol.* **1999**, *61* (Volume 61, 1999), 243–282. https://doi.org/10.1146/annurev.physiol.61.1.243.

(5) Basile, F.; Capaccia, C.; Zampini, D.; Biagetti, T.; Diverio, S.; Guelfi, G. Omics Insights into Animal Resilience and Stress Factors. *Animals* **2021**, *11* (1), 47. https://doi.org/10.3390/ani11010047.

(6) Costa-Mattioli, M.; Walter, P. The Integrated Stress Response: From Mechanism to Disease. *Science* **2020**, *368* (6489), eaat5314. https://doi.org/10.1126/science.aat5314.

(7) Hack, C. J. Integrated Transcriptome and Proteome Data: The Challenges Ahead. *Brief. Funct. Genomics* **2004**, *3* (3), 212–219. https://doi.org/10.1093/bfgp/3.3.212.

(8) Nie, L.; Wu, G.; Culley, D. E.; Scholten, J. C. M.; Zhang, W. Integrative Analysis of Transcriptomic and Proteomic Data: Challenges, Solutions and Applications. *Crit. Rev. Biotechnol.* **2007**, *27* (2), 63–75. https://doi.org/10.1080/07388550701334212.

(9) Liu, Y.; Beyer, A.; Aebersold, R. On the Dependency of Cellular Protein Levels on mRNA Abundance. *Cell* **2016**, *165* (3), 535–550. https://doi.org/10.1016/j.cell.2016.03.014.

(10) Ponomarenko, E. A.; Krasnov, G. S.; Kiseleva, O. I.; Kryukova, P. A.; Arzumanian, V. A.; Dolgalev, G. V.; Ilgisonis, E. V.; Lisitsa, A. V.; Poverennaya, E. V. Workability of mRNA Sequencing for Predicting Protein Abundance. *Genes* **2023**, *14* (11), 2065. https://doi.org/10.3390/genes14112065.

(11) Witze, E. S.; Old, W. M.; Resing, K. A.; Ahn, N. G. Mapping Protein Post-Translational Modifications with Mass Spectrometry. *Nat. Methods* **2007**, *4* (10), 798–806. https://doi.org/10.1038/nmeth1100.

(12) Müller, M. M. Post-Translational Modifications of Protein Backbones: Unique Functions, Mechanisms, and Challenges. *Biochemistry* **2018**, *57* (2), 177–185. https://doi.org/10.1021/acs.biochem.7b00861.

(13) Barber, K. W.; Rinehart, J. The ABCs of PTMs. *Nat. Chem. Biol.* **2018**, *14* (3), 188–192. https://doi.org/10.1038/nchembio.2572.

(14) Virág, D.; Dalmadi-Kiss, B.; Vékey, K.; Drahos, L.; Klebovich, I.; Antal, I.; Ludányi, K. Current Trends in the Analysis of Post-Translational Modifications. *Chromatographia* **2020**, *83* (1), 1–10. https://doi.org/10.1007/s10337-019-03796-9.

(15) Wong, J. W. H.; Cagney, G. An Overview of Label-Free Quantitation Methods in Proteomics by Mass Spectrometry. In *Proteome Bioinformatics*; Hubbard, S. J., Jones, A. R., Eds.; Humana Press: Totowa, NJ, 2010; pp 273–283. https://doi.org/10.1007/978-1-60761-444-9_18.

(16) Zhu, W.; Smith, J. W.; Huang, C.-M. Mass Spectrometry-Based Label-Free Quantitative Proteomics. *BioMed Res. Int.* **2010**, *2010* (1), 840518. https://doi.org/10.1155/2010/840518.

(17) Ong, S.-E.; Blagoev, B.; Kratchmarova, I.; Kristensen, D. B.; Steen, H.; Pandey, A.; Mann, M. Stable Isotope Labeling by Amino Acids in Cell Culture, SILAC, as a Simple and Accurate Approach to Expression Proteomics. *Mol. Cell. Proteomics* **2002**, *1* (5), 376–386.

(18) Thompson, A.; Schäfer, J.; Kuhn, K.; Kienle, S.; Schwarz, J.; Schmidt, G.; Neumann, T.; Hamon, C. Tandem Mass Tags: A Novel Quantification Strategy for Comparative Analysis of Complex Protein Mixtures by MS/MS. *Anal. Chem.* **2003**, *75* (8), 1895–1904. https://doi.org/10.1021/ac0262560.

(19) Wiese, S.; Reidegeld, K. A.; Meyer, H. E.; Warscheid, B. Protein Labeling by iTRAQ: A New Tool for Quantitative Mass Spectrometry in Proteome Research. *PROTEOMICS* **2007**, *7* (3), 340–350. https://doi.org/10.1002/pmic.200600422.

(20) Dieterich, D. C.; Link, A. J.; Graumann, J.; Tirrell, D. A.; Schuman, E. M. Selective Identification of Newly Synthesized Proteins in Mammalian Cells Using Bioorthogonal Noncanonical Amino Acid Tagging (BONCAT). *Proc. Natl. Acad. Sci.* **2006**, *103* (25), 9482–9487.

(21) Dieterich, D. C.; Lee, J. J.; Link, A. J.; Graumann, J.; Tirrell, D. A.; Schuman, E. M. Labeling, Detection and Identification of Newly Synthesized Proteomes with Bioorthogonal Non-Canonical Amino-Acid Tagging. *Nat. Protoc.* **2007**, *2* (3), 532–540. https://doi.org/10.1038/nprot.2007.52.

(22) Dieterich, D. C.; Hodas, J. J. L.; Gouzer, G.; Shadrin, I. Y.; Ngo, J. T.; Triller, A.; Tirrell, D. A.; Schuman, E. M. In Situ Visualization and Dynamics of Newly Synthesized Proteins in Rat Hippocampal Neurons. *Nat. Neurosci.* **2010**, *13*, 897. https://doi.org/10.1038/nn.2580.

(23) Rostovtsev, V. V.; Green, L. G.; Fokin, V. V.; Sharpless, K. B. A Stepwise Huisgen Cycloaddition Process: Copper(I)-Catalyzed Regioselective "Ligation" of Azides and Terminal Alkynes. *Angew. Chem. Int. Ed.* **2002**, *41* (14), 2596–2599. https://doi.org/10.1002/1521-3773(20020715)41:14<2596::AID-ANIE2596>3.0.CO;2-4.

(24) Tornøe, C. W.; Christensen, C.; Meldal, M. Peptidotriazoles on Solid Phase: [1,2,3]-Triazoles by Regiospecific Copper(I)-Catalyzed 1,3-Dipolar Cycloadditions of

Terminal Alkynes to Azides. *J. Org. Chem.* **2002**, *67* (9), 3057–3064. https://doi.org/10.1021/jo011148j.

(25) Agard, N. J.; Prescher, J. A.; Bertozzi, C. R. A Strain-Promoted [3 + 2] Azide−Alkyne Cycloaddition for Covalent Modification of Biomolecules in Living Systems. *J. Am. Chem. Soc.* **2004**, *126* (46), 15046–15047. https://doi.org/10.1021/ja044996f.

(26) Sletten, E. M.; Bertozzi, C. R. Bioorthogonal Chemistry: Fishing for Selectivity in a Sea of Functionality. *Angew. Chem. Int. Ed.* **2009**, *48* (38), 6974–6998. https://doi.org/10.1002/anie.200900942.

(27) Marchand, J. A.; Neugebauer, M. E.; Ing, M. C.; Lin, C.-I.; Pelton, J. G.; Chang, M. C. Y. Discovery of a Pathway for Terminal-Alkyne Amino Acid Biosynthesis. *Nature* **2019**, *567* (7748), 420–424. https://doi.org/10.1038/s41586-019-1020-y.

(28) Back, D.; Shaffer, B. T.; Loper, J. E.; Philmus, B. Untargeted Identification of Alkyne-Containing Natural Products Using Ruthenium-Catalyzed Azide Alkyne Cycloaddition Reactions Coupled to LC-MS/MS. *J. Nat. Prod.* **2022**, *85* (1), 105–114. https://doi.org/10.1021/acs.jnatprod.1c00798.

(29) Bagert, J. D.; Xie, Y. J.; Sweredoski, M. J.; Qi, Y.; Hess, S.; Schuman, E. M.; Tirrell, D. A. Quantitative, Time-Resolved Proteomic Analysis by Combining Bioorthogonal Noncanonical Amino Acid Tagging and Pulsed Stable Isotope Labeling by Amino Acids in Cell Culture. *Mol. Cell. Proteomics* **2014**, *13* (5), 1352–1358. https://doi.org/10.1074/mcp.M113.031914.

(30) D. Bagert, J.; Kessel, J. C. van; J. Sweredoski, M.; Feng, L.; Hess, S.; L. Bassler, B.; A. Tirrell, D. Time-Resolved Proteomic Analysis of Quorum Sensing in Vibrio Harveyi. *Chem. Sci.* **2016**, *7* (3), 1797–1806. https://doi.org/10.1039/C5SC03340C.

(31) Babin, B. M.; Atangcho, L.; van Eldijk, M. B.; Sweredoski, M. J.; Moradian, A.; Hess, S.; Tolker-Nielsen, T.; Newman, D. K.; Tirrell, D. A. Selective Proteomic Analysis of Antibiotic-Tolerant Cellular Subpopulations in Pseudomonas Aeruginosa Biofilms. *mBio* **2017**, *8* (5), 10.1128/mbio.01593-17. https://doi.org/10.1128/mbio.01593-17.

(32) Somasekharan, S. P.; Stoynov, N.; Rotblat, B.; Leprivier, G.; Galpin, J. D.; Ahern, C. A.; Foster, L. J.; Sorensen, P. H. B. Identification and Quantification of Newly Synthesized Proteins Translationally Regulated by YB-1 Using a Novel Click–SILAC Approach. *J. Proteomics* **2012**, *77*, e1–e10. https://doi.org/10.1016/j.jprot.2012.08.019.

(33) Schiapparelli, L. M.; McClatchy, D. B.; Liu, H.-H.; Sharma, P.; Yates, J. R.; Cline, H. T. Direct Detection of Biotinylated Proteins by Mass Spectrometry. *J. Proteome Res.* **2014**, *13* (9), 3966–3978. https://doi.org/10.1021/pr5002862.

(34) Wang, J.; Zhang, J.; Lee, Y.-M.; Koh, P.-L.; Ng, S.; Bao, F.; Lin, Q.; Shen, H.-M. Quantitative Chemical Proteomics Profiling of de Novo Protein Synthesis during Starvation-Mediated Autophagy. *Autophagy* **2016**, *12* (10), 1931–1944. https://doi.org/10.1080/15548627.2016.1196317.

(35) Howden, A. J. M.; Geoghegan, V.; Katsch, K.; Efstathiou, G.; Bhushan, B.; Boutureira, O.; Thomas, B.; Trudgian, D. C.; Kessler, B. M.; Dieterich, D. C.; Davis, B. G.; Acuto, O. QuaNCAT: Quantitating Proteome Dynamics in Primary Cells. *Nat. Methods* **2013**, *10* (4), 343–346. https://doi.org/10.1038/nmeth.2401.

(36) Hinz, F.; Dieterich, D.; Schuman, E. Teaching Old NCATs New Tricks: Using Non-Canonical Amino Acid Tagging to Study Neuronal Plasticity. *Curr. Opin. Chem. Biol.* **2013**, *17* (5), 738–746. https://doi.org/10.1016/j.cbpa.2013.07.021.

(37) Liang, Z.; Zhan, Y.; Shen, Y.; Wong, C. C. L.; Yates, J. R.; Plattner, F.; Lai, K.-O.; Ip, N. Y. The Pseudokinase CaMKv Is Required for the Activity-Dependent Maintenance of Dendritic Spines. *Nat. Commun.* **2016**, *7* (1), 13282. https://doi.org/10.1038/ncomms13282.

(38) Schanzenbächer, C. T.; Sambandan, S.; Langer, J. D.; Schuman, E. M. Nascent Proteome Remodeling Following Homeostatic Scaling at Hippocampal Synapses. *Neuron* **2016**, *92* (2), 358–371. https://doi.org/10.1016/j.neuron.2016.09.058.

(39) Schanzenbächer, C. T.; Langer, J. D.; Schuman, E. M. Time- and Polarity-Dependent Proteomic Changes Associated with Homeostatic Scaling at Central Synapses. *eLife* **2018**, *7*, e33322. https://doi.org/10.7554/eLife.33322.

(40) Hodas, J. J. L.; Nehring, A.; Höche, N.; Sweredoski, M. J.; Pielot, R.; Hess, S.; Tirrell, D. A.; Dieterich, D. C.; Schuman, E. M. Dopaminergic Modulation of the Hippocampal Neuropil Proteome Identified by Bioorthogonal Noncanonical Amino Acid Tagging (BONCAT). *PROTEOMICS* **2012**, *12* (15–16), 2464–2476. https://doi.org/10.1002/pmic.201200112.

(41) Bowling, H.; Bhattacharya, A.; Zhang, G.; Lebowitz, J. Z.; Alam, D.; Smith, P. T.; Kirshenbaum, K.; Neubert, T. A.; Vogel, C.; Chao, M. V.; Klann, E. BONLAC: A Combinatorial Proteomic Technique to Measure Stimulus-Induced Translational Profiles in Brain Slices. *Neuropharmacology* **2016**, *100*, 76–89. https://doi.org/10.1016/j.neuropharm.2015.07.017.

(42) Baron, D. M.; Matheny, T.; Lin, Y.-C.; Leszyk, J. D.; Kenna, K.; Gall, K. V.; Santos, D. P.; Tischbein, M.; Funes, S.; Hayward, L. J.; Kiskinis, E.; Landers, J. E.; Parker, R.; Shaffer, S. A.; Bosco, D. A. Quantitative Proteomics Identifies Proteins That Resist Translational Repression and Become Dysregulated in ALS-FUS. *Hum. Mol. Genet.* **2019**, *28* (13), 2143–2160. https://doi.org/10.1093/hmg/ddz048.

(43) Shin, J.; Rhim, J.; Kwon, Y.; Choi, S. Y.; Shin, S.; Ha, C.-W.; Lee, C. Comparative Analysis of Differentially Secreted Proteins in Serum-Free and Serum-Containing Media by Using BONCAT and Pulsed SILAC. *Sci. Rep.* **2019**, *9* (1), 3096. https://doi.org/10.1038/s41598-019-39650-z.

(44) Sridharan, D.; Dougherty, J. A.; Ahmed, U.; Sanghvi, S. K.; Alvi, S. B.; Park, K. H.; Islam, H.; Knoblaugh, S. E.; Singh, H.; Kirby, E. D.; Khan, M. Bioorthogonal Non-Canonical Amino Acid Tagging to Track Transplanted Human Induced Pluripotent Stem Cell-Specific Proteome. *Stem Cell Res. Ther.* **2024**, *15* (1), 186. https://doi.org/10.1186/s13287-024-03792-3.

(45) Glenn, W. S.; Stone, S. E.; Ho, S. H.; Sweredoski, M. J.; Moradian, A.; Hess, S.; Bailey-Serres, J.; Tirrell, D. A. Bioorthogonal Noncanonical Amino Acid Tagging (BONCAT) Enables Time-Resolved Analysis of Protein Synthesis in Native Plant Tissue. *Plant Physiol.* **2017**, *173* (3), 1543–1553. https://doi.org/10.1104/pp.16.01762.

(46) Liang, V.; Ullrich, M.; Lam, H.; Chew, Y. L.; Banister, S.; Song, X.; Zaw, T.; Kassiou, M.; Götz, J.; Nicholas, H. R. Altered Proteostasis in Aging and Heat Shock Response in C. Elegans Revealed by Analysis of the Global and de Novo Synthesized Proteome. *Cell. Mol. Life Sci.* **2014**, *71* (17), 3339–3361. https://doi.org/10.1007/s00018-014-1558-7.

(47) Yuet, K. P.; Doma, M. K.; Ngo, J. T.; Sweredoski, M. J.; Graham, R. L. J.; Moradian, A.; Hess, S.; Schuman, E. M.; Sternberg, P. W.; Tirrell, D. A. Cell-Specific Proteomic Analysis in Caenorhabditis Elegans. *Proc. Natl. Acad. Sci.* **2015**, *112* (9), 2705–2710. https://doi.org/10.1073/pnas.1421567112.

(48) Aburaya, S.; Yamauchi, Y.; Hashimoto, T.; Minakuchi, H.; Aoki, W.; Ueda, M. Neuronal Subclass-Selective Proteomic Analysis in Caenorhabditis Elegans. *Sci. Rep.* **2020**, *10* (1), 13840. https://doi.org/10.1038/s41598-020-70692-w.

(49) Shen, W.; Liu, H.-H.; Schiapparelli, L.; McClatchy, D.; He, H.; Yates, J. R.; Cline, H. T. Acute Synthesis of CPEB Is Required for Plasticity of Visual Avoidance Behavior in *Xenopus*. *Cell Rep.* **2014**, *6* (4), 737–747. https://doi.org/10.1016/j.celrep.2014.01.024.

(50) Liu, H.-H.; McClatchy, D. B.; Schiapparelli, L.; Shen, W.; Yates, J. R., III; Cline, H. T. Role of the Visual Experience-Dependent Nascent Proteome in Neuronal Plasticity. *eLife* **2018**, *7*, e33420. https://doi.org/10.7554/eLife.33420.

(51) McClatchy, D. B.; Ma, Y.; Liu, C.; Stein, B. D.; Martínez-Bartolomé, S.; Vasquez, D.; Hellberg, K.; Shaw, R. J.; Yates, J. R. Pulsed Azidohomoalanine Labeling in Mammals (PALM) Detects Changes in Liver-Specific LKB1 Knockout Mice. *J. Proteome Res.* **2015**, *14* (11), 4815–4822. https://doi.org/10.1021/acs.jproteome.5b00653.

(52) Calve, S.; Witten, A. J.; Ocken, A. R.; Kinzer-Ursem, T. L. Incorporation of Non-Canonical Amino Acids into the Developing Murine Proteome. *Sci. Rep.* **2016**, *6* (1), 32377. https://doi.org/10.1038/srep32377.

(53) Alvarez-Castelao, B.; Schanzenbächer, C. T.; Langer, J. D.; Schuman, E. M. Cell-Type-Specific Metabolic Labeling, Detection and Identification of Nascent Proteomes in Vivo. *Nat. Protoc.* **2019**, *14* (2), 556–575. https://doi.org/10.1038/s41596-018-0106-6.

(54) Evans, H. T.; Bodea, L.-G.; Götz, J. Cell-Specific Non-Canonical Amino Acid Labelling Identifies Changes in the de Novo Proteome during Memory Formation. *eLife* **2020**, *9*, e52990. https://doi.org/10.7554/eLife.52990.

(55) Oikonomou, G.; Prober, D. A. Attacking Sleep from a New Angle: Contributions from Zebrafish. *Curr. Opin. Neurobiol.* **2017**, *44*, 80–88. https://doi.org/10.1016/j.conb.2017.03.009.

(56) Tran, S.; Prober, D. A. Methods to Study Sleep in Zebrafish. In *Circadian Clocks*; Hirota, T., Hatori, M., Panda, S., Eds.; Springer US: New York, NY, 2022; pp 259–286. https://doi.org/10.1007/978-1-0716-2577-4_12.

(57) Jesuthasan, S. Fear, Anxiety, and Control in the Zebrafish. *Dev. Neurobiol.* **2012**, *72* (3), 395–403. https://doi.org/10.1002/dneu.20873.

(58) Ro, Y.; Noronha, M.; Mirza, B.; Ansari, R.; Gerlai, R. The Tapping Assay: A Simple Method to Induce Fear Responses in Zebrafish. *Behav. Res. Methods* **2022**, *54* (6), 2693–2706. https://doi.org/10.3758/s13428-021-01753-9.

(59) Santos, L. W.; Canzian, J.; Resmim, C. M.; Fontana, B. D.; Rosemberg, D. B. Contextual Fear Conditioning in Zebrafish: Influence of Different Shock Frequencies, Context, and Pharmacological Modulation on Behavior. *Neurobiol. Learn. Mem.* **2024**, *214*, 107963. https://doi.org/10.1016/j.nlm.2024.107963.

(60) Dreosti, E.; Lopes, G.; Kampff, A. R.; Wilson, S. W. Development of Social Behavior in Young Zebrafish. *Front. Neural Circuits* **2015**, *9*. https://doi.org/10.3389/fncir.2015.00039.

(61) Ogi, A.; Licitra, R.; Naef, V.; Marchese, M.; Fronte, B.; Gazzano, A.; Santorelli, F. M. Social Preference Tests in Zebrafish: A Systematic Review. *Front. Vet. Sci.* **2021**, *7*. https://doi.org/10.3389/fvets.2020.590057.

(62) Rea, V.; Van Raay, T. J. Using Zebrafish to Model Autism Spectrum Disorder: A Comparison of ASD Risk Genes Between Zebrafish and Their Mammalian Counterparts. *Front. Mol. Neurosci.* **2020**, *13*. https://doi.org/10.3389/fnmol.2020.575575.

(63) Tayanloo-Beik, A.; Hamidpour, S. K.; Abedi, M.; Shojaei, H.; Tavirani, M. R.; Namazi, N.; Larijani, B.; Arjmand, B. Zebrafish Modeling of Autism Spectrum Disorders, Current Status and Future Prospective. *Front. Psychiatry* **2022**, *13*. https://doi.org/10.3389/fpsyt.2022.911770.

(64) Roberts, A. C.; Bill, B. R.; Glanzman, D. L. Learning and Memory in Zebrafish Larvae. *Front. Neural Circuits* **2013**, *7*. https://doi.org/10.3389/fncir.2013.00126.

(65) Tan, J. K.; Nazar, F. H.; Makpol, S.; Teoh, S. L. Zebrafish: A Pharmacological Model for Learning and Memory Research. *Molecules* **2022**, *27* (21), 7374. https://doi.org/10.3390/molecules27217374.

(66) Reemst, K.; Shahin, H.; Shahar, O. D. Learning and Memory Formation in Zebrafish: Protein Dynamics and Molecular Tools. *Front. Cell Dev. Biol.* **2023**, *11*. https://doi.org/10.3389/fcell.2023.1120984.

(67) Darrow, K. O.; Harris, W. A. Characterization and Development of Courtship in Zebrafish, Danio Rerio. *Zebrafish* **2004**, *1* (1), 40–45. https://doi.org/10.1089/154585404774101662.

(68) Ninkovic, J.; Bally-Cuif, L. The Zebrafish as a Model System for Assessing the Reinforcing Properties of Drugs of Abuse. *Methods* **2006**, *39* (3), 262–274. https://doi.org/10.1016/j.ymeth.2005.12.007.

(69) Marques, J. C.; Li, M.; Schaak, D.; Robson, D. N.; Li, J. M. Internal State Dynamics Shape Brainwide Activity and Foraging Behaviour. *Nature* **2020**, *577* (7789), 239–243. https://doi.org/10.1038/s41586-019-1858-z.

(70) Prober, D. A.; Rihel, J.; Onah, A. A.; Sung, R.-J.; Schier, A. F. Hypocretin/Orexin Overexpression Induces An Insomnia-Like Phenotype in Zebrafish. *J. Neurosci.* **2006**, *26* (51), 13400–13410. https://doi.org/10.1523/JNEUROSCI.4332-06.2006.

(71) Clift, D.; Richendrfer, H.; Thorn, R. J.; Colwill, R. M.; Creton, R. High-Throughput Analysis of Behavior in Zebrafish Larvae: Effects of Feeding. *Zebrafish* **2014**, *11* (5), 455–461. https://doi.org/10.1089/zeb.2014.0989.

(72) Lee, D. A.; Oikonomou, G.; Prober, D. A. Large-Scale Analysis of Sleep in Zebrafish. *Bio-Protoc.* **2022**, *12* (3), e4313. https://doi.org/10.21769/BioProtoc.4313.

(73) Ahrens, M. B.; Li, J. M.; Orger, M. B.; Robson, D. N.; Schier, A. F.; Engert, F.; Portugues, R. Brain-Wide Neuronal Dynamics during Motor Adaptation in Zebrafish. *Nature* **2012**, *485* (7399), 471–477. https://doi.org/10.1038/nature11057.

(74) Leung, L. C.; Wang, G. X.; Madelaine, R.; Skariah, G.; Kawakami, K.; Deisseroth, K.; Urban, A. E.; Mourrain, P. Neural Signatures of Sleep in Zebrafish. *Nature* **2019**, *571* (7764), 198–204. https://doi.org/10.1038/s41586-019-1336-7.

(75) Hinz, F. I.; Dieterich, D. C.; Tirrell, D. A.; Schuman, E. M. Noncanonical Amino Acid Labeling in Vivo to Visualize and Affinity Purify Newly Synthesized Proteins in Larval Zebrafish. *ACS Chem. Neurosci.* **2012**, *3* (1), 40–49. https://doi.org/10.1021/cn2000876.

(76) Shahar, O. D.; Schuman, E. M. Large-Scale Cell-Type-Specific Imaging of Protein Synthesis in a Vertebrate Brain. *eLife* **2020**, *9*, e50564. https://doi.org/10.7554/eLife.50564.

(77) Rousseeuw, P. J. Silhouettes: A Graphical Aid to the Interpretation and Validation of Cluster Analysis. *J. Comput. Appl. Math.* **1987**, *20*, 53–65. https://doi.org/10.1016/0377-0427(87)90125-7.

(78) Mao, L.; Bryantsev, A. L.; Chechenova, M. B.; Shelden, E. A. Cloning, Characterization, and Heat Stress-Induced Redistribution of a Protein Homologous to Human Hsp27 in the Zebrafish *Danio Rerio*. *Exp. Cell Res.* **2005**, *306* (1), 230–241. https://doi.org/10.1016/j.yexcr.2005.02.007.

(79) Lam, P.; Harvie, E. A.; Huttenlocher, A. Heat Shock Modulates Neutrophil Motility in Zebrafish. *PLOS ONE* **2013**, *8* (12), e84436. https://doi.org/10.1371/journal.pone.0084436.

(80) Wang, C.; Chen, X.; Dai, Y.; Zhang, Y.; Sun, Y.; Cui, X. Comparative Transcriptome Analysis of Heat-Induced Domesticated Zebrafish during Gonadal Differentiation. *BMC Genomic Data* **2022**, *23* (1), 39. https://doi.org/10.1186/s12863-022-01058-6.

(81) Heldens, L.; Dirks, R. P.; Hensen, S. M. M.; Onnekink, C.; van Genesen, S. T.; Rustenburg, F.; Lubsen, N. H. Co-Chaperones Are Limiting in a Depleted Chaperone Network. *Cell. Mol. Life Sci.* **2010**, *67* (23), 4035–4048. https://doi.org/10.1007/s00018-010-0430-7.

(82) Gong, L.; Zhang, Q.; Pan, X.; Chen, S.; Yang, L.; Liu, B.; Yang, W.; Yu, L.; Xiao, Z.-X.; Feng, X.-H.; Wang, H.; Yuan, Z.-M.; Peng, J.; Tan, W.-Q.; Chen, J. P53 Protects Cells from Death at the Heatstroke Threshold Temperature. *Cell Rep.* **2019**, *29* (11), 3693-3707.e5. https://doi.org/10.1016/j.celrep.2019.11.032.

(83) Xu, K.; Xu, H.; Han, Z. Genome-Wide Identification of Hsp70 Genes in the Large Yellow Croaker (Larimichthys Crocea) and Their Regulated Expression Under Cold and Heat Stress. *Genes* **2018**, *9* (12), 590. https://doi.org/10.3390/genes9120590.

(84) Scieglinska, D.; Krawczyk, Z. Expression, Function, and Regulation of the Testis-Enriched Heat Shock *HSPA2* Gene in Rodents and Humans. *Cell Stress Chaperones* **2015**, *20* (2), 221–235. https://doi.org/10.1007/s12192-014-0548-x.

(85) Jerônimo, R.; Moraes, M. N.; de Assis, L. V. M.; Ramos, B. C.; Rocha, T.; Castrucci, A. M. de L. Thermal Stress in *Danio Rerio*: A Link between Temperature, Light, Thermo-TRP Channels, and Clock Genes. *J. Therm. Biol.* **2017**, *68*, 128–138. https://doi.org/10.1016/j.jtherbio.2017.02.009.

(86) Murtha, J. M.; Keller, E. T. Characterization of the Heat Shock Response in Mature Zebrafish (*Danio Rerio*). *Exp. Gerontol.* **2003**, *38* (6), 683–691. https://doi.org/10.1016/S0531-5565(03)00067-6.

(87) Murray, J. I.; Whitfield, M. L.; Trinklein, N. D.; Myers, R. M.; Brown, P. O.; Botstein, D. Diverse and Specific Gene Expression Responses to Stresses in Cultured Human Cells. *Mol. Biol. Cell* **2004**, *15* (5), 2361–2374. https://doi.org/10.1091/mbc.e03-11-0799.

(88) Marvin, M.; O'Rourke, D.; Kurihara, T.; Juliano, C. E.; Harrison, K. L.; Hutson, L. D. Developmental Expression Patterns of the Zebrafish Small Heat Shock Proteins. *Dev. Dyn.* **2008**, *237* (2), 454–463. https://doi.org/10.1002/dvdy.21414.

(89) Elicker, K. S.; Hutson, L. D. Genome-Wide Analysis and Expression Profiling of the Small Heat Shock Proteins in Zebrafish. *Gene* **2007**, *403* (1), 60–69. https://doi.org/10.1016/j.gene.2007.08.003.

(90) Krone, P. H.; Sass, J. B. Hsp 90α and Hsp 90β Genes Are Present in the Zebrafish and Are Differentially Regulated in Developing Embryos. *Biochem. Biophys. Res. Commun.* **1994**, *204* (2), 746–752. https://doi.org/10.1006/bbrc.1994.2522.

(91) Krone, P. H.; Lele, Z.; Sass, J. B. Heat Shock Genes and the Heat Shock Response in Zebrafish Embryos. *Biochem. Cell Biol. Biochim. Biol. Cell.* **1997**, *75* (5), 487–497.

(92) Du, S. J.; Li, H.; Bian, Y.; Zhong, Y. Heat-Shock Protein 90α1 Is Required for Organized Myofibril Assembly in Skeletal Muscles of Zebrafish Embryos. *Proc. Natl. Acad. Sci.* **2008**, *105* (2), 554–559. https://doi.org/10.1073/pnas.0707330105.

(93) Etard, C.; Behra, M.; Fischer, N.; Hutcheson, D.; Geisler, R.; Strähle, U. The UCS Factor Steif/Unc-45b Interacts with the Heat Shock Protein Hsp90a during Myofibrillogenesis. *Dev. Biol.* **2007**, *308* (1), 133–143. https://doi.org/10.1016/j.ydbio.2007.05.014.

(94) Rudeck, S.; Etard, C.; Khan, M. M.; Rottbauer, W.; Rudolf, R.; Strähle, U.; Just, S. A Compact Unc45b-Promoter Drives Muscle-Specific Expression in Zebrafish and Mouse. *genesis* **2016**, *54* (8), 431–438. https://doi.org/10.1002/dvg.22953.

(95) Yunoki, T.; Kariya, A.; Kondo, T.; Hayashi, A.; Tabuchi, Y. Gene Expression Analysis of Heat Shock Protein A Family Members Responsive to Hyperthermic Treatments in Normal Human Fibroblastic Cells. *Therm. Med.* **2012**, *28* (4), 73–85. https://doi.org/10.3191/thermalmed.28.73.

(96) Santacruz, H.; Vriz, S.; Angelier, N. Molecular Characterization of a Heat Shock Cognate cDNA of Zebrafish, Hsc70, and Developmental Expression of the Corresponding Transcripts. *Dev. Genet.* **1997**, *21* (3), 223–233. https://doi.org/10.1002/(SICI)1520-6408(1997)21:3<223::AID-DVG5>3.0.CO;2-9.

(97) Graser, R. T.; Malnar-Dragojevic, D.; Vincek, V. Cloning and Characterization of a 70 Kd Heat Shock Cognate (Hsc70) Gene from the Zebrafish (Danio Rerio). *Genetica* **1996**, *98* (3), 273–276. https://doi.org/10.1007/BF00057591.

(98) Cabezas-Sainz, P.; Coppel, C.; Pensado-López, A.; Fernandez, P.; Muinelo-Romay, L.; López-López, R.; Rubiolo, J. A.; Sánchez, L. Morphological Abnormalities and Gene Expression Changes Caused by High Incubation Temperatures in Zebrafish Xenografts with Human Cancer Cells. *Genes* **2021**, *12* (1), 113. https://doi.org/10.3390/genes12010113.

(99) Scott, G. R.; Johnston, I. A. Temperature during Embryonic Development Has Persistent Effects on Thermal Acclimation Capacity in Zebrafish. *Proc. Natl. Acad. Sci.* **2012**, *109* (35), 14247–14252. https://doi.org/10.1073/pnas.1205012109.

(100) Cristofre Martin, C.; Tang, P.; Barnardo, G.; Krone, P. H. Expression of the Chaperonin 10 Gene during Zebrafish Development. *Cell Stress Chaperones* **2001**, *6* (1), 38–43.

(101) Martin, C. C.; Tsang, C. H.; Beiko, R. G.; Krone, P. H. Expression and Genomic Organization of the Zebrafish Chaperonin Gene Complex. *Genome* **2002**, *45* (5), 804–811. https://doi.org/10.1139/g02-044.

(102) Sánchez-Vicente, I.; Lorenzo, O. Nitric Oxide Regulation of Temperature Acclimation: A Molecular Genetic Perspective. *J. Exp. Bot.* **2021**, *72* (16), 5789–5794. https://doi.org/10.1093/jxb/erab049.

(103) He, N.-Y.; Chen, L.-S.; Sun, A.-Z.; Zhao, Y.; Yin, S.-N.; Guo, F.-Q. A Nitric Oxide Burst at the Shoot Apex Triggers a Heat-Responsive Pathway in Arabidopsis. *Nat. Plants* **2022**, *8* (4), 434–450. https://doi.org/10.1038/s41477-022-01135-9.

(104) Demple, B. Signal Transduction by Nitric Oxide in Cellular Stress Responses. *Mol. Cell. Biochem.* **2002**, *234–235* (1–2), 11–18.

(105) Matsumoto, H.; Hayashi, S.; Hatashita, M.; Ohnishi, K.; Ohtsubo, T.; Kitai, R.; Shioura, H.; Ohnishi, T.; Kano, E. Nitric Oxide Is an Initiator of Intercellular Signal Transduction for Stress Response after Hyperthermia in Mutant P53 Cells of Human Glioblastoma. *Cancer Res.* **1999**, *59* (13), 3239–3244.

(106) Xu, W.; Liu, L.; Charles, I. G.; Moncada, S. Nitric Oxide Induces Coupling of Mitochondrial Signalling with the Endoplasmic Reticulum Stress Response. *Nat. Cell Biol.* **2004**, *6* (11), 1129–1134. https://doi.org/10.1038/ncb1188.

(107) Serra, M.; Saba, J. D. Sphingosine 1-Phosphate Lyase, a Key Regulator of Sphingosine 1-Phosphate Signaling and Function. *Adv. Enzyme Regul.* **2010**, *50* (1), 349–362. https://doi.org/10.1016/j.advenzreg.2009.10.024.

(108) Fyrst, H.; Saba, J. D. Sphingosine-1-Phosphate Lyase in Development and Disease: Sphingolipid Metabolism Takes Flight. *Biochim. Biophys. Acta BBA - Mol. Cell Biol. Lipids* **2008**, *1781* (9), 448–458. https://doi.org/10.1016/j.bbalip.2008.05.005.

(109) Xiao, S.; Peng, K.; Li, C.; Long, Y.; Yu, Q. The Role of Sphingosine-1-Phosphate in Autophagy and Related Disorders. *Cell Death Discov.* **2023**, *9* (1), 1–14. https://doi.org/10.1038/s41420-023-01681-x.

(110) Arya, R.; Mallik, M.; Lakhotia, S. C. Heat Shock Genes — Integrating Cell Survival and Death. *J. Biosci.* **2007**, *32* (3), 595–610. https://doi.org/10.1007/s12038-007-0059-3.

(111) Gu, Z. T.; Wang, H.; Li, L.; Liu, Y. S.; Deng, X. B.; Huo, S. F.; Yuan, F. F.; Liu, Z. F.; Tong, H. S.; Su, L. Heat Stress Induces Apoptosis through Transcription-Independent P53-Mediated Mitochondrial Pathways in Human Umbilical Vein Endothelial Cell. *Sci. Rep.* **2014**, *4* (1), 4469. https://doi.org/10.1038/srep04469.

(112) Oghbaei, H.; Hosseini, L.; Farajdokht, F.; Rahigh Aghsan, S.; Majdi, A.; Sadigh-Eteghad, S.; Sandoghchian Shotorbani, S.; Mahmoudi, J. Heat Stress Aggravates Oxidative Stress, Apoptosis, and Endoplasmic Reticulum Stress in the Cerebellum of Male C57 Mice. *Mol. Biol. Rep.* **2021**, *48* (8), 5881–5887. https://doi.org/10.1007/s11033-021-06582-9.

(113) Gillespie, C. S.; Sherman, D. L.; Blair, G. E.; Brophy, P. J. Periaxin, a Novel Protein of Myelinating Schwann Cells with a Possible Role in Axonal Ensheathment. *Neuron* **1994**, *12* (3), 497–508. https://doi.org/10.1016/0896-6273(94)90208-9.

(114) Scherer, S. S.; Xu, Y.; Bannerman, P. G. C.; Sherman, D. L.; Brophy, P. J. Periaxin Expression in Myelinating Schwann Cells: Modulation by Axon-Glial Interactions and Polarized Localization during Development. *Development* **1995**, *121* (12), 4265–4273. https://doi.org/10.1242/dev.121.12.4265.

(115) Kijima, K.; Numakura, C.; Shirahata, E.; Sawaishi, Y.; Shimohata, M.; Igarashi, S.; Tanaka, T.; Hayasaka, K. Periaxin Mutation Causes Early-Onset but Slow-Progressive Charcot-Marie-Tooth Disease. *J. Hum. Genet.* **2004**, *49* (7), 376–379. https://doi.org/10.1007/s10038-004-0162-3.

(116) Krecic, A. M.; Swanson, M. S. hnRNP Complexes: Composition, Structure, and Function. *Curr. Opin. Cell Biol.* **1999**, *11* (3), 363–371. https://doi.org/10.1016/S0955-0674(99)80051-9.

(117) Geuens, T.; Bouhy, D.; Timmerman, V. The hnRNP Family: Insights into Their Role in Health and Disease. *Hum. Genet.* **2016**, *135* (8), 851–867. https://doi.org/10.1007/s00439-016-1683-5.

(118) Kwon, Y. S.; Park, C.-B.; Lee, S.-M.; Zee, S.; Kim, G.-E.; Kim, Y.-J.; Sim, H.-J.; Kim, J.-H.; Seo, J.-S. Proteomic Analysis of Zebrafish (Danio Rerio) Embryos Exposed to Benzyl Benzoate. *Environ. Sci. Pollut. Res.* **2023**, *30* (10), 26375–26386. https://doi.org/10.1007/s11356-022-24081-7.

(119) Purushothaman, S.; Saxena, S.; Meghah, V.; Lakshmi, M. G. M.; Singh, S. K.; Swamy, C. V. B.; Idris, M. M. Proteomic and Gene Expression Analysis of Zebrafish Brain Undergoing Continuous Light/Dark Stress. *J. Sleep Res.* **2015**, *24* (4), 458–465. https://doi.org/10.1111/jsr.12287.

(120) Lucitt, M. B.; Price, T. S.; Pizarro, A.; Wu, W.; Yocum, A. K.; Seiler, C.; Pack, M. A.; Blair, I. A.; FitzGerald, G. A.; Grosser, T. Analysis of the Zebrafish Proteome during Embryonic Development*. *Mol. Cell. Proteomics* **2008**, *7* (5), 981–994. https://doi.org/10.1074/mcp.M700382-MCP200.

(121) Kwon, O. K.; Kim, S. J.; Lee, Y.-M.; Lee, Y.-H.; Bae, Y.-S.; Kim, J. Y.; Peng, X.; Cheng, Z.; Zhao, Y.; Lee, S. Global Analysis of Phosphoproteome Dynamics in Embryonic Development of Zebrafish (Danio Rerio). *PROTEOMICS* **2016**, *16* (1), 136–149. https://doi.org/10.1002/pmic.201500017.

(122) Banu, S.; Gaur, N.; Nair, S.; Ravikrishnan, T.; Khan, S.; Mani, S.; Bharathi, S.; Mandal, K.; Kuram, N. A.; Vuppaladadium, S.; Ravi, R.; Murthy, Ch. L. N.; Quoseena, M.; Babu, N. S.; Idris, M. M. Understanding the Complexity of Epimorphic Regeneration in Zebrafish Caudal Fin Tissue: A Transcriptomic and Proteomic Approach. *Genomics* **2022**, *114* (2), 110300. https://doi.org/10.1016/j.ygeno.2022.110300.

(123) Li, C.; Tan, X. F.; Lim, T. K.; Lin, Q.; Gong, Z. Comprehensive and Quantitative Proteomic Analyses of Zebrafish Plasma Reveals Conserved Protein Profiles between Genders and between Zebrafish and Human. *Sci. Rep.* **2016**, *6* (1), 24329. https://doi.org/10.1038/srep24329.

(124) Wang, N.; MacKenzie, L.; De Souza, A. G.; Zhong, H.; Goss, G.; Li, L. Proteome Profile of Cytosolic Component of Zebrafish Liver Generated by LC−ESI MS/MS Combined with Trypsin Digestion and Microwave-Assisted Acid Hydrolysis. *J. Proteome Res.* **2007**, *6* (1), 263–272. https://doi.org/10.1021/pr060367o.

(125) Lößner, C.; Wee, S.; Ler, S. G.; Li, R. H. X.; Carney, T.; Blackstock, W.; Gunaratne, J. Expanding the Zebrafish Embryo Proteome Using Multiple Fractionation Approaches and Tandem Mass Spectrometry. *PROTEOMICS* **2012**, *12* (11), 1879–1882. https://doi.org/10.1002/pmic.201100576.

(126) Alli Shaik, A.; Wee, S.; Li, R. H. X.; Li, Z.; Carney, T. J.; Mathavan, S.; Gunaratne, J. Functional Mapping of the Zebrafish Early Embryo Proteome and Transcriptome. *J. Proteome Res.* **2014**, *13* (12), 5536–5550. https://doi.org/10.1021/pr5005136.

(127) Tay, T. L.; Lin, Q.; Seow, T. K.; Tan, K. H.; Hew, C. L.; Gong, Z. Proteomic Analysis of Protein Profiles during Early Development of the Zebrafish,. *PROTEOMICS* **2006**, *6* (10), 3176–3188. https://doi.org/10.1002/pmic.200600030.

(128) Singh, S. K.; Sundaram, C. S.; Shanbhag, S.; Idris, M. M. Proteomic Profile of Zebrafish Brain Based on Two-Dimensional Gel Electrophoresis Matrix-Assisted Laser Desorption/Ionization MS/MS Analysis. *Zebrafish* **2010**, *7* (2), 169–177. https://doi.org/10.1089/zeb.2010.0657.

(129) Levesque, K. D.; Wright, P. A.; Bernier, N. J. Cross Talk without Cross Tolerance: Effect of Rearing Temperature on the Hypoxia Response of Embryonic Zebrafish. *Physiol. Biochem. Zool.* **2019**, *92* (4), 349–364. https://doi.org/10.1086/703178.

(130) Long, Y.; Li, L.; Li, Q.; He, X.; Cui, Z. Transcriptomic Characterization of Temperature Stress Responses in Larval Zebrafish. *PLOS ONE* **2012**, *7* (5), e37209. https://doi.org/10.1371/journal.pone.0037209.

(131) Ho, T.-N.; Paul, G. V.; Chen, Y.-H.; Hsu, T. Heat Stress Upregulates G-T Mismatch Binding Activities in Zebrafish (*Danio Rerio*) Embryos Preexposed and Nonexposed to a Sublethal Level of Cadmium (Cd). *Chemosphere* **2019**, *218*, 179–188. https://doi.org/10.1016/j.chemosphere.2018.11.038.

(132) Shoji, W.; Sato-Maeda, M. Application of Heat Shock Promoter in Transgenic Zebrafish. *DGD* **2008**, *50* (6), 401–406. https://doi.org/10.1111/j.1440-169X.2008.01038.x.

(133) de Alba, G.; López-Olmeda, J. F.; Sánchez-Vázquez, F. J. Rearing Temperature Conditions (Constant *vs.* Thermocycle) Affect Daily Rhythms of Thermal Tolerance and Sensing in Zebrafish. *J. Therm. Biol.* **2021**, *97*, 102880. https://doi.org/10.1016/j.jtherbio.2021.102880.

(134) Bazzini, A. A.; Lee, M. T.; Giraldez, A. J. Ribosome Profiling Shows That miR-430 Reduces Translation Before Causing mRNA Decay in Zebrafish. *Science* **2012**, *336* (6078), 233–237. https://doi.org/10.1126/science.1215704.

(135) Matern, M. S.; Beirl, A.; Ogawa, Y.; Song, Y.; Paladugu, N.; Kindt, K. S.; Hertzano, R. Transcriptomic Profiling of Zebrafish Hair Cells Using RiboTag. *Front. Cell Dev. Biol.* **2018**, *6*. https://doi.org/10.3389/fcell.2018.00047.

(136) Westman-Brinkmalm, A.; Abramsson, A.; Pannee, J.; Gang, C.; Gustavsson, M. K.; von Otter, M.; Blennow, K.; Brinkmalm, G.; Heumann, H.; Zetterberg, H. SILAC

Zebrafish for Quantitative Analysis of Protein Turnover and Tissue Regeneration. *J. Proteomics* **2011**, *75* (2), 425–434. https://doi.org/10.1016/j.jprot.2011.08.008.

(137) Nolte, H.; Konzer, A.; Ruhs, A.; Jungblut, B.; Braun, T.; Krüger, M. Global Protein Expression Profiling of Zebrafish Organs Based on in Vivo Incorporation of Stable Isotopes. *J. Proteome Res.* **2014**, *13* (4), 2162–2174. https://doi.org/10.1021/pr5000335.

(138) Konzer, A.; Ruhs, A.; Braun, H.; Jungblut, B.; Braun, T.; Krüger, M. Stable Isotope Labeling in Zebrafish Allows in Vivo Monitoring of Cardiac Morphogenesis. *Mol. Cell. Proteomics* **2013**, *12* (6), 1502–1512. https://doi.org/10.1074/mcp.M111.015594.

(139) Nolte, H.; Hölper, S.; Housley, M. P.; Islam, S.; Piller, T.; Konzer, A.; Stainier, D. Y. R.; Braun, T.; Krüger, M. Dynamics of Zebrafish Fin Regeneration Using a Pulsed SILAC Approach. *PROTEOMICS* **2015**, *15* (4), 739–751. https://doi.org/10.1002/pmic.201400316.

(140) Lee, D. A.; Andreev, A.; Truong, T. V.; Chen, A.; Hill, A. J.; Oikonomou, G.; Pham, U.; Hong, Y. K.; Tran, S.; Glass, L.; Sapin, V.; Engle, J.; Fraser, S. E.; Prober, D. A. Genetic and Neuronal Regulation of Sleep by Neuropeptide VF. *eLife* **2017**, *6*, e25727. https://doi.org/10.7554/eLife.25727.

(141) Perez-Riverol, Y.; Bandla, C.; Kundu, D. J.; Kamatchinathan, S.; Bai, J.; Hewapathirana, S.; John, N. S.; Prakash, A.; Walzer, M.; Wang, S.; Vizcaíno, J. A. The PRIDE Database at 20 Years: 2025 Update. *Nucleic Acids Res.* **2025**, *53* (D1), D543–D553. https://doi.org/10.1093/nar/gkae1011.

(142) Jones, J.; MacKrell, E. J.; Wang, T.-Y.; Lomenick, B.; Roukes, M. L.; Chou, T.-F. Tidyproteomics: An Open-Source R Package and Data Object for Quantitative Proteomics Post Analysis and Visualization. *BMC Bioinformatics* **2023**, *24* (1), 239. https://doi.org/10.1186/s12859-023-05360-7.

(143) Korotkevich, G.; Sukhov, V.; Budin, N.; Shpak, B.; Artyomov, M. N.; Sergushichev, A. Fast Gene Set Enrichment Analysis. bioRxiv February 1, 2021, p 060012. https://doi.org/10.1101/060012.

(144) Mao, L.; Shelden, E. A. Developmentally Regulated Gene Expression of the Small Heat Shock Protein Hsp27 in Zebrafish Embryos. *Gene Expr. Patterns* **2006**, *6* (2), 127–133. https://doi.org/10.1016/j.modgep.2005.07.002.

(145) Wu, Y. L.; Pan, X.; Mudumana, S. P.; Wang, H.; Kee, P. W.; Gong, Z. Development of a Heat Shock Inducible *Gfp* Transgenic Zebrafish Line by Using the Zebrafish *Hsp27* Promoter. *Gene* **2008**, *408* (1), 85–94. https://doi.org/10.1016/j.gene.2007.10.027.

(146) Xu, X.; Gupta, S.; Hu, W.; McGrath, B. C.; Cavener, D. R. Hyperthermia Induces the ER Stress Pathway. *PLOS ONE* **2011**, *6* (8), e23740. https://doi.org/10.1371/journal.pone.0023740.

(147) Xiao, H.; Wang, H.; He, Q.; Zhou, J.; Du, S. Gene Expression and Functional Analysis of Aha1a and Aha1b in Stress Response in Zebrafish. *Comp. Biochem. Physiol. B Biochem. Mol. Biol.* **2022**, *262*, 110777. https://doi.org/10.1016/j.cbpb.2022.110777.

(148) Das, S.; Bhattacharyya, N. P. Transcription Regulation of HYPK by Heat Shock Factor 1. *PLOS ONE* **2014**, *9* (1), e85552. https://doi.org/10.1371/journal.pone.0085552.

(149) Li, G.; Zhao, H.; Guo, H.; Wang, Y.; Cui, X.; Li, H.; Xu, B.; Guo, X. Analyses of the Function of DnaJ Family Proteins Reveal an Underlying Regulatory Mechanism of Heat Tolerance in Honeybee. *Sci. Total Environ.* **2020**, *716*, 137036. https://doi.org/10.1016/j.scitotenv.2020.137036.

(150) Srikanth, K.; Kwon, A.; Lee, E.; Chung, H. Characterization of Genes and Pathways That Respond to Heat Stress in Holstein Calves through Transcriptome Analysis. *Cell Stress Chaperones* **2017**, *22* (1), 29–42. https://doi.org/10.1007/s12192-016-0739-8.

(151) Han, C.; Chen, T.; Li, N.; Yang, M.; Wan, T.; Cao, X. HDJC9, a Novel Human Type C DnaJ/HSP40 Member Interacts with and Cochaperones HSP70 through the J Domain. *Biochem. Biophys. Res. Commun.* **2007**, *353* (2), 280–285. https://doi.org/10.1016/j.bbrc.2006.12.013.

(152) Pini, B.; Grosser, T.; Lawson, J. A.; Price, T. S.; Pack, M. A.; FitzGerald, G. A. Prostaglandin E Synthases in Zebrafish. *Arterioscler. Thromb. Vasc. Biol.* **2005**, *25* (2), 315–320. https://doi.org/10.1161/01.ATV.0000152355.97808.10.

(153) (Zhao, S.-J.; Guo, S.-N.; Zhu, Q.-L.; Yuan, S.-S.; Zheng, J.-L. Heat-Induced Oxidative Stress and Inflammation Involve in Cadmium Pollution History in the Spleen of Zebrafish. *Fish Shellfish Immunol.* **2018**, *72*, 1–8. https://doi.org/10.1016/j.fsi.2017.09.077.

(154) (Lim, M. Y.-T.; Bernier, N. J. Zebrafish Parental Progeny Investment in Response to Cycling Thermal Stress and Hypoxia: Deposition of Heat Shock Proteins but Not Cortisol. *J. Exp. Biol.* **2022**, *225* (21), jeb244715. https://doi.org/10.1242/jeb.244715.

(155) Eye-Specific Gene Expression Following Embryonic Ethanol Exposure in Zebrafish: Roles for Heat Shock Factor 1. *Reprod. Toxicol.* **2014**, *43*, 111–124. https://doi.org/10.1016/j.reprotox.2013.12.002.

(156) Yeh, F.-L.; Hsu, L.-Y.; Lin, B.-A.; Chen, C.-F.; Li, I.-C.; Tsai, S.-H.; Hsu, T. Cloning of Zebrafish (*Danio Rerio*) Heat Shock Factor 2 (HSF2) and Similar Patterns of HSF2 and HSF1 mRNA Expression in Brain Tissues. *Biochimie* **2006**, *88* (12), 1983–1988. https://doi.org/10.1016/j.biochi.2006.07.005.

Chapter III

TIME-RESOLVED PROTEOMIC ANALYSIS REVEALS CHANGES IN NEURONAL PROTEIN SYNTHESIS IN RESPONSE TO ANTIDEPRESSANT-LEVEL DOSES OF KETAMINE

3.1 Abstract

Major depressive disorder poses significant therapeutic challenges for patients, as traditional antidepressants are characterized by slow onset of action and limited effectiveness. Ketamine, a rapid-acting antidepressant, alleviates depressive symptoms within hours to days, yet the molecular basis of these rapid therapeutic effects remains poorly understood. Here, we employed bioorthogonal noncanonical amino acid tagging (BONCAT) coupled with mass spectrometry-based proteomics to investigate early changes in neuronal protein synthesis triggered by antidepressant-relevant doses of ketamine in primary embryonic rat cortical neuron cultures. Our BONCAT approach selectively captured azidohomoalanine (AHA)-labeled proteins synthesized within the first 24 hours of ketamine treatment, revealing a dose-dependent global increase in protein synthesis, with 91% and 68% of proteins displaying increased expression at 10 μM and 1 μM compared to controls, respectively. Differential expression analysis identified significant up- and down-regulated proteins associated with synaptic function and plasticity, cytoskeletal remodeling, cell signaling, metabolism, and RNA processing. In line with these results, functional enrichment analysis revealed that ketamine treatment induced significant alterations in pathway annotations related to synaptic processes, cytoskeletal proteins, and translation. These findings underscore BONCAT's ability to capture rapid, transient proteomic responses and illuminate early protein synthesis events triggered by low doses of ketamine, shedding light on the proteome dynamics underlying its rapid and sustained antidepressant effects.

3.2 Introduction

Major depressive disorder (MDD) is characterized by at least one extended episode involving changes in mood, interests, and cognition which significantly impact the mental and physical health of individuals diagnosed with the condition[1–3]. MDD is the second-most common cause of disability in the Unites States[4], and 1 in 6 individuals will experience MDD in their lifetime[5]. Given the high societal burden imposed by this disorder, developing treatment strategies is a top priority for the public health establishment.

Current first-line treatment regimens for MDD involve a class of medications known as selective serotonin reuptake inhibitors (SSRIs) which bind to reuptake transporters (SERT) for serotonin (5-HT) on serotonergic neurons[6–9]. While SSRIs have provided many patients with relief from depressive symptoms, 30-60% of MDD patients do not experience therapeutic effects from these drugs or eventually experience relapse in symptoms[10–14]. Furthermore, these compounds can give rise to unpleasant side effects, including sexual dysfunction, insomnia, nausea, fatigue, and weight gain from changes in appetite[15–17]. Perhaps most concerningly, even patients who do respond to SSRIs experience a "therapeutic lag" of 2-6 weeks before the drugs have a meaningful effect[18–21], a period that for some is accompanied by increased anxiety and risk of suicidality, particularly in adolescents[22,23].

In recent years, rapid-acting antidepressants (RAADs) have garnered considerable attention for their ability to alleviate depressive symptoms within hours to days[24–26]. Among the most widely studied of these RAADs, low, sub-dissociative doses of ketamine, an N-methyl-D-aspartate receptor (NMDAR) antagonist used for decades as a dissociative anesthetic, have demonstrated efficacy in MDD patients on a time scale much faster than SSRIs, with sustained effects lasting even after drug clearance[27–30]. This accelerated antidepressant effect is particularly beneficial for patients who are at high risk of self-harm or who have not responded to multiple rounds of conventional medications. These findings led to the approval of a nasal spray formulation of the *S*-enantiomer of ketamine (Spravato®, by Janssen Pharmaceuticals), approved by the FDA in 2019 for patients with treatment-resistant depression (TRD)[31]. While initially approved for use in conjunction with an oral

antidepressant, just this year, the FDA also approved its use as a standalone treatment, making it the first monotherapy for TRD.

Despite significant interest and clinical use, the mechanisms underlying ketamine's rapid antidepressant effects remain largely mysterious. Initially, ketamine was believed to exert its therapeutic effects through direct inhibition of NMDARs, particularly on GABAergic interneurons, leading to disinhibition and enhanced glutamatergic signaling[32,33]. This burst of activity is thought to trigger downstream signaling pathways, including mammalian target of rapamycin (mTOR)[34], brain-derived neurotrophic factor (BDNF)[35], and extracellular signal-regulated kinase (ERK)/mitogen-activated protein kinase (MAPK) cascades[36,37], which ultimately promote synaptogenesis and enhance synaptic plasticity[38,39]. Nevertheless, questions remain regarding which molecular and cellular pathways are altered by ketamine treatment, the temporal dynamics involved, and how these contribute to sustained antidepressant effects. A more complete understanding could pave the way for treatments that harness ketamine’s rapid antidepressant properties while minimizing its dissociative effects and the potential for abuse that can arise at higher doses[40–42].

Proteomic studies investigating ketamine's effects have begun to address some of these gaps. Previous proteomic analyses of cerebrospinal fluid (CSF), brain tissue, and neuronal cultures have identified ketamine-induced alterations in proteins and pathways associated with synaptic transmission, neuroplasticity, mitochondrial energy metabolism, immune responses, and oxidative stress[43–47]. Several of these studies specifically implicate changes in AMPA receptor signaling, mTOR-related pathways, and growth factor signaling cascades[44,47–49]. However, conventional proteomics approaches performed on whole lysates provide static snapshots of the proteome. The inability of these workflows to distinguish between proteins expressed before versus after ketamine exposure makes it challenging for them to capture rapid and transient changes that occur immediately after treatment. This temporal ambiguity is particularly problematic when studying a fast-acting compound like ketamine, whose effects are likely to evolve within hours of administration.

Time-resolved proteomic techniques that specifically isolate newly synthesized proteins offer a solution to this obstacle. By capturing changes in protein synthesis within defined time windows, these approaches can reveal early molecular events responsible initiating downstream therapeutic processes. One such technique is bioorthogonal noncanonical amino acid tagging (BONCAT)[50,51], which enables selective enrichment and identification of newly synthesized proteins via metabolic labeling with chemically modified amino acids. Most commonly, the azide-bearing methionine (Met) surrogate azidohomoalanine (AHA) is incorporated into newly synthesized proteins in competition with methionine after activation and charging by the host's endogenous methionyl-tRNA synthetase (MetRS). AHA-labeled proteins can then be affinity-purified via covalent attachment to alkyne-functionalized beads—either by a Cu(I)-catalyzed [3 + 2] azide-alkyne cycloaddition (CuAAC)[52,53], or by a strain-promoted [3 + 2] azide-alkyne cycloaddition (SPAAC)[54]—and subsequently identified using mass spectrometry[50,51]. Since azides and alkynes are rare in naturally occurring biological systems[55–57], the azide-alkyne "click" reaction is highly selective toward AHA-labeled proteins. Although depletion of methionine to maximize replacement by AHA can lead to altered protein abundances, competitive labeling at modest levels can be achieved without causing substantial disruption of the proteome [58]. Thus, by facilitating the separation of proteins expressed in response to drug treatment from pre-existing proteins, many of which are highly abundant and can obscure signal from newly synthesized proteins, BONCAT overcomes limitations of traditional proteomic methods. Indeed, BONCAT has been used to perform time-resolved proteomics in *in vitro* cultured neurons to examine transient changes in protein expression in response to a variety of pharmacological perturbations[59–63].

In this study, we used BONCAT to investigate the impact of antidepressant-relevant concentrations of ketamine on de novo protein synthesis in primary cortical neurons. By labeling, enriching, and analyzing proteins synthesized within the first 24 h of treatment, we uncovered significant and broad changes in the neuronal proteome induced by ketamine. Our data revealed a global increase in protein synthesis upon exposure to ketamine, as well as altered expression of proteins involved in synaptic plasticity, cytoskeletal remodeling, intra-

and intercellular signaling, metabolism, RNA processing, and translation. These findings shed new light on the molecular underpinnings of ketamine's antidepressant effects and illustrate the utility of BONCAT-based proteomics for investigating drug-dependent changes in the neuronal proteome.

3.3 Results and Discussion

BONCAT reveals ketamine-induced increase in neuronal protein synthesis

In order to investigate changes in neuronal protein expression underlying the rapid antidepressant effects of low doses of ketamine, primary embryonic rat cortical neurons were simultaneously treated with ketamine and AHA to label proteins synthesized during the first 24 h of treatment (Fig. 3.1). Choosing an appropriate *in vitro* concentration to elucidate ketamine's effects on neurons is not straightforward, as the actual concentration of ketamine experienced by its neuronal targets *in vivo* remains poorly defined. Our incomplete understanding of ketamine's neuropharmacology is due both to the unknown identity of the molecular mediator or mediators of its antidepressant action, as well as to the technical challenges of measuring drug levels within specific subcellular compartments[64]. Moreover, ketamine is metabolized on the timescale of minutes to hours[65–68], leading to variable concentrations of both parent compound and active metabolites in the brain that can only be roughly approximated *in vitro*. Past *in vitro* studies aiming to probe the mechanisms underlying ketamine's antidepressant effects have used concentrations ranging from 0.1 to 10 μM[37,69–73]. We selected two different concentrations to compare with untreated controls: 10 μM ketamine (racemate), representing the higher end of this range, to maximize the likelihood of detecting significant changes in protein expression in our BONCAT-enriched samples; and 1 μM ketamine (racemate), a mid-range dose that more closely reflects ketamine concentrations measured in cerebrospinal fluid (CSF) following administration of sub-anesthetic antidepressant doses of ketamine, which typically fall between 0.2 and 2.5 μM across studies[66,74–76].

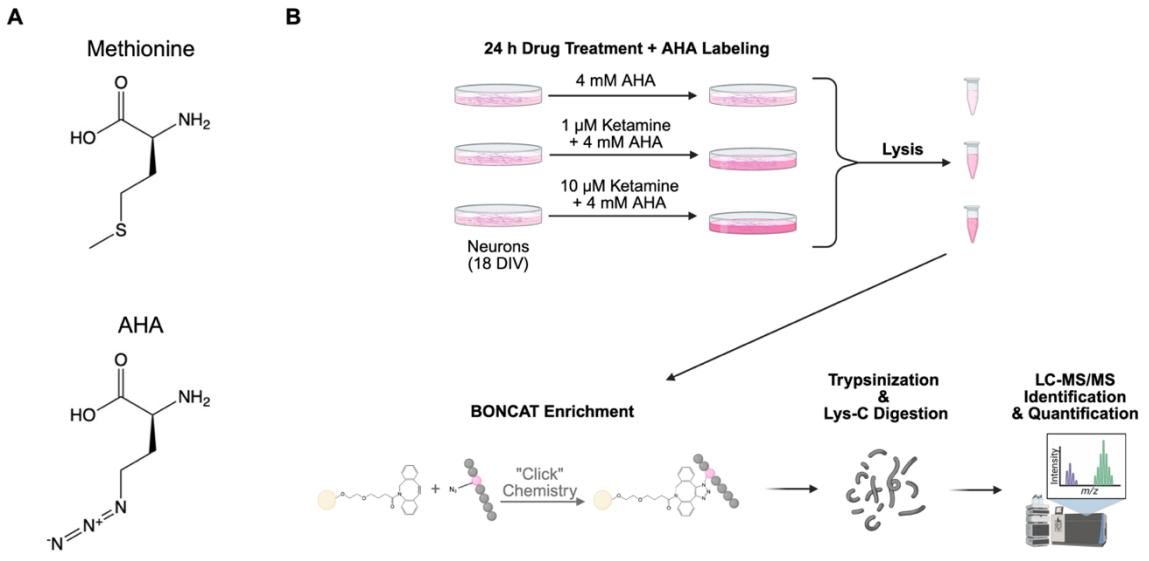

Figure 3.1. BONCAT enables labeling, chemical enrichment, identification, and proteomic analysis of newly synthesized proteins in primary neuron cultures. (A) Chemical structures of methionine and azidohomoalanine (AHA). (B) Schematic showing the experiment discussed in this paper. To investigate protein expression during treatment with low doses of ketamine, AHA was added to primary embryonic rat cortical neurons (18 DIV) alongside different concentrations of the drug. AHA-labeled proteins were enriched via covalent attachment to DBCO-agarose beads using copper-free strain-promoted [3 + 2] azide–alkyne cycloaddition. Peptides released via on-bead enzymatic digestion were subsequently identified via LC-MS/MS for downstream proteomic analysis. Created in BioRender. Miller, S. (2025) https://BioRender.com/tagz43n

Analysis of BONCAT-enriched samples via mass spectrometry revealed that ketamine-treated samples had overall higher raw abundances than untreated control samples. Of proteins identified in both 10 µM ketamine-treated samples and in untreated controls, 91% had higher average raw abundances in the treated samples (Fig. 3.2A). While less pronounced, this effect was also observed at lower doses, where 68% of proteins identified in both 1 µM ketamine-treated samples and in controls had higher average raw abundances in the ketamine-treated samples (Fig. 3.2B). Given that total cell lysate concentrations were normalized across all samples prior to enrichment, these results are indicative of greater AHA labeling and therefore greater levels of protein synthesis in neurons exposed to ketamine. Previously, Li et al. demonstrated that treatment with a sub-anesthetic dose of ketamine activates mTOR signaling in rat brains, leading to increased synthesis of various synapse-associated proteins[34]. More recently, preliminary results presented by Creeney et al. showed a rapid, dose-dependent increase in protein synthesis in primary cortical neuron cultures

treated with ketamine by measuring puromycin incorporation[77]. Our findings provide further evidence that ketamine induces a broad increase in protein synthesis across the neuronal proteome.

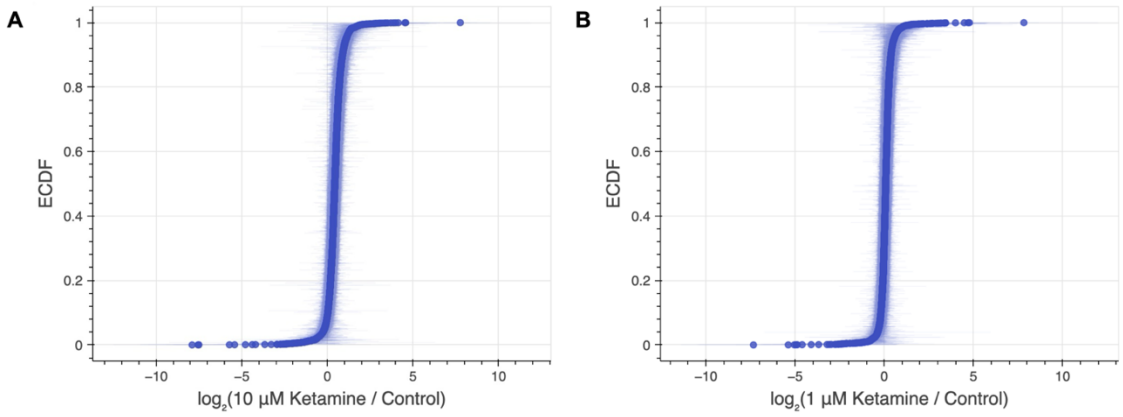

Figure 3.2. BONCAT proteomics reveals ketamine-induced increase in protein synthesis in primary cortical neurons treated with ketamine. (A) Empirical cumulative distribution function (ECDF) depicting the log ratios of the average raw abundances of proteins identified in neurons treated with 10 µM ketamine to their average raw abundances in untreated control samples. (D) ECDF depicting the log ratios of the average raw abundances of proteins identified in neurons treated with 1 µM ketamine to their average raw abundances in untreated control samples. Shading on ECDF curves represents 95% confidence intervals. n = 5 biological replicates for each condition.

Ketamine treatment results in significant changes in expression of proteins involved in synaptic function and plasticity, cytoskeletal dynamics, cell-cell signaling, metabolism, and RNA processing

Differential expression analysis of proteomics data from BONCAT-enriched samples revealed 62 significantly up-regulated proteins ($log_2FC > 1$, adj. $p < 0.05$) and 84 significantly down-regulated proteins ($log_2FC < 1$, adj. $p < 0.05$) in samples treated with 10 µM ketamine compared to controls (Fig. 3.3).

Changes in synapse-associated proteins suggest changes in synaptic function and plasticity induced by ketamine

Differential expression analysis of proteomics data from BONCAT-enriched samples revealed 62 significantly up-regulated proteins ($log_2FC > 1$, adj. $p < 0.05$) and 84

significantly down-regulated proteins ($log_2FC < 1$, adj. $p < 0.05$) in samples treated with 10 μM ketamine compared to controls (Fig. 3.3).

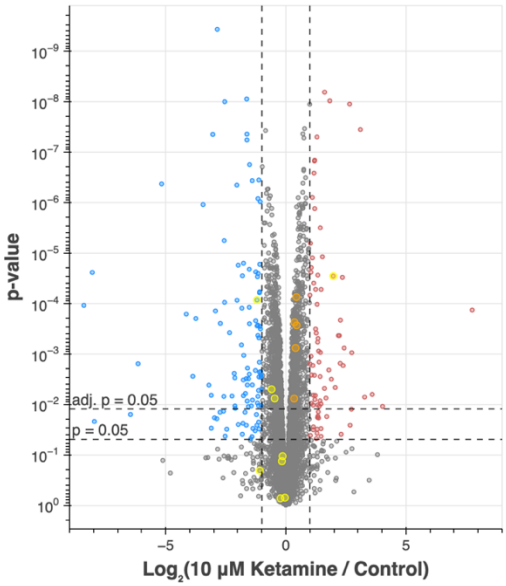

Figure 3.3. Differential expression analysis of BONCAT proteomics data identifies 146 proteins with significantly up- or down-regulated expression in 10 μM ketamine-treated neurons compared to untreated neurons. Volcano plot comparing expression of BONCAT-enriched proteins from primary cortical neurons treated with 10 μM ketamine to their expression in untreated controls. Fold change values were calculated via label-free quantification. Proteins significantly up-regulated in ketamine-treated neurons are depicted in red, whereas proteins significantly down-regulated in ketamine-treated neurons are depicted in blue. Yellow points designate semaphorins identified in the dataset, and orange points designate collapsin response mediator proteins identified in the dataset. Significance threshold was set to $|log_2(FC)| > 1$ and $p < 0.05$. Horizontal dashed lines depict $p = 0.05$ and Benjamini-Hochberg false-discovery rate (FDR)-adjusted $p = 0.05$.

Several of these proteins have been implicated in synaptic function and plasticity. Metabotropic glutamate receptor 1 (Grm1, $log_2FC = 2.19$, adj. $p = 0.00566$) is a member of a class of receptors known to modulate neuronal excitability and synaptic transmission[78]. While recent work has shown that metabotropic glutamate receptor 5 might play a role in ketamine's antidepressant effects[79,80], and metabotropic glutamate receptors 2 and 3 antagonists have been shown to enhance them[81], Grm1 has not yet been investigated in the context of ketamine treatment. Extracellular leucine-rich repeat protein (Elfn2, $log_2FC = 1.20$, adj. $p = 5.69 \times 10^{-5}$), which is also up-regulated, is a postsynaptic adhesion molecule that binds presynaptic group III metabotropic glutamate receptors, and *Elfn2* knockout mice

display a range of neuropsychiatric behaviors[82]. Activin receptor type-2A (Acvr2a, $\log_2$FC = 1.61, adj. p = $1.10\text{x}10^{-5}$) up-regulation in response to ketamine treatment is intriguing, as well, as activin has been shown to mediate the antidepressant response of mice to the SSRI fluoxetine[83], and to potentiate signaling via NMDARs[84]. Furthermore, we observed an increase in expression of proteins involved in calcium signaling and homeostasis, namely plasma membrane calcium-transporting ATPase 2 (Atp2b2, $\log_2$FC = 1.00, adj. p = 0.00201) and hippocalcin-like protein 4 (Hpcal4, $\log_2$FC = 1.47, adj. p = 0.00176), a neuronal calcium sensor. Additional significantly up-regulated proteins involved in synaptic plasticity include calcium/calmodulin-dependent phosphodiesterase 1B (Pde1b, $\log_2$FC = 1.34, adj. p = 0.00621), which plays a role in memory consolidation[85] and whose deletion results in a depression-like phenotype[86], protein-tyrosine kinase 2-beta (Ptk2b, $\log_2$FC = 1.19, adj. p = $5.69\text{x}10^{-5}$), a calcium-activated kinase involved in dendritic spine regulation and synaptic signaling[87,88], and MDGA1 (Mdga1, $\log_2$FC = 1.24, adj. p = 0.00482), which suppresses inhibitory synapse formation[89,90] and has been implicated in psychiatric disorders[91,92].

Proteins involved in synaptic function were also identified among proteins significantly down-regulated in response to treatment with 10 μM ketamine. Notably, a reduction in expression of SynGAP (Syngap1, $\log_2$FC = −2.85, adj. p = $2.52\text{x}10^{-6}$) has previously been demonstrated to enhance dendritic morphogenesis and excitatory synapse strength in human-induced pluripotent stem cells[93]. However, a seemingly contrasting second study by the same group of researchers showed that SynGAP1 promotes experience-dependent synapse strengthening in mouse brains *in vivo*[94]. It is possible that the role of SynGAP1 switches from developing neurons to mature circuits, but its function in modulating synaptic strength in the context of ketamine treatment is unknown. Another interesting down-regulated protein is tissue-type plasminogen activator (Plat, $\log_2$FC = −1.08, adj. p = $9.52\text{x}10^{-4}$), whose many roles include inducing synaptic vesicle endocytosis[95], influencing synaptic glutamate release[96], and conversion of proBDNF to BDNF (brain-derived neurotrophic factor)[97], a protein known to be involved in the pathophysiology of depression[98–100].

We also observed a significant reduction in expression of gamma-aminobutyric acid (GABA) receptor subunit epsilon (Gabre, $log_2FC = -1.63$, adj. $p = 1.10x10^{-5}$), which is involved in mediating inhibitory neurotransmission in the brain. GABA receptors, particularly $GABA_A$ receptors ($GABA_ARs$), have been implicated in the pathophysiology of depression and in studies examining ketamine's rapid-acting antidepressant effects. MDD is associated with reduced cortical GABA concentrations, impaired GABAergic inhibition, and altered $GABA_AR$ subunit expression; while there is no direct evidence that antidepressants reverse subunit-level transcriptional changes, chronic treatment with monoaminergic antidepressants has been shown to normalize brain GABA levels, restore inhibitory tone, and ameliorate behavioral and neuroendocrine abnormalities in both human patients and $GABA_AR$-deficient mouse models[101–103]. Furthermore, researchers have proposed that ketamine's RAAD effects involve inhibition of NMDARs on GABAergic cortical interneurons[104–106], and GABAAR-mutant mice, which display molecular and behavioral markers of depression, exhibit potentiation of cortical GABAergic synapses by ketamine[107]. While this specific $GABA_AR$ subunit has not been widely studied, it has been shown to be promiscuous in its ability to assemble into various positions in the receptor complex[108].

Another down-regulated protein involved in synaptic transmission is cystathionine beta-synthase (Cbs, $log_2FC = -3.44$, adj. $p = 1.68x10^{-4}$), which catalyzes the production of hydrogen sulfide, a gasotransmitter that has been detected in the brain and reported to be involved in neuromodulatory processes and synaptic remodeling[109,110]. We also observed the down-regulation of a few neuropeptides or neuropeptide precursors involved in neuronal signaling, including pro-neuropeptide Y (Npy, $log_2FC = -1.55$, adj. $p = 0.0204$), proenkephalin-A (Penk, $log_2FC = -2.34$, adj. $p = 0.00524$), and secretogranin-2 (Scg2, $log_2FC = -1.62$, adj. $p = 2.46x10^{-5}$). Other down-regulated synaptic proteins include slingshot protein phosphatase 1 (Ssh1, $log_2FC = -5.17$, adj. $p = 1.04x10^{-4}$), which is necessary for dendritic spine remodeling involved in structural plasticity[111], Kallikrein 8 (Klk8, $log_2FC = -2.73$, adj. $p = 0.00416$), a protease that regulates dendritic growth critical for long-term potentiation (LTP)[112,113], septin 9 (septin9, $log_2FC = -2.58$, adj. $p = 0.0340$), which promotes neurite outgrowth and also interferes with NDMA receptor subunit transport

into dendrites[114,115], and spermatogenesis-associated protein 5 (Spata5, $log_2FC = -2.55$, adj. $p = 0.00247$), which plays an important role in cortical neuron development and axonal growth[116]. Finally, we also detected significantly reduced expression of F-actin monooxygenase MICAL2 (Mical2, $log_2FC = -1.40$, adj. $p = 9.66x10^{-5}$), an inducer of actin depolymerization activated by semaphorin 3A[117–119] (Sema3a, $log_2FC = -1.20$, adj. $p = 0.00231$), a key regulator of axon guidance and dendritic growth also found in our data to be down-regulated in ketamine-treated samples[120].

Changes observed in expression of structural proteins involved in cytoskeletal dynamics and neuronal morphology

Several proteins mentioned above contribute to the remodeling of dendrites, axons, or synapses via interactions with cytoskeletal and other structural proteins in neurons. Other proteins involved in cytoskeletal dynamics or defining cell structure that were differentially expressed in neurons treated with 10 μM ketamine include failed axon connections homolog (Faxc, $log_2FC = 2.74$, adj. $p = 0.00936$), microtubule-associated scaffold protein 2 (Mtus2, $log_2FC = 1.06$, adj. $p = 0.00101$), tensin 1 (Tns1, $log_2FC = -1.12$, adj. $p = 9.66x10^{-5}$), tropomodulin-1 (Tmod1, $log_2FC = -1.15$, adj. $p = 0.00118$), actin filament-associated protein 1 (Afap1, $log_2FC = -1.76$, adj. $p = 9.23x10^{-4}$), cytoplasmic linker-associated protein 1 (Clasp1, $log_2FC = -1.61$, adj. $p = 0.0395$), and cytokeratins Krt1 ($log_2FC = -1.57$, adj. $p = 0.0469$), Krt10 ($log_2FC = -2.24$, adj. $p = 0.0336$), Krt17 ($log_2FC = -1.60$, adj. $p = 0.0149$), and Krt28 ($log_2FC = -2.12$, adj. $p = 0.0460$). Extracellular matrix proteins produced and secreted by neurons also play critical roles in neural circuit formation, axon guidance, and synaptogenesis[121]. La-related RNA-binding protein 6 (Larp6, $log_2FC = -2.10$, adj. $p = 0.0491$), which showed decreased expression in our dataset, post-transcriptionally regulates the expression of collagen, the most abundant protein in the ECM. The alteration in expression of this set of proteins paints a picture of altered neuronal morphology and rapid neural circuit restructuring in response to ketamine treatment.

Altered expression of signaling proteins in ketamine-treated neurons

Multiple significantly differentially expressed proteins in 10 μM ketamine-treated samples are involved in intracellular signal transduction. Up-regulation of adenylate cyclase type 6 (Adcy6, $\log_2$FC = 2.35, adj. p = 0.00126), which catalyzes the conversion of ATP to the second messenger cAMP, suggests enhanced cAMP-dependent signaling, a pathway known to modulate neuronal plasticity and synaptic transmission[122–125]. Additionally, two kinases involved in upstream ERK/MAPK signaling—MAP kinase kinase kinase 1 (Map3k1, $\log_2$FC = 1.20, adj. p = $1.74\text{x}10^{-4}$) and STE20-related kinase (Stk39, $\log_2$FC = 1.39, adj. p = 0.0463)—were also up-regulated. The ERK/MAPK signaling pathway is activated in diverse cellular processes, including cytoskeletal dynamics and stress responses, and has also been linked with depression[126,127]. Several small GTPases were also up-regulated, including Ras-related protein Rap-2 (Rap2c, $\log_2$FC = 1.79, adj. p = 0.0159) and Ras-like without CAAX 2 (Rit2, $\log_2$FC = 1.02, adj. p = $5.21\text{x}10^{-4}$). These proteins are involved in pathways that have been shown to play roles in neuronal synaptic plasticity, synapse formation, and neurite outgrowth[128–131]. Dysregulation of Rit2 expression has also been implicated in neuropsychiatric disorders, including Parkinson's disease and schizophrenia[132,133], raising the possibility that it may also play a role in the antidepressant action of ketamine.

Conversely, certain down-regulated proteins point to reduced activity of specific signaling modules. The hyperpolarization-activated cyclic nucleotide-gated channel 1 (Hcn1, $\log_2$FC = −1.08, adj. p = 0.00446) was significantly down-regulated. Hcn1 is a key regulator of neuronal excitability and rhythmic firing through its role in generating the inward hyperpolarization-activated current I_h[134,135]. Intriguingly, reduced Hcn1 expression or function has been associated with antidepressant-like behaviors in rodents[136], and ketamine has been reported to inhibit Hcn1–Hcn2 heteromeric channels in a subunit-specific manner[137]. Another study showed that HCN1 knockout mice failed to show ketamine-induced behavioral responses in a chronic stress model, highlighting the relevance of changes in Hcn1 expression to ketamine's mechanism of action[138]. Additional down-regulated signaling proteins include A-kinase anchor protein 13 (Akap13, $\log_2$FC = −1.14, adj. p = 0.0458), and TGF-beta-activated kinase binding protein 2 (Tab2, $\log_2$FC = −1.75, adj. p =

0.0103), which act respectively as a scaffold for complex assembly and as an adaptor for pathway activation in multiple intracellular signaling cascades[139–143].

Significant changes in expression of proteins involved in membrane trafficking, lipid composition, and vesicular transport

Treatment with 10 μM ketamine led to the up-regulation of several proteins involved in membrane trafficking and vesicular transport, consistent with increased synaptic remodeling. Tepsin ($log_2FC = 7.75$, adj. $p = 0.00301$), an accessory subunit of the AP-4 complex involved in neuronal lysosome transport, was significantly up-regulated, suggesting enhanced clathrin-mediated vesicle formation and trafficking[144]. Cubilin (Cubn, $log_2FC = 3.10$, adj. $p = 2.35x10^{-5}$), an endocytic receptor involved in cellular uptake of vitamins and lipoproteins, also exhibited increased expression[145,146], as did TBC1 domain family member 15 (Tbc1d15, $log_2FC = 2.38$, adj. $p = 0.0138$), a known Rab GTPase-activating protein, and Golgi membrane protein 1 (Golm1, $log_2FC = 1.24$, adj. $p = 0.00176$). These proteins are involved in endosomal sorting and trafficking from the Golgi apparatus, hinting at a general upregulation of intracellular transport systems. Changes in proteins involved in lipid metabolism were also observed; in addition to Golm1, which also plays a role in sphingolipid metabolism[147], phosphatidate cytidylyltransferase 1 (Cds1, $log_2FC = 1.36$, adj. $p = 0.00899$) and acid sphingomyelinase-like phosphodiesterase 3b (Smpdl3b, $log_2FC = 1.30$, adj. $p = 0.00257$) were up-regulated, implying increased synthesis and turnover of membrane lipids. These changes could support dynamic changes in membrane composition necessary for synaptic plasticity.

Meanwhile, several proteins involved in lipid transport and organelle dynamics were significantly down-regulated, including ATP-binding cassette sub-family A member 2 (Abca2, $log_2FC = -1.07$, adj. $p = 1.64x10^{-4}$), Golgin subfamily A member 4 (Golga4, $log_2FC = -1.10$, adj. $p = 0.0170$), and peroxisomal biogenesis factor 11 beta (Pex11b, $log_2FC = -1.20$, adj. $p = 0.00442$). Proteins related to fatty acid metabolism, including elongation of very long chain fatty acids protein 5 (Elovl5, $log_2FC = -1.65$, adj. $p = 0.0204$) and very-long-chain 3-hydroxyacyl-CoA dehydratase (Hacd2, $log_2FC = -3.87$, adj. $p = 0.0192$), were also

down-regulated, suggesting a decrease in production of certain membrane lipid species. Furthermore, dynein heavy chain domain 1 (Dnhd1, $\log_2$FC = −1.10, adj. p = 0.00193) and Rab27b ($\log_2$FC = −1.25, adj. p = 0.00113), both of which mediate vesicle transport and docking[148,149], were significantly differentially expressed, suggesting broad modulation of vesicle trafficking machinery.

Increase in proteins involved in cellular metabolism

Proteins involved in energy metabolism and mitochondrial function were up-regulated in ketamine-treated neurons. Nucleoside diphosphate kinase 5 (Ak5, $\log_2$FC = 1.43, adj. p = $3.17\text{x}10^{-4}$), which is involved in maintaining nucleotide pools for ATP and GTP synthesis[150], and mitochondrial ribonuclease P protein 1 (Prorp, $\log_2$FC = 1.32, adj. p = 0.0448), essential for mitochondrial tRNA processing[151], both showed increased expression. ATP-binding cassette sub-family D member 4 (Abcd4, $\log_2$FC = 1.01, adj. p = 0.0133), a transporter involved in vitamin B12 metabolism[152], was also up-regulated. These changes may reflect heightened metabolic demand in response to increased protein synthesis and synaptic remodeling.

Reduced expression of proteins with roles in RNA processing

Several proteins involved in transcriptional regulation, RNA processing, and translation and were significantly down-regulated following ketamine treatment. For example, Nol7 ($\log_2$FC = −1.01, adj. p = 0.0272) and Nol10 ($\log_2$FC = −1.09, adj. p = 0.00189), which are involved in ribosome biogenesis[153,154], both had significantly reduced expression. Notably, eukaryotic translation initiation factor 4E-binding protein 2 (Eif4ebp2, $\log_2$FC = −1.10, adj. p = 0.0127), a downstream target of mTOR signaling, was also down-regulated. This finding is particularly interesting given that 4E-BP2 plays a key role in regulating translation at the synapse and is critical for the rapid antidepressant effects of ketamine[155–157]. Furthermore, since 4E-BP2 represses translation by binding to eIF4E to block the formation of the translation initiation complex, a decrease in 4E-BP2 expression would result in an increase in cap-dependent translation, in agreement with the increase in protein synthesis we detected using BONCAT in neurons treated with ketamine.

Transcriptional regulators were also broadly down-regulated. Some zinc finger proteins, including Zfp518b ($log_2FC = -1.04$, adj. $p = 0.0196$), Zfp536 ($log_2FC = -1.51$, adj. $p = 6.39x10^{-5}$), Zfp91 ($log_2FC = -1.81$, adj. $p = 0.00122$), and Znf260 ($log_2FC = -8.40$, adj. $p = 0.00265$), showed significantly reduced expression, along with additional transcription factors such as MYB proto-oncogene-like 1 (Mybl1, $log_2FC = -1.03$, adj. $p = 0.0188$), PR/SET domain 15 (Prdm15, $log_2FC = -1.06$, adj. $p = 000482$), and BCL6 co-repressor (Bcor, $log_2FC = -1.51$, adj. $p = 0.00418$). This collective down-regulation suggests ketamine may suppress certain gene regulatory programs, potentially to shift transcriptional resources toward immediate-early or activity-dependent genes that support synaptic remodeling and plasticity.

Fifteen proteins found to be differentially expressed in neurons treated with 1 μM ketamine

Treatment with 1 μM ketamine resulted in fewer proteins being significantly up- or down-regulated in our normalized data after controlling for false discovery rate (FDR), likely a result of less pronounced changes in protein expression in response to lower doses of ketamine. We found six significantly up-regulated proteins and nine significantly down-regulated proteins in 1 μM ketamine-treated samples compared to controls (Fig. 3.4). The majority of these proteins were also found to be significantly differentially regulated in samples treated with 10 μM ketamine, including several discussed above: Tepsin ($log_2FC = 8.26$, adj. $p = 0.00303$) and Cubilin (Cubn, $log_2FC = 3.11$, adj. $p = 7.64x10^{-4}$), which are involved in membrane trafficking and vesicle formation, secondary messenger cAMP-synthesizing enzyme Adcy6 ($log_2FC = 1.83$, adj. $p = 0.0369$), mRNA spliceosome component Snrnp40 ($log_2FC = 1.24$, adj. $p = 0.0100$), and proteins involved in synapse formation, synaptic transmission, and neurite outgrowth such as Penk ($log_2FC = -1.64$, adj. $p = 0.0149$), Gabre ($log_2FC = -2.00$, adj. $p = 0.0149$), Ssh1 ($log_2FC = -5.26$, adj. $p = 0.0149$), Spata5 ($log_2FC = -2.47$, adj. $p = 0.0346$), and Cbs ($log_2FC = -2.90$, adj. $p = 0.00303$). Some proteins were found to be down-regulated in samples treated with 1 μM ketamine but not in

samples treated 10 μM ketamine. One such protein, protocadherin beta 4 (Pcdhb4, $\log_2$FC = −4.86, adj. p = 7.64x10^{-4}), is a cell adhesion molecule known to play a role in neural development and to be involved in multiple aspects of neural circuit formation, including dendrite arborization, axonal outgrowth, and synaptogenesis[158]. Another is Mapk11 ($\log_2$FC = −7.53, adj. p = 0.0113), another protein involved in MAPK signaling, mentioned above as one of the signaling pathways with components differentially expressed upon exposure to 10 μM ketamine.

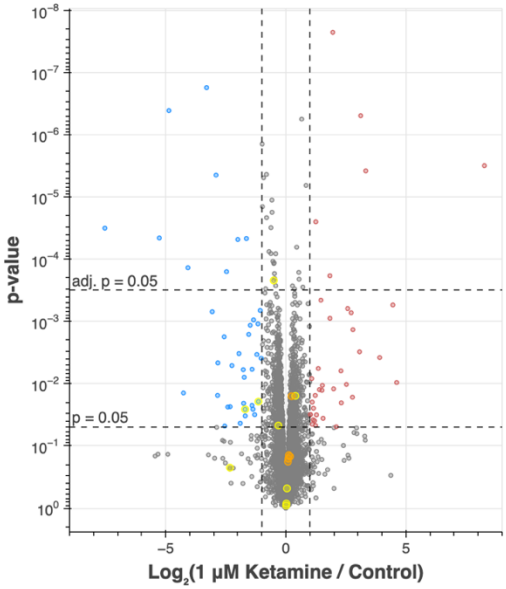

Figure 3.4. Differential expression analysis of BONCAT proteomics data identifies 15 proteins with significantly up- or down-regulated expression in 1 μM ketamine-treated neurons compared to untreated neurons. Volcano plot comparing expression of BONCAT-enriched proteins primary cortical neurons treated with 1 μM ketamine to their expression in untreated controls. Fold change values were calculated via label-free quantification. Proteins significantly up-regulated in ketamine-treated neurons are depicted in red, whereas proteins significantly down-regulated in ketamine-treated neurons are depicted in blue. Yellow points designate semaphorins identified in the dataset, and orange points designate collapsin response mediator proteins identified in the dataset. Significance threshold was set to $|\log_2(FC)| > 1$ and $p < 0.05$. Horizontal dashed lines depict p = 0.05 and Benjamini-Hochberg false-discovery rate (FDR)-adjusted p = 0.05.

General increase in expression of semaphorins and decrease in expression of collapsin-response mediator proteins

Our observation that Sema3a expression decreased in response to 10 μM ketamine treatment prompted us to investigate other semaphorins and other proteins in our dataset involved in

neurite outgrowth via semaphorin signaling. We identified nine semaphorin proteins in our dataset: Sema4a, Sema4f, Sema6a, Sema6d, Sema7a, Sema3e, Sema3c, Sema5b, and Sema3a. Class III semaphorins are soluble, whereas class IV, V, and VI semaphorins are transmembrane proteins and class VII semaphorins are membrane-bound through a glycosylphosphatidylinositol anchor. In our differential expression analysis comparing 10 μM ketamine-treated neurons to untreated controls, eight of the nine semaphorins detected had decreased expression ($log_2FC < 0$), although most of these changes were not statistically significant after FDR adjustment. The only up-regulated semaphorin in our dataset was Sema4a ($log_2FC = 1.97$, adj. $p = 0.00122$), which is primarily implicated in immune signaling by enhancing T-cell activation and less involved in neurite outgrowth (Fig. 3.3, Table 3.1)[159,160].

Table 3.1. Differential expression of semaphorin proteins identified in 10 μM ketamine treated samples and controls

Protein	Gene Name	Log_2FC	P-Value	FDR-Adj. P-Value
Semaphorin 4A	sema4a	1.973	2.90E-05	1.22E-03
Semaphorin 4F	sema4f	-0.039	7.12E-01	8.09E-01
Semaphorin 6A	sema6a	-0.134	1.07E-01	2.24E-01
Semaphorin 6D	sema6d	-0.162	1.35E-01	2.60E-01
Semaphorin 7A	sema7a	-0.225	7.35E-01	8.27E-01
Semaphorin 3E	sema3e	-0.466	7.70E-03	3.63E-02
Semaphorin 3C	sema3c	-0.593	5.06E-03	2.74E-02
Semaphorin 5B	sema5b	-1.086	2.07E-01	3.49E-01
Semaphorin 3A	sema3a	-1.198	8.63E-05	2.31E-03

Fold change values were calculated via label-free quantification. Both non-adjusted p-values as well as p-values adjusted for FDR using the Benjamini-Hochberg procedure are provided.

The three semaphorins with statistically significant decreases in expression in 10 μM ketamine-treated neurons after adjusting for FDR ($log_2FC < 0$, adj. $p < 0.05$) were the three identified Class III semaphorins. Sema3a ($log_2FC = -1.20$, adj. $p = 0.00231$) is the most studied semaphorin, known for its role in suppressing axon outgrowth by inducing growth cone collapse and promoting dendrite growth[161,162]. Although most soluble semaphorins have been found to mediate axon repulsion, some have a growth promoting effect on specific

neuronal subpopulations, including Sema3c, ($log_2FC = -0.593$, adj. $p = 0.0274$) which has been shown to promote the growth of axons in cortical neurons[163]. Sema3e exhibited a statistically significant change in expression in both 10 μM ketamine-treated neurons ($log_2FC = -0.466$, adj. $p = 0.0363$) as well as 1 μM ketamine-treated neurons ($log_2FC = -0.505$, adj. $p = 0.0403$) (Table 3.2). While Sema3e has not been as widely studied, Mata et al. demonstrated that Sema3e plays a role in the formation of neuronal connections during hippocampal development and propose that expression levels of Sema3e and its receptor plexin-D1 might modulate synapse formation in the adult brain[164].

Table 3.2. Differential expression of semaphorin proteins identified in 1 μM ketamine treated samples and controls

Protein	Gene Name	Log_2FC	P-Value	FDR-Adj. P-Value
Semaphorin 4A	sema4a	0.396	1.57E-02	2.21E-01
Semaphorin 6D	sema6d	0.047	4.83E-01	7.48E-01
Semaphorin 6A	sema6a	0.021	8.44E-01	9.38E-01
Semaphorin 4F	sema4f	0.014	9.09E-01	9.65E-01
Semaphorin 3C	sema3c	-0.311	4.71E-02	3.19E-01
Semaphorin 3E	sema3e	-0.505	2.20E-04	4.03E-02
Semaphorin 7A	sema7a	-1.139	1.94E-02	2.36E-01
Semaphorin 3A	sema3a	-1.694	2.58E-02	2.60E-01
Semaphorin 5B	sema5b	-2.324	2.24E-01	5.52E-01

Fold change values were calculated via label-free quantification. Both non-adjusted p-values as well as p-values adjusted for FDR using the Benjamini-Hochberg procedure are provided.

While Sema3e can bind directly to plexin-D1, most class III semaphorins must form a complex with neuropilin-1 or neuropilin-2, cell-surface glycoproteins, in order to bind to a plexin receptor. Sema3a binds to plexin-D1 exclusively through neuropilin-1, while Sema3c binds to plexin-D1 either via neuropilin-1 or neuropilin-2 binding, but can also bind directly to plexin-D1, plexin-A4, or plexin-B1 at higher concentrations[165]. We identified both neuropilins in our dataset, but their expression did not change significantly in response to ketamine treatment. Plexins also serve as the receptors for transmembrane-semaphorins, with which they interact directly[166]. We identified nine plexins in our dataset: plexin-D1, plexin-A1, plexin-A4, plexin-B3, plexin-B2, plexin-A3, plexin-B1, plexin-A2, and plexin-C1. None

of these had significant changes in expression in response to treatment with 1 μM ketamine, but upon exposure to 10 μM ketamine, three had changes in expression that were significant after adjusting for FDR: plexin-A1 ($log_2FC = 0.298$, adj. $p = 0.00303$), plexin-A4 ($log_2FC = 0.200$, adj. $p = 0.0382$), and plexin-A2 ($log_2FC = -0.243$, adj. $p = 0.0219$).

Collapsin response mediator proteins (CRMPs), also known as dihydropyrimidinase-like proteins or dihydropyrimidinase-related proteins, are a family of five cytosolic phosphoproteins involved in various aspects of nervous system development, including axon guidance, synapse maturation, and cell migration, with evidence for roles in adult synaptic plasticity as well[167,168]. CRMPs were initially discovered for their role as effectors of Sema3a signaling mediating growth cone collapse[169]. Interestingly, our data showed that all five CRMPs had modest (less than two-fold) but significant (adj. $p < 0.05$) increases expression in neurons treated with 10 μM ketamine compared to controls (Fig. 3.3, Table 3.3). In 1 μM ketamine-treated neurons, all five CRMPs had positive log_2FC values, but none passed the threshold of statistical significance after controlling for FDR (Fig. 3.4, Table 3.4). Altogether, our results showing changes in expression of various proteins involved in synapse formation and neurite outgrowth provide further evidence for hypotheses that ketamine rapidly promotes synaptogenesis[170–173] and alters neural connectivity in adult brains[174,175].

Table 3.3. Differential expression of collapsin response mediator proteins identified in 10 μM ketamine treated samples and controls

Protein	Gene Name	Log_2FC	P-Value	FDR-Adj. P-Value
Dihydropyrimidinase-related protein 5	dpysl5	0.450	2.74E-04	4.37E-03
Dihydropyrimidinase-related protein 2	dpysl2	0.440	7.53E-05	2.12E-03
Dihydropyrimidinase-related protein 4	dpysl4	0.407	7.70E-04	8.23E-03
Dihydropyrimidinase-related protein 3 (Isoform 2)	dpysl3	0.359	2.38E-04	4.08E-03
Dihydropyrimidinase-related protein 1	crmp1	0.346	7.73E-03	3.65E-02

Fold change values were calculated via label-free quantification. Both non-adjusted p-values as well as p-values adjusted for FDR using the Benjamini-Hochberg procedure are provided.

Table 3.4. Differential expression of collapsin response mediator proteins identified in 1 μM ketamine treated samples and controls

Protein	Gene Name	Log_2FC	P-Value	FDR-Adj. P-Value
Dihydropyrimidinase-related protein 5	dpysl5	0.239	1.59E-02	2.21E-01
Dihydropyrimidinase-related protein 1	crmp1	0.177	1.48E-01	4.72E-01
Dihydropyrimidinase-related protein 4	dpysl4	0.125	1.41E-01	4.67E-01
Dihydropyrimidinase-related protein 2	dpysl2	0.106	1.60E-01	4.83E-01
Dihydropyrimidinase-related protein 3 (Isoform 2)	dpysl3	0.090	1.79E-01	5.03E-01

Fold change values were calculated via label-free quantification. Both non-adjusted p-values as well as p-values adjusted for FDR using the Benjamini-Hochberg procedure are provided.

Functional enrichment analysis identifies pathways and processes significantly altered by ketamine treatment

We performed gene set enrichment analysis using the STRING enrichment API[176], which draws protein annotations from various databases, including Gene Ontology Resource, KEGG PATHWAY database, WikiPathways, Reactome Pathway Database, UniProt Keywords, PubMed publications, the JensenLab COMPARTMENTS subcellular localization database, Pfam domains, InterPro domains, and SMART domains.

Positive enrichment of synaptic processes

Given the number of significantly differentially expressed proteins involved in synaptic processes that we identified in our dataset and discussed above, it was not surprising that several pathways related to synaptic processes were found to be enriched in 10 μM ketamine-treated neurons (Fig. 3.5). These include pathways related to particular types of synapses ("glutamatergic synapse" and "dopaminergic synapse), cell-cell signaling ("GPCR downstream signaling" and "adrenergic signaling"), pathways related to synaptic vesicles and synaptic membranes, and pathways related to axons and axonal growth ("growth cone," "site of polarized growth," "presynaptic membrane," and "axon terminus"). These findings contribute to the body of work, mentioned above, that has found ketamine to rapidly induce synaptogenesis and rewiring of neuronal connectivity[170–175].

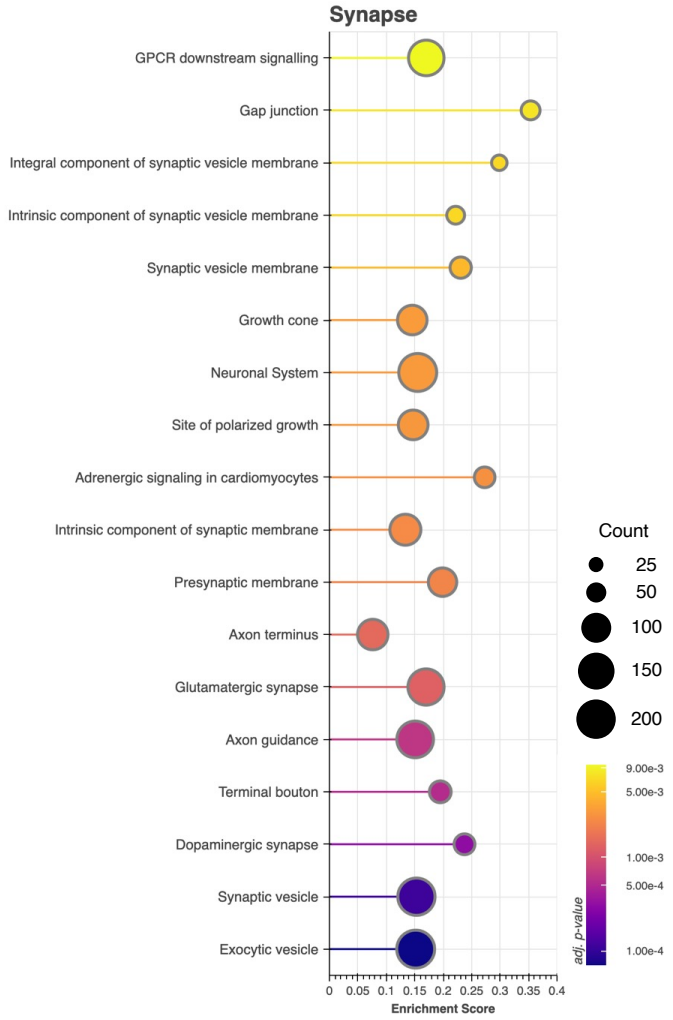

Figure 3.5. Positive enrichment of synapse-related pathways and processes in neurons treated with 10 µM ketamine. Functional enrichment analysis results for pathway annotations related to synaptic structures or functions. Circle size is proportional to the number of proteins in the dataset with that annotation ("Count"). Circle color corresponds to p-values (Kolmogorov-Smirnov) adjusted for multiple hypothesis testing using the Benjamini–Hochberg procedure.

Overall increase in expression of proteins related to cytoskeleton and cell structure

Annotations corresponding to cytoskeleton-related processes, pathways, and components were found to have significant enrichment in our dataset. Apart from annotations for "keratin filament" and "intermediate filament," which had negative enrichment scores, all other significantly altered pathways consisting of cytoskeleton proteins were positively enriched (Fig. 3.6). Some pathways—such as "intraflagellar transport," "cilium," and "cilium assembly"—may seem out of place in a neuronal dataset. Neurons do possess a single, non-

motile primary cilium that is increasingly recognized as a key neuronal signaling hub, involved in pathways like Sonic Hedgehog (Shh), Wnt, and GPCR signaling, all of which can affect neuronal development, morphogenesis, and function.[177–180]. However, closer examination of the proteins we identified with these annotations reveals that most of them can also be broadly categorized as components of the cytoskeleton or intracellular transport machinery (Fig. 3.7). These include tubulins and motor proteins (e.g., kinesins, dyneins) that are fundamental not only for building and moving molecules within primary cilia, but also for other microtubule-dependent processes, including those in axons and dendrites. "Ciliium" and "cilium assembly" proteins also include GPCR pathway components (e.g. Adcy3, Tacr1, Gnb1, Grk3) and kinases (e.g. Prkaca, Prkacb, Prkar2b, Prkar1a, Prkca, Grk3, Cdkl5, Akt1, Ttbk2, Csnk2b) that point to an overall modulation of neuronal signaling, as was discussed above in the context of our differential expression analysis.

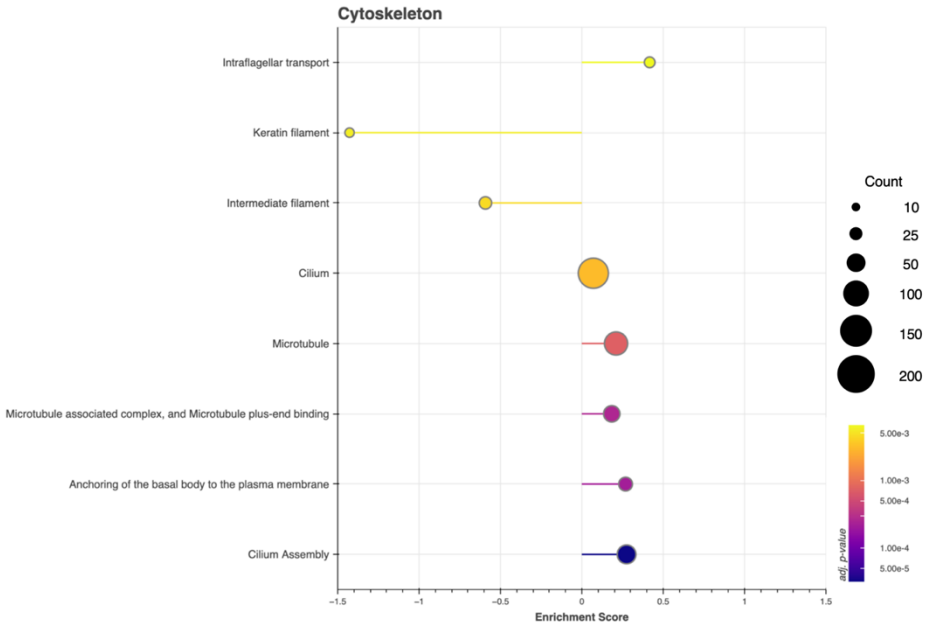

Figure 3.6. Enrichment of pathway annotations related to cytoskeleton and cell structure in neurons treated with 10 µM ketamine. Functional enrichment analysis results for pathway annotations related to cell structural components. Circle size is proportional to the number of proteins in the dataset with that annotation ("Count"). Circle color corresponds to p-values (Kolmogorov-Smirnov) adjusted for multiple hypothesis testing using the Benjamini–Hochberg procedure.

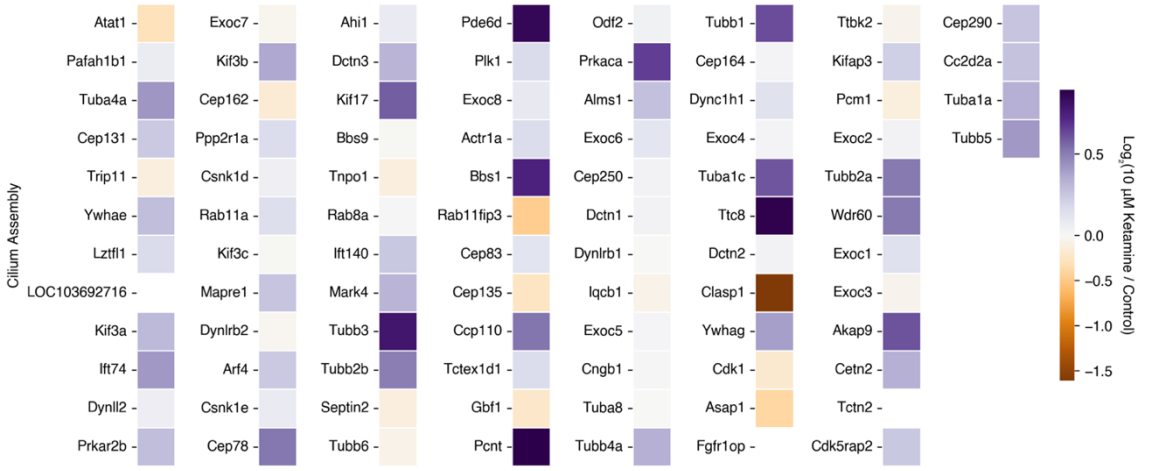

Figure 3.7. Several neuronal proteins with "cilium assembly" annotation are structural or cytoskeletal proteins. Heatmap depicts log_2FC values for proteins identified in 10 µM ketamine-treated neurons and untreated neurons calculated via label-free quantification from differential expression analysis.

Up-regulation of pathways implicated in cell cycle processes points to "moonlighting" of proteins involved in mitosis in post-mitotic neurons

A surprising set of positively enriched pathways in our dataset consisted of annotations broadly related to cell cycle or mitotic processes (Fig. 3.8). This was unexpected, since neurons are post-mitotic and do not undergo cell division. However, there is an increasing body of literature demonstrating that proteins traditionally linked to mitosis can have non-canonical, "moonlighting" functions in fully differentiated neurons. Several proteins, originally characterized for their roles in cell cycle progression, are now known to regulate aspects of neuronal development, function, and plasticity[181,182]. For example, multiple subunits of the Anaphase-Promoting Complex (APC/C)—including Anapc1, Anapc2, Anapc4, Anapc5, and Anapc7, which were among the proteins in our dataset with the KEGG annotation "oocyte meiosis" (Fig. 3.9A)—are central to controlling cell cycle progression but have also been implicated in synaptic plasticity and neurite growth. In neurons, the APC/C appears to help regulate the turnover of proteins that modulate axon and dendrite morphogenesis as well as synapse size and activity[183–186], including the postsynaptic glutamate receptor GluR2a[187], thereby contributing to the fine-tuning of neuronal connectivity.

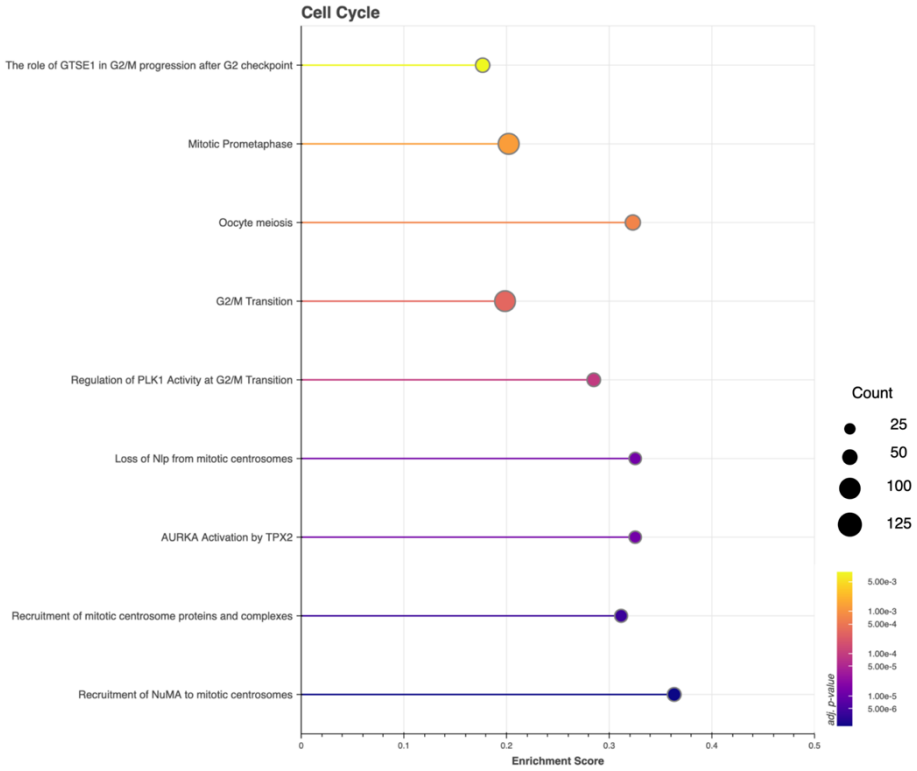

Figure 3.8. Cell cycle-related pathway annotations are positively enriched in neurons treated with 10 µM ketamine. Functional enrichment analysis results for pathway annotations related to aspects of mitosis or meiosis. Circle size is proportional to the number of proteins in the dataset with that annotation ("Count"). Circle color corresponds to p-values (Kolmogorov-Smirnov) adjusted for multiple hypothesis testing using the Benjamini–Hochberg procedure.

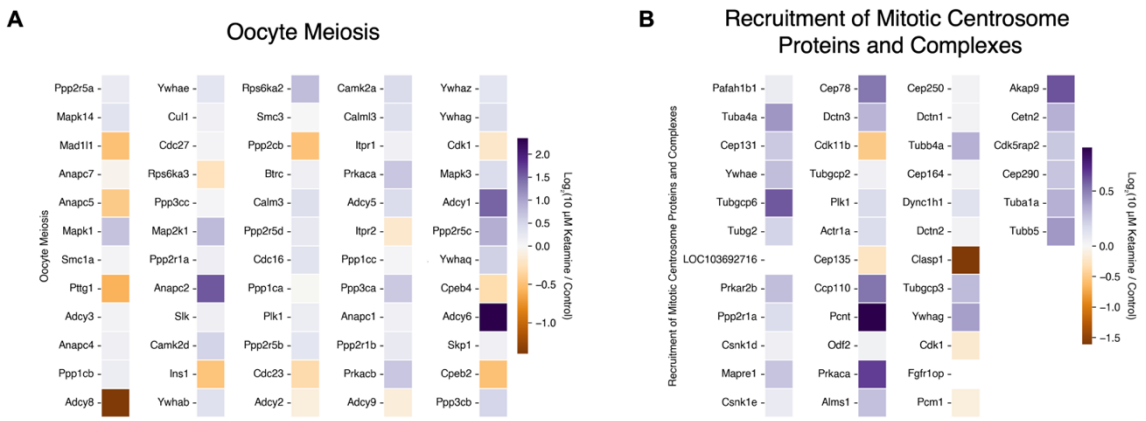

Figure 3.9. Annotations related to cell-cycle processes include several proteins that have been shown to play roles in neuronal plasticity and development. (A) Heatmap depicting $\log_2$FC values for proteins with the annotation "oocyte meiosis" identified in 10 µM ketamine-treated neurons and untreated neurons calculated via label-free quantification from differential expression analysis. (B) Heatmap depicting $\log_2$FC values for proteins with the annotation "recruitment of mitotic centrosome proteins and complexes" identified in 10 µM ketamine-treated neurons and untreated neurons calculated via label-free quantification from differential expression analysis.

Although best known for their roles in orchestrating mitosis, kinases such as cyclin-dependent kinase 1 (Cdk1), Cdk7, and Polo-like kinase 1 (Plk1) have also been shown to influence autophagy, cytoskeletal dynamics, and gene expression underlying neuronal morphogenesis and synaptic plasticity[188–191]. Cdk5rap2, which plays a necessary role in stabilizing centrosome microtubules during mitosis[192,193], is also known to bind to Cdk5r1 to activate Cdk5, a kinase critical for neuronal migration, axon guidance, and dendrite development[194–196]. Likewise, Pafah1b1, which has several cell cycle-related annotations, has also been shown to be essential for proper neuronal migration[197]. Therefore, while several of these proteins were included among those with cell cycle-related annotations in Fig. 3.8 (e.g. "recruitment of mitotic centrosome proteins and complexes," Fig. 3.9B), closer inspection of these groups of proteins reveals several with dual functions related to neuronal plasticity and neural circuit wiring.

While members of the kinesin family—such as Kif2a, Kif2c, Kif3a, and Kif3b—are involved in microtubule dynamics during cell division[198], in neurons, these motors are essential for axonal transport and the regulation of microtubule stability, ensuring the proper delivery of cargo along axons and dendrites[199,200]. Similarly, cytoplasmic dynein (e.g., Dync1h1), a key player in mitotic spindle function[201,202], is indispensable in neurons for retrograde transport, moving vesicles, organelles, and signaling endosomes that are critical for neuronal maintenance and plasticity[199,202,203]. Septin2, typically involved in cytokinesis[139,140], has also been observed in neurons, where it contributes to dendritic spine formation and synaptic stability through interactions with the actin cytoskeleton[114,204]. Collectively, these findings suggest that the enrichment of "cell cycle" pathways in our cortical neuron cultures likely reflects the alternative roles these proteins play in orchestrating cytoskeletal dynamics, vesicular trafficking, and synaptic remodeling, rather than an indication of cell division.

Negative enrichment of pathways related to translation observed in ketamine-treated neurons

We were intrigued to find that several pathways related to translation were negatively enriched in neurons treated with 10 μM ketamine (Fig. 3.10). Given the increase in AHA

labeling observed in these samples, suggestive of overall higher levels of protein synthesis, and Li et al.'s findings that sub-anesthetic doses of ketamine activate mTOR signaling and increase levels of synaptic proteins in the rat prefrontal cortex[34], one might have expected to see these pathways up-regulated. It is worth noting that there are conflicting reports regarding the role of mTOR signaling in mediating ketamine's rapid acting antidepressant effects. While some studies have demonstrated mTOR activation in response to ketamine treatment and that administration of mTOR antagonist rapamycin blocks ketamine's antidepressant effects[205–207], others have failed to replicate these results[35,208,209].

Activation of mTOR leads to increased protein synthesis via multiple mechanisms. By inhibiting translational repressors such as 4E-BP1 and 4E-BP2 and activating other kinases such as ribosomal kinase S6 that stimulate translation, mTOR can increase translation via mechanisms that do not necessarily depend on increased synthesis of translational machinery[210]. Indeed, as mentioned above, we did observe a significant decrease in expression of 4E-BP2 in response to ketamine treatment, which would be expected to result in increased protein synthesis (4E-BP1 was not among the proteins identified via LC-MS/MS). However, mTOR activation has been shown to also increase ribosome biogenesis by positively regulating ribosomal protein synthesis, as well as increasing transcription of ribosomal RNA[211,212]. The overall decrease in expression of proteins with ribosome-related annotations we observed in response to treatment with 10 μM ketamine (Fig. 3.10) is in contrast with hypotheses regarding mTOR activation. One study using pERK levels as a measure for mTOR activation in *in vitro* primary rat cortical neurons showed that, while sub-micromolar doses of ketamine led to significant increases in pERK, 1 μM and 10 μM doses did not[37]. This would suggest that the increase in protein synthesis observed in our ketamine-treated samples might occur via mechanisms involving post-translational modifications that ultimately activate translational machinery. Alternatively, differential regulation of translation at the mRNA transcript level could lead to increased synthesis of synaptic, axonal, dendritic, and cytoskeletal proteins but decreased expression of housekeeping proteins that make up translational machinery. Finally, non-mTOR pathways, such as MAPK signaling, could be responsible for the observed increase in protein synthesis[213,214].

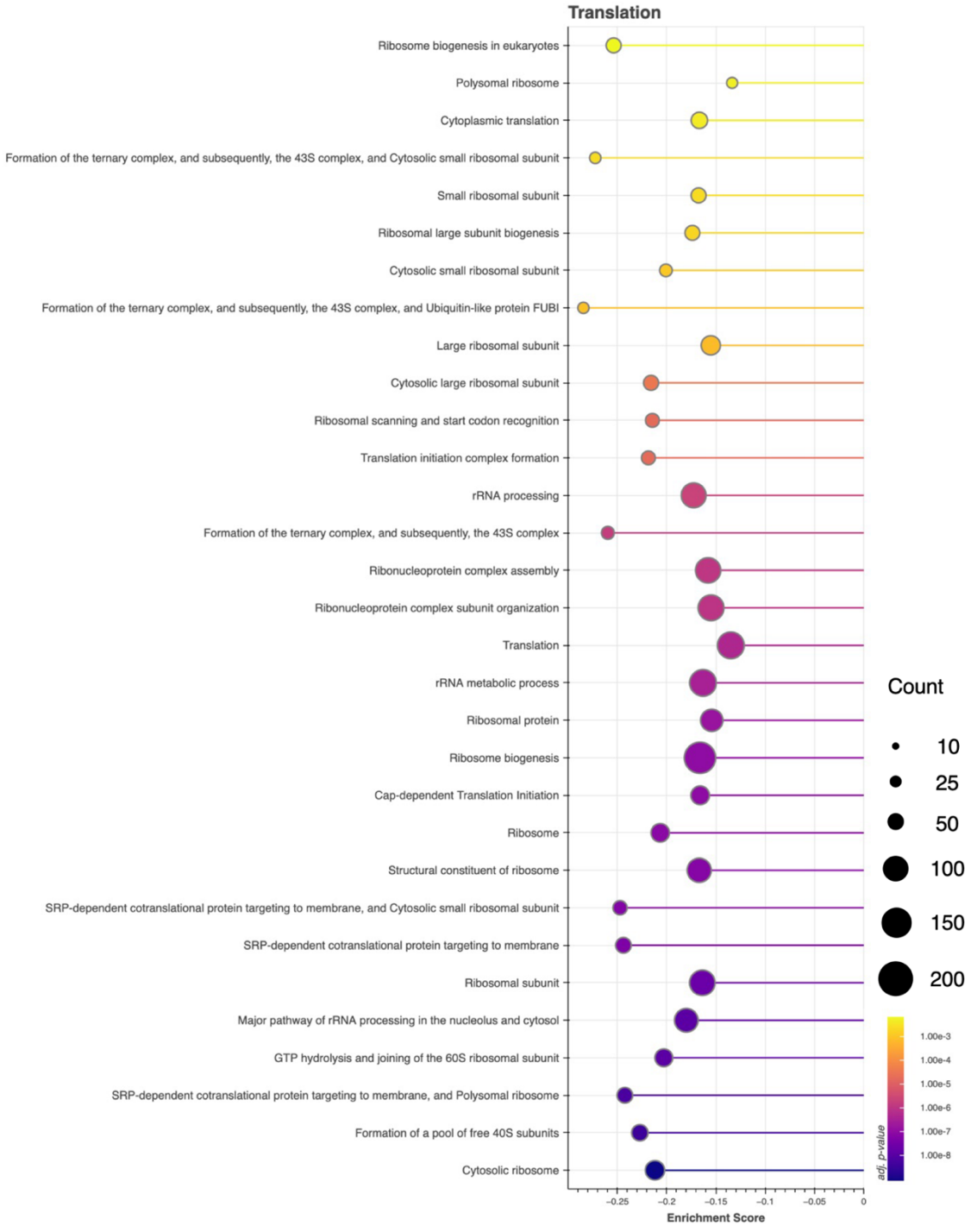

Figure 3.10. Negative enrichment of pathways and processes related to translation observed in 10 μM ketamine-treated neurons. Functional enrichment analysis results for pathway annotations related to translational machinery or processes. Circle size is proportional to the number of proteins in the dataset with that annotation ("Count"). Circle color corresponds to p-values (Kolmogorov-Smirnov) adjusted for multiple hypothesis testing using the Benjamini–Hochberg procedure.

Functional enrichment analysis reveals synapse-related pathways are up-regulated in neurons treated with 1 µM doses of ketamine

While functional enrichment analysis of data comparing protein expression in 1 µM ketamine-treated samples to controls predictably led to the identification of fewer significantly altered pathways than was observed in samples treated with higher doses, several interesting pathways were found to be differentially regulated. The majority of these significantly enriched pathways (21/36) were up-regulated pathways related to synaptic processes (Fig. 3.11), including synaptic signaling (e.g. "synaptic vesicle," "calmodulin

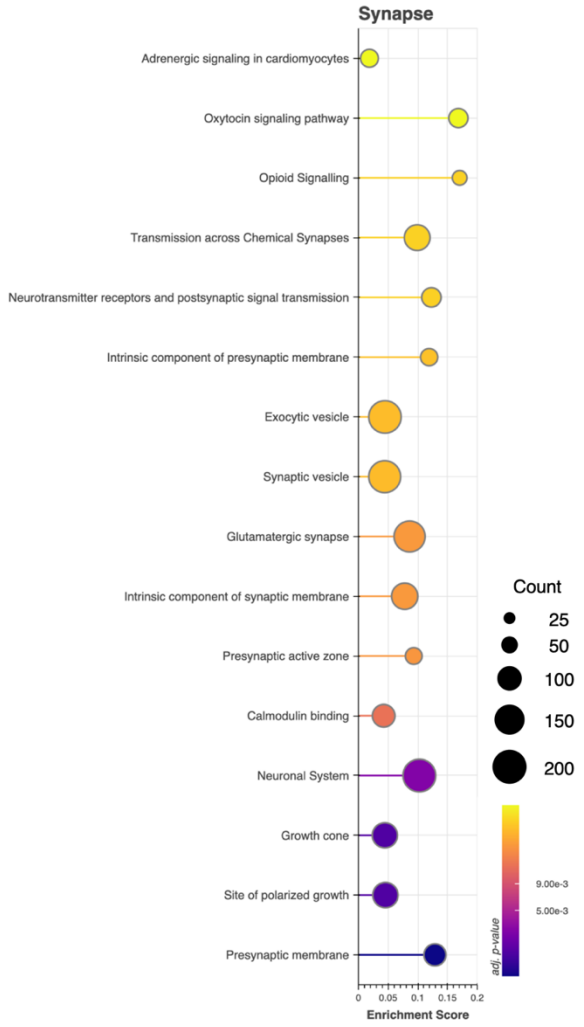

Figure 3.11. Positive enrichment of pathway annotations related to synaptic structures and functions in neurons treated with 1 µM ketamine. Functional enrichment analysis results for pathway annotations related to synaptic structures and processes. Circle size is proportional to the number of proteins in the dataset with that annotation ("Count"). Circle color corresponds to p-values (Kolmogorov-Smirnov) adjusted for multiple hypothesis testing using the Benjamini–Hochberg procedure.

binding," "glutamatergic synapse," "opioid signaling," "transmission across chemical synapses," "neurotransmitter receptors and postsynaptic signal transmission"), synaptogenesis ("growth cone," "site of polarized growth"), and synaptic structural components (e.g. "presynaptic active zone," "presynaptic membrane," "intrinsic component of synaptic membrane"). Other interesting positively enriched pathways in neurons exposed to 1 μM ketamine include "voltage-gated channel activity and ion homeostasis," indicative of changes in neuronal activity, "G-protein mediated events," "GTP-ase activity," and "GTP binding," which point to changes in G-protein signaling, and "microtubule," which agrees with aforementioned changes in expression of cytoskeletal proteins underlying neuronal morphogenesis and synaptic plasticity.

Functional enrichment analysis was able to identify broader patterns of protein expression changes whose directionality would not have been clear by simply examining individual up- or down-regulated proteins. Whereas analysis of differential expression data revealed synaptic and cytoskeletal proteins to be both significantly up- and down-regulated, functional enrichment analysis considering all proteins in our dataset revealed overall increases in these classes of proteins in ketamine-treated samples, highlighting its utility in proteomic data analysis.

3.4 Conclusion

In summary, our BONCAT-based proteomic analysis reveals that ketamine treatment leads to an increase in neuronal protein synthesis, accompanied by widespread changes in the expression of proteins involved in synaptic function, cytoskeletal dynamics, intracellular signaling, vesicle trafficking, metabolism, and gene regulation. These changes were most pronounced at 10 μM ketamine but were also detectable at a more physiologically relevant 1 μM dose when considering ketamine's rapid-acting antidepressant effects. Notably, we identified up-regulation of proteins that promote synaptic remodeling and plasticity, as well as down-regulation of proteins that may serve to inhibit such processes. Functional enrichment analyses revealed significant positive enrichment of synaptic, cytoskeletal, and intracellular signaling pathways, as well as surprising enrichment of mitotic pathways likely

reflecting non-canonical roles for these proteins in post-mitotic neurons. Together, our findings support and extend the hypothesis that ketamine rapidly enhances synaptic connectivity by promoting protein synthesis and dynamic remodeling of the neuronal proteome.

3.5 Materials and Methods

Primary neuron culture preparation and maintenance

The afternoon prior to cell plating, 10 cm dishes (Greiner Bio-One, 664160) were coated with 0.1 µg/mL poly-D-lysine (Sigma P6407) in an incubator at 37°C for 16-20 h. A few hours before plating cells, the poly-D-lysine solution was aspirated from the dishes, which were subsequently rinsed three times with cell culture grade water (Sigma-Aldrich, W3500) and allowed to air dry in a sterile cell culture hood. Dissociated E18 Sprague Dawley rat cortical cells were obtained from Transnetyx Tissue (formerly BrainBits, LLC). Plating of neurons was carried out following instructions provided by Transnetyx Tissue in their "E18 Dissociated Primary Neuronal Plating Protocol" with minor modifications; specifically, cells were spun down at 67 x g for 5 minutes and NbActiv4™ medium (Transnetyx Tissue) was used instead of NbActiv1™. Cells were plated at a density of $6x10^6$ cells per 10 cm dish (~100,000 cells/cm^2) in 15 mL NBActiv4™ medium containing 5% HyClone™ Defined Fetal Bovine Serum (FBS) (Cytiva, SH30070). After 24 h, a full medium exchange was performed, replacing the FBS-containing medium with 10 mL NBActiv4™ without serum. Every 3-4 days, a half medium exchange was performed by leaving behind 7.5 mL of spent medium, removing the rest, and adding 7.5 mL fresh, 37°C, CO_2-equilibrated NbActiv4™ medium.

Treatment and harvesting of cultured neurons

A 5 mM stock solution of racemic ketamine was prepared by combining equal volumes of previously prepared 5 mM stock solutions of *(R)*-ketamine hydrochloride (Cayman Chemical, 16519) and *(S)*-ketamine hydrochloride (Cayman Chemical, 9001961) in 1X PBS (Gibco, 10010-023). A 40 mM solution of AHA was prepared by dissolving AHA (Iris Biotech, HAA9280) in NbActiv4™. These were then diluted in NbActiv4™ to achieve a

solution of 8 mM AHA and either 0 μM, 2 μM, or 20 μM ketamine that was filtered under sterile conditions through a 0.2 μm filter and equilibrated in the incubator prior to neuron treatments. At 18 DIV, 7.5 mL of spent medium was left in each dish and 7.5 mL of the warmed, equilibrated treatment solution was added to each dish, resulting in a final concentration of 4 mM AHA and 0 μM, 1 μM, or 10 μM ketamine. The concentration of methionine in the medium is 0.2 mM.

After 24 h, the treatment solution was aspirated from each dish and cells were rinsed twice with 10 mL PBS with protease inhibitor cocktail (cOmplete Mini EDTA-free, Roche, 04-693-159-001) added at a ratio of 1 tablet per 50 mL PBS (PBS+PI). After the second rinse, 5 mL PBS+PI was added to each dish, dishes were thoroughly scraped with a cell scraper, and the liquid with released cells was transferred to a 15 mL Falcon tube on ice. Scraping and collection of cells were repeated with another 5 mL PBS+PI to ensure maximal harvesting and the cells were added to the same tube for each sample. Cells were centrifuged for 5 min at 5000 g, supernatants were carefully removed, and the remaining pellets were stored at -80°C until subsequent lysis.

Preparation of cell lysates

After thawing the cell pellets, 500 μL lysis buffer containing 1% Triton X-100 (Thermo Scientific, 85111), 1% (w/v) sodium dodecyl sulfate (Sigma-Aldrich, L5750), and 1:1000 EDTA-free protease inhibitors (Millipore, 539134) in 1X PBS were added to each tube. After pipetting up and down to suspend each pellet in the lysis buffer, the cell suspensions were transferred to 1.5-mL Eppendorf tubes provided by the BeatBox Tissue Kit 24x (PreOmics, P.O.00128) containing a magnetic bead for homogenization. Benzonase (Sigma-Aldrich, E8263-25KU) was added to each tube (1 μL per 500 μL lysate) and, after 5-10 min incubation, the tubes were placed in the PreOmics BeatBox tissue homogenizer for 10 min on the standard setting. Samples were then heated at 95°C for 10 min, followed by one more cycle of homogenization and heating. Lysates were cleared by centrifugation (20 min, 20,600 g, 4°C) and the supernatants were transferred to Protein LoBind tubes (Eppendorf, 02243108). Protein concentrations in each sample were measured using the Pierce™ BCA

Protein Assay Kit and normalized across all samples using 1% SDS in PBS to achieve the same mass of protein (typically 400-500 µg per sample) in a total volume of 500 µL. Lysates were stored at -80°C for further processing.

BONCAT enrichment and sample preparation for LC-MS/MS

For BONCAT analysis, protein lysates were first alkylated by adding 100 µL of 600 mM chloroacetamide (Sigma-Aldrich, C0267) prepared in 0.8% SDS/PBS, and incubating the mixture on a tube shaker at 65°C for 30 min at 1200 RPM in the dark. After alkylation, 600 µL of an 8 M urea / 0.85 M NaCl solution in PBS was added (4 M final concentration of urea), along with 30 µL aza-dibenzocyclooctyne (DBCO) agarose beads (Vector Laboratories, CCT-1034). The copper-free click reaction was then performed by gently rotating the mixture on a rotary wheel at low speed for 24 h in the dark at room temperature. Samples were centrifuged for 1 min at 1.5k RCF and the supernatant was removed. Reduction of samples was conducted by adding 500 µL of 5 mM dithiothreitol (Sigma-Aldrich, 43815) dissolved in 0.8% SDS/PBS, followed by incubation on a tube shaker at 70°C for 15 min at 1200 RPM in darkness. After centrifugation and removal of the supernatant, a second alkylation step was performed by adding 500 µL of 40 mM chloroacetamide to each sample and incubating on a rotary wheel for 30 min in the dark at room temperature. To reduce the amount of nonspecifically bound unlabeled protein, beads were rigorously washed first with 50 mL 0.8% (w/v) SDS in PBS, followed by 50 mL urea in 100 mM tris hydrochloride (pH = 8.0), and finally 50 mL 20% (v/v) acetonitrile (ACN) in doubly distilled water. For on-bead digestion, 0.1 µg trypsin and 0.05 µg endoproteinase LysC were added to each sample, and the mixture was incubated overnight at 37°C on a tube shaker at 1200 RPM. The next day, samples were centrifuged for 1 min at 1.5k RCF, and peptide-containing supernatants were transferred to Pierce™ Centrifuge Columns (Thermo Scientific, 89868). To maximize extraction of digested peptides, the beads were subjected to two additional washes, each using 50 µL of STOP solution from the PreOmics Phoenix Kit (P.O.00023, Lot Number 0000444362) which were added to the columns with the supernatants. Samples underwent a final centrifugation step at 1.5k RCF for 1 min to remove any residual DBCO-agarose resin. Desalting and purification of the peptides were performed

using the PreOmics Phoenix Kit following the manufacturer's instructions. After the final elution step, the purified peptides were vacuum concentrated to dryness and resuspended in 10 µL 0.2% formic acid for LC-MS/MS analysis.

LC-MS/MS analysis

Mass spectrometry was performed using an Eclipse mass spectrometer (Thermo Fisher Scientific, USA) coupled to a Vanquish Neo UHPLC system (Thermo Fisher Scientific, USA). Separation of peptides from BONCAT-enriched samples was carried out on an Aurora UHPLC column (25 cm × 75 µm, 1.7 µm C18, AUR3-25075C18-TS, Ion Opticks) with a constant flow rate of 0.35 µL/min over a 1-hour run. Ionization was conducted in positive mode at 1.6 kV. The chromatographic gradient consisted of 6% solvent B for 3.5 minutes, a linear increase to 25% B over 41.5 minutes, ramping to 40% B across the next 15 minutes, with a rapid increase to 98% B over 2 minutes, followed by a 5-minute hold at 98% B. Solvent B consisted of 80% acetonitrile (ACN, Fisher Scientific, A9554) and 0.2% formic acid (FA, Fisher Scientific, A11750) in water, and the remaining volume of solvent in each segment of the gradient consisted of Solvent A (2% ACN and 0.2% FA in water). MS1 scans were acquired in the Orbitrap at a resolution of 120,000 across an m/z range of 375–1600. The automatic gain control target was set to 106 with a maximum injection time of 50 ms. MS2 spectra were acquired in the ion trap using fast scan mode on precursors with charge states ranging from 2 to 7 and quadrupole isolation mode (1.2 m/z isolation window) with higher-energy collisional dissociation (HCD) activation type set to 30%. Dynamic exclusion was set to 30 s. The ion transfer tube temperature was maintained at 300°C, and the S-lens RF level was set to 30.

Proteomic data processing and analysis

Raw mass spectrometry data were processed using Proteome Discoverer 3.0 software with the SequestHT search engine, aligned against the Uniprot *Rattus norvegicus* proteome (UP000002494). Search parameters were as follows: oxidation (+15.995 Da, M) and deamidation (+0.984 Da, N) as dynamic modifications, and carbamidomethylation (+57.021 Da, C) as a fixed modification. The mass tolerance for precursor ions was set at 10 ppm, and

0.6 Da for fragment ions. Peptide-spectrum matches were filtered using a false discovery rate (FDR) threshold of 1%, validated via the Percolator Node using q-values. Peptide quantification was performed using the Minora LFQ node, which integrates the area under the curve from MS1 intensity data. Raw mass spectrometry data were deposited to the ProteomeXchange Consortium via the PRIDE[215] partner repository with the dataset identifier PXD064436.

Raw protein abundances were exported from Proteome Discoverer 3.0, imported into R, and processed using the Tidyproteomics package (version 1.7.3) (https://jeffsocal.github.io/tidyproteomics/index.html)[216]. Common contaminant proteins were filtered out and protein abundances were normalized across samples using median normalization. Differential expression analysis was conducted within the Tidyproteomics analysis pipeline utilizing the limma statistical framework (https://bioinf.wehi.edu.au/limma/). All data visualizations were generated using a separate Python analysis pipeline. All code is available upon request.

Functional enrichment analysis to identify significantly up- or down-regulated pathways and annotations was performed using "Proteins with Values/Ranks – Functional Enrichment Analysis" feature on the STRING database website (https://string-db.org, Version 12.0). For each comparison (i.e. 10 μM ketamine versus controls and 1 μM versus controls), the search input consisted of Uniprot accessions and log_2FC values for all proteins included in the differential expression analysis. FDR stringency was set to 0.01 for analysis of 10 μM vs control data and to 0.05 for analysis of the 1 μM vs control data. Significantly enriched pathway annotations were manually categorized as "Synapse," "Cytoskeleton," "Cell Cycle," and "Translation" for the purposes of visualizing functional enrichment analysis results. For annotations that appeared twice in the results, the one with the greater enrichment score was selected for plotting in the lollipop charts.

3.6 References

(1) Kupfer, D. J.; Frank, E.; Phillips, M. L. Major Depressive Disorder: New Clinical, Neurobiological, and Treatment Perspectives. *The Lancet* **2012**, *379* (9820), 1045–1055. https://doi.org/10.1016/S0140-6736(11)60602-8.

(2) Hofmann, S. G.; Curtiss ,Joshua; Carpenter ,Joseph K.; and Kind, S. Effect of Treatments for Depression on Quality of Life: A Meta-Analysis*. *Cogn. Behav. Ther.* **2017**, *46* (4), 265–286. https://doi.org/10.1080/16506073.2017.1304445.

(3) Marx, W.; Penninx, B. W. J. H.; Solmi, M.; Furukawa, T. A.; Firth, J.; Carvalho, A. F.; Berk, M. Major Depressive Disorder. *Nat. Rev. Dis. Primer* **2023**, *9* (1), 1–21. https://doi.org/10.1038/s41572-023-00454-1.

(4) Murray, C. J. L.; Lopez, A. D. Measuring the Global Burden of Disease. *N. Engl. J. Med.* **2013**, *369* (5), 448–457. https://doi.org/10.1056/NEJMra1201534.

(5) Kessler, R. C.; Berglund, P.; Demler, O.; Jin, R.; Merikangas, K. R.; Walters, E. E. Lifetime Prevalence and Age-of-Onset Distributions of DSM-IV Disorders in the National Comorbidity Survey Replication. *Arch. Gen. Psychiatry* **2005**, *62* (6), 593–602. https://doi.org/10.1001/archpsyc.62.6.593.

(6) Shaw, D. M.; Camps, F. E.; Eccleston, E. G. 5-Hydroxytryptamine in the Hind-Brain of Depressive Suicides. *Br. J. Psychiatry* **1967**, *113* (505), 1407–1411. https://doi.org/10.1192/bjp.113.505.1407.

(7) Åsberg, M.; Thorén, P.; Traskman, L.; Bertilsson, L.; Ringberger, V. "Serotonin Depression"—A Biochemical Subgroup Within the Affective Disorders? *Science* **1976**, *191* (4226), 478–480. https://doi.org/10.1126/science.1246632.

(8) Sarrias, M. J.; Artigas, F.; Martínez, E.; Gelpí, E.; Alvarez, E.; Udina, C.; Casas, M. Decreased Plasma Serotonin in Melancholic Patients: A Study with Clomipramine. *Biol. Psychiatry* **1987**, *22* (12), 1429–1438. https://doi.org/10.1016/0006-3223(87)90100-4.

(9) Weihs, K.; Wert, J. M. A Primary Care Focus on the Treatment of Patients With Major Depressive Disorder. *Am. J. Med. Sci.* **2011**, *342* (4), 324–330. https://doi.org/10.1097/MAJ.0b013e318210ff56.

(10) Tollefson, G. D.; Bosomworth, J. C.; Heiligenstein, J. H.; Potvin, J. H.; Holman, S. A Double-Blind, Placebo-Controlled Clinical Trial of Fluoxetine in Geriatric Patients With Major Depression. *Int. Psychogeriatr.* **1995**, *7* (1), 89–104. https://doi.org/10.1017/S1041610295001888.

(11) Trivedi, M. H.; Rush, A. J.; Wisniewski, S. R.; Nierenberg, A. A.; Warden, D.; Ritz, L.; Norquist, G.; Howland, R. H.; Lebowitz, B.; McGrath, P. J.; Shores-Wilson, K.; Biggs, M. M.; Balasubramani, G. K.; Fava, M.; STAR*D Study Team. Evaluation of Outcomes With Citalopram for Depression Using Measurement-Based Care in STAR*D: Implications for Clinical Practice. *Am. J. Psychiatry* **2006**, *163* (1), 28–40. https://doi.org/10.1176/appi.ajp.163.1.28.

(12) Rush, A. J.; Trivedi, M. H.; Wisniewski, S. R.; Nierenberg, A. A.; Stewart, J. W.; Warden, D.; Niederehe, G.; Thase, M. E.; Lavori, P. W.; Lebowitz, B. D.; McGrath, P. J.; Rosenbaum, J. F.; Sackeim, H. A.; Kupfer, D. J.; Luther, J.; Fava, M. Acute and Longer-Term Outcomes in Depressed Outpatients Requiring One or Several Treatment Steps: A STAR*D Report. *Am. J. Psychiatry* **2006**, *163* (11), 1905–1917. https://doi.org/10.1176/ajp.2006.163.11.1905.

(13) Warden, D.; Rush, A. J.; Trivedi, M. H.; Fava, M.; Wisniewski, S. R. The STAR*D Project Results: A Comprehensive Review of Findings. *Curr. Psychiatry Rep.* **2007**, *9* (6), 449–459. https://doi.org/10.1007/s11920-007-0061-3.

(14) Jakobsen, J. C.; Katakam, K. K.; Schou, A.; Hellmuth, S. G.; Stallknecht, S. E.; Leth-Møller, K.; Iversen, M.; Banke, M. B.; Petersen, I. J.; Klingenberg, S. L.; Krogh, J.; Ebert, S. E.; Timm, A.; Lindschou, J.; Gluud, C. Selective Serotonin Reuptake Inhibitors versus Placebo in Patients with Major Depressive Disorder. A Systematic Review with Meta-Analysis and Trial Sequential Analysis. *BMC Psychiatry* **2017**, *17* (1), 58. https://doi.org/10.1186/s12888-016-1173-2.

(15) Papakostas, G. I. Tolerability of Modern Antidepressants. *J. Clin. Psychiatry* **2008**, *69 Suppl E1*, 8–13.

(16) Moret, C.; Isaac, M.; Briley, M. Problems Associated with Long-Term Treatment with Selective Serotonin Reuptake Inhibitors. *J. Psychopharmacol. Oxf. Engl.* **2009**, *23* (8), 967–974. https://doi.org/10.1177/0269881108093582.

(17) Lee, S. H.; Paz-Filho, G.; Mastronardi, C.; Licinio, J.; Wong, M.-L. Is Increased Antidepressant Exposure a Contributory Factor to the Obesity Pandemic? *Transl. Psychiatry* **2016**, *6* (3), e759–e759. https://doi.org/10.1038/tp.2016.25.

(18) Belmaker, R. H.; Agam, G. Major Depressive Disorder. *N. Engl. J. Med.* **2008**, *358* (1), 55–68. https://doi.org/10.1056/NEJMra073096.

(19) Malhi, G. S.; Mann, J. J. Depression. *The Lancet* **2018**, *392* (10161), 2299–2312. https://doi.org/10.1016/S0140-6736(18)31948-2.

(20) Stahl, S. M. Mechanism of Action of Serotonin Selective Reuptake Inhibitors: Serotonin Receptors and Pathways Mediate Therapeutic Effects and Side Effects. *J. Affect. Disord.* **1998**, *51* (3), 215–235. https://doi.org/10.1016/S0165-0327(98)00221-3.

(21) Commons, K. G.; Linnros, S. E. Delayed Antidepressant Efficacy and the Desensitization Hypothesis. *ACS Chem. Neurosci.* **2019**, *10* (7), 3048–3052. https://doi.org/10.1021/acschemneuro.8b00698.

(22) Beasley, C. M.; Dornseif, B. E.; Pultz, J. A.; Bosomworth, J. C.; Sayler, M. E. Fluoxetine versus Trazodone: Efficacy and Activating-Sedating Effects. *J. Clin. Psychiatry* **1991**, *52* (7), 294–299.

(23) Jick, H.; Kaye, J. A.; Jick, S. S. Antidepressants and the Risk of Suicidal Behaviors. *JAMA* **2004**, *292* (3), 338–343. https://doi.org/10.1001/jama.292.3.338.

(24) Gould, T. D.; Zarate, C. A.; Thompson, S. M. Molecular Pharmacology and Neurobiology of Rapid-Acting Antidepressants. *Annu. Rev. Pharmacol. Toxicol.* **2019**, *59* (Volume 59, 2019), 213–236. https://doi.org/10.1146/annurev-pharmtox-010617-052811.

(25) Witkin, J. M.; Martin, A. E.; Golani, L. K.; Xu, N. Z.; Smith, J. L. Chapter Three - Rapid-Acting Antidepressants. In *Advances in Pharmacology*; Witkin, J. M., Ed.; Neuropsychotherapeutics; Academic Press, 2019; Vol. 86, pp 47–96. https://doi.org/10.1016/bs.apha.2019.03.002.

(26) Chen, T.; Cheng, L.; Ma, J.; Yuan, J.; Pi, C.; Xiong, L.; Chen, J.; Liu, H.; Tang, J.; Zhong, Y.; Zhang, X.; Liu, Z.; Zuo, Y.; Shen, H.; Wei, Y.; Zhao, L. Molecular Mechanisms of Rapid-Acting Antidepressants: New Perspectives for Developing Antidepressants. *Pharmacol. Res.* **2023**, *194*, 106837. https://doi.org/10.1016/j.phrs.2023.106837.

(27) Berman, R. M.; Cappiello, A.; Anand, A.; Oren, D. A.; Heninger, G. R.; Charney, D. S.; Krystal, J. H. Antidepressant Effects of Ketamine in Depressed Patients. *Biol. Psychiatry* **2000**, *47* (4), 351–354. https://doi.org/10.1016/S0006-3223(99)00230-9.

(28) Zarate, C. A., Jr; Singh, J. B.; Carlson, P. J.; Brutsche, N. E.; Ameli, R.; Luckenbaugh, D. A.; Charney, D. S.; Manji, H. K. A Randomized Trial of an N-Methyl-D-Aspartate Antagonist in Treatment-Resistant Major Depression. *Arch. Gen. Psychiatry* **2006**, *63* (8), 856–864. https://doi.org/10.1001/archpsyc.63.8.856.

(29) Chen, M.-H.; Li, C.-T.; Lin, W.-C.; Hong, C.-J.; Tu, P.-C.; Bai, Y.-M.; Cheng, C.-M.; Su, T.-P. Persistent Antidepressant Effect of Low-Dose Ketamine and Activation in the Supplementary Motor Area and Anterior Cingulate Cortex in Treatment-Resistant Depression: A Randomized Control Study. *J. Affect. Disord.* **2018**, *225*, 709–714. https://doi.org/10.1016/j.jad.2017.09.008.

(30) Riggs, L. M.; Gould, T. D. Ketamine and the Future of Rapid-Acting Antidepressants. *Annu. Rev. Clin. Psychol.* **2021**, *17* (Volume 17, 2021), 207–231. https://doi.org/10.1146/annurev-clinpsy-072120-014126.

(31) Daly, E. J.; Trivedi, M. H.; Janik, A.; Li, H.; Zhang, Y.; Li, X.; Lane, R.; Lim, P.; Duca, A. R.; Hough, D.; Thase, M. E.; Zajecka, J.; Winokur, A.; Divacka, I.; Fagiolini, A.; Cubała, W. J.; Bitter, I.; Blier, P.; Shelton, R. C.; Molero, P.; Manji, H.; Drevets, W. C.; Singh, J. B. Efficacy of Esketamine Nasal Spray Plus Oral Antidepressant Treatment for Relapse Prevention in Patients With Treatment-Resistant Depression: A Randomized Clinical Trial. *JAMA Psychiatry* **2019**, *76* (9), 893–903. https://doi.org/10.1001/jamapsychiatry.2019.1189.

(32) Gerhard, D. M.; Pothula, S.; Liu, R.-J.; Wu, M.; Li, X.-Y.; Girgenti, M. J.; Taylor, S. R.; Duman, C. H.; Delpire, E.; Picciotto, M.; Wohleb, E. S.; Duman, R. S. GABA Interneurons Are the Cellular Trigger for Ketamine's Rapid Antidepressant Actions. *J. Clin. Invest.* **2020**, *130* (3), 1336–1349. https://doi.org/10.1172/JCI130808.

(33) Pothula, S.; Kato, T.; Liu, R.-J.; Wu, M.; Gerhard, D.; Shinohara, R.; Sliby, A.-N.; Chowdhury, G. M. I.; Behar, K. L.; Sanacora, G.; Banerjee, P.; Duman, R. S. Cell-

Type Specific Modulation of NMDA Receptors Triggers Antidepressant Actions. *Mol. Psychiatry* **2021**, *26* (9), 5097–5111. https://doi.org/10.1038/s41380-020-0796-3.

(34) Li, N.; Lee, B.; Liu, R.-J.; Banasr, M.; Dwyer, J. M.; Iwata, M.; Li, X.-Y.; Aghajanian, G.; Duman, R. S. mTOR-Dependent Synapse Formation Underlies the Rapid Antidepressant Effects of NMDA Antagonists. *Science* **2010**, *329* (5994), 959–964. https://doi.org/10.1126/science.1190287.

(35) Autry, A. E.; Adachi, M.; Nosyreva, E.; Na, E. S.; Los, M. F.; Cheng, P.; Kavalali, E. T.; Monteggia, L. M. NMDA Receptor Blockade at Rest Triggers Rapid Behavioural Antidepressant Responses. *Nature* **2011**, *475* (7354), 91–95. https://doi.org/10.1038/nature10130.

(36) Réus, G. Z.; Vieira, F. G.; Abelaira, H. M.; Michels, M.; Tomaz, D. B.; dos Santos, M. A. B.; Carlessi, A. S.; Neotti, M. V.; Matias, B. I.; Luz, J. R.; Dal-Pizzol, F.; Quevedo, J. MAPK Signaling Correlates with the Antidepressant Effects of Ketamine. *J. Psychiatr. Res.* **2014**, *55*, 15–21. https://doi.org/10.1016/j.jpsychires.2014.04.010.

(37) Lepack, A. E.; Bang, E.; Lee, B.; Dwyer, J. M.; Duman, R. S. Fast-Acting Antidepressants Rapidly Stimulate ERK Signaling and BDNF Release in Primary Neuronal Cultures. *Neuropharmacology* **2016**, *111*, 242–252. https://doi.org/10.1016/j.neuropharm.2016.09.011.

(38) Zanos, P.; Gould, T. D. Mechanisms of Ketamine Action as an Antidepressant. *Mol. Psychiatry* **2018**, *23* (4), 801–811. https://doi.org/10.1038/mp.2017.255.

(39) Kang, M. J. Y.; Hawken, E.; Vazquez, G. H. The Mechanisms Behind Rapid Antidepressant Effects of Ketamine: A Systematic Review With a Focus on Molecular Neuroplasticity. *Front. Psychiatry* **2022**, *13*. https://doi.org/10.3389/fpsyt.2022.860882.

(40) Liu, Y.; Lin, D.; Wu, B.; Zhou, W. Ketamine Abuse Potential and Use Disorder. *Brain Res. Bull.* **2016**, *126*, 68–73. https://doi.org/10.1016/j.brainresbull.2016.05.016.

(41) Vines, L.; Sotelo, D.; Johnson, A.; Dennis, E.; Manza, P.; Volkow, N. D.; Wang, G.-J. Ketamine Use Disorder: Preclinical, Clinical, and Neuroimaging Evidence to Support Proposed Mechanisms of Actions. *Intell. Med.* **2022**, *2* (2), 61–68. https://doi.org/10.1016/j.imed.2022.03.001.

(42) Le, T. T.; Cordero, I. P.; Jawad, M. Y.; Swainson, J.; Di Vincenzo, J. D.; Jaberi, S.; Phan, L.; Lui, L. M. W.; Ho, R.; Rosenblat, J. D.; McIntyre, R. S. The Abuse Liability of Ketamine: A Scoping Review of Preclinical and Clinical Studies. *J. Psychiatr. Res.* **2022**, *151*, 476–496. https://doi.org/10.1016/j.jpsychires.2022.04.035.

(43) Xiao, Y.; Luo, H.; Yang, W. Z.; Zeng, Y.; Shen, Y.; Ni, X.; Shi, Z.; Zhong, J.; Liang, Z.; Fu, X.; Tu, H.; Sun, W.; Shen, W. L.; Hu, J.; Yang, J. A Brain Signaling Framework for Stress-Induced Depression and Ketamine Treatment Elucidated by Phosphoproteomics. *Front. Cell. Neurosci.* **2020**, *14*, 48. https://doi.org/10.3389/fncel.2020.00048.

(44) Wesseling, H.; Rahmoune, H.; Tricklebank, M.; Guest, P. C.; Bahn, S. A Targeted Multiplexed Proteomic Investigation Identifies Ketamine-Induced Changes in Immune Markers in Rat Serum and Expression Changes in Protein Kinases/Phosphatases in Rat Brain. *J. Proteome Res.* **2015**, *14* (1), 411–421. https://doi.org/10.1021/pr5009493.

(45) Weckmann, K.; Deery, M. J.; Howard, J. A.; Feret, R.; Asara, J. M.; Dethloff, F.; Filiou, M. D.; Iannace, J.; Labermaier, C.; Maccarrone, G.; Webhofer, C.; Teplytska, L.; Lilley, K.; Müller, M. B.; Turck, C. W. Ketamine's Antidepressant Effect Is Mediated by Energy Metabolism and Antioxidant Defense System. *Sci. Rep.* **2017**, *7* (1), 15788. https://doi.org/10.1038/s41598-017-16183-x.

(46) Zhou, N.; Shi, X.; Wang, R.; Wang, C.; Lan, X.; Liu, G.; Li, W.; Zhou, Y.; Ning, Y. Proteomic Patterns Associated with Ketamine Response in Major Depressive Disorders. *Cell Biol. Toxicol.* **2025**, *41* (1), 26. https://doi.org/10.1007/s10565-024-09981-3.

(47) Kang, M. J. Y.; Hawken, E.; Vazquez, G. H. The Mechanisms Behind Rapid Antidepressant Effects of Ketamine: A Systematic Review With a Focus on Molecular Neuroplasticity. *Front. Psychiatry* **2022**, *13*. https://doi.org/10.3389/fpsyt.2022.860882.

(48) Weckmann, K.; Deery, M. J.; Howard, J. A.; Feret, R.; Asara, J. M.; Dethloff, F.; Filiou, M. D.; Labermaier, C.; Maccarrone, G.; Lilley, K. S.; Mueller, M.; Turck, C. W. Ketamine's Effects on the Glutamatergic and GABAergic Systems: A Proteomics and Metabolomics Study in Mice. *Complex Psychiatry* **2019**, *5* (1), 42–51. https://doi.org/10.1159/000493425.

(49) Herzog, D. P.; Perumal, N.; Manicam, C.; Treccani, G.; Nadig, J.; Rossmanith, M.; Engelmann, J.; Jene, T.; Hasch, A.; van der Kooij, M. A.; Lieb, K.; Gassen, N. C.; Grus, F. H.; Müller, M. B. Longitudinal CSF Proteome Profiling in Mice to Uncover the Acute and Sustained Mechanisms of Action of Rapid Acting Antidepressant (2R,6R)-Hydroxynorketamine (HNK). *Neurobiol. Stress* **2021**, *15*, 100404. https://doi.org/10.1016/j.ynstr.2021.100404.

(50) Dieterich, D. C.; Link, A. J.; Graumann, J.; Tirrell, D. A.; Schuman, E. M. Selective Identification of Newly Synthesized Proteins in Mammalian Cells Using Bioorthogonal Noncanonical Amino Acid Tagging (BONCAT). *Proc. Natl. Acad. Sci.* **2006**, *103* (25), 9482–9487.

(51) Dieterich, D. C.; Lee, J. J.; Link, A. J.; Graumann, J.; Tirrell, D. A.; Schuman, E. M. Labeling, Detection and Identification of Newly Synthesized Proteomes with Bioorthogonal Non-Canonical Amino-Acid Tagging. *Nat. Protoc.* **2007**, *2* (3), 532–540. https://doi.org/10.1038/nprot.2007.52.

(52) Rostovtsev, V. V.; Green, L. G.; Fokin, V. V.; Sharpless, K. B. A Stepwise Huisgen Cycloaddition Process: Copper(I)-Catalyzed Regioselective "Ligation" of Azides and Terminal Alkynes. *Angew. Chem. Int. Ed.* **2002**, *41* (14), 2596–2599.

https://doi.org/10.1002/1521-3773(20020715)41:14<2596::AID-ANIE2596>3.0.CO;2-4.

(53) Tornøe, C. W.; Christensen, C.; Meldal, M. Peptidotriazoles on Solid Phase: [1,2,3]-Triazoles by Regiospecific Copper(I)-Catalyzed 1,3-Dipolar Cycloadditions of Terminal Alkynes to Azides. *J. Org. Chem.* **2002**, *67* (9), 3057–3064. https://doi.org/10.1021/jo011148j.

(54) Agard, N. J.; Prescher, J. A.; Bertozzi, C. R. A Strain-Promoted [3 + 2] Azide−Alkyne Cycloaddition for Covalent Modification of Biomolecules in Living Systems. *J. Am. Chem. Soc.* **2004**, *126* (46), 15046–15047. https://doi.org/10.1021/ja044996f.

(55) Sletten, E. M.; Bertozzi, C. R. Bioorthogonal Chemistry: Fishing for Selectivity in a Sea of Functionality. *Angew. Chem. Int. Ed.* **2009**, *48* (38), 6974–6998. https://doi.org/10.1002/anie.200900942.

(56) Marchand, J. A.; Neugebauer, M. E.; Ing, M. C.; Lin, C.-I.; Pelton, J. G.; Chang, M. C. Y. Discovery of a Pathway for Terminal-Alkyne Amino Acid Biosynthesis. *Nature* **2019**, *567* (7748), 420–424. https://doi.org/10.1038/s41586-019-1020-y.

(57) Back, D.; Shaffer, B. T.; Loper, J. E.; Philmus, B. Untargeted Identification of Alkyne-Containing Natural Products Using Ruthenium-Catalyzed Azide Alkyne Cycloaddition Reactions Coupled to LC-MS/MS. *J. Nat. Prod.* **2022**, *85* (1), 105–114. https://doi.org/10.1021/acs.jnatprod.1c00798.

(58) Bagert, J. D.; Xie, Y. J.; Sweredoski, M. J.; Qi, Y.; Hess, S.; Schuman, E. M.; Tirrell, D. A. Quantitative, Time-Resolved Proteomic Analysis by Combining Bioorthogonal Noncanonical Amino Acid Tagging and Pulsed Stable Isotope Labeling by Amino Acids in Cell Culture. *Mol. Cell. Proteomics* **2014**, *13* (5), 1352–1358. https://doi.org/10.1074/mcp.M113.031914.

(59) Hodas, J. J. L.; Nehring, A.; Höche, N.; Sweredoski, M. J.; Pielot, R.; Hess, S.; Tirrell, D. A.; Dieterich, D. C.; Schuman, E. M. Dopaminergic Modulation of the Hippocampal Neuropil Proteome Identified by Bioorthogonal Noncanonical Amino Acid Tagging (BONCAT). *PROTEOMICS* **2012**, *12* (15–16), 2464–2476. https://doi.org/10.1002/pmic.201200112.

(60) Zhang, G.; Bowling, H.; Hom, N.; Kirshenbaum, K.; Klann, E.; Chao, M. V.; Neubert, T. A. In-Depth Quantitative Proteomic Analysis of de Novo Protein Synthesis Induced by Brain-Derived Neurotrophic Factor. *J. Proteome Res.* **2014**, *13* (12), 5707–5714. https://doi.org/10.1021/pr5006982.

(61) Bowling, H.; Bhattacharya, A.; Zhang, G.; Lebowitz, J. Z.; Alam, D.; Smith, P. T.; Kirshenbaum, K.; Neubert, T. A.; Vogel, C.; Chao, M. V.; Klann, E. BONLAC: A Combinatorial Proteomic Technique to Measure Stimulus-Induced Translational Profiles in Brain Slices. *Neuropharmacology* **2016**, *100*, 76–89. https://doi.org/10.1016/j.neuropharm.2015.07.017.

(62) Schanzenbächer, C. T.; Sambandan, S.; Langer, J. D.; Schuman, E. M. Nascent Proteome Remodeling Following Homeostatic Scaling at Hippocampal Synapses. *Neuron* **2016**, *92* (2), 358–371. https://doi.org/10.1016/j.neuron.2016.09.058.

(63) Schanzenbächer, C. T.; Langer, J. D.; Schuman, E. M. Time- and Polarity-Dependent Proteomic Changes Associated with Homeostatic Scaling at Central Synapses. *eLife* **2018**, *7*, e33322. https://doi.org/10.7554/eLife.33322.

(64) Blumenfeld, Z.; Bera, K.; Castrén, E.; Lester, H. A. Antidepressants Enter Cells, Organelles, and Membranes. *Neuropsychopharmacology* **2024**, *49* (1), 246–261. https://doi.org/10.1038/s41386-023-01725-x.

(65) Clements, J. A.; Nimmo, W. S. PHARMACOKINETICS AND ANALGESIC EFFECT OF KETAMINE IN MAN. *Br. J. Anaesth.* **1981**, *53* (1), 27–30. https://doi.org/10.1093/bja/53.1.27.

(66) Lester, H. A.; Miwa, J. M.; Srinivasan, R. Psychiatric Drugs Bind to Classical Targets Within Early Exocytotic Pathways: Therapeutic Effects. *Biol. Psychiatry* **2012**, *72* (11), 907–915. https://doi.org/10.1016/j.biopsych.2012.05.020.

(67) Peltoniemi, M. A.; Hagelberg, N. M.; Olkkola, K. T.; Saari, T. I. Ketamine: A Review of Clinical Pharmacokinetics and Pharmacodynamics in Anesthesia and Pain Therapy. *Clin. Pharmacokinet.* **2016**, *55* (9), 1059–1077. https://doi.org/10.1007/s40262-016-0383-6.

(68) Kamp, J.; Jonkman, K.; Velzen, M. van; Aarts, L.; Niesters, M.; Dahan, A.; Olofsen, E. Pharmacokinetics of Ketamine and Its Major Metabolites Norketamine, Hydroxynorketamine, and Dehydronorketamine: A Model-Based Analysis. *Br. J. Anaesth.* **2020**, *125* (5), 750–761. https://doi.org/10.1016/j.bja.2020.06.067.

(69) Lepack, A. E.; Fuchikami, M.; Dwyer, J. M.; Banasr, M.; Duman, R. S. BDNF Release Is Required for the Behavioral Actions of Ketamine. *Int. J. Neuropsychopharmacol.* **2015**, *18* (1), pyu033. https://doi.org/10.1093/ijnp/pyu033.

(70) Cavalleri, L.; Merlo Pich, E.; Millan, M. J.; Chiamulera, C.; Kunath, T.; Spano, P. F.; Collo, G. Ketamine Enhances Structural Plasticity in Mouse Mesencephalic and Human iPSC-Derived Dopaminergic Neurons via AMPAR-Driven BDNF and mTOR Signaling. *Mol. Psychiatry* **2018**, *23* (4), 812–823. https://doi.org/10.1038/mp.2017.241.

(71) Lopez, J. P.; Lücken, M. D.; Brivio, E.; Karamihalev, S.; Kos, A.; De Donno, C.; Benjamin, A.; Yang, H.; Dick, A. L. W.; Stoffel, R.; Flachskamm, C.; Ressle, A.; Roeh, S.; Huettl, R.-E.; Parl, A.; Eggert, C.; Novak, B.; Yan, Y.; Yeoh, K.; Holzapfel, M.; Hauger, B.; Harbich, D.; Schmid, B.; Di Giaimo, R.; Turck, C. W.; Schmidt, M. V.; Deussing, J. M.; Eder, M.; Dine, J.; Theis, F. J.; Chen, A. Ketamine Exerts Its Sustained Antidepressant Effects via Cell-Type-Specific Regulation of *Kcnq2*. *Neuron* **2022**, *110* (14), 2283-2298.e9. https://doi.org/10.1016/j.neuron.2022.05.001.

(72) Yao, W.; Cao, Q.; Luo, S.; He, L.; Yang, C.; Chen, J.; Qi, Q.; Hashimoto, K.; Zhang, J. Microglial ERK-NRBP1-CREB-BDNF Signaling in Sustained Antidepressant

Actions of (R)-Ketamine. *Mol. Psychiatry* **2022**, *27* (3), 1618–1629. https://doi.org/10.1038/s41380-021-01377-7.

(73) Diniz, C. R. A. F.; Crestani, A. P.; Casarotto, P. C.; Biojone, C.; Cannarozzo, C.; Winkel, F.; Prozorov, M. A.; Kot, E. F.; Goncharuk, S. A.; Benette Marques, D.; Rakauskas Zacharias, L.; Autio, H.; Sahu, M. P.; Borges-Assis, A. B.; Leite, J. P.; Mineev, K. S.; Castrén, E.; Resstel, L. B. M. Fluoxetine and Ketamine Enhance Extinction Memory and Brain Plasticity by Triggering the P75 Neurotrophin Receptor Proteolytic Pathway. *Biol. Psychiatry* **2025**, *97* (3), 248–260. https://doi.org/10.1016/j.biopsych.2024.06.021.

(74) Geiger, Z.; VanVeller, B.; Lopez, Z.; Harrata, A. K.; Battani, K.; Wegman-Points, L.; Yuan, L.-L. Determination of Diffusion Kinetics of Ketamine in Brain Tissue: Implications for in Vitro Mechanistic Studies of Drug Actions. *Front. Neurosci.* **2021**, *15*. https://doi.org/10.3389/fnins.2021.678978.

(75) Ma, S.; Chen, M.; Jiang, Y.; Xiang, X.; Wang, S.; Wu, Z.; Li, S.; Cui, Y.; Wang, J.; Zhu, Y.; Zhang, Y.; Ma, H.; Duan, S.; Li, H.; Yang, Y.; Lingle, C. J.; Hu, H. Sustained Antidepressant Effect of Ketamine through NMDAR Trapping in the LHb. *Nature* **2023**, *622* (7984), 802–809. https://doi.org/10.1038/s41586-023-06624-1.

(76) Moaddel, R.; Farmer, C. A.; Yavi, M.; Kadriu, B.; Zhu, M.; Fan, J.; Chen, Q.; Lehrmann, E.; Fantoni, G.; De, S.; Mazucanti, C. H.; Acevedo-Diaz, E. E.; Yuan, P.; Gould, T. D.; Park, L. T.; Egan, J. M.; Ferrucci, L.; Zarate, C. A. Cerebrospinal Fluid Exploratory Proteomics and Ketamine Metabolite Pharmacokinetics in Human Volunteers after Ketamine Infusion. *iScience* **2023**, *26* (12), 108527. https://doi.org/10.1016/j.isci.2023.108527.

(77) Creeney, H.; Raval, P.; Srivastava, D. P.; Vernon, A. C. Ketamine Rapidly Stimulates Local Protein Synthesis in Primary Neuronal Cultures. *Eur. Neuropsychopharmacol.* **2019**, *29*, S346–S347. https://doi.org/10.1016/j.euroneuro.2018.11.538.

(78) Niswender, C. M.; Conn, P. J. Metabotropic Glutamate Receptors: Physiology, Pharmacology, and Disease. *Annu. Rev. Pharmacol. Toxicol.* **2010**, *50* (Volume 50, 2010), 295–322. https://doi.org/10.1146/annurev.pharmtox.011008.145533.

(79) Elmeseiny, O. S. A.; Müller, H. K. A Molecular Perspective on mGluR5 Regulation in the Antidepressant Effect of Ketamine. *Pharmacol. Res.* **2024**, *200*, 107081. https://doi.org/10.1016/j.phrs.2024.107081.

(80) Gokalp, D.; Unal, G. The Role of mGluR5 on the Therapeutic Effects of Ketamine in Wistar Rats. *Psychopharmacology (Berl.)* **2024**, *241* (7), 1399–1415. https://doi.org/10.1007/s00213-024-06571-3.

(81) Pałucha-Poniewiera, A. The Role of mGlu2/3 Receptor Antagonists in the Enhancement of the Antidepressant-like Effect of Ketamine. *Pharmacol. Biochem. Behav.* **2022**, *220*, 173454. https://doi.org/10.1016/j.pbb.2022.173454.

(82) Dunn, H. A.; Zucca, S.; Dao, M.; Orlandi, C.; Martemyanov, K. A. ELFN2 Is a Postsynaptic Cell Adhesion Molecule with Essential Roles in Controlling Group III

mGluRs in the Brain and Neuropsychiatric Behavior. *Mol. Psychiatry* **2019**, *24* (12), 1902–1919. https://doi.org/10.1038/s41380-019-0512-3.

(83) Gergues, M. M.; Yohn, C. N.; Bharadia, A.; Levinstein, M. R.; Samuels, B. A. Dentate Gyrus Activin Signaling Mediates the Antidepressant Response. *Transl. Psychiatry* **2021**, *11* (1), 1–16. https://doi.org/10.1038/s41398-020-01156-y.

(84) Kurisaki, A.; Inoue, I.; Kurisaki, K.; Yamakawa, N.; Tsuchida, K.; Sugino, H. Activin Induces Long-Lasting *N*-Methyl-d-Aspartate Receptor Activation via Scaffolding PDZ Protein Activin Receptor Interacting Protein 1. *Neuroscience* **2008**, *151* (4), 1225–1235. https://doi.org/10.1016/j.neuroscience.2007.12.012.

(85) McQuown, S.; Xia, S.; Baumgärtel, K.; Barido, R.; Anderson, G.; Dyck, B.; Scott, R.; Peters, M. Phosphodiesterase 1b (PDE1B) Regulates Spatial and Contextual Memory in Hippocampus. *Front. Mol. Neurosci.* **2019**, *12*. https://doi.org/10.3389/fnmol.2019.00021.

(86) Hufgard, J. R.; Williams, M. T.; Vorhees, C. V. Phosphodiesterase-1b Deletion Confers Depression-like Behavioral Resistance Separate from Stress-Related Effects in Mice. *Genes Brain Behav.* **2017**, *16* (8), 756–767. https://doi.org/10.1111/gbb.12391.

(87) Giralt, A.; Brito, V.; Chevy, Q.; Simonnet, C.; Otsu, Y.; Cifuentes-Díaz, C.; de Pins, B.; Coura, R.; Alberch, J.; Ginés, S.; Poncer, J.-C.; Girault, J.-A. Pyk2 Modulates Hippocampal Excitatory Synapses and Contributes to Cognitive Deficits in a Huntington's Disease Model. *Nat. Commun.* **2017**, *8* (1), 15592. https://doi.org/10.1038/ncomms15592.

(88) de Pins, B.; Mendes, T.; Giralt, A.; Girault, J.-A. The Non-Receptor Tyrosine Kinase Pyk2 in Brain Function and Neurological and Psychiatric Diseases. *Front. Synaptic Neurosci.* **2021**, *13*. https://doi.org/10.3389/fnsyn.2021.749001.

(89) Toledo, A.; Letellier, M.; Bimbi, G.; Tessier, B.; Daburon, S.; Favereaux, A.; Chamma, I.; Vennekens, K.; Vanderlinden, J.; Sainlos, M.; de Wit, J.; Choquet, D.; Thoumine, O. MDGAs Are Fast-Diffusing Molecules That Delay Excitatory Synapse Development by Altering Neuroligin Behavior. *eLife* **2022**, *11*, e75233. https://doi.org/10.7554/eLife.75233.

(90) Kim, S.; Jang, G.; Kim, H.; Lim, D.; Han, K. A.; Um, J. W.; Ko, J. MDGAs Perform Activity-Dependent Synapse Type-Specific Suppression via Distinct Extracellular Mechanisms. *Proc. Natl. Acad. Sci.* **2024**, *121* (26), e2322978121. https://doi.org/10.1073/pnas.2322978121.

(91) Li, J.; Liu, J.; Feng, G.; Li, T.; Zhao, Q.; Li, Y.; Hu, Z.; Zheng, L.; Zeng, Z.; He, L.; Wang, T.; Shi, Y. The *MDGA*1 Gene Confers Risk to Schizophrenia and Bipolar Disorder. *Schizophr. Res.* **2011**, *125* (2), 194–200. https://doi.org/10.1016/j.schres.2010.11.002.

(92) Wang, X.; Wei, H.; Hu, Z.; Jiang, J.; Dong, X.; Zhu, J.; Chen, H.; Brose, N.; Lipstein, N.; Xu, T.; Connor, S. A.; Ma, D.; Xie, Y. Chronic Stress Induces Depression through

MDGA1-Neuroligin2 Mediated Suppression of Inhibitory Synapses in the Lateral Habenula. *Theranostics* **2025**, *15* (5), 1842–1863. https://doi.org/10.7150/thno.104282.

(93) Llamosas, N.; Arora, V.; Vij, R.; Kilinc, M.; Bijoch, L.; Rojas, C.; Reich, A.; Sridharan, B.; Willems, E.; Piper, D. R.; Scampavia, L.; Spicer, T. P.; Miller, C. A.; Holder, J. L.; Rumbaugh, G. SYNGAP1 Controls the Maturation of Dendrites, Synaptic Function, and Network Activity in Developing Human Neurons. *J. Neurosci.* **2020**, *40* (41), 7980–7994. https://doi.org/10.1523/JNEUROSCI.1367-20.2020.

(94) Llamosas, N.; Michaelson, S. D.; Vaissiere, T.; Rojas, C.; Miller, C. A.; Rumbaugh, G. Syngap1 Regulates Experience-Dependent Cortical Ensemble Plasticity by Promoting in Vivo Excitatory Synapse Strengthening. *Proc. Natl. Acad. Sci.* **2021**, *118* (34), e2100579118. https://doi.org/10.1073/pnas.2100579118.

(95) Yepes, M.; Wu, F.; Torre, E.; Cuellar-Giraldo, D.; Jia, D.; Cheng, L. Tissue-Type Plasminogen Activator Induces Synaptic Vesicle Endocytosis in Cerebral Cortical Neurons. *Neuroscience* **2016**, *319*, 69–78. https://doi.org/10.1016/j.neuroscience.2016.01.046.

(96) Varangot, A.; Lebatard, S.; Bellemain-Sagnard, M.; Lebouvier, L.; Hommet, Y.; Vivien, D. Modulations of the Neuronal Trafficking of Tissue-Type Plasminogen Activator (tPA) Influences Glutamate Release. *Cell Death Dis.* **2023**, *14* (1), 1–15. https://doi.org/10.1038/s41419-022-05543-9.

(97) Tsai, S.-J. Role of Tissue-Type Plasminogen Activator and Plasminogen Activator Inhibitor-1 in Psychological Stress and Depression. *Oncotarget* **2017**, *8* (68), 113258–113268. https://doi.org/10.18632/oncotarget.19935.

(98) Yang, T.; Nie, Z.; Shu, H.; Kuang, Y.; Chen, X.; Cheng, J.; Yu, S.; Liu, H. The Role of BDNF on Neural Plasticity in Depression. *Front. Cell. Neurosci.* **2020**, *14*. https://doi.org/10.3389/fncel.2020.00082.

(99) Porter, G. A.; O'Connor, J. C. Brain-Derived Neurotrophic Factor and Inflammation in Depression: Pathogenic Partners in Crime? *World J. Psychiatry* **2022**, *12* (1), 77–97. https://doi.org/10.5498/wjp.v12.i1.77.

(100) Correia, A. S.; Cardoso, A.; Vale, N. BDNF Unveiled: Exploring Its Role in Major Depression Disorder Serotonergic Imbalance and Associated Stress Conditions. *Pharmaceutics* **2023**, *15* (8), 2081. https://doi.org/10.3390/pharmaceutics15082081.

(101) Shen, Q.; Lal, R.; Luellen, B. A.; Earnheart, J. C.; Andrews, A. M.; Luscher, B. γ-Aminobutyric Acid-Type A Receptor Deficits Cause Hypothalamic-Pituitary-Adrenal Axis Hyperactivity and Antidepressant Drug Sensitivity Reminiscent of Melancholic Forms of Depression. *Biol. Psychiatry* **2010**, *68* (6), 512–520. https://doi.org/10.1016/j.biopsych.2010.04.024.

(102) Luscher, B.; Shen, Q.; Sahir, N. The GABAergic Deficit Hypothesis of Major Depressive Disorder. *Mol. Psychiatry* **2011**, *16* (4), 383–406. https://doi.org/10.1038/mp.2010.120.

(103) Luscher, B.; Fuchs, T. Chapter Five - GABAergic Control of Depression-Related Brain States. In *Advances in Pharmacology*; Rudolph, U., Ed.; Diversity and Functions of GABA Receptors: A Tribute to Hanns Möhler, Part B; Academic Press, 2015; Vol. 73, pp 97–144. https://doi.org/10.1016/bs.apha.2014.11.003.

(104) Luscher, B.; Feng, M.; Jefferson, S. J. Chapter Two - Antidepressant Mechanisms of Ketamine: Focus on GABAergic Inhibition. In *Advances in Pharmacology*; Duman, R. S., Krystal, J. H., Eds.; Rapid Acting Antidepressants; Academic Press, 2020; Vol. 89, pp 43–78. https://doi.org/10.1016/bs.apha.2020.03.002.

(105) Gerhard, D. M.; Pothula, S.; Liu, R.-J.; Wu, M.; Li, X.-Y.; Girgenti, M. J.; Taylor, S. R.; Duman, C. H.; Delpire, E.; Picciotto, M.; Wohleb, E. S.; Duman, R. S. GABA Interneurons Are the Cellular Trigger for Ketamine's Rapid Antidepressant Actions. *J. Clin. Invest.* **2020**, *130* (3), 1336–1349. https://doi.org/10.1172/JCI130808.

(106) Lazarevic, V.; Yang, Y.; Flais, I.; Svenningsson, P. Ketamine Decreases Neuronally Released Glutamate via Retrograde Stimulation of Presynaptic Adenosine A1 Receptors. *Mol. Psychiatry* **2021**, *26* (12), 7425–7435. https://doi.org/10.1038/s41380-021-01246-3.

(107) Ren, Z.; Pribiag, H.; Jefferson, S. J.; Shorey, M.; Fuchs, T.; Stellwagen, D.; Luscher, B. Bidirectional Homeostatic Regulation of a Depression-Related Brain State by Gamma-Aminobutyric Acidergic Deficits and Ketamine Treatment. *Biol. Psychiatry* **2016**, *80* (6), 457–468. https://doi.org/10.1016/j.biopsych.2016.02.009.

(108) Bollan, K. A.; Baur, R.; Hales, T. G.; Sigel, E.; Connolly, C. N. The Promiscuous Role of the Epsilon Subunit in GABAA Receptor Biogenesis. *Mol. Cell. Neurosci.* **2008**, *37* (3), 610–621. https://doi.org/10.1016/j.mcn.2007.12.011.

(109) Chen, X.; Jhee, K.-H.; Kruger, W. D. Production of the Neuromodulator H2S by Cystathionine β-Synthase via the Condensation of Cysteine and Homocysteine*. *J. Biol. Chem.* **2004**, *279* (50), 52082–52086. https://doi.org/10.1074/jbc.C400481200.

(110) Kamat, P. K.; Kalani, A.; Tyagi, N. Chapter Eleven - Role of Hydrogen Sulfide in Brain Synaptic Remodeling. In *Methods in Enzymology*; Cadenas, E., Packer, L., Eds.; Hydrogen Sulfide in Redox Biology, Part B; Academic Press, 2015; Vol. 555, pp 207–229. https://doi.org/10.1016/bs.mie.2014.11.025.

(111) Zhou, L.; Jones, E. V.; Murai, K. K. EphA Signaling Promotes Actin-Based Dendritic Spine Remodeling through Slingshot Phosphatase*. *J. Biol. Chem.* **2012**, *287* (12), 9346–9359. https://doi.org/10.1074/jbc.M111.302802.

(112) Ishikawa, Y.; Tamura, H.; Shiosaka, S. Diversity of Neuropsin (KLK8)-Dependent Synaptic Associativity in the Hippocampal Pyramidal Neuron. *J. Physiol.* **2011**, *589* (14), 3559–3573. https://doi.org/10.1113/jphysiol.2011.206169.

(113) Konar, A.; Kumar, A.; Maloney, B.; Lahiri, D. K.; Thakur, M. K. A Serine Protease KLK8 Emerges as a Regulator of Regulators in Memory: Microtubule Protein Dependent Neuronal Morphology and PKA-CREB Signaling. *Sci. Rep.* **2018**, *8* (1), 9928. https://doi.org/10.1038/s41598-018-27640-6.

(114) Radler, M. R.; Spiliotis, E. T. Right Place, Right Time - Spatial Guidance of Neuronal Morphogenesis by Septin GTPases. *Curr. Opin. Neurobiol.* **2022**, *75*, 102557. https://doi.org/10.1016/j.conb.2022.102557.

(115) Bai, X.; Karasmanis, E. P.; Spiliotis, E. T. Septin 9 Interacts with Kinesin KIF17 and Interferes with the Mechanism of NMDA Receptor Cargo Binding and Transport. *Mol. Biol. Cell* **2016**, *27* (6), 897–906. https://doi.org/10.1091/mbc.E15-07-0493.

(116) Puusepp, S.; Kovacs-Nagy, R.; Alhaddad, B.; Braunisch, M.; Hoffmann, G. F.; Kotzaeridou, U.; Lichvarova, L.; Liiv, M.; Makowski, C.; Mandel, M.; Meitinger, T.; Pajusalu, S.; Rodenburg, R. J.; Safiulina, D.; Strom, T. M.; Talvik, I.; Vaarmann, A.; Wilson, C.; Kaasik, A.; Haack, T. B.; Õunap, K. Compound Heterozygous SPATA5 Variants in Four Families and Functional Studies of SPATA5 Deficiency. *Eur. J. Hum. Genet.* **2018**, *26* (3), 407–419. https://doi.org/10.1038/s41431-017-0001-6.

(117) Lundquist, M. R.; Storaska, A. J.; Liu, T.-C.; Larsen, S. D.; Evans, T.; Neubig, R. R.; Jaffrey, S. R. Redox Modification of Nuclear Actin by MICAL-2 Regulates SRF Signaling. *Cell* **2014**, *156* (3), 563–576. https://doi.org/10.1016/j.cell.2013.12.035.

(118) Galloni, C.; Carra, D.; Abella, J. V. G.; Kjær, S.; Singaravelu, P.; Barry, D. J.; Kogata, N.; Guérin, C.; Blanchoin, L.; Way, M. MICAL2 Enhances Branched Actin Network Disassembly by Oxidizing Arp3B-Containing Arp2/3 Complexes. *J. Cell Biol.* **2021**, *220* (8), e202102043. https://doi.org/10.1083/jcb.202102043.

(119) Hou, S. T.; Nilchi, L.; Li, X.; Gangaraju, S.; Jiang, S. X.; Aylsworth, A.; Monette, R.; Slinn, J. Semaphorin3A Elevates Vascular Permeability and Contributes to Cerebral Ischemia-Induced Brain Damage. *Sci. Rep.* **2015**, *5* (1), 7890. https://doi.org/10.1038/srep07890.

(120) Shelly, M.; Cancedda, L.; Lim, B. K.; Popescu, A. T.; Cheng, P.; Gao, H.; Poo, M. Semaphorin3A Regulates Neuronal Polarization by Suppressing Axon Formation and Promoting Dendrite Growth. *Neuron* **2011**, *71* (3), 433–446. https://doi.org/10.1016/j.neuron.2011.06.041.

(121) Wareham, L. K.; Baratta, R. O.; Del Buono, B. J.; Schlumpf, E.; Calkins, D. J. Collagen in the Central Nervous System: Contributions to Neurodegeneration and Promise as a Therapeutic Target. *Mol. Neurodegener.* **2024**, *19* (1), 11. https://doi.org/10.1186/s13024-024-00704-0.

(122) Kandel, E. R. The Molecular Biology of Memory: cAMP, PKA, CRE, CREB-1, CREB-2, and CPEB. *Mol. Brain* **2012**, *5* (1), 14. https://doi.org/10.1186/1756-6606-5-14.

(123) Lee, D. Global and Local Missions of cAMP Signaling in Neural Plasticity, Learning, and Memory. *Front. Pharmacol.* **2015**, *6*. https://doi.org/10.3389/fphar.2015.00161.

(124) Shahoha, M.; Cohen, R.; Ben-Simon, Y.; Ashery, U. cAMP-Dependent Synaptic Plasticity at the Hippocampal Mossy Fiber Terminal. *Front. Synaptic Neurosci.* **2022**, *14*. https://doi.org/10.3389/fnsyn.2022.861215.

(125) Yamada, D.; Davidson, A. M.; Hige, T. Cyclic Nucleotide-Induced Bidirectional Long-Term Synaptic Plasticity in Drosophila Mushroom Body. *J. Physiol.* **2024**, *602* (9), 2019–2045. https://doi.org/10.1113/JP285745.

(126) Fukunaga, K.; Miyamoto, E. Role of MAP Kinase in Neurons. *Mol. Neurobiol.* **1998**, *16* (1), 79–95. https://doi.org/10.1007/BF02740604.

(127) Iroegbu, J. D.; Ijomone, O. K.; Femi-Akinlosotu, O. M.; Ijomone, O. M. ERK/MAPK Signalling in the Developing Brain: Perturbations and Consequences. *Neurosci. Biobehav. Rev.* **2021**, *131*, 792–805. https://doi.org/10.1016/j.neubiorev.2021.10.009.

(128) Zhang, L.; Zhang, P.; Wang, G.; Zhang, H.; Zhang, Y.; Yu, Y.; Zhang, M.; Xiao, J.; Crespo, P.; Hell, J. W.; Lin, L.; Huganir, R. L.; Zhu, J. J. Ras and Rap Signal Bidirectional Synaptic Plasticity via Distinct Subcellular Microdomains. *Neuron* **2018**, *98* (4), 783-800.e4. https://doi.org/10.1016/j.neuron.2018.03.049.

(129) Chen, X.; Shibata, A. C.; Hendi, A.; Kurashina, M.; Fortes, E.; Weilinger, N. L.; MacVicar, B. A.; Murakoshi, H.; Mizumoto, K. Rap2 and TNIK Control Plexin-Dependent Tiled Synaptic Innervation in C. Elegans. *eLife* **2018**, *7*, e38801. https://doi.org/10.7554/eLife.38801.

(130) Spencer, M. L.; Shao, H.; Tucker, H. M.; Andres, D. A. Nerve Growth Factor-Dependent Activation of the Small GTPase Rin*. *J. Biol. Chem.* **2002**, *277* (20), 17605–17615. https://doi.org/10.1074/jbc.M111400200.

(131) Shi, G.-X.; Han, J.; Andres, D. A. Rin GTPase Couples Nerve Growth Factor Signaling to P38 and B-Raf/ERK Pathways to Promote Neuronal Differentiation*. *J. Biol. Chem.* **2005**, *280* (45), 37599–37609. https://doi.org/10.1074/jbc.M507364200.

(132) Gao, A. Y. L.; Montagna, D. R.; Hirst, W. D.; Temkin, P. A. RIT2 Regulates Autophagy Lysosomal Pathway Induction and Protects against α-Synuclein Pathology in a Cellular Model of Parkinson's Disease. *Neurobiol. Dis.* **2024**, *199*, 106568. https://doi.org/10.1016/j.nbd.2024.106568.

(133) Daneshmandpour, Y.; Darvish, H.; Emamalizadeh, B. RIT2: Responsible and Susceptible Gene for Neurological and Psychiatric Disorders. *Mol. Genet. Genomics* **2018**, *293* (4), 785–792. https://doi.org/10.1007/s00438-018-1451-4.

(134) Biel, M.; Wahl-Schott, C.; Michalakis, S.; Zong, X. Hyperpolarization-Activated Cation Channels: From Genes to Function. *Physiol. Rev.* **2009**, *89* (3), 847–885. https://doi.org/10.1152/physrev.00029.2008.

(135) Sartiani, L.; Mannaioni, G.; Masi, A.; Novella Romanelli, M.; Cerbai, E. The Hyperpolarization-Activated Cyclic Nucleotide–Gated Channels: From Biophysics to Pharmacology of a Unique Family of Ion Channels. *Pharmacol. Rev.* **2017**, *69* (4), 354–395. https://doi.org/10.1124/pr.117.014035.

(136) Lewis, A. S.; Vaidya, S. P.; Blaiss, C. A.; Liu, Z.; Stoub, T. R.; Brager, D. H.; Chen, X.; Bender, R. A.; Estep, C. M.; Popov, A. B.; Kang, C. E.; Veldhoven, P. P. V.; Bayliss, D. A.; Nicholson, D. A.; Powell, C. M.; Johnston, D.; Chetkovich, D. M. Deletion of the Hyperpolarization-Activated Cyclic Nucleotide-Gated Channel

Auxiliary Subunit TRIP8b Impairs Hippocampal Ih Localization and Function and Promotes Antidepressant Behavior in Mice. *J. Neurosci.* **2011**, *31* (20), 7424–7440. https://doi.org/10.1523/JNEUROSCI.0936-11.2011.

(137) Chen, X.; Shu, S.; Bayliss, D. A. HCN1 Channel Subunits Are a Molecular Substrate for Hypnotic Actions of Ketamine. *J. Neurosci.* **2009**, *29* (3), 600–609. https://doi.org/10.1523/JNEUROSCI.3481-08.2009.

(138) LI Jing, C. F. Inhibition of HCN1 Channels by Ketamine Accounts for Its Antidepressant Actions. *J. Sichuan Univ. Med. Sci. Ed.* **2014**, *45* (6).

(139) Diviani, D.; Soderling, J.; Scott, J. D. AKAP-Lbc Anchors Protein Kinase A and Nucleates Gα12-Selective Rho-Mediated Stress Fiber Formation*. *J. Biol. Chem.* **2001**, *276* (47), 44247–44257. https://doi.org/10.1074/jbc.M106629200.

(140) Shibolet, O.; Giallourakis, C.; Rosenberg, I.; Mueller, T.; Xavier, R. J.; Podolsky, D. K. AKAP13, a RhoA GTPase-Specific Guanine Exchange Factor, Is a Novel Regulator of TLR2 Signaling. *J. Biol. Chem.* **2007**, *282* (48), 35308–35317. https://doi.org/10.1074/jbc.M704426200.

(141) Cariolato, L.; Cavin, S.; Diviani, D. A-Kinase Anchoring Protein (AKAP)-Lbc Anchors a PKN-Based Signaling Complex Involved in A1-Adrenergic Receptor-Induced P38 Activation*. *J. Biol. Chem.* **2011**, *286* (10), 7925–7937. https://doi.org/10.1074/jbc.M110.185645.

(142) Takaesu, G.; Kishida, S.; Hiyama, A.; Yamaguchi, K.; Shibuya, H.; Irie, K.; Ninomiya-Tsuji, J.; Matsumoto, K. TAB2, a Novel Adaptor Protein, Mediates Activation of TAK1 MAPKKK by Linking TAK1 to TRAF6 in the IL-1 Signal Transduction Pathway. *Mol. Cell* **2000**, *5* (4), 649–658. https://doi.org/10.1016/S1097-2765(00)80244-0.

(143) Kanayama, A.; Seth, R. B.; Sun, L.; Ea, C.-K.; Hong, M.; Shaito, A.; Chiu, Y.-H.; Deng, L.; Chen, Z. J. TAB2 and TAB3 Activate the NF-κB Pathway through Binding to Polyubiquitin Chains. *Mol. Cell* **2004**, *15* (4), 535–548. https://doi.org/10.1016/j.molcel.2004.08.008.

(144) Majumder, P.; Edmison, D.; Rodger, C.; Patel, S.; Reid, E.; Gowrishankar, S. AP-4 Regulates Neuronal Lysosome Composition, Function, and Transport via Regulating Export of Critical Lysosome Receptor Proteins at the Trans-Golgi Network. *Mol. Biol. Cell* **2022**, *33* (12), ar102. https://doi.org/10.1091/mbc.E21-09-0473.

(145) Kozyraki, R.; Fyfe, J.; Kristiansen, M.; Gerdes, C.; Jacobsen, C.; Cui, S.; Christensen, E. I.; Aminoff, M.; de la Chapelle, A.; Krahe, R.; Verroust, P. J.; Moestrup, S. K. The Intrinsic Factor–Vitamin B12 Receptor, Cubilin, Is a High-Affinity Apolipoprotein A-I Receptor Facilitating Endocytosis of High-Density Lipoprotein. *Nat. Med.* **1999**, *5* (6), 656–661. https://doi.org/10.1038/9504.

(146) Christensen, E. I.; Birn, H. Megalin and Cubilin: Multifunctional Endocytic Receptors. *Nat. Rev. Mol. Cell Biol.* **2002**, *3* (4), 258–267. https://doi.org/10.1038/nrm778.

(147) Nagaraj, M.; Höring, M.; Ahonen, M. A.; Nguyen, V. D.; Zhou, Y.; Vihinen, H.; Jokitalo, E.; Liebisch, G.; Nidhina Haridas, P. A.; Olkkonen, V. M. GOLM1 Depletion Modifies Cellular Sphingolipid Metabolism and Adversely Affects Cell Growth. *J. Lipid Res.* **2022**, *63* (9), 100259. https://doi.org/10.1016/j.jlr.2022.100259.

(148) Muresan, V.; Stankewich, M. C.; Steffen, W.; Morrow, J. S.; Holzbaur, E. L. F.; Schnapp, B. J. Dynactin-Dependent, Dynein-Driven Vesicle Transport in the Absence of Membrane Proteins: A Role for Spectrin and Acidic Phospholipids. *Mol. Cell* **2001**, *7* (1), 173–183. https://doi.org/10.1016/S1097-2765(01)00165-4.

(149) Underwood, R.; Wang, B.; Carico, C.; Whitaker, R. H.; Placzek, W. J.; Yacoubian, T. A. The GTPase Rab27b Regulates the Release, Autophagic Clearance, and Toxicity of α-Synuclein. *J. Biol. Chem.* **2020**, *295* (23), 8005–8016. https://doi.org/10.1074/jbc.RA120.013337.

(150) Solaroli, N.; Panayiotou, C.; Johansson, M.; Karlsson, A. Identification of Two Active Functional Domains of Human Adenylate Kinase 5. *FEBS Lett.* **2009**, *583* (17), 2872–2876. https://doi.org/10.1016/j.febslet.2009.07.047.

(151) Hochberg, I.; Demain, L. A. M.; Richer, J.; Thompson, K.; Urquhart, J. E.; Rea, A.; Pagarkar, W.; Rodríguez-Palmero, A.; Schlüter, A.; Verdura, E.; Pujol, A.; Quijada-Fraile, P.; Amberger, A.; Deutschmann, A. J.; Demetz, S.; Gillespie, M.; Belyantseva, I. A.; McMillan, H. J.; Barzik, M.; Beaman, G. M.; Motha, R.; Ng, K. Y.; O'Sullivan, J.; Williams, S. G.; Bhaskar, S. S.; Lawrence, I. R.; Jenkinson, E. M.; Zambonin, J. L.; Blumenfeld, Z.; Yalonetsky, S.; Oerum, S.; Rossmanith, W.; Yue, W. W.; Zschocke, J.; Munro, K. J.; Battersby, B. J.; Friedman, T. B.; Taylor, R. W.; O'Keefe, R. T.; Newman, W. G. Bi-Allelic Variants in the Mitochondrial RNase P Subunit PRORP Cause Mitochondrial tRNA Processing Defects and Pleiotropic Multisystem Presentations. *Am. J. Hum. Genet.* **2021**, *108* (11), 2195–2204. https://doi.org/10.1016/j.ajhg.2021.10.002.

(152) Coelho, D.; Kim, J. C.; Miousse, I. R.; Fung, S.; du Moulin, M.; Buers, I.; Suormala, T.; Burda, P.; Frapolli, M.; Stucki, M.; Nürnberg, P.; Thiele, H.; Robenek, H.; Höhne, W.; Longo, N.; Pasquali, M.; Mengel, E.; Watkins, D.; Shoubridge, E. A.; Majewski, J.; Rosenblatt, D. S.; Fowler, B.; Rutsch, F.; Baumgartner, M. R. Mutations in ABCD4 Cause a New Inborn Error of Vitamin B12 Metabolism. *Nat. Genet.* **2012**, *44* (10), 1152–1155. https://doi.org/10.1038/ng.2386.

(153) McCool, M. A.; Bryant ,Carson J.; Huang ,Hannah; Ogawa ,Lisa M.; Farley-Barnes ,Katherine I.; Sondalle ,Samuel B.; Abriola ,Laura; Surovtseva ,Yulia V.; and Baserga, S. J. Human Nucleolar Protein 7 (NOL7) Is Required for Early Pre-rRNA Accumulation and Pre-18S rRNA Processing. *RNA Biol.* **2023**, *20* (1), 257–271. https://doi.org/10.1080/15476286.2023.2217392.

(154) Kaiser, R. W. J.; Ignarski, M.; Van Nostrand, E. L.; Frese, C. K.; Jain, M.; Cukoski, S.; Heinen, H.; Schaechter, M.; Seufert, L.; Bunte, K.; Frommolt, P.; Keller, P.; Helm, M.; Bohl, K.; Höhne, M.; Schermer, B.; Benzing, T.; Höpker, K.; Dieterich, C.; Yeo, G. W.; Müller, R.-U.; Fabretti, F. A Protein-RNA Interaction Atlas of the Ribosome

Biogenesis Factor AATF. *Sci. Rep.* **2019**, *9* (1), 11071. https://doi.org/10.1038/s41598-019-47552-3.

(155) Banko, J. L.; Poulin, F.; Hou, L.; DeMaria, C. T.; Sonenberg, N.; Klann, E. The Translation Repressor 4E-BP2 Is Critical for eIF4F Complex Formation, Synaptic Plasticity, and Memory in the Hippocampus. *J. Neurosci.* **2005**, *25* (42), 9581–9590. https://doi.org/10.1523/JNEUROSCI.2423-05.2005.

(156) Aguilar-Valles, A.; De Gregorio, D.; Matta-Camacho, E.; Eslamizade, M. J.; Khlaifia, A.; Skaleka, A.; Lopez-Canul, M.; Torres-Berrio, A.; Bermudez, S.; Rurak, G. M.; Simard, S.; Salmaso, N.; Gobbi, G.; Lacaille, J.-C.; Sonenberg, N. Antidepressant Actions of Ketamine Engage Cell-Specific Translation via eIF4E. *Nature* **2021**, *590* (7845), 315–319. https://doi.org/10.1038/s41586-020-03047-0.

(157) Lewis, V.; Rodrigue, B.; Arsenault, E.; Zhang, M.; Taghavi-Abkuh, F.-F.; Silva, W. C. C.; Myers, M.; Matta-Camacho, E.; Aguilar-Valles, A. Translational Control by Ketamine and Its Implications for Comorbid Cognitive Deficits in Depressive Disorders. *J. Neurochem.* **2023**, *166* (1), 10–23. https://doi.org/10.1111/jnc.15652.

(158) Peek, S. L.; Mah, K. M.; Weiner, J. A. Regulation of Neural Circuit Formation by Protocadherins. *Cell. Mol. Life Sci.* **2017**, *74* (22), 4133–4157. https://doi.org/10.1007/s00018-017-2572-3.

(159) Kumanogoh, A.; Marukawa, S.; Suzuki, K.; Takegahara, N.; Watanabe, C.; Ch'ng, E.; Ishida, I.; Fujimura, H.; Sakoda, S.; Yoshida, K.; Kikutani, H. Class IV Semaphorin Sema4A Enhances T-Cell Activation and Interacts with Tim-2. *Nature* **2002**, *419* (6907), 629–633. https://doi.org/10.1038/nature01037.

(160) Lu, N.; Li, Y.; Zhang, Z.; Xing, J.; Sun, Y.; Yao, S.; Chen, L. Human Semaphorin-4A Drives Th2 Responses by Binding to Receptor ILT-4. *Nat. Commun.* **2018**, *9* (1), 742. https://doi.org/10.1038/s41467-018-03128-9.

(161) Luo, Y.; Raible, D.; Raper, J. A. Collapsin: A Protein in Brain That Induces the Collapse and Paralysis of Neuronal Growth Cones. *Cell* **1993**, *75* (2), 217–227. https://doi.org/10.1016/0092-8674(93)80064-L.

(162) Shelly, M.; Cancedda, L.; Lim, B. K.; Popescu, A. T.; Cheng, P.; Gao, H.; Poo, M. Semaphorin3A Regulates Neuronal Polarization by Suppressing Axon Formation and Promoting Dendrite Growth. *Neuron* **2011**, *71* (3), 433–446. https://doi.org/10.1016/j.neuron.2011.06.041.

(163) Bagnard, D.; Lohrum, M.; Uziel, D.; Püschel, A. W.; Bolz, J. Semaphorins Act as Attractive and Repulsive Guidance Signals during the Development of Cortical Projections. *Development* **1998**, *125* (24), 5043–5053. https://doi.org/10.1242/dev.125.24.5043.

(164) Mata, A.; Gil, V.; Pérez-Clausell, J.; Dasilva, M.; González-Calixto, M. C.; Soriano, E.; García-Verdugo, J. M.; Sanchez-Vives, M. V.; del Río, J. A. New Functions of Semaphorin 3E and Its Receptor PlexinD1 during Developing and Adult Hippocampal Formation. *Sci. Rep.* **2018**, *8* (1), 1381. https://doi.org/10.1038/s41598-018-19794-0.

(165) Toledano, S.; Nir-Zvi, I.; Engelman, R.; Kessler, O.; Neufeld, G. Class-3 Semaphorins and Their Receptors: Potent Multifunctional Modulators of Tumor Progression. *Int. J. Mol. Sci.* **2019**, *20* (3), 556. https://doi.org/10.3390/ijms20030556.

(166) Tamagnone, L.; Artigiani, S.; Chen, H.; He, Z.; Ming, G.; Song, H.; Chedotal, A.; Winberg, M. L.; Goodman, C. S.; Poo, M.; Tessier-Lavigne, M.; Comoglio, P. M. Plexins Are a Large Family of Receptors for Transmembrane, Secreted, and GPI-Anchored Semaphorins in Vertebrates. *Cell* **1999**, *99* (1), 71–80. https://doi.org/10.1016/S0092-8674(00)80063-X.

(167) Nakamura, F.; Ohshima, T.; Goshima, Y. Collapsin Response Mediator Proteins: Their Biological Functions and Pathophysiology in Neuronal Development and Regeneration. *Front. Cell. Neurosci.* **2020**, *14*. https://doi.org/10.3389/fncel.2020.00188.

(168) Desprez, F.; Ung, D. C.; Vourc'h, P.; Jeanne, M.; Laumonnier, F. Contribution of the Dihydropyrimidinase-like Proteins Family in Synaptic Physiology and in Neurodevelopmental Disorders. *Front. Neurosci.* **2023**, *17*. https://doi.org/10.3389/fnins.2023.1154446.

(169) Goshima, Y.; Nakamura, F.; Strittmatter, P.; Strittmatter, S. M. Collapsin-Induced Growth Cone Collapse Mediated by an Intracellular Protein Related to UNC-33. *Nature* **1995**, *376* (6540), 509–514. https://doi.org/10.1038/376509a0.

(170) Zunszain, P. A.; Horowitz, M. A.; Cattaneo, A.; Lupi, M. M.; Pariante, C. M. Ketamine: Synaptogenesis, Immunomodulation and Glycogen Synthase Kinase-3 as Underlying Mechanisms of Its Antidepressant Properties. *Mol. Psychiatry* **2013**, *18* (12), 1236–1241. https://doi.org/10.1038/mp.2013.87.

(171) Wu, H.; Savalia, N. K.; Kwan, A. C. Ketamine for a Boost of Neural Plasticity: How, but Also When? *Biol. Psychiatry* **2021**, *89* (11), 1030–1032. https://doi.org/10.1016/j.biopsych.2021.03.014.

(172) Kopelman, J.; Keller, T. A.; Panny, B.; Griffo, A.; Degutis, M.; Spotts, C.; Cruz, N.; Bell, E.; Do-Nguyen, K.; Wallace, M. L.; Mathew, S. J.; Howland, R. H.; Price, R. B. Rapid Neuroplasticity Changes and Response to Intravenous Ketamine: A Randomized Controlled Trial in Treatment-Resistant Depression. *Transl. Psychiatry* **2023**, *13* (1), 1–9. https://doi.org/10.1038/s41398-023-02451-0.

(173) Piazza, M. K.; Kavalali, E. T.; Monteggia, L. M. Ketamine Induced Synaptic Plasticity Operates Independently of Long-Term Potentiation. *Neuropsychopharmacology* **2024**, *49* (11), 1758–1766. https://doi.org/10.1038/s41386-024-01895-2.

(174) Rengasamy, M.; Mathew, S.; Howland, R.; Griffo, A.; Panny, B.; Price, R. Neural Connectivity Moderators and Mechanisms of Ketamine Treatment among Treatment-Resistant Depressed Patients: A Randomized Controlled Trial. *eBioMedicine* **2024**, *99*. https://doi.org/10.1016/j.ebiom.2023.104902.

(175) Moujaes, F.; Ji, J. L.; Rahmati, M.; Burt, J. B.; Schleifer, C.; Adkinson, B. D.; Savic, A.; Santamauro, N.; Tamayo, Z.; Diehl, C.; Kolobaric, A.; Flynn, M.; Rieser, N.;

Fonteneau, C.; Camarro, T.; Xu, J.; Cho, Y.; Repovs, G.; Fineberg, S. K.; Morgan, P. T.; Seifritz, E.; Vollenweider, F. X.; Krystal, J. H.; Murray, J. D.; Preller, K. H.; Anticevic, A. Ketamine Induces Multiple Individually Distinct Whole-Brain Functional Connectivity Signatures. *eLife* **2024**, *13*, e84173. https://doi.org/10.7554/eLife.84173.

(176) Franceschini, A.; Szklarczyk, D.; Frankild, S.; Kuhn, M.; Simonovic, M.; Roth, A.; Lin, J.; Minguez, P.; Bork, P.; von Mering, C.; Jensen, L. J. STRING v9.1: Protein-Protein Interaction Networks, with Increased Coverage and Integration. *Nucleic Acids Res.* **2013**, *41* (D1), D808–D815. https://doi.org/10.1093/nar/gks1094.

(177) Liu, S.; Trupiano, M. X.; Simon, J.; Guo, J.; Anton, E. S. Chapter Three - The Essential Role of Primary Cilia in Cerebral Cortical Development and Disorders. In *Current Topics in Developmental Biology*; Bashaw, G. J., Ed.; Molecular Mechanisms of Neural Development and Insights into Disease; Academic Press, 2021; Vol. 142, pp 99–146. https://doi.org/10.1016/bs.ctdb.2020.11.003.

(178) Hilgendorf, K. I.; Johnson, C. T.; Jackson, P. K. The Primary Cilium as a Cellular Receiver: Organizing Ciliary GPCR Signaling. *Curr. Opin. Cell Biol.* **2016**, *39*, 84–92. https://doi.org/10.1016/j.ceb.2016.02.008.

(179) Toro-Tapia, G.; Das, R. M. Primary Cilium Remodeling Mediates a Cell Signaling Switch in Differentiating Neurons. *Sci. Adv.* **2020**, *6* (21), eabb0601. https://doi.org/10.1126/sciadv.abb0601.

(180) Coschiera, A.; Yoshihara, M.; Lauter, G.; Ezer, S.; Pucci, M.; Li, H.; Kavšek, A.; Riedel, C. G.; Kere, J.; Swoboda, P. Primary Cilia Promote the Differentiation of Human Neurons through the WNT Signaling Pathway. *BMC Biol.* **2024**, *22* (1), 48. https://doi.org/10.1186/s12915-024-01845-w.

(181) Thome, K. C.; Dhar, S. K.; Quintana, D. G.; Delmolino, L.; Shahsafaei, A.; Dutta, A. Subsets of Human Origin Recognition Complex (ORC) Subunits Are Expressed in Non-Proliferating Cells and Associate with Non-ORC Proteins*. *J. Biol. Chem.* **2000**, *275* (45), 35233–35241. https://doi.org/10.1074/jbc.M005765200.

(182) Huang, Z.; Zang, K.; Reichardt, L. F. The Origin Recognition Core Complex Regulates Dendrite and Spine Development in Postmitotic Neurons. *J. Cell Biol.* **2005**, *170* (4), 527–535. https://doi.org/10.1083/jcb.200505075.

(183) Li, M.; Shin, Y.-H.; Hou, L.; Huang, X.; Wei, Z.; Klann, E.; Zhang, P. The Adaptor Protein of the Anaphase Promoting Complex Cdh1 Is Essential in Maintaining Replicative Lifespan and in Learning and Memory. *Nat. Cell Biol.* **2008**, *10* (9), 1083–1089. https://doi.org/10.1038/ncb1768.

(184) Kim, A. H.; Puram, S. V.; Bilimoria, P. M.; Ikeuchi, Y.; Keough, S.; Wong, M.; Rowitch, D.; Bonni, A. A Centrosomal Cdc20-APC Pathway Controls Dendrite Morphogenesis in Postmitotic Neurons. *Cell* **2009**, *136* (2), 322–336. https://doi.org/10.1016/j.cell.2008.11.050.

(185) Delgado-Esteban, M.; García-Higuera, I.; Maestre, C.; Moreno, S.; Almeida, A. APC/C-Cdh1 Coordinates Neurogenesis and Cortical Size during Development. *Nat. Commun.* **2013**, *4* (1), 2879. https://doi.org/10.1038/ncomms3879.

(186) Bobo-Jiménez, V.; Delgado-Esteban, M.; Angibaud, J.; Sánchez-Morán, I.; de la Fuente, A.; Yajeya, J.; Nägerl, U. V.; Castillo, J.; Bolaños, J. P.; Almeida, A. APC/CCdh1-Rock2 Pathway Controls Dendritic Integrity and Memory. *Proc. Natl. Acad. Sci.* **2017**, *114* (17), 4513–4518. https://doi.org/10.1073/pnas.1616024114.

(187) van Roessel, P.; Elliott, D. A.; Robinson, I. M.; Prokop, A.; Brand, A. H. Independent Regulation of Synaptic Size and Activity by the Anaphase-Promoting Complex. *Cell* **2004**, *119* (5), 707–718. https://doi.org/10.1016/j.cell.2004.11.028.

(188) Chen, L.-L.; Wang ,Yong-Bo; Song ,Ju-Xian; Deng ,Wan-Kun; Lu ,Jia-Hong; Ma ,Li-Li; Yang ,Chuan-Bin; Li ,Min; and Xue, Y. Phosphoproteome-Based Kinase Activity Profiling Reveals the Critical Role of MAP2K2 and PLK1 in Neuronal Autophagy. *Autophagy* **2017**, *13* (11), 1969–1980. https://doi.org/10.1080/15548627.2017.1371393.

(189) Schmetsdorf, S.; Gärtner, U.; Arendt, T. Constitutive Expression of Functionally Active Cyclin-Dependent Kinases and Their Binding Partners Suggests Noncanonical Functions of Cell Cycle Regulators in Differentiated Neurons. *Cereb. Cortex* **2007**, *17* (8), 1821–1829. https://doi.org/10.1093/cercor/bhl091.

(190) Nie, B.-X.; Zhao, G.; Yuan, X.-F.; Yu, L.-X.; Zhang, J.; Yuan, Y.; Liu, Y.; Hu, J.; Song, E.; Zhou, Y.-C.; Shu, J. Inhibition of CDK1 Attenuates Neuronal Apoptosis and Autophagy and Confers Neuroprotection after Chronic Spinal Cord Injury in Vivo. *J. Chem. Neuroanat.* **2022**, *119*, 102053. https://doi.org/10.1016/j.jchemneu.2021.102053.

(191) He, G.; Yang, X.; Wang, G.; Qi, J.; Mao, R.; Wu, Z.; Zhou, Z. Cdk7 Is Required for Activity-Dependent Neuronal Gene Expression, Long-Lasting Synaptic Plasticity and Long-Term Memory. *Front. Mol. Neurosci.* **2017**, *10*. https://doi.org/10.3389/fnmol.2017.00365.

(192) Fong, K.-W.; Choi, Y.-K.; Rattner, J. B.; Qi, R. Z. CDK5RAP2 Is a Pericentriolar Protein That Functions in Centrosomal Attachment of the γ-Tubulin Ring Complex. *Mol. Biol. Cell* **2008**, *19* (1), 115–125. https://doi.org/10.1091/mbc.e07-04-0371.

(193) Watanabe, S.; Meitinger, F.; Shiau, A. K.; Oegema, K.; Desai, A. Centriole-Independent Mitotic Spindle Assembly Relies on the PCNT–CDK5RAP2 Pericentriolar Matrix. *J. Cell Biol.* **2020**, *219* (12), e202006010. https://doi.org/10.1083/jcb.202006010.

(194) Dhavan, R.; Tsai, L.-H. A Decade of CDK5. *Nat. Rev. Mol. Cell Biol.* **2001**, *2* (10), 749–759. https://doi.org/10.1038/35096019.

(195) Zhu, J.; Li, W.; Mao, Z. Cdk5: Mediator of Neuronal Development, Death and the Response to DNA Damage. *Mech. Ageing Dev.* **2011**, *132* (8), 389–394. https://doi.org/10.1016/j.mad.2011.04.011.

(196) Pao, P.-C.; Tsai, L.-H. Three Decades of Cdk5. *J. Biomed. Sci.* **2021**, *28* (1), 79. https://doi.org/10.1186/s12929-021-00774-y.

(197) Hirotsune, S.; Fleck, M. W.; Gambello, M. J.; Bix, G. J.; Chen, A.; Clark, G. D.; Ledbetter, D. H.; McBain, C. J.; Wynshaw-Boris, A. Graded Reduction of Pafah1b1 (Lis1) Activity Results in Neuronal Migration Defects and Early Embryonic Lethality. *Nat. Genet.* **1998**, *19* (4), 333–339. https://doi.org/10.1038/1221.

(198) Goshima, G.; Vale, R. D. The Roles of Microtubule-Based Motor Proteins in Mitosis : Comprehensive RNAi Analysis in the Drosophila S2 Cell Line. *J. Cell Biol.* **2003**, *162* (6), 1003–1016. https://doi.org/10.1083/jcb.200303022.

(199) Goldstein, L. S. B.; Yang, Z. Microtubule-Based Transport Systems in Neurons: The Roles of Kinesins and Dyneins. *Annu. Rev. Neurosci.* **2000**, *23* (Volume 23, 2000), 39–71. https://doi.org/10.1146/annurev.neuro.23.1.39.

(200) Morfini, G.; Szebenyi, G.; Richards, B.; Brady, S. T. Regulation of Kinesin: Implications for Neuronal Development. *Dev. Neurosci.* **2001**, *23* (4–5), 364–376. https://doi.org/10.1159/000048720.

(201) Bader, J. R.; Vaughan, K. T. Dynein at the Kinetochore: Timing, Interactions and Functions. *Semin. Cell Dev. Biol.* **2010**, *21* (3), 269–275. https://doi.org/10.1016/j.semcdb.2009.12.015.

(202) Schiavo, G.; Greensmith, L.; Hafezparast, M.; Fisher, E. M. C. Cytoplasmic Dynein Heavy Chain: The Servant of Many Masters. *Trends Neurosci.* **2013**, *36* (11), 641–651. https://doi.org/10.1016/j.tins.2013.08.001.

(203) Ahmad, F. J.; Echeverri, C. J.; Vallee, R. B.; Baas, P. W. Cytoplasmic Dynein and Dynactin Are Required for the Transport of Microtubules into the Axon. *J. Cell Biol.* **1998**, *140* (2), 391–401. https://doi.org/10.1083/jcb.140.2.391.

(204) Tada, T.; Simonetta, A.; Batterton, M.; Kinoshita, M.; Edbauer, D.; Sheng, M. Role of Septin Cytoskeleton in Spine Morphogenesis and Dendrite Development in Neurons. *Curr. Biol.* **2007**, *17* (20), 1752–1758. https://doi.org/10.1016/j.cub.2007.09.039.

(205) Yang, C.; Hu ,Yi-Min; Zhou ,Zhi-Qiang; Zhang ,Guang-Fen; and Yang, J.-J. Acute Administration of Ketamine in Rats Increases Hippocampal BDNF and mTOR Levels during Forced Swimming Test. *Ups. J. Med. Sci.* **2013**, *118* (1), 3–8. https://doi.org/10.3109/03009734.2012.724118.

(206) Li, N.; Liu, R.-J.; Dwyer, J. M.; Banasr, M.; Lee, B.; Son, H.; Li, X.-Y.; Aghajanian, G.; Duman, R. S. Glutamate *N*-Methyl-D-Aspartate Receptor Antagonists Rapidly Reverse Behavioral and Synaptic Deficits Caused by Chronic Stress Exposure. *Biol. Psychiatry* **2011**, *69* (8), 754–761. https://doi.org/10.1016/j.biopsych.2010.12.015.

(207) Harraz, M. M.; Tyagi, R.; Cortés, P.; Snyder, S. H. Antidepressant Action of Ketamine via mTOR Is Mediated by Inhibition of Nitrergic Rheb Degradation. *Mol. Psychiatry* **2016**, *21* (3), 313–319. https://doi.org/10.1038/mp.2015.211.

(208) Popp, S.; Behl, B.; Joshi, J. J.; Lanz, T. A.; Spedding, M.; Schenker, E.; Jay, T. M.; Svenningsson, P.; Caudal, D.; Cunningham, J. I.; Deaver, D.; Bespalov, A. In Search of the Mechanisms of Ketamine's Antidepressant Effects: How Robust Is the Evidence behind the mTor Activation Hypothesis. F1000Research April 11, 2016. https://doi.org/10.12688/f1000research.8236.1.

(209) Abdallah, C. G.; Averill, L. A.; Gueorguieva, R.; Goktas, S.; Purohit, P.; Ranganathan, M.; Sherif, M.; Ahn, K.-H.; D'Souza, D. C.; Formica, R.; Southwick, S. M.; Duman, R. S.; Sanacora, G.; Krystal, J. H. Modulation of the Antidepressant Effects of Ketamine by the mTORC1 Inhibitor Rapamycin. *Neuropsychopharmacology* **2020**, *45* (6), 990–997. https://doi.org/10.1038/s41386-020-0644-9.

(210) Yang, M.; Lu, Y.; Piao, W.; Jin, H. The Translational Regulation in mTOR Pathway. *Biomolecules* **2022**, *12* (6), 802. https://doi.org/10.3390/biom12060802.

(211) Mayer, C.; Grummt, I. Ribosome Biogenesis and Cell Growth: mTOR Coordinates Transcription by All Three Classes of Nuclear RNA Polymerases. *Oncogene* **2006**, *25* (48), 6384–6391. https://doi.org/10.1038/sj.onc.1209883.

(212) Iadevaia, V.; Liu, R.; Proud, C. G. mTORC1 Signaling Controls Multiple Steps in Ribosome Biogenesis. *Semin. Cell Dev. Biol.* **2014**, *36*, 113–120. https://doi.org/10.1016/j.semcdb.2014.08.004.

(213) Kelleher, R. J.; Govindarajan, A.; Jung, H.-Y.; Kang, H.; Tonegawa, S. Translational Control by MAPK Signaling in Long-Term Synaptic Plasticity and Memory. *Cell* **2004**, *116* (3), 467–479. https://doi.org/10.1016/S0092-8674(04)00115-1.

(214) Cargnello, M.; Roux, P. P. Activation and Function of the MAPKs and Their Substrates, the MAPK-Activated Protein Kinases. *Microbiol. Mol. Biol. Rev.* **2011**, *75* (1), 50–83. https://doi.org/10.1128/mmbr.00031-10.

(215) Perez-Riverol, Y.; Bandla, C.; Kundu, D. J.; Kamatchinathan, S.; Bai, J.; Hewapathirana, S.; John, N. S.; Prakash, A.; Walzer, M.; Wang, S.; Vizcaíno, J. A. The PRIDE Database at 20 Years: 2025 Update. *Nucleic Acids Res.* **2025**, *53* (D1), D543–D553. https://doi.org/10.1093/nar/gkae1011.

(216) Jones, J.; MacKrell, E. J.; Wang, T.-Y.; Lomenick, B.; Roukes, M. L.; Chou, T.-F. Tidyproteomics: An Open-Source R Package and Data Object for Quantitative Proteomics Post Analysis and Visualization. *BMC Bioinformatics* **2023**, *24* (1), 239. https://doi.org/10.1186/s12859-023-05360-7.

Chapter IV

INVESTIGATIONS OF PROTEIN SYNTHESIS UNDERLYING BEHAVIORAL PHENOMENA IN ZEBRAFISH USING BONCAT PROTEOMICS

4.1 Abstract

Understanding how temporally controlled changes in protein synthesis regulate behavioral phenomena remains a central challenge in neuroscience. Here, we applied the bioorthogonal noncanonical amino acid tagging (BONCAT) proteomics tools we developed and validated in Chapter II to investigate circadian rhythms in protein synthesis and the proteomic response to low-dose ketamine treatment in zebrafish larvae, a model organism that has gained popularity in the field of neuroscience alongside technological advancements in research methodologies.

Using BONCAT, we identified consistent evidence for increased protein synthesis during the night compared to during the day at six days post-fertilization, although this finding did not generalize reliably across different stages of larval development. Differential expression analyses across multiple night/day comparisons revealed limited overlap in significantly regulated proteins, suggesting substantial variability or context-dependence in circadian protein synthesis patterns. Additionally, our analysis identified few known circadian clock components, with no statistically significant rhythmic expression after correction for multiple comparisons.

In parallel, seeking to extend our *in vitro* findings from Chapter III to an *in vivo* model, we explored proteomic shifts in zebrafish larvae induced by low-dose ketamine treatment known to produce rapid-acting antidepressant effects. Our BONCAT-based approach captured early proteomic responses to treatment with 1 μM ketamine, demonstrating the technique's potential for dissecting rapid drug-induced changes in protein synthesis that conventional methods typically overlook. However, differing results obtained from two separate

experiments and lack of statistically significant changes in protein expression led us to set this project aside, as it pointed to the need for further optimization of the BONCAT method in zebrafish and for experimental validation that the doses of ketamine used would indeed induce the behavioral effects we aimed to study.

Though limitations such as experimental variability restricted conclusive biological insights, this work highlights the advantages and challenges of using BONCAT to capture temporally resolved proteome dynamics. Our findings lay the groundwork for future investigations into the molecular mechanisms underlying complex behaviors, further advancing the application of BONCAT in behavioral neuroscience and translational research.

4.2 Introduction

Behavioral phenomena, including sleep-wake cycles, learning, memory, and responses to environmental stimuli or pharmacological interventions, are fundamentally regulated by temporally controlled changes in protein synthesis[1–3]. Proteins synthesized at specific times facilitate synaptic remodeling, cellular responses, and metabolic adaptations essential for behavioral flexibility and survival. While the transcriptional regulation of these processes has been extensively studied, increasing evidence highlights the critical role of translational regulation—the direct control of protein synthesis independent of mRNA abundance—as an integral mechanism in shaping behavior[4–7].

Zebrafish larvae serve as an ideal model to investigate these dynamic biological processes due to their genetic tractability, rapid development, and robust, quantifiable behaviors[8–11]. At larval stages, zebrafish display robust and evolutionarily conserved circadian rhythms in sleep-wake behaviors, locomotor activity, and environmental responsiveness, clearly observable from as early as five days post-fertilization (dpf)[12,13]. Moreover, the transparency and small size of zebrafish larvae enable non-invasive monitoring of brain activity and high-throughput video tracking, making them particularly suitable for studying the molecular and cellular mechanisms underlying observable behavioral phenomena[14–16].

To take full advantage of the zebrafish model and to better understand the molecular underpinnings of behaviors of interest, methods capable of monitoring dynamic protein synthesis are required. Proteomic analyses have long provided insights into protein expression linked to behavioral phenomena, yet traditional proteomic techniques typically measure steady-state protein levels and cannot readily differentiate between newly synthesized proteins and pre-existing protein pools. This limitation hampers their ability to detect rapid and transient events in protein synthesis associated with behavioral states or pharmacological responses. To address this, bioorthogonal noncanonical amino acid tagging (BONCAT) has emerged as a powerful tool for time-resolved proteomics[17–20]. BONCAT involves metabolic labeling of newly synthesized proteins using chemically modified amino acid analogs, such as azidohomoalanine (AHA), enabling their selective enrichment via Cu(I)-catalyzed [3 + 2] azide-alkyne cycloaddition (CuAAC)[21,22], or by a strain-promoted [3 + 2] azide-alkyne cycloaddition (SPAAC)[23], referred to collectively as "click chemistry." This approach facilitates targeted analysis of proteins synthesized during defined, biologically relevant time windows.

In our previous work, detailed in Chapter II, we validated BONCAT as a useful method for monitoring protein synthesis over short time scales in larval zebrafish, demonstrating its ability to detect otherwise obscured molecular responses to environmental stressors. Building upon this methodological foundation, we sought to leverage BONCAT proteomics to dissect the proteomic changes underlying specific behavioral phenomena and pharmacological responses in zebrafish larvae. Specifically, we undertook studies addressing two major questions: first, the circadian regulation of protein synthesis, and second, the proteomic response to low doses of ketamine, an anesthetic and antidepressant known to rapidly alter neuronal activity and behavior.

Circadian rhythms in protein synthesis have been documented to exhibit distinct rhythmic profiles independent of transcriptional fluctuations, varying significantly across tissues and developmental stages[24]. Thus, an accurate understanding of circadian patterns in protein synthesis requires direct proteomic measurements rather than indirect inference from mRNA

studies. Motivated by the aim of linking circadian protein synthesis to behavior, we used BONCAT proteomics to investigate day/night differences in protein synthesis rates in zebrafish larvae across multiple developmental stages.

Simultaneously, we expanded our investigation of BONCAT proteomics to explore protein synthesis responses to pharmacological perturbations, specifically to low doses of ketamine. A rapid-acting antidepressant at sub-anesthetic doses, ketamine has garnered significant clinical interest due to its ability to alleviate depressive symptoms within hours to days, much faster than traditional antidepressants[25–30]. Despite extensive research and clinical use, the molecular mechanisms underlying ketamine's rapid antidepressant effects remain incompletely understood[31–33]. Previous proteomic analyses of neuronal tissues and cell cultures have implicated changes in synaptic transmission, neuroplasticity, metabolism, and cellular signaling following ketamine exposure[34–39]. However, these conventional proteomic studies, based on whole-cell lysates, lack the temporal resolution to distinguish immediate proteomic changes induced by drug exposure from baseline protein expression. In order to more directly probe the early ketamine-induced shifts in protein expression that might mediate its rapid therapeutic effects, we employed BONCAT to specifically label and identify proteins synthesized in zebrafish larvae during treatment with low, antidepressant-relevant doses of ketamine.

In this chapter, we employ BONCAT proteomics in both circadian and pharmacological contexts, presenting an in-depth exploration of the application of the methods we developed to study behavioral states and drug responses in zebrafish larvae. Although our findings did not yield the consistency of results across experiments required for publication, they offer valuable methodological insights and illustrate the current capabilities and limitations of BONCAT for time-resolved proteomic analyses of behavioral phenomena. Thus, the work described herein lays the foundation for future work to improve upon these techniques and use them to unravel the molecular underpinnings of complex behaviors, providing a critical step towards enhancing the utility of BONCAT proteomics in behavioral neuroscience and translational research.

4.3 Results and Discussion

Protein synthesis in 6 dpf zebrafish larvae is higher during night than during day, but this finding does not reliably generalize across other stages of zebrafish development

Intrigued by our initial finding that proteins labeled with AHA for 12 h during night (9 pm – 9 am) and proteins labeled with AHA for 12 h during the day (9 am – 9 pm) in zebrafish larvae could be resolved into distinct, linearly separable clusters, we wondered whether time-resolved BONCAT proteomics could uncover circadian differences in protein synthesis during day versus night. When we inspected our raw LC-MS/MS data from this experiment more closely, we observed that proteins identified in both day and night samples had overall higher raw abundances in samples labeled with AHA at night, indicative of greater levels of protein synthesis during this time window (Fig. 4.1A).

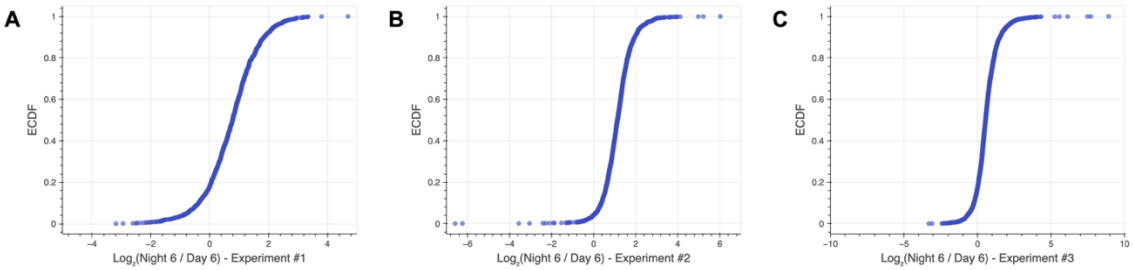

Figure 4.1. Elevated protein synthesis during night 6 compared to day 6 in zebrafish larvae observed across multiple BONCAT proteomics experiments. (A-C) Empirical cumulative distribution function (ECDF) curves depicting the log ratios of the average raw abundances of proteins identified after BONCAT enrichment in zebrafish larvae (6 dpf) treated with 4 mM AHA for 12 h during the night to their average raw abundances in zebrafish larvae (6 dpf) treated with 4 mM AHA for 12 h during the day. Data are shown from (A) the first experiment, (B) the second experiment, and (C) the third experiment testing this night 6 versus day 6 comparison. n = 3 biological replicates for each condition in all three experiments.

We repeated this experiment several times to confirm whether this finding could be replicated. Additionally, in order to determine whether this might be a phenomenon specific to zebrafish larvae at 6 dpf ("night 6" vs "day 6"), or whether it could be related to developmental stages in zebrafish larvae rather than true circadian effects, we also performed AHA labeling in zebrafish during other time windows surrounding this stage of development. Specifically, we performed AHA labeling for 12 h periods during the day at 5 dpf ("day 5"), during the night at 5 dpf ("night 5"), during the day at 7 dpf ("day 7"), and during the night

at 7 dpf ("night 7"). These comparisons could not all be done at once due to limitations in sample handling during the BONCAT enrichment process, so different pairwise comparisons were performed across separate experiments. We did not perform AHA labeling outside the 5 dpf to 7 dpf age range, since circadian sleep/wake behaviors are not typically studied in zebrafish prior to 5 dpf, and after 7 dpf, the fish can no longer survive solely off their yolk sack and must be placed on a juvenile fish diet, leading to the introduction of potential confounding factors in our data.

In total, we carried out five versions of this experiment, labeling newly synthesized proteins in zebrafish larvae with AHA for 12 h during different combinations of day and night time windows and performing proteomic analyses on BONCAT-enriched samples. Some specific night/day comparisons were repeated across experiments (e.g. Night 6 vs Day 6, Night 6 vs Day 7), while others (Night 5 vs Day 5, Night 7 vs Day 7, Night 5 vs Day 6) were only tested once.

The increase in protein synthesis during night 6 compared to day 6 was observed across all three experiments in which this comparison was tested (Figs. 4.1A-C), with 82%, 96%, and 82% of proteins identified in both night 6-labeled and day 6-labeled samples having higher average raw abundances in night 6-labeled samples, respectively. However, other night/day comparisons did not produce this result as consistently. While one experiment comparing night 5 to day 5 showed somewhat similar raw abundances for proteins detected in both sets of samples (Fig. 4.2A, 51% of proteins with higher raw abundances in samples labeled during night 5 than day 5), a second attempt resulted in 67% of proteins having higher abundances in samples labeled during night 5 than day 5 (Fig. 4.2B). An even greater difference was observed across two experiments comparing protein synthesis during night 6 to day 7; in one experiment, 55% of proteins had higher raw abundances during night 6 than during day 7 (Fig. 4.2C), while in a second experiment, 89% of proteins had higher raw abundances during night 6 than during day 7 (Fig. 4.2D). Finally, we performed one comparison of AHA labeling during night 7 to labeling during day 7, which revealed only a modest increase in

protein synthesis during night, with 60% of proteins having higher raw abundances in night 7-labeled samples than in day 7-labeled samples (Fig. 4.2E).

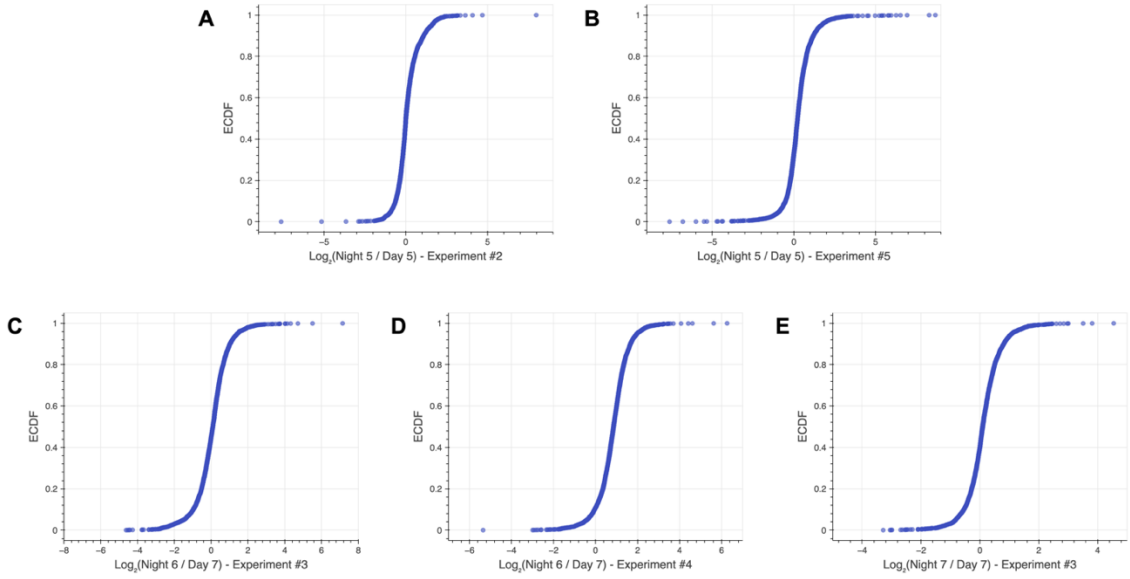

Figure 4.2. Increase in protein synthesis during night compared to day was observed in some other night/day comparisons, but not consistently across experiments. (A-E) ECDF curves depicting the log ratios of the average raw abundances of proteins identified after BONCAT enrichment in zebrafish larvae treated with 4 mM AHA for 12 h during the night to their average raw abundances in zebrafish larvae treated with 4 mM AHA for 12 h during the day. Data are shown from (A) night 5 versus day 5 comparison from the second experiment conducted of five total BONCAT experiments conducted, (B) night 5 versus day 5 comparison from the fifth experiment, (C) night 6 versus day 7 comparison from the third experiment, (D) night 6 versus day 7 comparison from the fourth experiment, and (E) night 7 versus day 7 comparison from the third experiment. n = 3 biological replicates for each condition in the data plotted in (A), (C), (D), and (E). n = 4 biological replicates for each condition in the data plotted in (B).

The increase in protein synthesis observed across various experiments cannot be attributed to animal growth during development, since the protein concentrations measured in lysates derived from 150 zebrafish larvae of various ages did not increase in proportion to fish age. Furthermore, normalization of lysate concentrations prior to BONCAT enrichment ensures that greater raw abundances correspond to increased AHA labeling and thus rates of protein synthesis. Nevertheless, while we did reliably see elevated protein synthesis during night 6 compared to day 6, we were not able to confirm whether this is truly a circadian phenomenon irrespective of zebrafish age or developmental stage.

There is limited past research investigating overall levels of protein synthesis during night versus day across a range of organisms. The majority of research on nighttime protein synthesis is related to muscle recovery and growth, demonstrating increased protein synthesis at night after ingestion of protein after exercise[40–45]. Circadian fluctuations in protein synthesis levels during normal sleep/wake cycles have not been as widely explored. A report by Adam and Oswald in 1983 reviewing numerous studies concluded that peak rates of protein synthesis and cellular proliferation occur during an organism's sleep phase[46]. A later study by Ramm and Smith showed that slow wave sleep specifically is associated with higher rates of protein synthesis throughout the brain[47]. They did not observe a similar increase in protein synthesis during REM sleep, although earlier research by Drucker-Colín et al. demonstrated that protein synthesis inhibitors decreased total REM sleep time without altering slow-wave sleep time. These results are not necessarily in conflict, as it is possible that protein synthesis is necessary for the maintenance of normal REM sleep but that this protein synthesis does not increase relative to daytime levels. More recent research has shown that there are circadian fluctuations in protein synthesis and translational regulation, with signal transducers involved in protein synthesis (i.e. mTOR, p70S6K, and ERK) showing circadian rhythms of phosphorylation that differ in phase across different muscle tissues[48]. Therefore, while we were not able to conclusively determine whether overall protein synthesis increases overnight in zebrafish larvae using BONCAT, it is possible that there is elevated protein synthesis at night during more narrow time windows, certain sleep phases, or specific tissues or brain regions, which would be challenging to detect via AHA labeling of whole fish.

Only a small subset of circadian clock components were identified in our BONCAT proteomics experiments

We conducted differential expression analysis of our BONCAT proteomics data for all eight day-night comparisons from across five experiments. Since the difference in overall protein synthesis during night versus day was variable across experiments (Fig. 4.1, Fig. 4.2), we calculated $\log_2$(Fold Change) ($\log_2$FC) values for proteins using median normalized abundances to determine changes in expression of proteins relative to the total amount of

protein synthesis in a particular condition. All fold changes were calculated with average protein abundances from samples labeled at night in the numerator and average protein abundances from samples labeled during day in the denominator, so $\log_2FC > 0$ corresponds to higher levels of expression at night, whereas $\log_2FC < 0$ corresponds to higher levels of expression during day.

We first examined whether any proteins encoded by the known circadian clock genes in zebrafish were identified in our datasets (i.e. Clock, Period, Timeless, Cry or Bmal proteins)[49,50]. None were identified in our first experiment. Cry3a was identified in our second experiment, and while it was not identified in any samples labeled during night 5, its expression was higher during day 6 than during night 6 ($\log_2FC = -1.999$, $p = 0.00446$, FDR-adj. $p = 0.144$).

In our third experiment, we identified Timeless, Cry3a, and Cry5, but Cry3a was only identified in samples labeled during day 6 or day 7, preventing the calculation of a $\log_2FC$ value associated with night/day expression. Timeless did not have a strong change in expression in any night/day comparison from this experiment (Night 6 / Day 6: $\log_2FC = -0.264$, $p = 0.556$, FDR-adj. $p = 0.751$; Night 6 / Day 7: $\log_2FC = 0.0970$, $p = 0.727$, FDR-adj. $p = 0.840$; Night 7 / Day 7: $\log_2FC = -0.297$, $p = 0.394$, FDR-adj. $p = 0.752$). Cry5 was not identified in samples labeled during day 6 or night 6, but it had increased expression during day 7 compared to during night 7 ($\log_2FC = -1.246$, $p = 0.0249$, FDR-adj. $p = 0.362$).

In our fourth experiment comparing night 6 to day 7, we also identified Timeless, Cry3a, and Cry6. Once again, Cry3a was not identified in samples labeled during night 6, so no log2FC value could be calculated. As was previously observed, Timeless expression did not change significantly between night and day ($\log_2FC = -0.307$, $p = 0.642$, FDR-adj. $p = 0.869$). Unlike the prior experiment, however, Cry5 exhibited no notable change in expression in this dataset ($\log_2FC = -0.341$, $p = 0.549$, FDR-adj. $p = 0.820$).

In our final experiment, where we compared protein synthesis during night 5 during day 5, the only circadian clock proteins we identified were timeless and cry2. Once again, Timeless did not have a significant change in expression during night versus day ($log_2FC = -0.0808$, $p = 0.830$, FDR-adj. $p = 0.945$), while Cry2 had a modest decrease in expression ($log_2FC = -0.881$, $p = 0.0479$, FDR-adj. $p = 0.395$).

In summary, we identified relatively few proteins known to be involved in circadian clock regulation in our various night/day comparison, and none of those for which log_2FC values could be calculated had statistically significant changes after adjusting for false discovery rate (FDR). Nevertheless, if considering non-adjusted p-values, Cry proteins had significantly reduced expression during night compared to during day in 3 of the 4 datasets in which they were identified. This is in line with what would be expected for Cry expression, since it is known that Cry transcription is induced by daylight in both zebrafish and mice, resulting in peak expression levels during the day[50–52].

Differential expression analysis and functional enrichment analysis across multiple night-vs-day comparisons reveals some consistent findings between experiments but mostly variable results

Although we identified thousands of proteins in our experiments probing protein synthesis during night versus day in zebrafish, relatively few had statistically significant changes in expression (FDR-adj. $p < 0.05$) when considering normalized data. While some proteins were found to be significantly up- or down-regulated across multiple experiments, most significantly differentially regulated proteins in any particular night/day comparison did not have a significant change in expression in any other day/night comparison. No proteins were found to have statistically significant increases or decreases in expression ($|log_2FC| > 1$, FDR-adj. $p < 0.05$) across all eight night/day differential expression analyses performed, nor were any found to be significantly differentially regulated across the five night/day comparisons with higher protein synthesis at night than day (>65% proteins with higher raw abundances in samples labeled with AHA at night compared to those labeled with AHA during day). Even if only considering the experiments comparing protein expression during night 6 versus

day 6, no proteins were found to be statistically significantly differentially regulated across all three.

We then expanded our aggregated analysis of our night/day BONCAT proteomics datasets to consider proteins with $|\log_2 FC| > 1$ and $p < 0.05$, rather than the most stringent threshold of FDR-adj. $p < 0.05$. Even with the expanded set of proteins considered, none were found to have consistent up- or down-regulation across all eight comparisons. Only one protein, fatty acid binding protein 10a (Fabp10a, highlighted in bright green in Figs. 4.3A-E), was

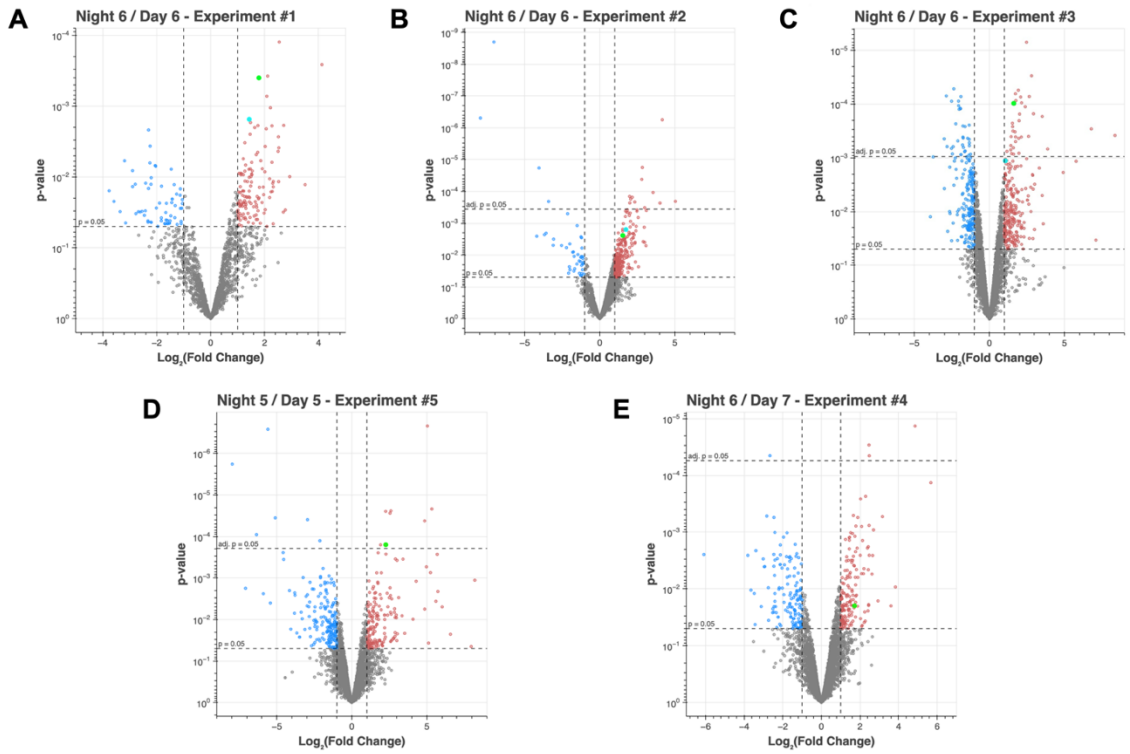

Figure 4.3. Differential expression analysis of BONCAT proteomics data identifies several up- and down-regulated proteins in each experiment, but the specific proteins identified differ across experiments. (A-E) Volcano plots comparing median-normalized abundances of BONCAT-enriched proteins from zebrafish larvae treated with 4 mM AHA for 12 h during the night to their expression in zebrafish larvae treated with 4 mM AHA for 12 h during the day from the five night/day comparisons where at least 65% of proteins identified had higher raw abundances during the night than during the day. Fold change values were calculated via label-free quantification. Proteins with $\log_2(FC) > 1$ and $p < 0.05$ that are up-regulated during the night are depicted in red, whereas proteins with $\log_2(FC) < 1$ and $p < 0.05$ that are down-regulated during the night are depicted in blue. Horizontal dashed lines depict $p = 0.05$ and Benjamini-Hochberg false-discovery rate (FDR)-adjusted $p = 0.05$. The lime green point highlights Fabp10a, which was the only protein with $|\log_2(FC)| > 1$ and $p < 0.05$ across all five comparisons. The cyan point highlights Plg, the only additional protein with $|\log_2(FC)| > 1$ and $p < 0.05$ in the three day 6 versus night 6 comparisons. n = 3 biological replicates for each condition in the data plotted in (A), (B), (C), and (E). n = 4 biological replicates for each condition in the data plotted in (D).

up-regulated across all five night/day comparisons where protein synthesis was found to be higher at night, and one additional protein (Plasminogen, or Plg, highlighted in cyan in Figs. 4.3A-C) was found to be up-regulated in the three night 6 versus day 6 comparisons. Fabp10a is predicted to be involved in fatty acid transport, and plasminogen is predicted to be involved in proteolysis.

While it is customary to perform differential expression analysis on normalized data as we have done above, we also examined the results of differential expression analysis performed on raw protein abundance data for each of our night/day comparisons (Figs. 4.4A-E). For the comparisons where raw abundances were higher in samples labeled during night than those labeled during day, differential expression analysis of raw data results in more proteins being up-regulated and more proteins with positive $\log_2$FC values having $p < 0.05$ or FDR-adj. $p < 0.05$. Still, however, no significantly up-regulated proteins were shared across all eight night/day comparisons, either considering FDR-adj p-values or non-adjusted p-values. Even the subsets of comparisons described above (i.e. the five comparisons where protein synthesis at night was at least 65% higher during night than day, or the three night 6 versus day 6 comparisons) did not share any proteins with $|\log_2\text{FC}| > 1$ and FDR-adj. $p < 0.05$.

Broadening the scope of the aggregated analysis to include any proteins with non-adjusted p-values less than 0.05, we identified 57 proteins that were up-regulated ($\log_2\text{FC} > 1$, $p < 0.05$) across the three night 6 versus day 6 comparisons (Figs. 4.4A-C, Table 4.1), 15 of which were also up-regulated in the two additional analyses where samples labeled during the night had greater AHA labeling than samples labeled during the day (Figs. 4.4D-E, Table 4.1, rows highlighted green).

At an individual level, none of the proteins from this group stood out as particularly biologically interesting in the context of sleep. We examined the list of proteins to identify what broader functional classes of proteins were represented amongst those with higher expression at night. We found several secreted proteins found in plasma (sex hormone-binding globulin, fibrinogen beta chain, plasminogen, serotransferrin, complement component C3a, ceruloplasmin, apolipoprotein Bb, apolipoprotein A-Ib, high-density

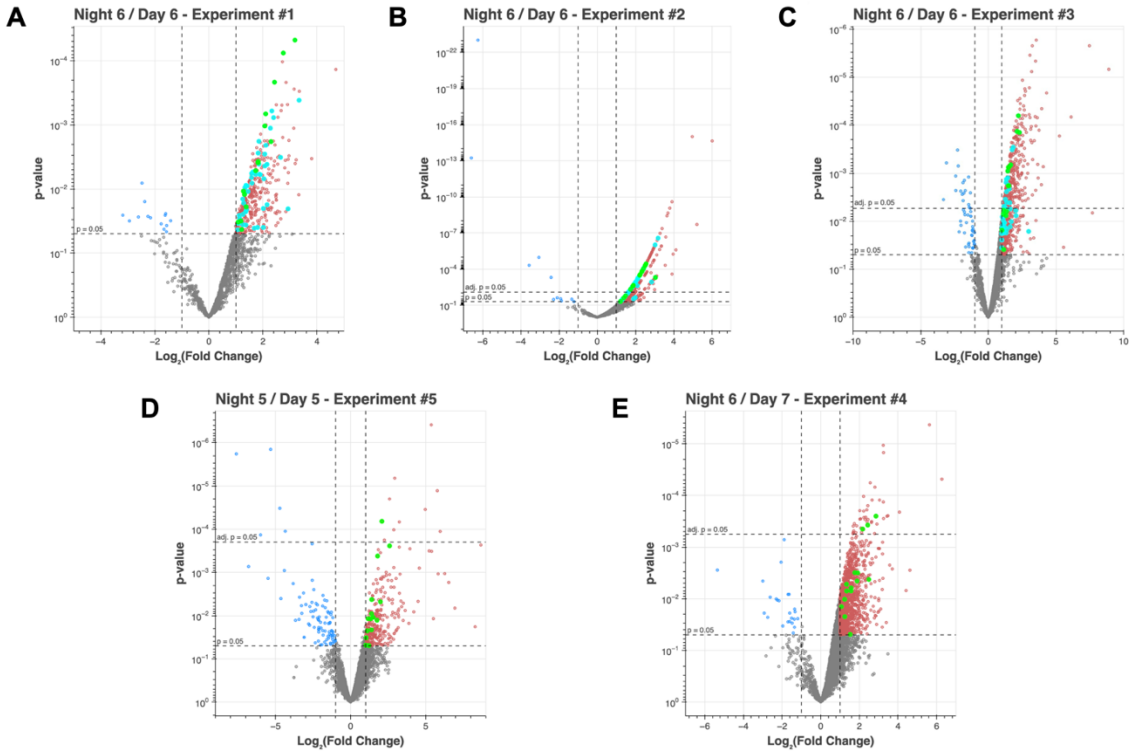

Figure 4.4. Differential expression analysis of raw abundance data from multiple BONCAT proteomics experiments identifies more proteins that are consistently up-regulated across night/day comparisons. (A-E) Volcano plots comparing raw abundances of BONCAT-enriched proteins from zebrafish larvae treated with 4 mM AHA for 12 h during the night to their expression in zebrafish larvae treated with 4 mM AHA for 12 h during the day from the five night/day comparisons where at least 65% of proteins identified had higher raw abundances during the night than during the day. Fold change values were calculated via label-free quantification. Proteins with $\log_2(FC) > 1$ and $p < 0.05$ that are up-regulated during the night are depicted in red, whereas proteins with $\log_2(FC) < 1$ and $p < 0.05$ that are down-regulated during the night are depicted in blue. Horizontal dashed lines depict $p = 0.05$ and Benjamini-Hochberg false-discovery rate (FDR)-adjusted $p = 0.05$. The lime green points highlight proteins with $|\log_2(FC)| > 1$ and $p < 0.05$ across all five comparisons. The cyan points highlight proteins with $|\log_2(FC)| > 1$ and $p < 0.05$ in the three day 6 versus night 6 comparisons. n = 3 biological replicates for each condition in the data plotted in (A), (B), (C), and (E). n = 4 biological replicates for each condition in the data plotted in (D).

lipoprotein-binding protein), multiple collagen proteins that extracellular matrix (ECM) components, and cytoskeletal and trafficking proteins (myosin heavy chain b, actin-related protein 3, coatomer subunit α, BRO1 domain–containing protein BROX). Several proteins could be categorized as being involved in RNA-binding and translation (eIF3 subunit F, 40S ribosomal protein S27, polyadenylate-binding protein 1A) or being involved in proteostasis (Hsp90β, Hsc70, and proteasome 26S subunits). Finally, there were several proteins

involved in cellular metabolism (fructose-bisphosphate aldolase, UTP–glucose-1-phosphate uridylyltransferase, glutathione reductase, thioredoxin-like 1, aldo-keto reductase A3, homogentisate 1,2-dioxygenase, very-long-chain 3-oxoacyl-CoA reductase, S-adenosylmethionine synthase) and more specifically lipid metabolism (fatty acid-binding protein 10a, cytochrome P450 family 8 and family 24 enzymes, acetyl-CoA C-myristoyltransferase, short-chain dehydrogenase/reductase 16C). Overall, several classes of proteins with a broad range of biological functions were represented amongst those with elevated expression during night versus day, which most likely reflects an overall increase in protein synthesis in these samples rather than a prioritization of a particular subset of proteins.

Table 4.1. Proteins up-regulated in multiple night/day comparisons across different experiments

Protein	Gene Name	Log_2FC	P-Value	FDR-Adj. P-Value
Sex hormone-binding globulin	shbg	2.991	1.64E-02	8.75E-02
Fibrinogen beta chain	fgb	2.309	1.42E-04	1.05E-02
Fatty acid-binding protein 10-A, liver basic	fabp10a	2.231	6.37E-05	8.74E-03
Fructose-bisphosphate aldolase	aldob	2.139	1.35E-04	1.05E-02
Solute carrier family 2 member 2	slc2a2	2.056	7.70E-03	6.09E-02
Acetyl-CoA C-myristoyltransferase	scp2a	2.038	6.01E-03	5.31E-02
Procollagen, type IX, alpha 2	col9a2	1.857	2.89E-04	1.31E-02
Collagen, type XI, alpha 2	col11a2	1.774	3.27E-04	1.37E-02
Eukaryotic translation initiation factor 3, subunit F (Fragment)	eif3f	1.713	1.02E-02	7.12E-02
Plasminogen	plg	1.668	6.75E-04	1.94E-02
Claudin b	cldnb	1.633	5.60E-03	5.12E-02
Serotransferrin	tfa	1.629	1.31E-02	7.98E-02
Glutathione reductase	gsr	1.595	4.15E-03	4.32E-02
Aldo-keto reductase family 7, member A3 (aflatoxin aldehyde reductase)	akr7a3	1.570	2.14E-03	3.18E-02
Si:ch1073-464p5.5	si:ch1073-464p5.5	1.538	7.51E-04	1.95E-02
Heat shock protein 90, beta (grp94), member 1	hsp90b1	1.527	1.83E-03	2.93E-02
Cytochrome P450, family 8, subfamily B, polypeptide 1 (Fragment)	cyp8b1	1.493	7.56E-04	1.95E-02
High density lipoprotein-binding protein a	hdlbpa	1.490	1.76E-03	2.84E-02
Complement component c3a, duplicate 1	c3a.1	1.486	1.84E-03	2.93E-02
Zgc:110425	N/A	1.459	1.26E-03	2.49E-02
Zgc:112265 (Fragment)	itih3b.2	1.448	9.04E-04	2.09E-02
Putative oxidoreductase GLYR1	glyr1	1.394	1.48E-02	8.38E-02

Thioredoxin-like 1	txnl1	1.369	6.31E-03	5.48E-02
Tgm2b protein	tgm2b	1.367	4.09E-03	4.32E-02
Carboxylic ester hydrolase (Fragment)	ces2a	1.355	2.45E-03	3.41E-02
40S ribosomal protein S27	rps27l	1.345	1.33E-03	2.54E-02
Carboxymethylenebutenolidase homolog	cmbl	1.321	1.76E-02	9.10E-02
Homogentisate 1,2-dioxygenase	hgd	1.318	1.55E-03	2.73E-02
Zgc:172051 (Fragment)	N/A	1.316	7.71E-03	6.09E-02
Zgc:163061	N/A	1.275	3.52E-03	4.03E-02
High mobility group box 1b	hmgb1b	1.269	5.24E-03	4.91E-02
Ceruloplasmin	cp	1.243	1.35E-02	8.06E-02
Apolipoprotein Bb, tandem duplicate 1	apobb.1	1.240	5.59E-03	5.12E-02
Myosin, heavy chain b	myhb	1.211	1.08E-02	7.31E-02
UTP--glucose-1-phosphate uridylyltransferase	ugp2a	1.188	6.93E-03	5.73E-02
Collagen, type II, alpha 1b	col2a1b	1.175	1.63E-02	8.75E-02
Coatomer subunit alpha	copa	1.167	7.82E-03	6.11E-02
Proteasome (Prosome, macropain) 26S subunit, ATPase, 1a	psmc1a	1.161	4.94E-03	4.83E-02
Polyadenylate-binding protein 1A	pabpc1a	1.159	6.55E-03	5.59E-02
Si:dkey-261m9.12	si:dkey-261m9.12	1.153	1.47E-02	8.35E-02
Proteasome 26S subunit, ATPase 3	psmc3	1.152	3.90E-02	1.44E-01
Non-specific serine/threonine protein kinase	stk10	1.149	1.10E-02	7.35E-02
Apolipoprotein A-Ib	apoa1b	1.143	5.96E-03	5.28E-02
Guanine nucleotide-binding protein-like 3	gnl3	1.142	1.47E-02	8.35E-02
Actin-related protein 3	actr3	1.142	1.77E-02	9.10E-02
BRO1 domain-containing protein BROX	brox	1.131	1.77E-02	9.10E-02
Short chain dehydrogenase/reductase family 16C, member 5	sdr16c5b	1.121	7.22E-03	5.91E-02
Dolichyl-diphosphooligosaccharide--protein glycosyltransferase subunit 2	rpn2	1.107	9.41E-03	6.87E-02
AHNAK nucleoprotein	ahnak	1.090	1.22E-02	7.77E-02
Actinodin2	and2	1.088	1.40E-02	8.16E-02
Very-long-chain 3-oxoacyl-CoA reductase-A	hsd17b12a	1.067	1.39E-02	8.14E-02
Cytochrome P450, family 24, subfamily A, polypeptide 1	cyp24a1	1.043	8.14E-03	6.22E-02
Heat shock cognate 71 kDa protein	hspa8	1.040	1.35E-02	8.06E-02
78 kDa glucose-regulated protein	hspa5	1.019	1.54E-02	8.61E-02
EWS RNA-binding protein 1b	ewsr1b	1.014	2.48E-02	1.10E-01
S-adenosylmethionine synthase	mat1a	1.011	3.58E-02	1.37E-01
Collagen, type IV, alpha 2	col4a2	1.011	1.82E-02	9.18E-02

Fold change values were calculated via label-free quantification. Both non-adjusted p-values as well as p-values adjusted for FDR using the Benjamini-Hochberg procedure are shown. Rows highlighted in green are proteins that were up-regulated in all five analyses where samples labeled during the night had greater AHA labeling than samples labeled during the day.

We performed functional enrichment analysis for all eight night/day comparisons using the STRING database API to identify annotations or pathways that were significantly positively or negatively enriched amongst proteins synthesized during night versus day. Several comparisons revealed annotations related to endopeptidase activity or regulation to be positively enriched during the night, particularly in the night 6 / day 6 comparison in the first experiment (Table S4.1), night 6 / day 7 in the third experiment (Table S4.2), night 6 / day 7 in the fourth experiment (Table S4.3), and night 5 / day 5 comparison in the fifth experiment (Table S4.4). Most of the annotations enriched in the night 6 / day 6 comparison from our second experiment were related to translation and gene expression, which is perhaps unsurprising given the increase in protein synthesis observed at night in this experiment (Table S4.5). Meanwhile, functional enrichment analysis of the night 6 / day 6 comparison from our third experiment revealed primarily annotations related to collagen and ECM, although a couple of brain-related annotations ("neuronal system" and "transmission across chemical synapses") were both negatively enriched (Table S4.6). The two night 6 / day 7 comparisons (third and fourth experiments) both had a relatively large number annotations significantly positively or negatively enriched, including several annotations related to gene regulation and ECM, as well as amino acid metabolism and transport.

While our datasets exploring circadian changes in protein expression did not reveal enough reproducible or significant results to warrant publishing this work, it is possible that the data we collected contain other interesting information if analyzed through different lenses. For example, across our various experiments performing AHA labeling during different day or night periods spanning the day of 5 dpf through the night of 7 dpf, we incidentally collected a larval zebrafish development dataset spanning 72 hours with six consecutive 12 h time windows. With careful analysis taking into account the fact that that these datasets were collected across various experiments, one could look at these results in aggregate to determine if there are any interesting temporal patterns in protein synthesis during this window of zebrafish development.

Treatment of zebrafish with low, antidepressant-relevant doses of ketamine shows increase in protein synthesis consistent with results in *in vitro* primary cortical neuron cultures

Seeking to identify a behavioral phenomenon that would be interesting to explore at the proteomic level using BONCAT, we considered drug treatments that have been shown to cause observable behavioral changes in zebrafish. Encouraged by the observations we uncovered in *in vitro* primary rat embryonic cortical neuron cultures treated with low doses of ketamine using BONCAT (Chapter III), we aimed to extend our findings *in vivo* using zebrafish.

There have been a few studies of ketamine's effects on zebrafish behavior and brain activity, but all of these used higher doses of ketamine than those typically used *in vitro* to study ketamine's antidepressant effects (0.1 to 10 μM[53–58]). One paper found that ketamine produces changes in adult zebrafish locomotor behavior resembling those associated with psychosis in other animals, but the concentrations they used correspond to approximately 15 μM ketamine[59]. Other researchers reported dose-dependent anxiolytic effects of ketamine in adult zebrafish after 20 min of treatment, however these results were most pronounced at relatively high, sedative doses of 146 μM and 219 μM[60]. More recently, zebrafish larvae have been used as a model to investigate the neurological basis of ketamine's antidepressant effects. Andalman et al. reported that ketamine delays the emergence of passivity in zebrafish exposed to a behavioral challenge and, at a neural level, prevents the progressive increase in activity of ventral habenula neurons observed in untreated fish following stress[61]. However, their treatment protocol, which involved 20 min of exposure to 182 μM ketamine followed by 1 hour of recovery prior to behavior and imaging experiments, bears little resemblance to ketamine antidepressant treatment protocols in rodents or humans. Finally, using the most extreme treatment of 730 μM ketamine for 30 min followed by a 1 hour washout, Duque et al. demonstrated that ketamine-treated zebrafish larvae displayed prolonged increased behavioral perseverance in futile swimming conditions, and that this effect is linked to ketamine's hyperactivation of the norepinephrine-astroglia circuit responsible for passivity[62].

For our BONCAT experiments in zebrafish larvae, we chose a sub-dissociative, sub-anesthetic dose of 1 µM ketamine, which falls within the range of concentrations more commonly used to study ketamine's antidepressant effects and more closely approximates the concentration in cerebrospinal fluid (CSF) following *in vivo* administration of antidepressant doses of ketamine (0.2-2.5 µM[63–65]). Our first attempt at this experiment involved treating zebrafish larvae (5 dpf) with 1 µM ketamine (racemate) and 4 mM AHA. BONCAT-enriched samples were subjected to LC-MS/MS analysis without undergoing desalting to minimize protein loss, and while this led to some samples initially clogging the column, we were able to successfully run and obtain data for all samples.

We identified and obtained raw abundance values for 3,660 proteins. Comparing the average raw abundances of proteins identified in samples from both treatment groups revealed that 85% had higher average raw abundances in ketamine-treated samples compared to controls (Fig. 4.5). This result is indicative of greater AHA labeling, and thus of increased protein synthesis, in ketamine-treated samples compared to controls, in agreement with our results in *in vitro* primary neuron cultures (Chapter III, Fig. 3.2).

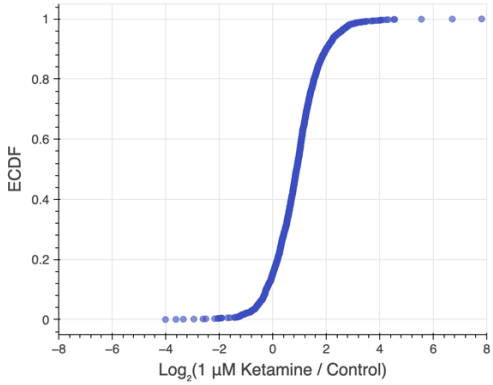

Figure 4.5. BONCAT proteomics reveals ketamine-induced increase in protein synthesis in zebrafish larvae treated with 1 µM ketamine. ECDF depicting the log ratios of the average raw abundances of proteins identified after BONCAT enrichment in zebrafish larvae (5 dpf) treated for 12 h with 1 µM ketamine (racemate) and 4 mM AHA to their average raw abundances in control samples treated only with 4 mM AHA. n = 4 biological replicates for each condition.

Differences in protein expression between ketamine-treated and control zebrafish larvae were also revealed via principal component analysis (PCA). We observed clear segregation and linear separability of ketamine-treated and untreated control samples (Fig. 4.6),

suggesting that drug treatment drives distinct patterns in the proteomics data that are well-captured by the first two principal components, which together account for over half of the total variance.

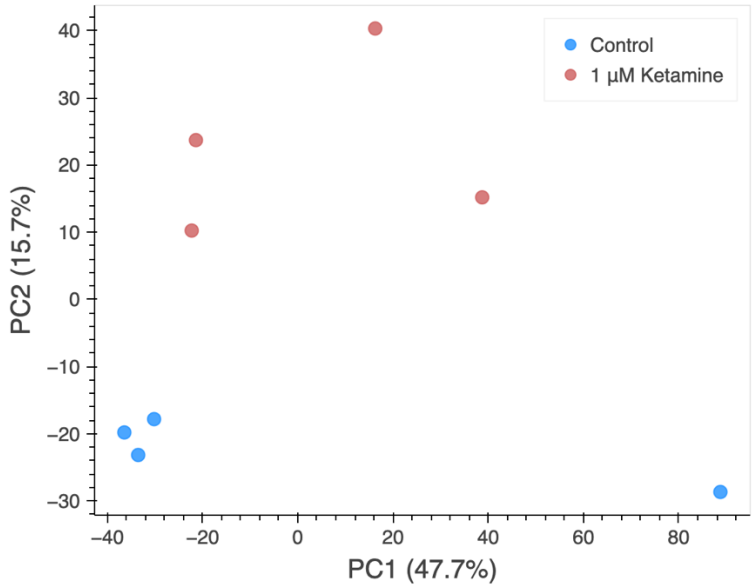

Figure 4.6. Principal component analysis shows clustering and linear separability of samples by treatment condition. PCA was performed using median normalized abundance data from BONCAT-enriched samples derived from zebrafish larvae (5 dpf) treated for 12 h with 1 µM ketamine (racemate) and 4 mM AHA and from control zebrafish larvae treated only with 4 mM AHA. n = 4 biological replicates per condition.

Analysis of BONCAT proteomics data reveals up- and down-regulated proteins and pathways in zebrafish larvae treated with ketamine compared to controls

We performed differential expression analysis on median normalized data to determine, relative to the total amount of protein synthesis in a particular condition, which proteins were up- or down-regulated in ketamine-treated zebrafish. While 97 proteins were found to have at least two-fold higher or lower expression in ketamine-treated samples with an associated p-value of less than 0.05 (Fig. 4.7), after adjusting for FDR, none of these p-values passed the threshold of statistical significance (FDR-adj. $p < 0.05$).

Nevertheless, we examined the proteins with $|\log_2 FC| > 1$ and $p < 0.05$ and identified several with potentially interesting biological functions in the context of low-dose ketamine treatment. The protein with the second highest increase in expression in ketamine-treated

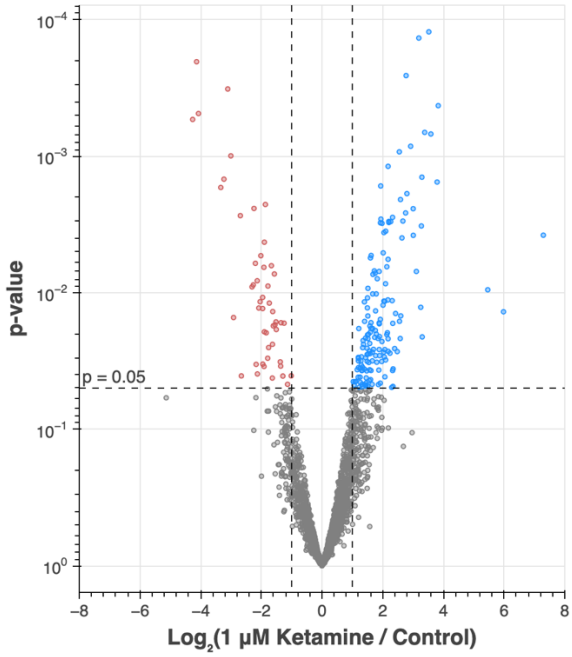

Figure 4.7. Differential expression analysis of BONCAT proteomics data reveals proteins with increased or decreased expression in zebrafish larvae treated with 1 µM ketamine compared to untreated zebrafish larvae. Volcano plot comparing median normalized abundances of BONCAT-enriched proteins from zebrafish larvae (5 dpf) treated for 12 h with 1 µM ketamine (racemate) and 4 mM AHA to those from control zebrafish larvae (5 dpf) treated only with 4 mM AHA. Fold change values were calculated via label-free quantification. Proteins with $\log_2(FC) > 1$ and $p < 0.05$ that are up-regulated in fish treated with ketamine are depicted in red, whereas proteins with $\log_2(FC) < 1$ and $p < 0.05$ that are down-regulated in fish treated with ketamine are depicted in blue. Horizontal dashed line depicts $p = 0.05$. No proteins passed the threshold for statistical significance (FDR-adj. $p < 0.05$) after adjusting for FDR using the Benjamini-Hochberg procedure.

zebrafish larvae was aldehyde dehydrogenase (Aldh2, $\log_2FC = 4.568$, $p = 0.03947$). A study performed in mice showed that *aldh2* knock-out mice have more severe bladder inflammation than wildtype mice exposed to chronic ketamine treatment[66], which could suggest that the increase in Aldh2 expression observed in our experiment might have anti-inflammatory effects. The authors of this study also reported a dose-dependent increase in expression of inducible nitric oxide synthase, which produces the proinflammatory mediator nitric oxide, in wildtype mice with chronic low- or high-dose treatment with ketamine. In agreement with their results, we observed increased expression of nitric oxide synthase-trafficking protein (Nostrin, $\log_2FC = 1.452$ $p = 0.0489$), as well as increased expression of nitric oxide synthase (Nos2b, $\log_2FC = 1.119$, $p = 0.536$) which did not pass the $p < 0.05$ threshold.

A protein from an uncharacterized gene predicted to be a glutamate receptor subunit was also found to be up-regulated (si:ch211-251b21.1, $\log_2$FC = 1.246, p = 0.0143), which is intriguing given the role of glutamate in hypothesized mechanisms for ketamine's antidepressant effects. Both human patients with MDD and animal models for depression have altered glutamate metabolism[67] and lower levels of glutamate in particular brain regions[68–73].

Ketamine is known to inhibit N-methyl-D-aspartate receptors (NMDARs), which are glutamate receptors, and it was initially suspected that antagonism of NMDARs on GABAergic interneurons leads to enhanced glutamate signaling[74,75], eventually resulting in increased synaptic plasticity and synaptogenesis[76,77]. Additionally, in our *in vitro* experiments described in Chapter III, we found that primary neurons treated with ketamine had increased expression of metabotropic glutamate receptor 1 (Grm1) and that "glutamatergic synapse" was amongst the annotations found via functional enrichment analysis to be significantly up-regulated in ketamine-treated neurons.

Several proteins involved in translation were found to be amongst those with $|\log_2 FC| > 1$ and $p < 0.05$ (Table 4.2). Nine ribosomal proteins had increased expression (Rps8, Rpl15, Rps11, Rps5, Rpl3, Rps6, Rpl22, Rpl36a, and Rps13), while three ribosomal proteins had decreased expression (Rps15a, Rps18, and Rplp2). Two eukaryotic translation initiation factor (EIF) proteins were found to be down-regulated (Eif5 and Eif4g2b). Translation-associated proteins such as protein pelota homolog (Pelo) and SRA stem-loop-interacting RNA-binding protein (Slirp) were also down-regulated, whereas signal recognition particle subunit SRP68 (Srp68) was up-regulated. These relatively strong shifts in expression of translational machinery components might be related to the overall increase in protein synthesis discussed above that we observed in zebrafish larvae exposed to ketamine (Fig. 4.5). We also saw significant changes in expression of proteins involved in translation in our BONCAT proteomics data from cultured primary neurons treated with ketamine (Chapter III), although our *in vitro* data showed that these proteins and pathways were mainly down-regulated, whereas our *in vivo* data from zebrafish showed some proteins increasing in

expression and others decreasing. Furthermore, Li et al. reported that low doses of ketamine activate mTOR signaling in mice, resulting in increased expression of synaptic proteins in the rat prefrontal cortex[78], and this mTOR activation could also give rise to increased translation more broadly, including increased expression of ribosomal proteins.

Table 4.2. Proteins involved in translation found to be differentially regulated in zebrafish larvae treated with 1 µM ketamine.

Protein	Gene Name	Log_2FC	P-Value
40S ribosomal protein S8	rps8	3.181	0.0234
Ribosomal protein L15	rpl15	2.998	0.0334
40S ribosomal protein S11	rps11	2.426	0.0262
Ribosomal protein S5	rps5	1.799	0.0291
Signal recognition particle subunit SRP68	srp68	1.792	0.0412
Ribosomal protein L3	rpl3	1.479	0.0250
40S ribosomal protein S6	rsp6	1.432	0.0191
Ribosomal protein L22	rpl22	1.311	0.0330
60S ribosomal protein L36a	rpl36a	1.305	0.0208
40S ribosomal protein S13	rps13	1.092	0.0497
Protein pelota homolog	pelo	-1.026	0.0323
Eukaryotic translation initiation factor 4, gamma 2b	eif4g2b	-1.305	0.0333
SRA stem-loop-interacting RNA-binding protein	slirp	-1.638	0.0146
Eukaryotic translation initiation factor 5	eif5	-1.790	0.0102
40S ribosomal protein S15a	rps15a	-1.917	0.0165
40S ribosomal protein S18	rps18	-2.184	0.0115
60S acidic ribosomal protein P2	rplp2	-3.911	0.0016

Fold change values were calculated via label-free quantification. P-values shown are not adjusted for FDR.

Finally, we identified six crystallin proteins (a combination of β- and γ-crystallins) to be amongst the 69 proteins with $log_2FC > 1$ and $p < 0.05$. This class of proteins is found in the eye lens and plays a role in the development of the zebrafish visual system. It is unclear what this might imply beyond the possibility that ketamine could influence larval zebrafish eye development, which could result from altered protein synthesis in the eye downstream of

signaling pathways such as mTOR, which has been shown to be stimulated by ketamine treatment[78].

We examined our differential expression data for semaphorins and collapsin response mediator proteins (CRMPs), as we observed that these classes of proteins had interesting changes in expression in our *in vitro* primary neuron experiments (Chapter III). We did not identify any semaphorins in our zebrafish BONCAT proteomics data, and while we did identify six CRMPs, they did not have the same pattern of expression as what we observed in cultured neurons, where we observed an overall increase in expression of CRMPs. In zebrafish treated with ketamine, Dpysl4 was found to be more strongly down-regulated ($log_2FC = 2.040$, $p = 0.0117$), whereas the other CRMPs identified had no significant change in expression ($p > 0.05$). Of these, four had positive log_2FC values (Dpysl2b, Dpysl2a, Dpysl3, Dpysl5b) and one had a negative log_2FC value (Dpysl5a). Ultimately, however, the lack of statistical significance associated with these results makes it impossible to draw meaningful conclusions regarding how low-dose ketamine treatment affects CRMP expression in zebrafish.

We performed functional enrichment analysis to determine whether any annotations across several databases were significantly positively or negatively enriched in ketamine-treated zebrafish larvae compared to controls. Only seven pathway annotations were found to be significantly altered (FDR-adj. $p < 0.05$), all of which were negatively enriched in ketamine-treated samples (Table 4.3). The one potentially interesting down-regulated pathway in ketamine-treated fish given our own results, as well as existing research on ketamine's effects on protein synthesis, was "cytoplasmic ribosomal proteins". This result agrees with the down-regulation of several proteins involved in translation that we observed in our differential expression analysis results, as well as with our functional enrichment analysis results in our *in vitro* BONCAT experiments with cultured primary neurons (Chapter III), where various pathway annotations related to translation were found to be down-regulated in response to ketamine treatment. The rest of the down-regulated annotations identified were related to extracellular matrix components, such as collagen, or proteins found in heart tissue.

Table 4.3. Seven annotations from various pathway annotation databases were significantly negatively enriched in ketamine-treated zebrafish larvae compared to controls.

Annotation Database	Annotation	Genes in Set Mapped	Enrichment Score	Direction	FDR-Adj. P-Value
GO Molecular Function	Extracellular matrix structural constituent	31/155	0.754	Down	0.0219
GO Cellular Component	Collagen trimer	27/104	1.01	Down	0.0049
WikiPathways	Cytoplasmic ribosomal proteins	55/78	0.344	Down	0.0495
TISSUES	Heart ventricle	103/172	0.247	Down	0.0245
TISSUES	Right ventricle	96/160	0.266	Down	0.0245
COMPARTMENTS	Collagen trimer	25/69	1.01	Down	0.0072
Pfam	Collagen triple helix repeat (20 copies)	30/92	0.899	Down	0.0025

Functional enrichment analysis was performed using the STRING database API. P-values (Kolmogorov-Smirnov) were adjusted for multiple hypothesis testing using the Benjamini–Hochberg procedure.

Second attempt testing low-dose ketamine treatment of zebrafish larvae was unable to reproduce results of initial experiment

In an effort to acquire data with greater statistical significance, we attempted this experiment a second time using more samples per condition (n=6 per condition instead of n=4 per condition in the first iteration of the experiment analyzed above). We also used slightly more mature zebrafish larvae (6 dpf rather than 5 dpf), as these would be closer in age to those used in the work of Andalman et al. and of Duque et al. investigating ketamine in zebrafish[61,62]. Unfortunately, one sample was lost during the BONCAT enrichment protocol due to a faulty bead washing column and another two samples (Ctl 6 and Ket 1) were discarded as outliers, since the range of raw abundance values detected in those samples via LC-MS/MS were substantially lower than those detected in the rest of the samples (Fig. 4.8).

We identified fewer proteins in this experiment than we did in the previous one (2,279 proteins). This may have been due to our desalting the samples prior to LC-MS/MS analysis to avoid their clogging the column, as this multi-step process for sample purification can lead to substantial protein loss. While we did once again observe greater protein synthesis in ketamine-treated zebrafish larvae compared to untreated controls, the effect was not as strong as the previous experiment; in this attempt, only 68% of proteins identified in both conditions

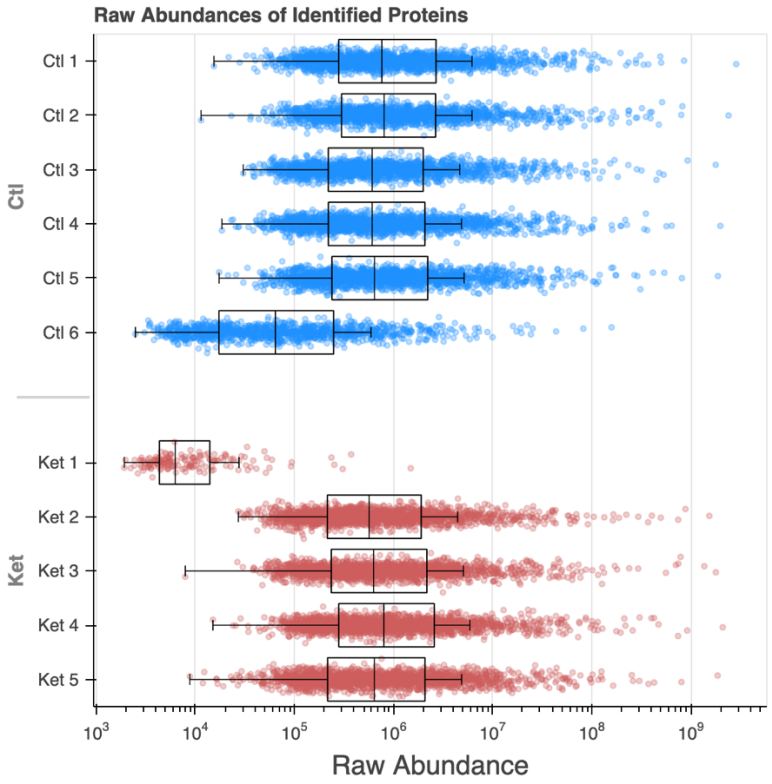

Figure 4.8. Two samples from second BONCAT proteomics experiment investigating the effect of ketamine treatment on protein synthesis in zebrafish larvae were discarded as outliers due to overall lower raw abundances. Scatter plot depicts raw abundance values (unitless) from LC-MS/MS analysis for all proteins identified in each sample. The top and bottom of each box are the 75th and 25th percentiles of the data, respectively. The line in the middle of each box is the median protein abundance for that sample. The whiskers extend to the maximum of the set of data points that are less than 1.5 times the interquartile range beyond the edges of the box. "Ctl 6" and "Ket 1" were ultimately discarded as outliers given the substantially lower raw abundance values detected in those samples.

after BONCAT enrichment had higher raw abundances in the ketamine-treated samples (Fig. 4.9A). We also did not see clear separation or clustering of samples via PCA after normalizing raw abundances across all samples (Fig. 4.9B). These results indicate that drug treatment was not the primary driver of variability in the dataset captured by the first two principal components, or that the effect size attributable to sample treatment condition is small relative to overall variance in the data.

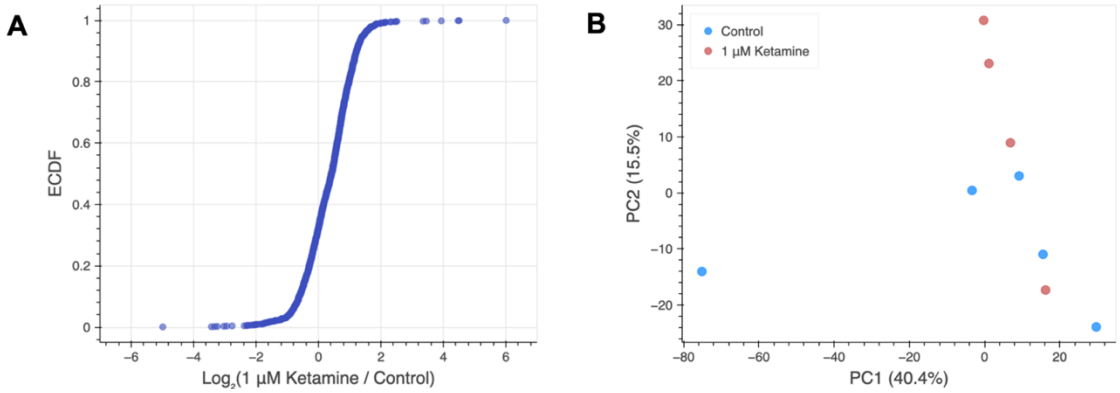

Figure 4.9. Second BONCAT proteomics experiment investigating protein synthesis in ketamine-treated zebrafish larvae produced different results than initial attempt. (A) ECDF depicting the log ratios of the average raw abundances of proteins identified after BONCAT enrichment in zebrafish larvae (6 dpf) treated for 12 h with 1 µM ketamine (racemate) and 4 mM AHA to their average raw abundances in control samples treated only with 4 mM AHA. (B) PCA plot shows less defined clustering and poor separation between ketamine-treated and control samples. PCA was performed using median normalized abundance data. n = 5 biological replicates for untreated control larvae. n = 4 biological replicates for ketamine-treated larvae.

Differential expression analysis of this dataset revealed 55 proteins with $|\log_2 FC| > 1$ and $p < 0.05$, with 18 proteins up-regulated and 37 proteins down-regulated (Fig. 4.10). Similar to the previous experiment, however, none of the p-values in the dataset were less than 0.05 after adjusting for multiple hypothesis testing. None of these 55 proteins overlapped with the 97 proteins found in the previous dataset to have $|\log_2 FC| > 1$ and $p < 0.05$. Nevertheless, several interesting proteins did appear. In particular, the protein with the second highest $\log_2 FC$ value was Grin2db ($\log_2 FC = 3.803$, $p = 0.00435$), which encodes a subunit of the NMDA receptor. Although different from the uncharacterized gene predicted to encode a glutamate receptor subunit in the first experiment, it was interesting that glutamate receptor subunits were up-regulated in both analyses.

Only one of these 55 proteins encoded a ribosomal protein (Rpl23, $\log_2 FC = 2.595$, $p = 0.00434$), unlike the previous experiment were several proteins involved in translation were found to have more pronounced and primarily decreasing shifts in expression. Instead, in this experiment, we found several proteins with $|\log_2 FC| > 1$ and $p < 0.05$ that are expressed in the brain and play interesting roles in synaptic plasticity, dendritic spine remodeling, transport of synaptic cargos and neurotransmitters, brain development, and neurite

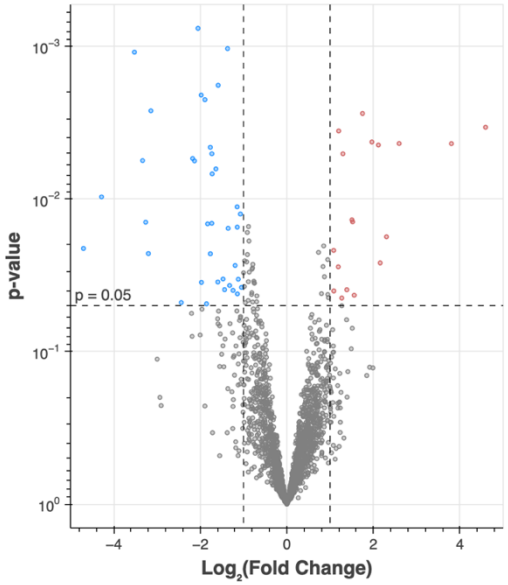

Figure 4.10. Differential expression analysis of BONCAT proteomics data reveals fewer up- or down-regulated proteins in second attempted experiment comparing zebrafish larvae treated with 1 µM ketamine to untreated controls. Volcano plot comparing median normalized abundances of BONCAT-enriched proteins from zebrafish larvae (6 dpf) treated for 12 h with 1 µM ketamine (racemate) and 4 mM AHA to those from control zebrafish larvae (6 dpf) treated only with 4 mM AHA. Fold change values were calculated via label-free quantification. Proteins with $\log_2(FC) > 1$ and $p < 0.05$ that are up-regulated in fish treated with ketamine are depicted in red, whereas proteins with $\log_2(FC) < 1$ and $p < 0.05$ that are down-regulated in fish treated with ketamine are depicted in blue. Horizontal dashed line depicts $p = 0.05$. No proteins passed the threshold for statistical significance (FDR-adj. $p < 0.05$) after adjusting for FDR using the Benjamini-Hochberg procedure.

outgrowth. In addition to Grin2db, other neuronally expressed proteins include non-muscle myosin IIA heavy chain (Myh14, $\log_2FC = 4.593$, $p = 0.00340$), annexin A3 (Anxa3b, $\log_2FC = 1.504$, $p = 0.0137$), cofilin 1 (Cfl1, $\log_2FC = 1.387$, $p = 0.0394$), kinectin 1 (Ktn1, $\log_2FC = -1.122$, $p = 0.0336$), GABA transporter 1 (Slc6a1a, $\log_2FC = -1.243$, $p = 0.0398$), hippocalcin (Hpca, $\log_2FC = -1.475$, $p = 0.0335$), stress-induced phosphoprotein 1 (Stip1, $\log_2FC = -1.594$, $p = 0.0351$), growth arrest-specific 6 (Gas6, $\log_2FC = -1.893$, $p = 0.00224$), and SWI/SNF-related, actin-dependent chromatin remodeler A1 (Smarca1, $\log_2FC = -3.142$, $p = 0.00265$).

We also identified several cytoskeletal or cytoskeleton-interacting proteins amongst those with $|\log_2FC| > 1$ and $p < 0.05$. These include some of the proteins mentioned above that have structural functions in neurons (e.g. Myh14, Cfl1, Ktn1, Smarca1, Anxa3b), which

interact with or modify actins, as well as thymosin β (Tmsb1, $\log_2$FC = 1.557, p = 0.0428), nebulin fragment (Neb, $\log_2$FC = −1.831, p = 0.0146), collagen XXVIII α2a (Col28a2a, $\log_2$FC = −3.262, p = 0.0142), and centromere protein F (Cenpf, $\log_2$FC = −4.699, p = 0.0211).

These results are in alignment with those from our BONCAT experiment in cultured primary neurons, where we found several synapse-associated proteins and structural proteins to be significantly differentially expressed in response to ketamine treatment. Although our zebrafish data lack the statistical significance required to draw confident conclusions without follow up experiments confirming the changes in expression of these proteins, altogether, our *in* vitro and *in vivo* data paint a picture of rapid synaptic plasticity, altered neuronal morphology, and neural circuit rewiring in upon exposure to sub-dissociative, antidepressant-level doses of ketamine.

We performed functional enrichment analysis on the data from this second experiment to determine which pathway annotations were significantly up- or down-regulated in ketamine-treated fish compared to controls. No pathways related to synaptic functions, cytoskeletal components, or translation were found to be enriched in either set of samples. The only six annotations found to be significantly altered were annotations for heart-related structures (“atrium,” “right atrium,” “cardiovascular system,” “right ventricle,” “heart,” “heart ventricle”), the latter two of which were also negatively enriched in ketamine-treated fish in the first experiment.

Having observed somewhat different results across two attempted experiments, we decided against continuing to use BONCAT proteomics to investigate ketamine-induced changes in protein synthesis in zebrafish larvae. While time constraints prevented us from pursuing this further, we believe that increasing the number of samples per condition, as well as continuing to optimize the BONCAT enrichment and proteomics sample preparation processes, would improve reproducibility across experiments and increase the likelihood of identifying statistically significant, biologically interesting changes in protein expression.

4.4 Conclusions and Future Directions

Our ultimate goal in developing *in vivo* BONCAT proteomics methods is to understand molecular changes underlying transient behavioral phenomena. The work summarized in this chapter describes the first attempts at using BONCAT in zebrafish to do time-resolved proteomics to shed light on questions in behavioral neuroscience. We first aimed to probe circadian changes in protein expression underlying sleep wake behaviors, and later sought to identify changes in protein synthesis that might drive ketamine's rapid-acting antidepressant effects at low doses. While our BONCAT proteomics data revealed some interesting changes in protein synthesis in both sets of experiments, our results did not pass the threshold of statistical significance or the level or reproducibility across experiments required to draw strong biological conclusions. However, with additional work to improve the BONCAT method in zebrafish, we are optimistic that BONCAT proteomics will be able to reveal meaningful molecular level insights into sleep, depression, and many other behaviors being studied in this exciting model organism.

There are multiple parts of the BONCAT enrichment process that could be further optimized for more efficient separation of AHA-labeled proteins. For example, in our early BONCAT experiments in zebrafish, we found that adjusting the volume of DBCO-agarose beads used in the enrichment seemed to have an effect on the relative abundances of proteins identified in labeled versus unlabeled samples. Further testing could identify the optimal bead quantity to reduce background without excessively reducing the number of proteins identified. Additionally, background from unlabeled proteins might be reduced by replacing agarose beads with magnetic beads, which we hypothesize would have less non-specific adsorption of unlabeled proteins. Magnetic beads would also likely simplify and reduce the number of required wash steps, resulting in less bead loss and therefore less protein loss. Thus, magnetic beads have the potential minimize background signal from non-AHA-labeled proteins while maximizing the retention of AHA-labeled proteins.

The usefulness of BONCAT proteomics for answering neuroscientific questions in zebrafish would further benefit from the implementation of cell-type-specific labeling strategies,

particularly within neurons. In our experiments, most AHA-labeled proteins likely originated from tissues outside the brain, limiting the specificity and interpretability of our proteomics data as it applies to brain-based phenomena. To address this issue, we dedicated considerable effort toward reproducing results published by Shahar et al., who successfully demonstrated cell-type-specific labeling of newly synthesized proteins in larval zebrafish neurons by expressing a modified methionyl tRNA synthetase (MetRS) capable of charging the bulkier azide-bearing noncanonical amino acid ANL under the control of a neuron-specific promoter[79]. However, in our hands, their *Tg(Elavl3:Gal4, UAS:CFP-T2A-MetRS^{L270G})* transgenic fish line showed mosaic expression of the mutant MetRS in the brain rather than pan-neuronal epxression. We observed slightly stronger albeit asymmetrical expression in the habenula and weak, sparse expression across the rest of the brain that varied from larva to larva (data not shown but available upon request). MetRS expression levels, evaluated based on CFP signal intensity, correlated with ANL labeling visualized via FUNCAT experiments. Our efforts to engineer a similar transgenic fish line by injecting embryos with a redesigned plasmid construct were also unsuccessful. The development of a stable transgenic fish line with strong pan-neuronal expression of the mutant MetRS is a necessary first step for achieving cell-type-specific time-resolved BONCAT proteomics in zebrafish. From there, the methodological improvements suggested earlier would be critical, since the affinity purification of ANL-labeled proteins from a subset of cells in zebrafish larvae presents an even more complicated enrichment problem than AHA labeling across the whole animal.

Finally, before going further with studies of ketamine in zebrafish larvae, it would be worthwhile to test whether such low doses of ketamine (1 μM) produce the desired antidepressant-like effect in this animal model using a relevant behavioral assay. Even though the small size and permeable skin of zebrafish larvae facilitate the uptake of drugs from their surrounding medium, it is possible that pharmacokinetics of drug absorption and metabolism by zebrafish larvae would require higher concentrations of ketamine in the swimming water to achieve the necessary concentration in brain tissue to give rise to antidepressant effects. Andalman et al. and Duque et al. reported antidepressant-like effects

from ketamine treatment in zebrafish larvae, but both groups used recovery periods prior to testing behavior[61,62]. Therefore, one would need to determine whether it is possible to elicit similar antidepressant effects in fish from sub-anesthetic doses of ketamine before performing time-resolved BONCAT proteomics under these conditions to draw conclusions relevant to the behavioral phenomenon of interest.

4.5 Materials and Methods

Zebrafish Husbandry

Animal husbandry and all experimental procedures involving zebrafish were performed in accordance with the California Institute of Technology Institutional Animal Care and Use Committee (IACUC) guidelines and by the Office of Laboratory Animal Resources at the California Institute of Technology (animal protocol 1836). All experiments used wildtype (hybrid TLAB) zebrafish 4-7 days post fertilization (dpf). Sex is not yet defined at this stage of development. Fish were raised in an incubator at 28.5°C in petri dishes containing E3 embryo medium (5 mM NaCl, 0.17 mM KCl, 0.33 mM $CaCl_2$, 0.33 mM $MgSO_4$) at a density of 50 zebrafish larvae per dish.

AHA labeling for BONCAT and FUNCAT in zebrafish larvae

To initiate labeling of newly synthesized proteins in zebrafish larvae, E3 was removed from petri dishes and replaced with 20 mL 4 mM AHA (Iris Biotech, HAA9280) dissolved in E3, filtered with a 0.2 μM filter, and brought to 28.5°C prior to treatment. Fish treated with AHA for 12 h were administered AHA either at 6 dpf at 9 am (day) or at 6 dpf at 9 pm (night). Fish treated with ketamine and untreated controls in those experiments were labeled for 12 h during the day. To perform treatments, E3 removed from petri dishes and replaced with 20 mL of E3 with 4 mM AHA and, for ketamine-treated samples, with 1 μM ketamine. Larvae were left in the 28.5°C incubator for the duration of labeling. After the desired labeling time, the 4 mM AHA solution was removed from the dishes, and fish were rinsed three times with E3 prior to collection. Zebrafish larvae were collected in 5-mL Eppendorf tubes (150 fish collected from three dishes per 5-mL tube) and placed on ice for euthanasia. After 1 hour, fish were transferred from the 5-mL tubes to 1.5-mL Eppendorf tubes. All E3 was removed

from the tube, and the remaining pellet of zebrafish was stored at −80°C until subsequent lysis and chemical enrichment.

Preparation of zebrafish lysates

After thawing, 500 µL lysis buffer containing 0.2% (w/v) n-dodecyl-β-maltoside (Thermo Fisher Scientific, 329370010), 2.5% (w/v) sodium dodecyl sulfate (Sigma-Aldrich, L5750), and 1:1000 EDTA-free protease inhibitors (Millipore, 539134) in 1X PBS was added to each tube containing zebrafish larvae. Zebrafish tissue was homogenized using a handheld motorized pestle for approximately 1 minute per sample, until mostly homogeneous by eye. Samples were transferred to 15-mL falcon tubes on ice for sonication, which was performed 4 x 30 s at 30% amplitude (QSonica), cycling through samples to allow foam at the surface to settle between sonication intervals. After sonication, benzonase (Sigma-Aldrich, E8263-25KU) was added to each sample at a ratio of 1:500, or 1 µL benzonase per tube, and left to incubate at room temperature for 5 min to degrade DNA and RNA in the samples that may not have been sheared via sonication. Samples were transferred to 1.5-mL Protein LoBind tubes (Eppendorf, 02243108), heated at 95°C for 10 min on a heating block, and cleared by centrifugation (20 min, 20,600 g, 4°C). Supernatants were transferred to new Protein LoBind tubes. Protein concentrations in each lysate were measured using the Pierce™ BCA Protein Assay Kit (performed on aliquots of lysates diluted 10-fold to ensure the concentrations measured were within the assay's dynamic range) and normalized across all samples using 2.5% SDS in PBS, resulting in each sample containing the same mass of protein (typically 1-3 mg) in a total volume of 500 µL. Lysates were stored at −80°C for further processing.

BONCAT enrichment and sample preparation for mass spectrometry

Lysates were first alkylated by treatment with 100 µL of 600 mM chloroacetamide (Sigma-Aldrich, C0267) in 0.8% SDS/PBS and incubation on a tube shaker at 65°C for 30 min in the dark at 1200 RPM. Following alkylation, 600 µL of 8 M urea / 0.85 M NaCl in PBS were added to the lysate (final concentration of urea: 4 M) along with 30 µL aza-dibenzocyclooctyne (DBCO) agarose beads (Vector Laboratories, CCT-1034). The copper-free click reaction was incubated on a rotary wheel at a low speed in the dark at room

temperature for 24 h. Samples were centrifuged at 1.5k RCF for 1 min, the supernatant was removed, and samples were reduced by adding 500 µL of 5 mM dithiothreitol (Sigma-Aldrich, 43815) in 0.8% SDS/PBS to each sample and incubating on a tube shaker for 15 min at 70°C and 1200 RPM in the dark. After centrifugation and removal of supernatant, samples were subjected to another alkylation step using 500 µL of 40 mM chloroacetamide and placement on a rotary wheel in the dark at room temperature for 30 min. Beads were then subjected to a series of thorough wash steps to remove nonspecifically bound proteins, first with 50 mL 0.8% (w/v) SDS in PBS, then with 50 mL urea in 100 mM tris hydrochloride (pH = 8.0), and finally with 50 mL 20% (v/v) acetonitrile (ACN) in doubly distilled water. Washed beads were transferred to 1.5-mL Protein LoBind tubes using 10% ACN in 50 mM ammonium bicarbonate, using 500 µL, then 300 µL, then 300 µL solution to ensure maximal resuspension and collection of beads from the columns. Samples were centrifuged at 1.5k RCF for 1 min and all but 100 µL of the supernatant was removed.

On-bead digestion was carried out by adding 0.1 µg trypsin and 0.05 µg endoproteinase LysC to each sample and incubating overnight on a tube shaker at 37°C and 1200 RPM. The following morning, samples were spun down at 1.5k RCF for 1 min and the peptide-containing supernatants were transferred to Pierce™ Centrifuge Columns (Thermo Scientific, 89868). The process of collecting peptides was repeated with three additional bead washes. For the first, 100 µL 20% ACN in LC-MS Grade Pierce™ Water (Thermo Scientific, 51140) was added to each tube, samples were centrifuged for 1.5k RCF for 1 min, and supernatant was transferred to the Pierce™ Centrifuge Columns. This was repeated two more times, each with 100 µL 20% ACN solution which were combined in the Pierce™ Centrifuge Columns. Samples were then centrifuged at 1.5k RCF for 1 min to remove any DBCO-agarose resin carried over in the supernatants. Tubes containing the flow-through were placed on a SpeedVac and vacuum concentrated until dry.

Samples were resuspended in 0.2% formic acid in LC-MS grade water and desalted using C18 ZipTips (Millipore, ZTC18S096) following instructions provided by the manufacturer. Activation solution consisted of 100% ACN, equilibration solution and wash solution were

both 0.2% formic acid in LC-MS grade water, and elution solution was 0.2% FA and 70% ACN in LC-MS grade water. Eluted peptides were vacuum concentrated to dryness and resuspended in 10 µL 0.2% formic acid for subsequent LC-MS/MS analysis.

LC-MS/MS analysis

All samples were analyzed on an Eclipse mass spectrometer (Thermo Fisher Scientific, USA) coupled to a Vanquish Neo UHPLC system (Thermo Fisher Scientific, USA). Peptides from BONCAT-enriched samples were separated on an Aurora UHPLC Column (25 cm x 75 µm, 1.7 µm C18, AUR3-25075C18-TS, Ion Opticks) with a flow rate of 0.35 µL/min for a total duration of 1 h and ionized at 1.6 kV in the positive ion mode. The gradient was composed of 6% solvent B (3.5 min), 6-25% B (41.5 min), 25-40% B (15 min), 40–98% B (2 min) and 98% B (5min), with the remaining volume composed of solvent A, where solvent A is 2% acetonitrile (ACN, Fisher Scientific, A9554) and 0.2% formic acid (FA, Fisher Scientific, A11750) in water, and solvent B is 80% ACN and 0.2% formic acid in water. For samples from whole lysates, 2 µg of peptides were separated on an Aurora Frontier™ column (60 cm × 75 µm, 1.7 µm C18, AUR3-60075C18, Ion Opticks) at 0.30 µL/min for a total duration of 2 h and ionized at 1.8 kV. The gradient was composed of 6% solvent B (7.5 min), 6-25% B (82.5 min), 25-40% B (30 min), 40–98% B (1 min) and 98% B (9 min). MS1 scans were acquired in the Orbitrap at the resolution of 120,000 from 375 to 1,600 m/z. Automatic gain control (AGC) was set to a target of 106 and a maximum injection time of 50 ms. MS2 scans were acquired in the ion trap using fast scan rate on precursors with 2-7 charge states and quadrupole isolation mode (isolation window: 1.2 m/z) with higher-energy collisional dissociation (HCD, 30%) activation type. Dynamic exclusion was set to 30 s. Ion transfer tube temperature was 300°C and the S-lens RF level was set to 30.

Proteomic data processing and analysis

MS raw files were searched against the Uniprot *Danio rerio* proteome (UP000000437) using the Proteome Discoverer 3.0 software based on the SequestHT algorithm. Oxidation / +15.995 Da (M), deamidated / +0.984 Da (N) were set as dynamic modifications; carbamidomethylation / +57.021 Da (C) was set as a fixed modification. The precursor mass

tolerance was set to 10 ppm; fragment mass tolerance was set to 0.6 Da. The maximum false peptide discovery rate was specified as 0.01 using the Percolator Node validated by q-value. The relative abundance of parental peptides was calculated by integration of the area under the curve of the MS1 peaks using the Minora LFQ node.

Raw protein quantification data exported from Proteome Discoverer 3.0 was imported into R and analyzed using the Tidyproteomics package (version 1.7.3) (https://jeffsocal.github.io/tidyproteomics/index.html)[80]. Once imported, the data were filtered for common protein contaminants and normalized between runs via median normalization. Differential expression analysis was performed in the Tidyproteomics package using the limma algorithms (https://bioinf.wehi.edu.au/limma/). All plots were generated using a separate analysis pipeline in Python. Jupyter notebooks with Python code can be provided upon request.

Functional enrichment analysis to identify significantly up- or down-regulated pathways and annotations was performed using "Proteins with Values/Ranks – Functional Enrichment Analysis" feature on the STRING database website (https://string-db.org, Version 12.0). For each comparison, the search input consisted of Uniprot accessions and log_2FC values for all proteins included in the differential expression analysis. FDR stringency was set to 0.05.

4.6 Supplementary Information

Table S4.1. Functional enrichment analysis reveals pathway and process annotations that are positively or negatively enriched during night 6 compared to during day 6 (Experiment #1).

Annotation Database	Annotation	Genes in Set Mapped	Enrichment Score	Direction	FDR-Adj. P-Value
GO Function	Peptidase regulator activity	14/189	2.4998	Down	0.0269
GO Function	Endopeptidase regulator activity	13/153	2.57826	Down	0.0269
GO Function	Endopeptidase inhibitor activity	11/144	2.66862	Down	0.0399
STRING clusters	Mixed, incl. HDR through Single Strand Annealing (SSA), and ATP-dependent DNA damage sensor activity	4/75	6.14054	Up	0.0116
InterPro	Thrombospondin type-1 (TSP1) repeat	3/42	5.97392	Up & Down	0.0427
InterPro	Thrombospondin type-1 (TSP1) repeat superfamily	3/42	5.97392	Up & Down	0.0427
SMART	Thrombospondin type 1 repeats	3/85	5.97392	Up & Down	0.026

Functional enrichment analysis was performed using the STRING database API. P-values (calculated using the Aggregate Fold Change, or AFC, method) were adjusted for multiple hypothesis testing using the Benjamini–Hochberg procedure.

Table S4.2. Functional enrichment analysis reveals pathway and process annotations that are positively or negatively enriched during night 6 compared to during day 7 (Experiment #3).

Annotation Database	Annotation	Genes in Set Mapped	Enrichment Score	Direction	FDR-Adj. P-Value
GO Process	Nucleosome assembly	16/99	4.53048	Up	2.29E-05
GO Process	Chromosome condensation	13/40	5.47061	Up	2.29E-05
GO Process	Negative regulation of DNA recombination	11/47	6.45358	Up	2.29E-05
GO Process	Negative regulation of DNA metabolic process	19/107	3.69843	Up	2.29E-05
GO Process	protein-DNA complex assembly	20/180	3.73841	Up	2.29E-05
GO Process	Extracellular matrix organization	63/280	1.86735	Up	4.87E-05
GO Process	Lipid localization	64/385	0.839171	Down	0.0012
GO Process	Small molecule catabolic process	126/329	0.578288	Down	0.0029
GO Process	Lipid transport	57/342	0.809251	Down	0.0037
GO Process	Small molecule biosynthetic process	93/383	0.660069	Down	0.0037
GO Process	Alpha-amino acid catabolic process	44/99	0.623444	Down	0.0044
GO Process	Regulation of DNA recombination	21/98	3.59374	Up	0.0051
GO Process	protein-DNA complex subunit organization	28/210	2.95083	Up	0.0079
GO Process	Chromatin organization	88/577	1.23204	Up	0.0081
GO Process	Negative regulation of nucleobase-containing compound metabolic process	135/1071	0.954562	Up	0.0121
GO Process	Chromatin assembly	23/143	3.24442	Up	0.0134
GO Process	Carboxylic acid catabolic process	93/224	0.591531	Down	0.0192
GO Process	Organic hydroxy compound transport	22/119	1.10595	Down	0.0226
GO Process	Chromosome organization	119/867	0.958441	Up	0.0236
GO Process	Nucleosome organization	23/128	3.41003	Up	0.0258
GO Process	Cellular amino acid catabolic process	51/115	0.622548	Down	0.0262
GO Process	Chromatin remodeling	45/263	1.90657	Up	0.0281
GO Function	Structural constituent of chromatin	18/160	4.29991	Up	1.06E-05
GO Function	Nucleosome binding	20/51	3.64261	Up	1.06E-05
GO Function	Nucleosomal DNA binding	14/28	5.07123	Up	1.06E-05
GO Function	Extracellular matrix structural constituent	53/155	1.97449	Up	0.00014
GO Function	Double-stranded DNA binding	98/2035	1.51644	Up	0.0011
GO Function	Lipid transporter activity	27/188	1.06134	Down	0.0031
GO Function	Chromatin DNA binding	23/82	3.27015	Up	0.0077
GO Function	Chromatin binding	80/467	1.17463	Up	0.0142
GO Function	Serine-type endopeptidase activity	31/211	1.10156	Down	0.0142

GO Function	Peptidase activity	127/761	0.426841	Down	0.0142
GO Function	Endopeptidase activity	88/523	0.54428	Down	0.0386
GO Component	Nucleosome	20/173	3.93161	Up	1.34E-05
GO Component	Extracellular matrix	106/498	1.30308	Up	1.34E-05
GO Component	Collagen-containing extracellular matrix	90/310	1.34049	Up	0.00014
GO Component	Collagen trimer	45/104	2.31324	Up	0.00021
GO Component	DNA packaging complex	28/245	3.07383	Up	0.0013
GO Component	Chromatin	79/534	1.36864	Up	0.0166
STRING clusters	Mixed, incl. Complement activation, and Common Pathway of Fibrin Clot Formation	46/144	1.1022	Down	8.2E-06
STRING clusters	Apoptosis induced DNA fragmentation, and DNA binding, bending	14/33	3.9296	Up	0.000015
STRING clusters	Apoptosis induced DNA fragmentation, and HMG box A DNA-binding domain, conserved site	10/22	5.09028	Up	0.000015
STRING clusters	Linker histone H1/H5, and G protein-coupled receptor 37 orphan	6/15	6.64443	Up	0.000015
STRING clusters	Linker histone H1/H5, and G protein-coupled receptor 37 orphan	4/10	7.24186	Up	0.000036
STRING clusters	Collagen biosynthesis and modifying enzymes, and Glycosyl transferase family 2	16/37	2.84357	Up	0.00027
STRING clusters	G protein-coupled receptor 37 orphan, and Linker histone H1/H5	3/5	7.67284	Up	0.00035
STRING clusters	Protein folding, and Cellular response to heat stress	59/139	0.542517	Down	0.0027
STRING clusters	Protein folding, and DnaJ molecular chaperone homology domain	60/167	0.529432	Down	0.0046
STRING clusters	Collagen biosynthesis and modifying enzymes, and TRIC channel	12/24	2.65028	Up	0.0066
STRING clusters	Mixed, incl. Complement activation, and Common Pathway of Fibrin Clot Formation	27/101	1.10716	Down	0.01
STRING clusters	Mixed, incl. Chaperone-mediated protein folding, and Chaperone binding	28/64	0.649456	Down	0.0112
STRING clusters	Unfolded protein binding, and Cellular response to heat stress	43/91	0.592723	Down	0.0143
STRING clusters	Mixed, incl. Chaperone-mediated protein folding, and Chaperone binding	30/70	0.582327	Down	0.0143
STRING clusters	C-terminal tandem repeated domain in type 4 procollagens, and NCAM1 interactions	9/11	2.86607	Up	0.0214

STRING clusters	Mixed, incl. mRNA editing complex, and N6-methyladenosine-containing RNA binding	7/27	3.28243	Up	0.0251
STRING clusters	Glycine, serine and threonine metabolism, and One carbon pool by folate	31/63	0.57426	Down	0.0282
STRING clusters	Mixed, incl. mRNA editing complex, and N6-methyladenosine-containing RNA binding	8/40	2.96902	Up	0.0284
KEGG	Protein processing in endoplasmic reticulum	67/197	0.491342	Down	0.0256
KEGG	ECM-receptor interaction	37/101	1.52847	Up	0.0256
Reactome	Apoptosis induced DNA fragmentation	11/24	3.78349	Up	0.00011
Reactome	Metabolism of amino acids and derivatives	110/211	0.590925	Down	0.00011
Reactome	Collagen chain trimerization	12/21	3.2725	Up	0.00049
Reactome	Non-integrin membrane-ECM interactions	13/24	2.81948	Up	0.0025
Reactome	Integrin cell surface interactions	20/56	1.95669	Up	0.0111
Reactome	Assembly of collagen fibrils and other multimeric structures	16/42	2.1028	Up	0.0251
COMPARTMENTS	Extracellular matrix	75/275	1.51738	Up	9.42E-05
COMPARTMENTS	Collagen-containing extracellular matrix	61/199	1.80313	Up	0.00015
COMPARTMENTS	Extracellular space	63/354	0.865203	Down	0.00055
COMPARTMENTS	Extracellular region	197/1274	0.481223	Up & Down	0.00065
COMPARTMENTS	Collagen trimer	35/69	2.50049	Up	0.0057
COMPARTMENTS	Complex of collagen trimers	10/15	2.95899	Up	0.0057
COMPARTMENTS	Fibrillar collagen trimer	8/10	3.02463	Up	0.0225
COMPARTMENTS	Banded collagen fibril	8/10	3.02463	Up	0.0225
COMPARTMENTS	Protein-lipid complex	14/46	1.40367	Down	0.0309
COMPARTMENTS	Plasma lipoprotein particle	14/46	1.40367	Down	0.0309
COMPARTMENTS	Lipoprotein particle	14/46	1.40367	Down	0.0309
UniProt Keywords	Zinc-finger	131/2077	0.969685	Up	0.00053
UniProt Keywords	Oxidoreductase	116/358	0.51899	Down	0.0018
UniProt Keywords	Protease	76/361	0.742443	Down	0.0018
UniProt Keywords	Zinc	195/2455	0.502859	Up	0.0118
UniProt Keywords	Serine protease	21/107	1.26667	Down	0.0135
UniProt Keywords	Chromosome	29/139	2.47783	Up	0.0224
Pfam	Collagen triple helix repeat (20 copies)	44/92	2.25865	Up	0.00091
InterPro	Linker histone H1/H5, domain H15	5/16	6.53213	Up	4.91E-05
InterPro	Linker histone H1/H5	5/14	6.53213	Up	4.91E-05

InterPro	NAD(P)-binding domain superfamily	54/134	0.653363	Down	0.0015
SMART	Domain in histone families 1 and 5	12/26	6.02503	Up	1.03E-05
SMART	Fibrillar collagens C-terminal domain	14/18	2.78538	Up	0.00087
SMART	Thrombospondin N-terminal - like domains.	12/25	2.74723	Up	0.0035
SMART	Trypsin-like serine protease	23/141	1.18059	Down	0.0223
SMART	Fibronectin type 3 domain	42/246	1.2027	Up	0.0223
SMART	C-terminal tandem repeated domain in type 4 procollagens	4/6	4.43579	Up	0.0223
SMART	K homology RNA-binding domain	21/41	0.626374	Up	0.031
SMART	Zinc finger	49/1197	1.2691	Up	0.031
SMART	Transglutaminase/protease-like homologues	6/14	3.19111	Up	0.031
SMART	Alpha-2-Macroglobulin	11/24	1.39996	Down	0.031
SMART	Alpha-2-macroglobulin family	11/24	1.39996	Down	0.031
SMART	A-macroglobulin receptor	11/24	1.39996	Down	0.031

Functional enrichment analysis was performed using the STRING database API. P-values (calculated either using the Aggregate Fold Change method or, for larger terms or terms with an unambiguous signal, using a Kolmogorov-Smirnov test) were adjusted for multiple hypothesis testing using the Benjamini–Hochberg procedure.

Table S4.3. Functional enrichment analysis reveals pathway and process annotations that are positively or negatively enriched during night 6 compared to during day 7 (Experiment #4).

Annotation Database	Annotation	Genes in Set Mapped	Enrichment Score	Direction	FDR-Adj. P-Value
GO Process	Negative regulation of DNA recombination	14/47	2.52579	Up	0.00012
GO Process	Nucleosome assembly	17/99	1.76283	Up	0.0025
GO Process	Chromosome condensation	14/40	2.01387	Up	0.0025
GO Process	Negative regulation of proteolysis	54/230	0.856771	Down	0.0029
GO Process	Negative regulation of endopeptidase activity	47/178	0.819646	Down	0.0208
GO Process	Regulation of proteolysis	118/546	0.548303	Down	0.0208
GO Process	Negative regulation of nucleobase-containing compound metabolic process	141/1071	0.627549	Up	0.0208
GO Process	Negative regulation of DNA metabolic process	21/107	1.66354	Up	0.0208
GO Process	Nucleosome organization	23/128	1.51571	Up	0.0234
GO Process	Regulation of DNA recombination	22/98	1.52509	Up	0.0274
GO Process	Negative regulation of hydrolase activity	55/240	0.780066	Down	0.0278
GO Process	Organic acid catabolic process	97/226	0.499549	Down	0.0292
GO Process	Proteolysis involved in protein catabolic process	129/702	0.232824	Down	0.0292
GO Process	Alpha-amino acid catabolic process	46/99	0.654099	Down	0.0297
GO Process	Macromolecule catabolic process	177/973	0.217922	Down	0.03
GO Process	Cellular amino acid catabolic process	53/115	0.726907	Down	0.03
GO Process	Carboxylic acid catabolic process	96/224	0.501706	Down	0.03
GO Process	protein-DNA complex subunit organization	27/210	1.34346	Up	0.03
GO Process	Small molecule catabolic process	130/329	0.54978	Down	0.0332
GO Function	Structural constituent of chromatin	17/160	1.90626	Up	0.0002
GO Function	Nucleosomal DNA binding	14/28	2.16774	Up	0.0002
GO Function	Chromatin DNA binding	20/82	1.56849	Up	0.0009
GO Function	Endopeptidase inhibitor activity	45/144	0.87913	Down	0.0018
GO Function	Peptidase inhibitor activity	46/155	0.854473	Down	0.0031
GO Function	Endopeptidase regulator activity	47/153	0.835594	Down	0.0051
GO Function	Double-stranded DNA binding	139/2035	0.527051	Up	0.0087
GO Function	Serine-type endopeptidase inhibitor activity	27/94	0.981159	Down	0.0087
GO Function	Extracellular matrix structural constituent	49/155	0.469572	Up	0.0087
GO Function	Peptidase regulator activity	55/189	0.707803	Down	0.0087
GO Function	Enzyme inhibitor activity	65/304	0.653753	Down	0.0287
GO Component	Nucleosome	19/173	1.66366	Up	0.00057

GO Component	Peptidase complex	47/108	0.507841	Down	0.00057
GO Component	DNA packaging complex	28/245	1.64689	Up	0.00061
GO Component	Proteasome complex	41/67	0.52215	Down	0.00095
GO Component	Endopeptidase complex	43/86	0.481869	Down	0.0014
GO Component	Collagen-containing extracellular matrix	80/310	0.416717	Up	0.0071
GO Component	Collagen trimer	39/104	0.602241	Up	0.0072
GO Component	Extracellular matrix	96/498	0.402037	Up	0.0097
GO Component	Proteasome accessory complex	21/29	0.654084	Down	0.0135
STRING clusters	Mixed, incl. Complement activation, and Common Pathway of Fibrin Clot Formation	52/144	1.20235	Down	4.87E-05
STRING clusters	Mixed, incl. Complement activation, and Common Pathway of Fibrin Clot Formation	35/101	1.28682	Down	0.00019
STRING clusters	Mixed, incl. Proteasome complex, and ERAD pathway	57/144	0.628073	Down	0.00026
STRING clusters	Proteasome	37/51	0.6133	Down	0.00065
STRING clusters	Proteasome complex, and Proteasome assembly	40/74	0.539558	Down	0.00068
STRING clusters	Proteasome, and Proteasome assembly	39/63	0.528211	Down	0.00092
STRING clusters	Apoptosis induced DNA fragmentation, and DNA binding, bending	13/33	1.96761	Up	0.002
STRING clusters	Apoptosis induced DNA fragmentation, and HMG box A DNA-binding domain, conserved site	10/22	2.33705	Up	0.002
STRING clusters	Common Pathway of Fibrin Clot Formation, and Coagulation	22/45	1.45283	Down	0.0053
STRING clusters	Linker histone H1/H5, and G protein-coupled receptor 37 orphan	6/15	2.63117	Up	0.0316
STRING clusters	Mixed, incl. Myosin II complex, and Striated muscle thin filament	56/125	0.109606	Up	0.0417
STRING clusters	Amino acid import across plasma membrane, and Amino acid transport across the plasma membrane	11/51	1.71995	Down	0.0417
STRING clusters	Amino acid import across plasma membrane, and Amino acid transport across the plasma membrane	10/42	1.82768	Down	0.0417
STRING clusters	Mixed, incl. Collagen biosynthesis and modifying enzymes, and Collagen fibril organization	29/74	0.771011	Up	0.0417
STRING clusters	Collagen biosynthesis and modifying enzymes, and Glycosyl transferase family 2	16/37	1.329	Up	0.0417
STRING clusters	Mixed, incl. Common Pathway of Fibrin Clot Formation, and Acute inflammatory response	19/40	1.22377	Down	0.0417

STRING clusters	Mixed, incl. Protein-lipid complex, and LDL remodeling	10/29	1.78248	Down	0.0417
STRING clusters	Phototransduction, and Detection of visible light	23/77	0.755352	Up	0.0417
STRING clusters	Mixed, incl. Steroid biosynthetic process, and Cytochrome P450	32/190	0.708489	Down	0.0417
KEGG	Proteasome	36/55	0.531377	Down	0.0022
KEGG	Steroid hormone biosynthesis	14/62	1.51839	Down	0.0148
KEGG	Glycine, serine and threonine metabolism	26/44	1.05716	Down	0.0148
KEGG	ECM-receptor interaction	37/101	0.754505	Up	0.0187
KEGG	Metabolism of xenobiotics by cytochrome P450	29/62	0.701543	Down	0.0213
KEGG	Focal adhesion	91/264	0.447812	Up	0.034
Reactome	ABC-family proteins mediated transport	38/82	0.679712	Down	0.00051
Reactome	Metabolism of amino acids and derivatives	112/211	0.576275	Down	0.00051
Reactome	G1/S Transition	31/98	0.630497	Down	0.0014
Reactome	Cross-presentation of soluble exogenous antigens (endosomes)	26/61	0.652882	Down	0.0017
Reactome	Autodegradation of Cdh1 by Cdh1:APC/C	25/55	0.713296	Down	0.0017
Reactome	APC/C:Cdc20 mediated degradation of Securin	26/59	0.652882	Down	0.0017
Reactome	APC/C:Cdh1 mediated degradation of Cdc20 and other APC/C:Cdh1 targeted proteins in late mitosis/early G1	26/65	0.652882	Down	0.0017
Reactome	Cdc20:Phospho-APC/C mediated degradation of Cyclin A	27/64	0.629669	Down	0.0017
Reactome	SCF(Skp2)-mediated degradation of p27/p21	27/55	0.647998	Down	0.0017
Reactome	Autodegradation of the E3 ubiquitin ligase COP1	26/45	0.652882	Down	0.0017
Reactome	Regulation of ornithine decarboxylase (ODC)	26/43	0.652882	Down	0.0017
Reactome	Metabolism of polyamines	28/50	0.671606	Down	0.0017
Reactome	Transport of small molecules	169/566	0.317539	Down	0.0017
Reactome	Mitotic G1 phase and G1/S transition	33/123	0.585409	Down	0.0017
Reactome	Asymmetric localization of PCP proteins	27/54	0.712306	Down	0.0017
Reactome	Degradation of AXIN	26/46	0.652882	Down	0.0017
Reactome	Hedgehog ligand biogenesis	30/57	0.631844	Down	0.0017
Reactome	Deubiquitination	58/227	0.552542	Down	0.0017
Reactome	UCH proteinases	34/82	0.636582	Down	0.0017
Reactome	CDK-mediated phosphorylation and removal of Cdc6	26/64	0.652882	Down	0.0017
Reactome	Cyclin E associated events during G1/S transition	28/64	0.655492	Down	0.0017
Reactome	Ubiquitin Mediated Degradation of Phosphorylated Cdc25A	26/45	0.652882	Down	0.0017

Reactome	Cyclin A:Cdk2-associated events at S phase entry	28/65	0.655492	Down	0.0017
Reactome	Ubiquitin-dependent degradation of Cyclin D	26/44	0.652882	Down	0.0017
Reactome	The role of GTSE1 in G2/M progression after G2 checkpoint	26/44	0.652882	Down	0.0017
Reactome	Regulation of RUNX3 expression and activity	26/47	0.649092	Down	0.0017
Reactome	MAPK6/MAPK4 signaling	32/71	0.568618	Down	0.0026
Reactome	DNA Replication Pre-Initiation	32/115	0.58454	Down	0.0026
Reactome	APC/C-mediated degradation of cell cycle proteins	29/78	0.574642	Down	0.003
Reactome	Degradation of DVL	28/51	0.606492	Down	0.003
Reactome	Regulation of RUNX2 expression and activity	28/45	0.580464	Down	0.003
Reactome	Ub-specific processing proteases	49/162	0.558467	Down	0.0031
Reactome	Assembly of the pre-replicative complex	31/100	0.592132	Down	0.0034
Reactome	RUNX1 regulates transcription of genes involved in differentiation of HSCs	27/58	0.546831	Down	0.0043
Reactome	CLEC7A (Dectin-1) signaling	33/73	0.524426	Down	0.0059
Reactome	G2/M Checkpoints	36/130	0.384419	Down	0.0063
Reactome	Dectin-1 mediated noncanonical NF-kB signaling	29/52	0.53392	Down	0.0067
Reactome	Degradation of GLI1 by the proteasome	29/49	0.53088	Down	0.0067
Reactome	Regulation of RAS by GAPs	29/57	0.56915	Down	0.0067
Reactome	NIK-->noncanonical NF-kB signaling	29/52	0.53392	Down	0.0067
Reactome	Orc1 removal from chromatin	29/63	0.53088	Down	0.0067
Reactome	FBXL7 down-regulates AURKA during mitotic entry and in early mitosis	29/47	0.53088	Down	0.0067
Reactome	Transcriptional regulation by RUNX2	29/55	0.553415	Down	0.0067
Reactome	Drug ADME	34/118	0.508984	Down	0.0067
Reactome	GSK3B and BTRC:CUL1-mediated-degradation of NFE2L2	29/44	0.534713	Down	0.0067
Reactome	Formation of Fibrin Clot (Clotting Cascade)	15/44	1.37157	Down	0.0093
Reactome	Intrinsic Pathway of Fibrin Clot Formation	11/35	1.6052	Down	0.0097
Reactome	Synthesis of DNA	31/109	0.437416	Down	0.0115
Reactome	Neddylation	46/194	0.371543	Down	0.0135
Reactome	Activation of NF-kappaB in B cells	30/54	0.493922	Down	0.0168
Reactome	Antigen processing-Cross presentation	32/104	0.517878	Down	0.0168
Reactome	Hedgehog on state	30/72	0.478433	Down	0.0168
Reactome	Nuclear events mediated by NFE2L2	30/48	0.507619	Down	0.0168

Reactome	S Phase	36/137	0.296173	Down	0.0174
Reactome	KEAP1-NFE2L2 pathway	36/66	0.500482	Down	0.0196
Reactome	Phase II - Conjugation of compounds	32/75	0.690939	Down	0.0203
Reactome	Oxygen-dependent proline hydroxylation of Hypoxia-inducible Factor Alpha	29/55	0.507694	Down	0.0242
Reactome	Transcriptional regulation by RUNX3	29/67	0.345124	Down	0.0242
Reactome	GLI3 is processed to GLI3R by the proteasome	32/53	0.459285	Down	0.0249
Reactome	Common Pathway of Fibrin Clot Formation	11/18	1.44833	Down	0.0277
Reactome	Nucleotide catabolism	10/28	1.50897	Down	0.0301
Reactome	PCP/CE pathway	39/81	0.505793	Down	0.0314
Reactome	Protein localization	30/100	0.621969	Down	0.0314
Reactome	AUF1 (hnRNP D0) binds and destabilizes mRNA	30/50	0.510137	Down	0.0342
Reactome	DNA Replication	37/142	0.380637	Down	0.0342
Reactome	Biological oxidations	61/177	0.552029	Down	0.0364
Reactome	Apoptosis induced DNA fragmentation	12/24	1.25964	Up	0.0386
Reactome	PTEN Regulation	39/129	0.214148	Down	0.0468
Reactome	Transcriptional regulation by RUNX1	39/147	0.335262	Down	0.0468
TISSUES	Heart	183/399	0.164741	Down	0.0264
TISSUES	Cardiovascular system	199/504	0.157028	Down	0.0345
COMPARTMENTS	Peptidase complex	49/111	0.478981	Down	0.0016
COMPARTMENTS	Proteasome complex	41/73	0.501555	Down	0.0021
COMPARTMENTS	Collagen-containing extracellular matrix	55/199	0.739842	Up	0.0026
COMPARTMENTS	Endopeptidase complex	44/87	0.451999	Down	0.0036
COMPARTMENTS	Extracellular matrix	66/275	0.57039	Up	0.0151
COMPARTMENTS	Chromosome	90/728	0.67535	Up	0.0273
UniProt Keywords	DNA-binding	90/992	0.83844	Up	0.00019
UniProt Keywords	Protease	88/361	0.430487	Down	0.0206
UniProt Keywords	Proteasome	28/45	0.422081	Down	0.0245
Pfam	Collagen triple helix repeat (20 copies)	42/92	0.516248	Up	0.0384
InterPro	Beta/gamma crystallin	21/43	0.674033	Up	0.0097
InterPro	Gamma-crystallin-like	21/43	0.674033	Up	0.0097
SMART	Domain in histone families 1 and 5	12/26	2.5201	Up	6.22E-05
SMART	Beta/gamma crystallins	26/62	0.605431	Up	0.0057
SMART	Fibrillar collagens C-terminal domain	11/18	1.60743	Up	0.0224
SMART	Alpha-2-Macroglobulin	11/24	1.658	Down	0.0224

SMART	Alpha-2-macroglobulin family	11/24	1.658	Down	0.0224
SMART	A-macroglobulin receptor	11/24	1.658	Down	0.0224

Functional enrichment analysis was performed using the STRING database API. P-values (calculated either using the Aggregate Fold Change method or, for larger terms or terms with an unambiguous signal, using a Kolmogorov-Smirnov test) were adjusted for multiple hypothesis testing using the Benjamini–Hochberg procedure.

Table S4.4. Functional enrichment analysis reveals pathway and process annotations that are positively or negatively enriched during night 5 compared to during day 5 (Experiment #5).

Annotation Database	Annotation	Genes in Set Mapped	Enrichment Score	Direction	FDR-Adj. P-Value
GO Process	Negative regulation of hydrolase activity	56/240	0.5887	Down	0.0088
GO Process	Negative regulation of peptidase activity	49/185	0.574876	Down	0.0301
GO Process	Negative regulation of endopeptidase activity	48/178	0.584089	Down	0.0301
GO Process	Regulation of endopeptidase activity	69/313	0.480488	Down	0.0301
GO Process	Regulation of peptidase activity	78/341	0.408551	Down	0.0357
GO Function	Endopeptidase inhibitor activity	44/144	0.596041	Down	0.0091
GO Function	Peptidase inhibitor activity	45/155	0.585744	Down	0.0091
GO Function	Peptidase regulator activity	56/189	0.49356	Down	0.0091
GO Function	Endopeptidase regulator activity	47/153	0.615448	Down	0.0091
STRING clusters	Mixed, incl. Complement activation, and Common Pathway of Fibrin Clot Formation	27/101	0.908669	Down	0.0045
STRING clusters	Mixed, incl. Complement activation, and Common Pathway of Fibrin Clot Formation	45/144	0.640356	Down	0.0424
Reactome	Integrin cell surface interactions	21/56	1.2835	Down	0.0259
COMPARTMENTS	Extracellular region	185/1274	0.28682	Down	0.0159
Pfam	Collagen triple helix repeat (20 copies)	38/92	0.793453	Down	0.0388
SMART	Leucine-rich repeats, typical (most populated) subfamily	9/163	2.13623	Up	0.0247

Functional enrichment analysis was performed using the STRING database API. P-values (calculated using the Kolmogorov-Smirnov test, with the exception of the last annotation from the SMART database, for which the p-value was calculated using the Aggregate Fold Change method) were adjusted for multiple hypothesis testing using the Benjamini–Hochberg procedure.

Table S4.5. Functional enrichment analysis reveals pathway and process annotations that are positively or negatively enriched during night 6 compared to during day 6 (Experiment #2).

Annotation Database	Annotation	Genes in Set Mapped	Enrichment Score	Direction	FDR-Adj. P-Value
GO Process	Negative regulation of DNA recombination	11/47	2.73413	Down	0.0039
GO Process	Chromosome condensation	12/40	2.32589	Down	0.0087
GO Process	Negative regulation of DNA metabolic process	14/107	2.13926	Down	0.0087
GO Process	Nucleosome assembly	16/99	1.79695	Down	0.018
GO Process	Nucleosome organization	19/128	1.58917	Down	0.018
GO Process	protein-DNA complex assembly	17/180	1.75998	Down	0.018
GO Process	protein-DNA complex subunit organization	20/210	1.56814	Down	0.018
GO Process	Intermediate filament cytoskeleton organization	27/67	0.988753	Down	0.0225
GO Function	Nucleosomal DNA binding	12/28	2.68112	Down	0.00048
GO Function	Structural constituent of ribosome	77/175	0.718973	Down	0.002
GO Function	Structural constituent of chromatin	17/160	1.92656	Down	0.002
GO Function	Nucleosome binding	18/51	1.81574	Down	0.002
GO Function	Chromatin DNA binding	20/82	1.63202	Down	0.0032
GO Function	Microtubule binding	21/277	0.496392	Up	0.0038
GO Function	Calcium ion binding	110/813	0.253156	Up	0.0076
GO Component	Nucleosome	20/173	1.72453	Down	0.0021
GO Component	Cytosolic large ribosomal subunit	31/44	1.19905	Down	0.0021
GO Component	Ribosome	83/199	0.672735	Down	0.0086
GO Component	Cytosolic ribosome	51/71	0.818397	Down	0.0086
GO Component	Large ribosomal subunit	38/99	0.943483	Down	0.0147
GO Component	Ribosomal subunit	65/155	0.719749	Down	0.0147
GO Component	Ribonucleoprotein complex	189/603	0.479515	Down	0.0233
STRING clusters	Cytoplasmic ribosomal proteins, and Translation elongation factor EFG/EF2, domain IV	74/107	0.757481	Down	0.0015
STRING clusters	Cytoplasmic ribosomal proteins, and High mobility group protein HMGN	72/101	0.774706	Down	0.0015
STRING clusters	Cytoplasmic ribosomal proteins, and Small ribosomal subunit	70/96	0.772469	Down	0.0015
STRING clusters	Cytoplasmic ribosomal proteins	69/86	0.788524	Down	0.0015
STRING clusters	Cytoplasmic ribosomal proteins	66/81	0.784499	Down	0.0015
STRING clusters	Cytoplasmic ribosomal proteins	62/71	0.760025	Down	0.0015
STRING clusters	Cytoplasmic ribosomal proteins	31/38	1.12352	Down	0.0015
STRING clusters	Cytoplasmic ribosomal proteins	26/31	1.13729	Down	0.0017
STRING clusters	Cytoplasmic ribosomal proteins	65/76	0.709597	Down	0.0019
STRING clusters	Cytoplasmic ribosomal proteins	57/66	0.810714	Down	0.0019

STRING clusters	Cytoplasmic ribosomal proteins, and Translational elongation	81/122	0.65952	Down	0.003
STRING clusters	Cytoplasmic ribosomal proteins, and Translational elongation	80/113	0.660514	Down	0.0048
STRING clusters	Apoptosis induced DNA fragmentation, and DNA binding, bending	12/33	2.11616	Down	0.006
STRING clusters	Apoptosis induced DNA fragmentation, and HMG box A DNA-binding domain, conserved site	9/22	2.49196	Down	0.006
STRING clusters	Cytoplasmic ribosomal proteins	52/60	0.779636	Down	0.007
STRING clusters	Cytoplasmic ribosomal proteins	47/55	0.803219	Down	0.0087
STRING clusters	Mixed, incl. Complement activation, and Common Pathway of Fibrin Clot Formation	17/101	1.5842	Down	0.0112
STRING clusters	Linker histone H1/H5, and G protein-coupled receptor 37 orphan	5/15	3.31832	Down	0.0113
STRING clusters	Complement activation, classical pathway, and Lectin pathway of complement activation	4/32	3.56036	Down	0.0279
STRING clusters	Eukaryotic Translation Initiation, and Translation factor activity, RNA binding	104/178	0.51569	Down	0.0311
KEGG	Ribosome	74/129	0.782067	Down	0.00097
KEGG	Calcium signaling pathway	36/290	0.343834	Up	0.0124
Reactome	L13a-mediated translational silencing of Ceruloplasmin expression	78/95	0.821073	Down	0.0014
Reactome	SRP-dependent cotranslational protein targeting to membrane	65/80	0.871833	Down	0.0014
Reactome	Formation of a pool of free 40S subunits	74/88	0.802139	Down	0.0014
Reactome	Cap-dependent Translation Initiation	78/98	0.821073	Down	0.0014
Reactome	Translation	88/194	0.749958	Down	0.0014
Reactome	Nonsense Mediated Decay (NMD) enhanced by the Exon Junction Complex (EJC)	72/95	0.862546	Down	0.0014
Reactome	GTP hydrolysis and joining of the 60S ribosomal subunit	77/95	0.81284	Down	0.0017
Reactome	Nonsense Mediated Decay (NMD) independent of the Exon Junction Complex (EJC)	66/78	0.840237	Down	0.0017
Reactome	Metabolism of RNA	190/480	0.505396	Down	0.0025
Reactome	Major pathway of rRNA processing in the nucleolus and cytosol	81/158	0.768246	Down	0.0077
WikiPathways	Cytoplasmic ribosomal proteins	64/78	0.904816	Down	0.00014
COMPARTMENTS	Ribosome	57/152	0.680912	Down	0.0078
UniProt Keywords	Calcium	102/561	0.305497	Up	0.0062
UniProt Keywords	Ribosomal protein	63/107	0.792152	Down	0.0062

SMART	Domain in histone families 1 and 5	12/26	2.54552	Down	0.00045

Functional enrichment analysis was performed using the STRING database API. P-values (calculated either using the Aggregate Fold Change method or, for larger terms or terms with an unambiguous signal, using a Kolmogorov-Smirnov test) were adjusted for multiple hypothesis testing using the Benjamini–Hochberg procedure.

Table S4.6. Functional enrichment analysis reveals pathway and process annotations that are positively or negatively enriched during night 6 compared to during day 6 (Experiment #3).

Annotation Database	Annotation	Genes in Set Mapped	Enrichment Score	Direction	FDR-Adj. P-Value
GO Function	Extracellular matrix structural constituent	52/155	0.446725	Down	0.0053
GO Component	Collagen trimer	44/104	0.721092	Up & Down	0.00093
STRING clusters	Mixed, incl. Complement activation, and Common Pathway of Fibrin Clot Formation	28/101	1.27547	Down	6.5E-07
STRING clusters	Mixed, incl. Complement activation, and Common Pathway of Fibrin Clot Formation	47/144	0.776784	Down	7.88E-05
STRING clusters	Mixed, incl. Activation of the phototransduction cascade, and cGMP binding	12/26	2.43862	Up	0.0231
STRING clusters	Mixed, incl. ABC-type transporter activity, and Inward rectifier potassium channel transmembrane domain	13/99	1.72214	Down	0.024
KEGG	Proteasome	36/55	0.201073	Down	0.0281
Reactome	Degradation of the extracellular matrix	35/107	0.561804	Up & Down	0.0161
Reactome	Transmission across Chemical Synapses	55/189	0.691752	Up	0.0446
Reactome	Neuronal System	65/300	0.544995	Up	0.0448
COMPARTMENTS	Collagen-containing extracellular matrix	61/199	0.621368	Up & Down	0.0045
COMPARTMENTS	Collagen trimer	34/69	0.623686	Down	0.0059
COMPARTMENTS	Extracellular region	194/1274	0.279739	Up & Down	0.0265
Pfam	Collagen triple helix repeat (20 copies)	42/92	0.644959	Up & Down	0.00064
SMART	Complement component C1q domain.	4/47	4.51621	Up	0.0171

Functional enrichment analysis was performed using the STRING database API. P-values (calculated using the Kolmogorov-Smirnov test, with the exception of the annotations "Mixed, incl. Activation of the phototransduction cascade, and cGMP binding," "Mixed, incl. ABC-type transporter activity, and Inward rectifier potassium channel transmembrane domain," and "Complement component C1q domain," for which p-values were calculated using the Aggregate Fold Change method) were adjusted for multiple hypothesis testing using the Benjamini–Hochberg procedure.

4.7 References

(1) Cirelli, C.; Gutierrez, C. M.; Tononi, G. Extensive and Divergent Effects of Sleep and Wakefulness on Brain Gene Expression. *Neuron* **2004**, *41* (1), 35–43. https://doi.org/10.1016/S0896-6273(03)00814-6.

(2) Sutton, M. A.; Schuman, E. M. Dendritic Protein Synthesis, Synaptic Plasticity, and Memory. *Cell* **2006**, *127* (1), 49–58. https://doi.org/10.1016/j.cell.2006.09.014.

(3) Wu, J.; McCallum, S. E.; Glick, S. D.; Huang, Y. Inhibition of the Mammalian Target of Rapamycin Pathway by Rapamycin Blocks Cocaine-Induced Locomotor Sensitization. *Neuroscience* **2011**, *172*, 104–109. https://doi.org/10.1016/j.neuroscience.2010.10.041.

(4) Costa-Mattioli, M.; Sossin, W. S.; Klann, E.; Sonenberg, N. Translational Control of Long-Lasting Synaptic Plasticity and Memory. *Neuron* **2009**, *61* (1), 10–26. https://doi.org/10.1016/j.neuron.2008.10.055.

(5) Buffington, S. A.; Huang, W.; Costa-Mattioli, M. Translational Control in Synaptic Plasticity and Cognitive Dysfunction. *Annu. Rev. Neurosci.* **2014**, *37* (Volume 37, 2014), 17–38. https://doi.org/10.1146/annurev-neuro-071013-014100.

(6) Choe, H. K.; Cho, J. Comprehensive Genome-Wide Approaches to Activity-Dependent Translational Control in Neurons. *Int. J. Mol. Sci.* **2020**, *21* (5), 1592. https://doi.org/10.3390/ijms21051592.

(7) Xu, Z.-X.; Kim, G. H.; Tan, J.-W.; Riso, A. E.; Sun, Y.; Xu, E. Y.; Liao, G.-Y.; Xu, H.; Lee, S.-H.; Do, N.-Y.; Lee, C. H.; Clipperton-Allen, A. E.; Kwon, S.; Page, D. T.; Lee, K. J.; Xu, B. Elevated Protein Synthesis in Microglia Causes Autism-like Synaptic and Behavioral Aberrations. *Nat. Commun.* **2020**, *11* (1), 1797. https://doi.org/10.1038/s41467-020-15530-3.

(8) Gerlai, R. A Small Fish with a Big Future: Zebrafish in Behavioral Neuroscience. *Rev. Neurosci.* **2011**, *22* (1), 3–4. https://doi.org/10.1515/RNS.2011.002.

(9) Kalueff, A. V.; Stewart, A. M.; Gerlai, R. Zebrafish as an Emerging Model for Studying Complex Brain Disorders. *Trends Pharmacol. Sci.* **2014**, *35* (2), 63–75. https://doi.org/10.1016/j.tips.2013.12.002.

(10) Doszyn, O.; Dulski, T.; Zmorzynska, J. Diving into the Zebrafish Brain: Exploring Neuroscience Frontiers with Genetic Tools, Imaging Techniques, and Behavioral Insights. *Front. Mol. Neurosci.* **2024**, *17*. https://doi.org/10.3389/fnmol.2024.1358844.

(11) Firdous, S. M.; Pal, S.; Khanam, S.; Zakir, F. Behavioral Neuroscience in Zebrafish: Unravelling the Complexity of Brain-Behavior Relationships. *Naunyn. Schmiedebergs Arch. Pharmacol.* **2024**, *397* (12), 9295–9313. https://doi.org/10.1007/s00210-024-03275-5.

(12) Oikonomou, G.; Prober, D. A. Attacking Sleep from a New Angle: Contributions from Zebrafish. *Curr. Opin. Neurobiol.* **2017**, *44*, 80–88. https://doi.org/10.1016/j.conb.2017.03.009.

(13) Tran, S.; Prober, D. A. Methods to Study Sleep in Zebrafish. In *Circadian Clocks*; Hirota, T., Hatori, M., Panda, S., Eds.; Springer US: New York, NY, 2022; pp 259–286. https://doi.org/10.1007/978-1-0716-2577-4_12.

(14) Ahrens, M. B.; Li, J. M.; Orger, M. B.; Robson, D. N.; Schier, A. F.; Engert, F.; Portugues, R. Brain-Wide Neuronal Dynamics during Motor Adaptation in Zebrafish. *Nature* **2012**, *485* (7399), 471–477. https://doi.org/10.1038/nature11057.

(15) Clift, D.; Richendrfer, H.; Thorn, R. J.; Colwill, R. M.; Creton, R. High-Throughput Analysis of Behavior in Zebrafish Larvae: Effects of Feeding. *Zebrafish* **2014**, *11* (5), 455–461. https://doi.org/10.1089/zeb.2014.0989.

(16) Lee, D. A.; Oikonomou, G.; Prober, D. A. Large-Scale Analysis of Sleep in Zebrafish. *Bio-Protoc.* **2022**, *12* (3), e4313. https://doi.org/10.21769/BioProtoc.4313.

(17) Dieterich, D. C.; Link, A. J.; Graumann, J.; Tirrell, D. A.; Schuman, E. M. Selective Identification of Newly Synthesized Proteins in Mammalian Cells Using Bioorthogonal Noncanonical Amino Acid Tagging (BONCAT). *Proc. Natl. Acad. Sci.* **2006**, *103* (25), 9482–9487.

(18) Dieterich, D. C.; Lee, J. J.; Link, A. J.; Graumann, J.; Tirrell, D. A.; Schuman, E. M. Labeling, Detection and Identification of Newly Synthesized Proteomes with Bioorthogonal Non-Canonical Amino-Acid Tagging. *Nat. Protoc.* **2007**, *2* (3), 532–540. https://doi.org/10.1038/nprot.2007.52.

(19) Schanzenbächer, C. T.; Sambandan, S.; Langer, J. D.; Schuman, E. M. Nascent Proteome Remodeling Following Homeostatic Scaling at Hippocampal Synapses. *Neuron* **2016**, *92* (2), 358–371. https://doi.org/10.1016/j.neuron.2016.09.058.

(20) Alvarez-Castelao, B.; Schanzenbächer, C. T.; Hanus, C.; Glock, C.; tom Dieck, S.; Dörrbaum, A. R.; Bartnik, I.; Nassim-Assir, B.; Ciirdaeva, E.; Mueller, A.; Dieterich, D. C.; Tirrell, D. A.; Langer, J. D.; Schuman, E. M. Cell-Type-Specific Metabolic Labeling of Nascent Proteomes in Vivo. *Nat. Biotechnol.* **2017**, *35* (12), 1196–1201. https://doi.org/10.1038/nbt.4016.

(21) Rostovtsev, V. V.; Green, L. G.; Fokin, V. V.; Sharpless, K. B. A Stepwise Huisgen Cycloaddition Process: Copper(I)-Catalyzed Regioselective "Ligation" of Azides and Terminal Alkynes. *Angew. Chem. Int. Ed.* **2002**, *41* (14), 2596–2599. https://doi.org/10.1002/1521-3773(20020715)41:14<2596::AID-ANIE2596>3.0.CO;2-4.

(22) Tornøe, C. W.; Christensen, C.; Meldal, M. Peptidotriazoles on Solid Phase: [1,2,3]-Triazoles by Regiospecific Copper(I)-Catalyzed 1,3-Dipolar Cycloadditions of Terminal Alkynes to Azides. *J. Org. Chem.* **2002**, *67* (9), 3057–3064. https://doi.org/10.1021/jo011148j.

(23) Agard, N. J.; Prescher, J. A.; Bertozzi, C. R. A Strain-Promoted [3 + 2] Azide−Alkyne Cycloaddition for Covalent Modification of Biomolecules in Living Systems. *J. Am. Chem. Soc.* **2004**, *126* (46), 15046–15047. https://doi.org/10.1021/ja044996f.

(24) Lyu, J.; Zhuang ,Yanrong; and Lin, Y. Circadian Regulation of Translation. *RNA Biol.* **2024**, *21* (1), 959–969. https://doi.org/10.1080/15476286.2024.2408524.

(25) Gould, T. D.; Zarate, C. A.; Thompson, S. M. Molecular Pharmacology and Neurobiology of Rapid-Acting Antidepressants. *Annu. Rev. Pharmacol. Toxicol.* **2019**, *59* (Volume 59, 2019), 213–236. https://doi.org/10.1146/annurev-pharmtox-010617-052811.

(26) Witkin, J. M.; Martin, A. E.; Golani, L. K.; Xu, N. Z.; Smith, J. L. Chapter Three - Rapid-Acting Antidepressants. In *Advances in Pharmacology*; Witkin, J. M., Ed.; Neuropsychotherapeutics; Academic Press, 2019; Vol. 86, pp 47–96. https://doi.org/10.1016/bs.apha.2019.03.002.

(27) Berman, R. M.; Cappiello, A.; Anand, A.; Oren, D. A.; Heninger, G. R.; Charney, D. S.; Krystal, J. H. Antidepressant Effects of Ketamine in Depressed Patients. *Biol. Psychiatry* **2000**, *47* (4), 351–354. https://doi.org/10.1016/S0006-3223(99)00230-9.

(28) Zarate, C. A., Jr; Singh, J. B.; Carlson, P. J.; Brutsche, N. E.; Ameli, R.; Luckenbaugh, D. A.; Charney, D. S.; Manji, H. K. A Randomized Trial of an N-Methyl-D-Aspartate Antagonist in Treatment-Resistant Major Depression. *Arch. Gen. Psychiatry* **2006**, *63* (8), 856–864. https://doi.org/10.1001/archpsyc.63.8.856.

(29))Chen, M.-H.; Li, C.-T.; Lin, W.-C.; Hong, C.-J.; Tu, P.-C.; Bai, Y.-M.; Cheng, C.-M.; Su, T.-P. Persistent Antidepressant Effect of Low-Dose Ketamine and Activation in the Supplementary Motor Area and Anterior Cingulate Cortex in Treatment-Resistant Depression: A Randomized Control Study. *J. Affect. Disord.* **2018**, *225*, 709–714. https://doi.org/10.1016/j.jad.2017.09.008.

(30) Daly, E. J.; Trivedi, M. H.; Janik, A.; Li, H.; Zhang, Y.; Li, X.; Lane, R.; Lim, P.; Duca, A. R.; Hough, D.; Thase, M. E.; Zajecka, J.; Winokur, A.; Divacka, I.; Fagiolini, A.; Cubała, W. J.; Bitter, I.; Blier, P.; Shelton, R. C.; Molero, P.; Manji, H.; Drevets, W. C.; Singh, J. B. Efficacy of Esketamine Nasal Spray Plus Oral Antidepressant Treatment for Relapse Prevention in Patients With Treatment-Resistant Depression: A Randomized Clinical Trial. *JAMA Psychiatry* **2019**, *76* (9), 893–903. https://doi.org/10.1001/jamapsychiatry.2019.1189.

(31) Matveychuk, D.; Thomas, R. K.; Swainson, J.; Khullar, A.; MacKay, M.-A.; Baker, G. B.; Dursun, S. M. Ketamine as an Antidepressant: Overview of Its Mechanisms of Action and Potential Predictive Biomarkers. *Ther. Adv. Psychopharmacol.* **2020**, *10*, 2045125320916657. https://doi.org/10.1177/2045125320916657.

(32) Lullau, A. P. M.; Haga, E. M. W.; Ronold, E. H.; Dwyer, G. E. Antidepressant Mechanisms of Ketamine: A Review of Actions with Relevance to Treatment-Resistance and Neuroprogression. *Front. Neurosci.* **2023**, *17*. https://doi.org/10.3389/fnins.2023.1223145.

(33) Krystal, J. H.; Kavalali, E. T.; Monteggia, L. M. Ketamine and Rapid Antidepressant Action: New Treatments and Novel Synaptic Signaling Mechanisms. *Neuropsychopharmacology* **2024**, *49* (1), 41–50. https://doi.org/10.1038/s41386-023-01629-w.

(34) Wesseling, H.; Rahmoune, H.; Tricklebank, M.; Guest, P. C.; Bahn, S. A Targeted Multiplexed Proteomic Investigation Identifies Ketamine-Induced Changes in Immune Markers in Rat Serum and Expression Changes in Protein Kinases/Phosphatases in Rat Brain. *J. Proteome Res.* **2015**, *14* (1), 411–421. https://doi.org/10.1021/pr5009493.

(35) Weckmann, K.; Deery, M. J.; Howard, J. A.; Feret, R.; Asara, J. M.; Dethloff, F.; Filiou, M. D.; Iannace, J.; Labermaier, C.; Maccarrone, G.; Webhofer, C.; Teplytska, L.; Lilley, K.; Müller, M. B.; Turck, C. W. Ketamine's Antidepressant Effect Is Mediated by Energy Metabolism and Antioxidant Defense System. *Sci. Rep.* **2017**, *7* (1), 15788. https://doi.org/10.1038/s41598-017-16183-x.

(36) Xiao, Y.; Luo, H.; Yang, W. Z.; Zeng, Y.; Shen, Y.; Ni, X.; Shi, Z.; Zhong, J.; Liang, Z.; Fu, X.; Tu, H.; Sun, W.; Shen, W. L.; Hu, J.; Yang, J. A Brain Signaling Framework for Stress-Induced Depression and Ketamine Treatment Elucidated by Phosphoproteomics. *Front. Cell. Neurosci.* **2020**, *14*, 48. https://doi.org/10.3389/fncel.2020.00048.

(37) Weckmann, K.; Deery, M. J.; Howard, J. A.; Feret, R.; Asara, J. M.; Dethloff, F.; Filiou, M. D.; Labermaier, C.; Maccarrone, G.; Lilley, K. S.; Mueller, M.; Turck, C. W. Ketamine's Effects on the Glutamatergic and GABAergic Systems: A Proteomics and Metabolomics Study in Mice. *Complex Psychiatry* **2019**, *5* (1), 42–51. https://doi.org/10.1159/000493425.

(38) Herzog, D. P.; Perumal, N.; Manicam, C.; Treccani, G.; Nadig, J.; Rossmanith, M.; Engelmann, J.; Jene, T.; Hasch, A.; van der Kooij, M. A.; Lieb, K.; Gassen, N. C.; Grus, F. H.; Müller, M. B. Longitudinal CSF Proteome Profiling in Mice to Uncover the Acute and Sustained Mechanisms of Action of Rapid Acting Antidepressant (2R,6R)-Hydroxynorketamine (HNK). *Neurobiol. Stress* **2021**, *15*, 100404. https://doi.org/10.1016/j.ynstr.2021.100404.

(39) Zhou, N.; Shi, X.; Wang, R.; Wang, C.; Lan, X.; Liu, G.; Li, W.; Zhou, Y.; Ning, Y. Proteomic Patterns Associated with Ketamine Response in Major Depressive Disorders. *Cell Biol. Toxicol.* **2025**, *41* (1), 26. https://doi.org/10.1007/s10565-024-09981-3.

(40) Holwerda, A. M.; Kouw, I. W.; Trommelen, J.; Halson, S. L.; Wodzig, W. K.; Verdijk, L. B.; van Loon, L. J. Physical Activity Performed in the Evening Increases the Overnight Muscle Protein Synthetic Response to Presleep Protein Ingestion in Older Men123. *J. Nutr.* **2016**, *146* (7), 1307–1314. https://doi.org/10.3945/jn.116.230086.

(41) Trommelen, J.; Holwerda, A. M.; Kouw, I. W. K.; Langer, H.; Halson, S. L.; Rollo, I.; Verdijk, L. B.; Van Loon, L. J. C. Resistance Exercise Augments Postprandial

Overnight Muscle Protein Synthesis Rates. *Med. Sci. Sports Exerc.* **2016**, *48* (12), 2517. https://doi.org/10.1249/MSS.0000000000001045.

(42) Kouw, I. W.; Holwerda, A. M.; Trommelen, J.; Kramer, I. F.; Bastiaanse, J.; Halson, S. L.; Wodzig, W. K.; Verdijk, L. B.; van Loon, L. J. Protein Ingestion before Sleep Increases Overnight Muscle Protein Synthesis Rates in Healthy Older Men: A Randomized Controlled Trial. *J. Nutr.* **2017**, *147* (12), 2252–2261. https://doi.org/10.3945/jn.117.254532.

(43) Trommelen, J.; Kouw, I. W. K.; Holwerda, A. M.; Snijders, T.; Halson, S. L.; Rollo, I.; Verdijk, L. B.; van Loon, L. J. C. Presleep Dietary Protein-Derived Amino Acids Are Incorporated in Myofibrillar Protein during Postexercise Overnight Recovery. *Am. J. Physiol.-Endocrinol. Metab.* **2018**, *314* (5), E457–E467. https://doi.org/10.1152/ajpendo.00273.2016.

(44) Snijders, T.; Trommelen, J.; Kouw, I. W. K.; Holwerda, A. M.; Verdijk, L. B.; van Loon, L. J. C. The Impact of Pre-Sleep Protein Ingestion on the Skeletal Muscle Adaptive Response to Exercise in Humans: An Update. *Front. Nutr.* **2019**, *6*. https://doi.org/10.3389/fnut.2019.00017.

(45) Reis, C. E. G.; Loureiro, L. M. R.; Roschel, H.; da Costa, T. H. M. Effects of Pre-Sleep Protein Consumption on Muscle-Related Outcomes — A Systematic Review. *J. Sci. Med. Sport* **2021**, *24* (2), 177–182. https://doi.org/10.1016/j.jsams.2020.07.016.

(46) Adam, K.; Oswald, I. Protein Synthesis, Bodily Renewal and the Sleep-Wake Cycle. *Clin. Sci.* **1983**, *65* (6), 561–567. https://doi.org/10.1042/cs0650561.

(47) Ramm, P.; Smith, C. T. Rates of Cerebral Protein Synthesis Are Linked to Slow Wave Sleep in the Rat. *Physiol. Behav.* **1990**, *48* (5), 749–753. https://doi.org/10.1016/0031-9384(90)90220-X.

(48) Chang, S.; Yoshihara, T.; Machida, S.; Naito, H. Circadian Rhythm of Intracellular Protein Synthesis Signaling in Rat Cardiac and Skeletal Muscles. *Biochem. Biophys. Rep.* **2017**, *9*, 153–158. https://doi.org/10.1016/j.bbrep.2016.12.005.

(49) Zhong, Z.; Wang, M.; Huang, G.; Zhang, S.; Wang, H. Molecular Genetic and Genomic Analyses of Zebrafish Circadian Rhythmicity. In *Biological Timekeeping: Clocks, Rhythms and Behaviour*; Kumar, V., Ed.; Springer India: New Delhi, 2017; pp 193–209. https://doi.org/10.1007/978-81-322-3688-7_8.

(50) Sacksteder, R. E.; Kimmey, J. M. Immunity, Infection, and the Zebrafish Clock. *Infect. Immun.* **2022**, *90* (9), e00588-21. https://doi.org/10.1128/iai.00588-21.

(51) Takahashi, J. S. Transcriptional Architecture of the Mammalian Circadian Clock. *Nat. Rev. Genet.* **2017**, *18* (3), 164–179. https://doi.org/10.1038/nrg.2016.150.

(52) Mazur, M.; Rakus, K.; Adamek, M.; Surachetpong, W.; Chadzinska, M.; Pijanowski, L. Effects of Light and Circadian Clock on the Antiviral Immune Response in Zebrafish. *Fish Shellfish Immunol.* **2023**, *140*, 108979. https://doi.org/10.1016/j.fsi.2023.108979.

(53) Lepack, A. E.; Fuchikami, M.; Dwyer, J. M.; Banasr, M.; Duman, R. S. BDNF Release Is Required for the Behavioral Actions of Ketamine. *Int. J. Neuropsychopharmacol.* **2015**, *18* (1), pyu033. https://doi.org/10.1093/ijnp/pyu033.

(54) Lepack, A. E.; Bang, E.; Lee, B.; Dwyer, J. M.; Duman, R. S. Fast-Acting Antidepressants Rapidly Stimulate ERK Signaling and BDNF Release in Primary Neuronal Cultures. *Neuropharmacology* **2016**, *111*, 242–252. https://doi.org/10.1016/j.neuropharm.2016.09.011.

(55) Cavalleri, L.; Merlo Pich, E.; Millan, M. J.; Chiamulera, C.; Kunath, T.; Spano, P. F.; Collo, G. Ketamine Enhances Structural Plasticity in Mouse Mesencephalic and Human iPSC-Derived Dopaminergic Neurons via AMPAR-Driven BDNF and mTOR Signaling. *Mol. Psychiatry* **2018**, *23* (4), 812–823. https://doi.org/10.1038/mp.2017.241.

(56) Lopez, J. P.; Lücken, M. D.; Brivio, E.; Karamihalev, S.; Kos, A.; De Donno, C.; Benjamin, A.; Yang, H.; Dick, A. L. W.; Stoffel, R.; Flachskamm, C.; Ressle, A.; Roeh, S.; Huettl, R.-E.; Parl, A.; Eggert, C.; Novak, B.; Yan, Y.; Yeoh, K.; Holzapfel, M.; Hauger, B.; Harbich, D.; Schmid, B.; Di Giaimo, R.; Turck, C. W.; Schmidt, M. V.; Deussing, J. M.; Eder, M.; Dine, J.; Theis, F. J.; Chen, A. Ketamine Exerts Its Sustained Antidepressant Effects via Cell-Type-Specific Regulation of *Kcnq2*. *Neuron* **2022**, *110* (14), 2283-2298.e9. https://doi.org/10.1016/j.neuron.2022.05.001.

(57) Yao, W.; Cao, Q.; Luo, S.; He, L.; Yang, C.; Chen, J.; Qi, Q.; Hashimoto, K.; Zhang, J. Microglial ERK-NRBP1-CREB-BDNF Signaling in Sustained Antidepressant Actions of (R)-Ketamine. *Mol. Psychiatry* **2022**, *27* (3), 1618–1629. https://doi.org/10.1038/s41380-021-01377-7.

(58) Diniz, C. R. A. F.; Crestani, A. P.; Casarotto, P. C.; Biojone, C.; Cannarozzo, C.; Winkel, F.; Prozorov, M. A.; Kot, E. F.; Goncharuk, S. A.; Benette Marques, D.; Rakauskas Zacharias, L.; Autio, H.; Sahu, M. P.; Borges-Assis, A. B.; Leite, J. P.; Mineev, K. S.; Castrén, E.; Resstel, L. B. M. Fluoxetine and Ketamine Enhance Extinction Memory and Brain Plasticity by Triggering the P75 Neurotrophin Receptor Proteolytic Pathway. *Biol. Psychiatry* **2025**, *97* (3), 248–260. https://doi.org/10.1016/j.biopsych.2024.06.021.

(59) Zakhary, S. M.; Ayubcha, D.; Ansari, F.; Kamran, K.; Karim, M.; Leheste, J. R.; Horowitz, J. M.; Torres, G. A Behavioral and Molecular Analysis of Ketamine in Zebrafish. *Synapse* **2011**, *65* (2), 160–167. https://doi.org/10.1002/syn.20830.

(60) De Campos, E. G.; Bruni, A. T.; De Martinis, B. S. Ketamine Induces Anxiolytic Effects in Adult Zebrafish: A Multivariate Statistics Approach. *Behav. Brain Res.* **2015**, *292*, 537–546. https://doi.org/10.1016/j.bbr.2015.07.017.

(61) Andalman, A. S.; Burns, V. M.; Lovett-Barron, M.; Broxton, M.; Poole, B.; Yang, S. J.; Grosenick, L.; Lerner, T. N.; Chen, R.; Benster, T.; Mourrain, P.; Levoy, M.; Rajan, K.; Deisseroth, K. Neuronal Dynamics Regulating Brain and Behavioral State Transitions. *Cell* **2019**, *177* (4), 970-985.e20. https://doi.org/10.1016/j.cell.2019.02.037.

(62) Duque, M.; Chen, A. B.; Hsu, E.; Narayan, S.; Rymbek, A.; Begum, S.; Saher, G.; Cohen, A. E.; Olson, D. E.; Li, Y.; Prober, D. A.; Bergles, D. E.; Fishman, M. C.; Engert, F.; Ahrens, M. B. Ketamine Induces Plasticity in a Norepinephrine-Astroglial Circuit to Promote Behavioral Perseverance. *Neuron* **2025**, *113* (3), 426-443.e5. https://doi.org/10.1016/j.neuron.2024.11.011.

(63) Geiger, Z.; VanVeller, B.; Lopez, Z.; Harrata, A. K.; Battani, K.; Wegman-Points, L.; Yuan, L.-L. Determination of Diffusion Kinetics of Ketamine in Brain Tissue: Implications for in Vitro Mechanistic Studies of Drug Actions. *Front. Neurosci.* **2021**, *15*. https://doi.org/10.3389/fnins.2021.678978.

(64) Ma, S.; Chen, M.; Jiang, Y.; Xiang, X.; Wang, S.; Wu, Z.; Li, S.; Cui, Y.; Wang, J.; Zhu, Y.; Zhang, Y.; Ma, H.; Duan, S.; Li, H.; Yang, Y.; Lingle, C. J.; Hu, H. Sustained Antidepressant Effect of Ketamine through NMDAR Trapping in the LHb. *Nature* **2023**, *622* (7984), 802–809. https://doi.org/10.1038/s41586-023-06624-1.

(65) Moaddel, R.; Farmer, C. A.; Yavi, M.; Kadriu, B.; Zhu, M.; Fan, J.; Chen, Q.; Lehrmann, E.; Fantoni, G.; De, S.; Mazucanti, C. H.; Acevedo-Diaz, E. E.; Yuan, P.; Gould, T. D.; Park, L. T.; Egan, J. M.; Ferrucci, L.; Zarate, C. A. Cerebrospinal Fluid Exploratory Proteomics and Ketamine Metabolite Pharmacokinetics in Human Volunteers after Ketamine Infusion. *iScience* **2023**, *26* (12), 108527. https://doi.org/10.1016/j.isci.2023.108527.

(66) Xi, X. J.; Chen, S. H.; Mi, H. Aldh2 Gene Reduces Oxidative Stress in the Bladder by Regulating the NF-κB Pathway in a Mouse Model of Ketamine-induced Cystitis. *Exp. Ther. Med.* **2020**, *20* (5), 1–1. https://doi.org/10.3892/etm.2020.9239.

(67) Kim, J. S.; Schmid-Burgk, W.; Claus, D.; Kornhuber, H. H. Increased Serum Glutamate in Depressed Patients. *Arch. Für Psychiatr. Nervenkrankh.* **1982**, *232* (4), 299–304. https://doi.org/10.1007/BF00345492.

(68) Kugaya, A.; Sanacora, G. Beyond Monoamines: Glutamatergic Function in Mood Disorders. *CNS Spectr.* **2005**, *10* (10), 808–819. https://doi.org/10.1017/S1092852900010403.

(69) Yildiz-Yesiloglu, A.; Ankerst, D. P. Review of 1H Magnetic Resonance Spectroscopy Findings in Major Depressive Disorder: A Meta-Analysis. *Psychiatry Res. Neuroimaging* **2006**, *147* (1), 1–25. https://doi.org/10.1016/j.pscychresns.2005.12.004.

(70) Tordera, R. M.; Totterdell, S.; Wojcik, S. M.; Brose, N.; Elizalde, N.; Lasheras, B.; Del Rio, J. Enhanced Anxiety, Depressive-like Behaviour and Impaired Recognition Memory in Mice with Reduced Expression of the Vesicular Glutamate Transporter 1 (VGLUT1). *Eur. J. Neurosci.* **2007**, *25* (1), 281–290. https://doi.org/10.1111/j.1460-9568.2006.05259.x.

(71) Almeida, R. F.; Thomazi, A. P.; Godinho, G. F.; Saute, J. A. M.; Wofchuk, S. T.; Souza, D. O.; Ganzella, M. Effects of Depressive-Like Behavior of Rats on Brain Glutamate Uptake. *Neurochem. Res.* **2010**, *35* (8), 1164–1171. https://doi.org/10.1007/s11064-010-0169-4.

(72) Lee, Y.; Son, H.; Kim, G.; Kim, S.; Lee, D. H.; Roh, G. S.; Kang, S. S.; Cho, G. J.; Choi, W. S.; Kim, H. J. Glutamine Deficiency in the Prefrontal Cortex Increases Depressive-like Behaviours in Male Mice. *J. Psychiatry Neurosci.* **2013**, *38* (3), 183–191. https://doi.org/10.1503/jpn.120024.

(73) Moriguchi, S.; Takamiya, A.; Noda, Y.; Horita, N.; Wada, M.; Tsugawa, S.; Plitman, E.; Sano, Y.; Tarumi, R.; ElSalhy, M.; Katayama, N.; Ogyu, K.; Miyazaki, T.; Kishimoto, T.; Graff-Guerrero, A.; Meyer, J. H.; Blumberger, D. M.; Daskalakis, Z. J.; Mimura, M.; Nakajima, S. Glutamatergic Neurometabolite Levels in Major Depressive Disorder: A Systematic Review and Meta-Analysis of Proton Magnetic Resonance Spectroscopy Studies. *Mol. Psychiatry* **2019**, *24* (7), 952–964. https://doi.org/10.1038/s41380-018-0252-9.

(74) Gerhard, D. M.; Pothula, S.; Liu, R.-J.; Wu, M.; Li, X.-Y.; Girgenti, M. J.; Taylor, S. R.; Duman, C. H.; Delpire, E.; Picciotto, M.; Wohleb, E. S.; Duman, R. S. GABA Interneurons Are the Cellular Trigger for Ketamine's Rapid Antidepressant Actions. *J. Clin. Invest.* **2020**, *130* (3), 1336–1349. https://doi.org/10.1172/JCI130808.

(75) Pothula, S.; Kato, T.; Liu, R.-J.; Wu, M.; Gerhard, D.; Shinohara, R.; Sliby, A.-N.; Chowdhury, G. M. I.; Behar, K. L.; Sanacora, G.; Banerjee, P.; Duman, R. S. Cell-Type Specific Modulation of NMDA Receptors Triggers Antidepressant Actions. *Mol. Psychiatry* **2021**, *26* (9), 5097–5111. https://doi.org/10.1038/s41380-020-0796-3.

(76) Zanos, P.; Gould, T. D. Mechanisms of Ketamine Action as an Antidepressant. *Mol. Psychiatry* **2018**, *23* (4), 801–811. https://doi.org/10.1038/mp.2017.255.

(77) Kang, M. J. Y.; Hawken, E.; Vazquez, G. H. The Mechanisms Behind Rapid Antidepressant Effects of Ketamine: A Systematic Review With a Focus on Molecular Neuroplasticity. *Front. Psychiatry* **2022**, *13*. https://doi.org/10.3389/fpsyt.2022.860882.

(78) Li, N.; Lee, B.; Liu, R.-J.; Banasr, M.; Dwyer, J. M.; Iwata, M.; Li, X.-Y.; Aghajanian, G.; Duman, R. S. mTOR-Dependent Synapse Formation Underlies the Rapid Antidepressant Effects of NMDA Antagonists. *Science* **2010**, *329* (5994), 959–964. https://doi.org/10.1126/science.1190287.

(79) Shahar, O. D.; Schuman, E. M. Large-Scale Cell-Type-Specific Imaging of Protein Synthesis in a Vertebrate Brain. *eLife* **2020**, *9*, e50564. https://doi.org/10.7554/eLife.50564.

(80) Jones, J.; MacKrell, E. J.; Wang, T.-Y.; Lomenick, B.; Roukes, M. L.; Chou, T.-F. Tidyproteomics: An Open-Source R Package and Data Object for Quantitative Proteomics Post Analysis and Visualization. *BMC Bioinformatics* **2023**, *24* (1), 239. https://doi.org/10.1186/s12859-023-05360-7.